Improvement of heat-led CHPs based upon ORC-technology

Tobias Gabriel Erhart

Institute of Electric and Electronic Engineering

University of Strathclyde, Glasgow

Submitted in fulfilment of the requirements for the degree of

Doctor of Philosophy in Electronic Engineering

2015-08-24

Supervisors

Prof. Dr. habil. Ursula Eicker

University of Applied Sciences Stuttgart
Department of Building Physics
Centre for Sustainable Energy Technology - zafh.net Schellingstrasse 24
70190 Stuttgart, Germany

Prof. Dr David Infield
Institute of Energy and Environment
Royal College Building
University of Strathclyde
204 George Street Glasgow

G1 1XW, Scotland Date:

Signatures:

Declaration

This thesis is the result of the author's original research. It has been composed by the author and has not been previously submitted for examination which has led to the award of a degree.

Date: 2016-03-12

Signature:

"The fool doth think he is wise, but the wise man knows himself to be

a fool."

William Shakespeare

Acknowledgements

This thesis has been generously supported by Landesstiftung BadenWu¨rttemberg with a scholarship. This thesis concludes the results of two research projects (POLYCITY, RecoORC). I would like to thank all project partners in industry and research for their assistance and collaboration. Many thanks to the team of the Stadtwerke Esslingen. Wolfgang Lotz for his trust in research. Jochen Fink and Marc Hagenloch for their great collaboration. Ju¨rgen G¨olz for his immense practical skills, knowledge and all our fruitful discussions. Andreas
Schad and his mechanical team for a great collaboration. Prof. Dr.-Ing. Martin Mu¨ller for introducing me to the field of power generation and ORC.

I am grateful for the support of my supervisors, colleagues, friends and family. They helping me to cope with the challenges of a full position, a thesis and starting a family. Special thanks go to: Andreas Trinkle for showing me good practice in programming and for his outstanding work on the OPC-client and the EMtool. Eric Duminil for teaching me ruby and backing up my data. Alesio Barone and Luca Abbiati for their contribution. Dr Sylvain Quoilin for his inspiring work. Furthermore, I would like to express my gratitude to all developers of great, free software (GNUplot, modelica, MikTex,
Texmaker, Git, Tourtoise, FluidProp, CycleTempo, ExternalMedia Library, ThermoPower Library, CoolProp Library,...), especially Prof. Dr Francesco Casella for his modelica libraries.

Abstract

Drawn by the benefits of decentralised and renewable power supply, over 150 Organic Rankine Cycle systems, in a range from 400kW$_{el}$ to 2MW$_{el}$, have been installed in Central Europe between 1998 to 2014. The majority of modules are biomass fired and heat-led by district heating networks. Combined heat and power (CHP) using the ORC technology has a great potential to provide heat and the electric base

load for households. The impact of such systems in terms of CO_2 and primary energy consumption is very low in comparison to conventional heating systems (gas, oil). With rising fuel prices over the last years, the economic situation has become critical for many of these facilities and improvements in efficiency are essential.

The research reported here, concludes five years of practical and theoretical experiences and investigations. An operating power plant with a design power of $1MW_{el}$ has served as validation. Monitoring data have been gathered over a period of eight years for the entire biomass power plant including the district heating network. In addition, a detailed measuring campaign was conducted for three years on the ORC-unit. Approaches to improve the performance of power plants of this category have been developed based on the long-term monitoring.

- The influence of a condenser reservoir controller is very limited, based on the proportions of the thermal inertia. Control implementation of the heat rejection systems is vital in order to obtain smooth load transitions. The control of the heat rejection system has been optimized in order to provide stable sink temperatures. It could be shown that this measure leads to a smoother operation of the unit.
- Acceptable electrical efficiencies can only be achieved with high pressure ratios across the turbine. Therefore, the recuperator was focused upon. A significant increase of power output (2% points) could be achieved by improving the heat transfer while reducing the pressure losses across the aggregate.
- Besides the frictions losses, the potential of the cycle can only be utilized if the fluid contains no contaminants, such as low-boilers or inert gases. If this is the case, the condenser can reach a minimum of pressure. Quality management and, if necessary, fluid recycling are vital. Approaches for these two points are discussed. The implementation of a fluid management system for working fluid contaminated with low-boilers and high-boilers is shown. The effectiveness of these measures are proved by

monitoring data. It could be shown, that 54% to 63% of the MDM contained in contaminated working fluid can be recycled with just one distilling procedure.

In addition to the practical experiences gained, the obtained data of the ORC-unit has been used to develop, calibrate and validate correlations and computer models. The data inform partial models and cycle models, of physical and empirical nature, to simulate ORC units of that type in modelica.

- A turbine model for single-stage, super-sonic axial units has been developed. It is accurate within a range of ±0.5%.
- The steady-state validation of the pre-heater model show a fair correlation within boundaries of ±5%. Taking a look a the correlation quality of the dynamic component model of the preheater, even better results can be expected. With a nodal model of only two nodes the entire calculation correlates within a range of ±0.5%
- The comparison of the various pool boiling correlation in literature has shown that evaporation of siloxanes in a kettle-type tube evaporator cannot be solved without significant adaptations. While the most correlations delivered a good trend the offsets are enormous. Therefore, a new correlation for this specific case has been developed. Finally a correlation based on was chosen with the basic structure of Gorenflo's approach using the pressure correlation function of Mostinski. The prediction quality, with a range of ±8%, is fairly good for a boiling correlation.
- The proposed model for the recuperator unit correlates within a range of ±5% in the relevant U-value range of 200W/m²K to 325W/m²K. The deviation for lower U-values can exceed 10%, but it is only relevant during start-ups
- The simulation results show that an operational mode with a low super-heating rate lead to higher thermal efficiencies. This implies a reduction of fuel in the furnace therefrom including all

consequences. The fuel mass flow is reduced, which leads to a decrease of wear on the transport systems and heat exchangers. Additionally this strategy lowers the risk of hot spots in the ORC, leading to a longer cycle fluid lifespan and a win-win(-win) situation economically speaking. The electric efficiency improves by 1%-point almost across the whole load range. The surplus during an average year amounts up to 28000e for the case study unit.

Nomenclature

Roman Symbols

ΔH_c^0	Heat of combustion, see LCV [kJ/kg],[MWh/m³]
ΔT	temperature difference [K]
$\dot{m}$	mass flow [kg/s]
$\dot{V}$	volume flow [l/s] or [m³/h]
A	Area [m²]
a	attraction parameter [-]
A_{chn}	chain formation Helmholtz Energy [J] of a molecule
A_{id}	ideal Helmholtz Energy [J] of a molecule
A_{seg}	segmental interaction Helmholtz Energy [J] of a molecule
A/F	Helmholtz Energy [J]
adj. R^2	adjusted coefficient of determination
b	repulsion parameter [-]
Bo/Bg	Boiling number [-]
E	Helmholtz Energy [kJ/kg]
F_A	attractive dispersion Helmholtz Energy [J] of a molecule
f_{DW}	Darcy-Weisbach friction factor
F_H	hard-body Helmholtz Energy [J] of a molecule
F_{pol}	polar interaction Helmholtz Energy [J] of a molecule
h_0	specific enthalpy reference state [kJ/kg]
h_{evap}	specific enthalpy of evaporation [kJ/kg]
h_l	specific enthalpy of liquid [kJ/kg]

h_v specific enthalpy of vapour [kJ/kg]

J moment of inertia [kgm^2]

Ja Jakob number [-]

k Boltzmann Constant 1.38064852J/K

m mass [kg]

N absolute number of molecules [-]

N number of tubes [-]

N_A Avogadro Number [1/mol]

Nu Nusselt number, named after Wilhelm Nußelt [-]

p absolute pressure [Pa]

p pressure [bar]

p_{cond} pressure inside the condenser vessel

p_c critical pressure of the cycle fluid, here 14.15bar

p_r reduced pressure of the cycle fluid, $\frac{p}{p_c}$ p_{sat} saturation

pressure of pure component in the condenser PPMCC Pearson

product-moment correlation coefficient

Pr Prandlt number, named after Ludwig Prandtl [-]

Q energy, thermal [MWh_{th}] R gas

Constant [J/molK]

r radius [m]

R^2 coefficient of determination

r_s reciprocal pressure ratio [Pa/Pa]

Ra Rayleigh number [-]

Re	Reynolds number [-]
Sh	Sherwood number [-]
STP	Standard Temperature and Pressure, 273.15K and 101325Pa
T_c	critical temperature of the cycle fluid, here for MDM 290.935K
T_r	reduced temperature [-]
U	heat transfer coefficient [W/(m²K)]
u	wood moisture according to EN 844-4 [kg/kg]
V_c	critical volume [m³/kg]
V_m	critical molar volume [m³/mol]
W	work, electrical [MWh_{el}]
$\dot{X}_i$	load state interval

Greek Symbols

α	angular acceleration [rad/s²]
α	convective heat transfer coefficient [W/m²K]
α	polynomial adaptation factor of the attraction parameter [-]
$\bar{\eta}_{el,an}$	annual weighted mean degree of efficiency
β	pressure ratio [-],[Pa/Pa]
	Error [%]
	Surface roughness [mm],[m]
η_{el}	electric degree of efficiency
η_{mech}	mechanical degree of efficiency
η_{th}	thermal degree of efficiency
Γ	specific mass flow per unit length [kg/ms]
κ_i	pure component parameter, for i=0 to i=3 [-]

λ	thermal conductivity [W/mK]
λ_{com}	stoichiometric air-fuel equivalence ratio of combustion
μ	dynamic viscosity [Ns/m^2],[Pas]
ω	Acentric Factor [-]
ω	angular velocity [rad/s]
Φ	heat rate [MW$_{th}$] or [kW$_{th}$]
Φ	heat transfer rate, heat rate [kW]
ρ	density [kg/m^3]
ρ_c	critical density [kg/m^3]
ρ_r	reduced Density [-]
Θ	complementary reduced temperature [-]
ϑ	temperature [$^\circ C$]
ζ	fitting friction number

Subscripts

amb ambient an

annual

aux auxiliary boil

boiling bub bubble

bun bundle c critical

car Carnot

cold cold side of heat exchanger

cond condenser, condensing

conv	convective
df	dry fuel
dh	district heating
dsh	de-super-heat
el	electric
feed	feed flow output
fg	flue gas
fin	fin, used as surface enhancement
fuel	fuel
furn	furnace
geo	geodetic
gr	gross
hot	hot side of heat exchanger
HTRI	Heat Transfer Research Inc.
liq	liquid
log	logarithmic
loss	loss, dissipation
nb	nucleate boiling
net	net
$NPSH_R$	Net Positive Suction Head Required
off	offset
ONB	On-set point of Nucleate Boiling
OTS	Off The Shelf
para	parasitic

pip pipe r

reduced

ret return flow input RSME

Root Square Mean Error s

isentropic sat saturated sc

sub-cool seg segment

SSE Sum of Squares due to Error surf

surface tc thermal conversion

th thermal to

thermal oil tot

total

tube property of a tube

vap vapour

Acronyms

CAS Chemical Abstracts Service Registry Number

CFD Computational Fluid Dynamics

CHP Mass Spectroscopy

CSV Character Separated Values

DH District Heating

DWFF Darcy-Weisbach Friction Factor

EBIT Earnings Before Interest and Tax

EEE Department of Electrical and Electronic Engineering

EEG	Gesetz fu¨r den Vorrang Erneuerbarer Energien - German Renewable Energy Act
EES	Engineering Equation Solver (by F-Software)
EOS	Equations-of-State
FTP	File Transfer Protocol
GC	Gas Chromatography
HPR	Heat-to-Power Ratio
HS	Head space sample
LCV/LHV	Lower calorific heating value
LMTD	Logarithmic Mean Temperature Difference
MDM	Octamethyltrisiloxane,Dimethyl-Bis(Trimethylsilyloxy)Silane (CAS 107-51-7), cycle fluid
OPC-UA	OLE for Process Control-Unified Architecture
P-Bus	PROFIBUS®, Process Field Bus
P235GH	low alloyed boiler steel according to DIN EN 10028-2
PHE	Plate Heat Exchanger
PHR	Power-to-Heat Ratio
PID	Proportional-Integral-Differential
PPMCC	Pearson product-moment correlation coefficient
PSHE	Plate Shell Heat Exchanger
SME	Small and Medium Enterprises
STT	Shell and Tube Type
SWE	Stadtwerke Esslingen GmbH&Co.KG, local supply company
T66	Therminol® 66 thermal oil used in the transfer cycle of the power plant

TUV¨ Technischer Uberwachungsverein¨

TCP/IP Transmission Control Protocol/Internet Protocol

Document Structure

- Chapter I (Introduction): gives a brief introduction from historical development to state-of-the-art technology. The context between technical and economical aspects and the current market situation for ORC-power plants is described.
- Chapter II (Methodology): the methodology of this work is described.
- Chapter III (The case study Scharnhauser Park): the case study "Scharnhauser Park", which serves as validation system for this work is described in detail.
- Chapter IV (Data acquisition): monitoring of operational data for the case study are described in detail. It contains the entire process from the physical sensor layer to the data processing and post-processing.
- Chapter V (Modelling): the approach to the modelling of all relevant sub-systems and systems is described in this chapter. It concludes the simulation of heat transfer, mass transport, control and energy conversion
- Chapter VI (Validation results): validation results, based on the data of the case study, are presented in this chapter.
- Chapter VII (Monitoring results - operational experience): as an additional practical approach to the topic, gathered operational experience of several years is reported and evaluated.
- Chapter VIII (Simulation results and improved operation strategies): simulation results of parametric studies are evaluated.
- Chapter IX (Discussion of results - final conclusions): simulation results of parametric studies are evaluated under the consideration of operational experiences. The technical results are concatenated with economic key figures. Recommendations

for the operation of biomass fuelled heat-led ORC plants are given.

- Appendix A (Technical reference and source code): technical appendix containing simulation details, correlation parameters, data sheets and program code.
- Appendix B (Publications of the author): appendix for nontechnical and organisational issues.

Enjoy reading!

Contents

List of Figures

Chapter 1

Introduction

With the implementation of the Electric Grid Access Act [1] in 1991 and the successive Renewable Energy Sources Act[2] (RES) in 2000 [11] the production of Combined Heat and Power (CHP) in small and medium sized plants has become interesting from an economic point of view. A wide range of these technologies are applied today. The common steam turbine processes, operating with high temperatures and pressures and enormous dimensions, are not suitable for such comparably small-scale facilities. Therefore technologies that have been neglected in the past, or that have been used in small market niches, were further developed. In this field, wood gasification, the Stirling engine, the steam engine, the KalinaCycle and the Organic-Rankine-Cycle have to be mentioned. Since the beginning of the 1980s the ORC-technology has continuously and successfully been developed. First of all carriers of thermal springs and wood processing companies invested in that concept. Especially the need to enlarge their core business and finding a synergy under the constraint of low personnel and economical resources, led to the decision for this allegedly low maintenance technology. In the recent years reaching the facility scale of 2MW electric output ensured to operate a plant economically. The promotion of biomass by the RES-Act can turn the concept into a rather attractive investment, even as stand-alone-plant. Compared with common energy carriers this combination has a very low Primary Energy Factor (PEF)[3] of up to 0.2 [4]. The CO_2 savings related to user end energy (including transportation losses) are over 60% to de-centralised gas and oil boilers (Figure 1.1). Taking a look at the PEFs of de-centralized co-generation solutions in Figure 1.2, the useful end energy generated from such power plants has significantly lower impact on primary energy consumption than conventional

[1] Stromeinspeisungsgesetz, (StromEinspG)

[2] Gesetz fu¨r den Vorrang Erneuerbarer Energien, Erneuerbare-Energien-Gesetz (EEG)

[3] According to DIN EN 15603[12], the primary energy factors is the quotient of primary energy carrier and the end user energy. It describes how much useful energy is dissipated while transporting, distribution, transmission, generation and processing to the utilization site.

[4] by definition this value can be lower

technologies. The operation of various facilities over the last years and the increasing number of the ones being built show the difficulties as well as the potential. Besides other applications, such as geothermal or solar, over 150 biomass CHP facilities have been constructed in the last decade all over Europe. Their electric outputs reach from 400kW to 2.2MW per unit. This variety of CHP has become a common technology, particularly in Germany, Austria, Italy and France. Municipalities and local supply companies are diversifying their business portfolio from water and gas service to a local or regional, decentralised energy infrastructure. In this context CHP technologies have become a part of their repertoire. Multiple points argue for a combination of heat and electric power:

- Consumption or conversion of renewable and sustainable local resources.
- A local or regional supply chain with creation of value.
- Feasible Investment cost for SMEs (≤ 10 MMe).
- The availability of a mature technology in an adequate quality.
- Reasonable heat to power ratio and a high contemporaneity of both.
- Both, base load and medium to peak load capability.
- The quickly changing conditions of the energy market with constantly increasing production costs.
- A small number of alternatives with a 24 hours respectively 72 hours unmanned operation. The German boiler code demands manned operation if steam is used in a category V pressure vessel (e.g. steam with more than 120 °C and cycle volume larger than 50l).
- The promotion of this technology politically, by incentives and/or subsidies.

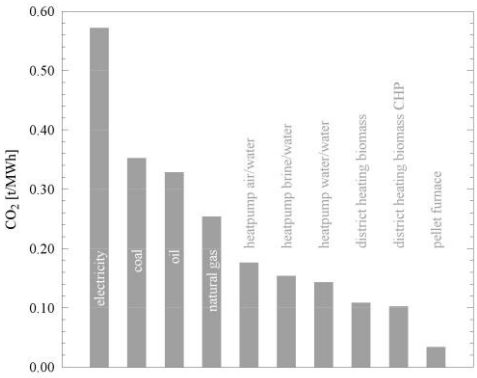

Figure 1.1: CO_2 emissions of various concepts, related to end energy

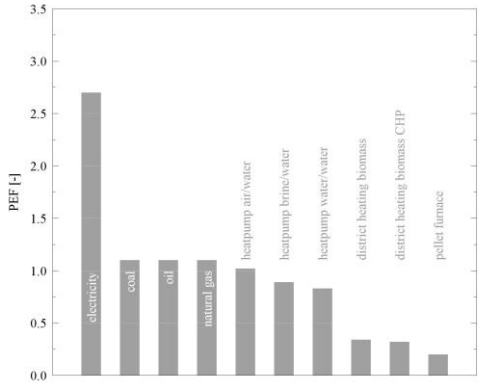

Figure 1.2: Primary Energy Factor of heating concepts, related to end energy

The recent development in Germany shows success stories as well as many suppliers that have underestimated the running costs and maintenance of such power plants. A brief view on the history of the water steam cycle proves that even after a long period of development remarkable improvements can be achieved. Further increase in reliability and efficiency can be expected in the next years, as the ORC-technology has made the leap from experimental to standard technology.

1.1 History of ORC

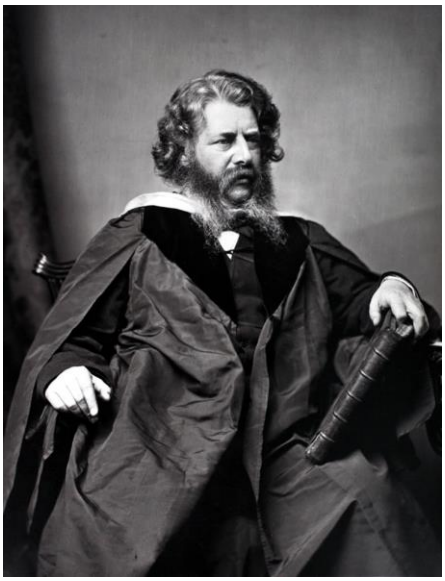

Figure 1.3: William J.M. Rankine [University of Glasgow]

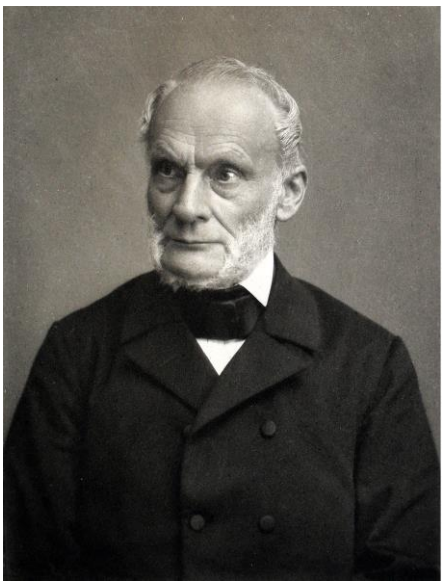

Figure 1.4: Rudolf Clausius [1, 2]

The ORC process is based upon the works of the Scottish engineer and physicist William John Macquorn Rankine (*?*5.7.1820 †24.12.1872) and the German physicist Rudolf Julius Emanuel Clausius (*?*2.2.1822 †24.08.1888), both gentlemen are depicted in Figures 1.3 and 1.4. Within his publication "Manual of the Steam Engine and Other Prime Movers" (1859) Rankine described the conversion of thermal energy into mechanical energy. Almost at the same time (1856) Clausius published his thoughts about energy conversion in his version of the Second Law of
Thermodynamics. He was the first one to introduce an extensive property called Entropy. Back then, the process was solely based on water as a working fluid. Since that time the majority of power plants for the energy production are based on the Clausius-Rankine-Process. The basic concept has been improved and nowadays steam-cycles are complex and sophisticated. However, the usage of water limits the cycle layout to certain pressure and temperature levels. As a consequence, water has been replaced by fluids of organic descent. With this Organic-Rankine-Process the process design overcomes the above mentioned limitations.

1.1.1 First ORC applications

The first known commercial application of Organic-Rankine-Cycles were indeed mobile applications. In the 1880s steam engines had become elaborate enough to

use them in smaller ships and boats. Along the US coast motor boats became very popular for private use. With a rising number of such pleasure boats, the authorities had to face the dangers that come with a steam engine: fires and explosions. Thus, the operation of such vessels was restricted, a certified steam engineer was required on-board to run the engine. In order to circumvent these restrictions, in 1883 Frank W. Ofeldt handed in a patent for a closed loop “steam” engine operating without water [Paul Towne, The Naphtha Engine, 1991]. The fluid in the cycle was Naphtha. Within a few years the Naphtha Launches became very popular. The Gas Engine and Power Company NYC claimed having sold over 500 launches by 1890 [The Rudder, July 1980]. The engine was an ORC-cycle with a piston expander. One part of liquid Naphtha was taken from a tank and burnt in a small boiler, pre-heating and evaporating another part of the Naphtha in a closed loop. The vapour was then expanded in a three piston engine. After expansion the vapour was condensed using a pipe going under water along the hull of the vessel. The engines were lighter (lower pressure), more compact, easier to operate and the fuel had a much higher specific energy content than cord firewood. Naphtha and whale oil served as lubricant in this engine type. The concept was very sophisticated and robust. At that time the available engine sizes ranged from 1hp (/SI0.7457kW) to 16hp (11.9312kW) of mechanical power. Until outboard petrol and diesel engines became reliable enough ORC was the state of the art to motorise small boats. Figures 1.5 and 1.6 show a typical Naphtha Launch and a cross section through the above mentioned three cylinder engine.

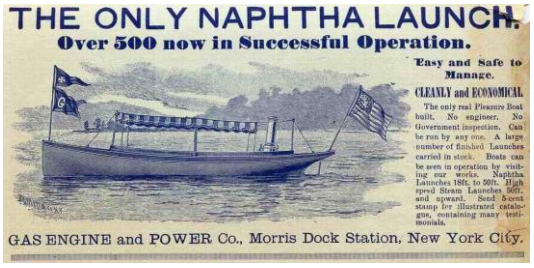

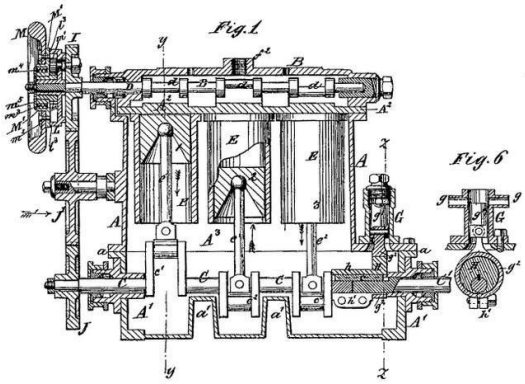

Figure 1.5: magazine article on Naphta enfuelled launches [The Rudder, 1890]

Figure 1.6: drawing of a Naphtha gine [Towne, 1991]

1.1.2 Early (industrial) ORC applications

It took quite a while from the aforementioned mobile solutions to the first industrially used ORC plant. In the 1960s, Tabor and Bronicki developed low temperature micro-ORC units in a electrical power range up to 10kW$_{el}$ [13]. This development was the basis for the company of Ormat Turbines, which was founded in 1965 by Lucien and Yehudit Bronicki. In the year 1967 the first medium-scale geothermal unit was taken into operation in the Soviet Union. The American ORC market is dominated by the company of Ormat Industries, formerly Ormat

Turbines. Besides several large geothermal power plants, which is the main field of the business operations, their portfolio contains auxiliary power stations based on natural gas boilers. Great advances in ORC technology were done in the late seventies and early eighties by the research group of Angelino, Gaia and Macchi. Their work was the foundation for the Company of Turboden which later became the European market leader for ORC technology. In Europe the first successful long-term testing of a biomass fuelled ORC-plant has been undertaken in 1999. In Admont, Austria the company of STIA set-up an 400kW$_{el}$ biomass driven unit. In many publications (Obernberger, Hammerschmid, Bini et al. [14–16]) this power plant and the following project, with a larger engine, in Lienz have been assessed. The two sites were co-funded by the European Commission within the the fifth Frame Work Programme. For biomass fuelled systems, the reliability as well as the feasibility have been proven within these projects.

1.2 Energy market situation in Germany

In order to set energy demand, energy consumption and energy conversion especially in terms of ORC into relation a brief look at energy market situation is necessary. Incentives on the one hand side and purchase prices for fuel can either balance or imbalance the market. With economic-political instruments (incentives, taxes, guaranteed grid access) certain technologies or branches can be promoted or inhibited. As the grid-feed-in tariffs are constant over the period of operation (for each facility) the main economic variable is the fuel market price.

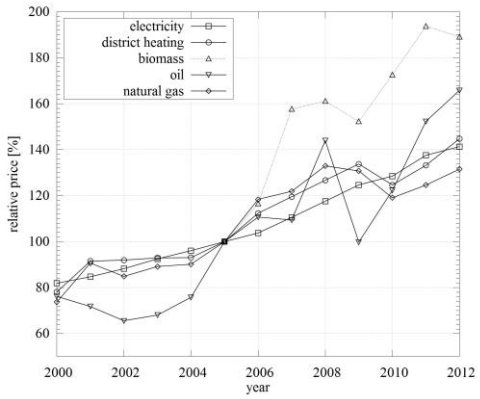

Figure 1.7: energy prices development in Germany

Table 1.1: feed-in tariffs [ct/kWh] according to EEG [17–19]

$P_{el} \leq$ year	$P_{el} \leq$ 150kW	$P_{el} \leq$ 500kW	$P_{el} \leq$ 5MW
2004	21.5	19.9	16.9
2005	21.33	19.75	16.77
2006	21.16	19.6	16.64
2007	20.99	19.46	16.51
2008	20.83	19.32	16.38
2014	13.66	11.78	10.55

The above Figure 1.7 on the left shows a comparison of the statistical energy prices for end users in Germany. All values are normalised and related to the year 2005, when the statistical monitoring of biomass prices began in Germany. It is common practice, to couple district heating prices to the natural gas price. Biomass increased more than other energy carriers since then. For suppliers with long term contracts this causes a deficit. This deficit can only be compensated by decreasing other costs such as personnel or increasing the efficiency. The EEG triggered a development in the early 2000s. During one decade the share of renewable energies (including hydro-power) in electric generation reached 23%, the coverage of thermal demand was 10.4% [20]. Within this part, biomass covers 27.1% of the electric generation and 74% of the thermal energy [20]. According to the rated peak power the electric generation from biomass has the highest proportion in electricity production. While all biogenous fuels have a share of 8.7% in the rated power, their share in electric production reached 25.9% in 2012 [20]. Since the evolution of renewable energies was a success in the last years, the incentives have been in the focus of political controversies in Germany. As a consequence, the EEG has been revised in the years 2009, 2012 and 2014.

Table 1.1 provides an overview on the incentive structure. The total incentives are a result of a basic tariff and number of bonuses (CHP-bonus, renewable-bonus, technology-bonus, et cetera). With the EEG 2012 the CHP-bonus was cancelled and a heat consumption became obligatory. The generator requires a minimum of 60% running in CHP-mode to fulfil this criterion. In the latest version of the EEG most bonuses have been reduced or cancelled for systems

using solid biomass. As a result the feed-in tariffs are significantly lower than in the beginning, as the last line in the Table 1.1 shows.

1.3 ORC today

The majority of ORC-modules in Germany are biomass fired and heat-led by the thermal demand of a district heating network. The technology of ORC has become a market relevant issue in the recent years. In the 1980s and 1990s only a few manufacturers, mainly small start-ups, produced ORCs. Some of those companies have failed, some grew and many of them have been taken over by large international market players, such as Pratt& Whitney, Bosch et cetera. The quantity and type of ORC systems depend very much on national legal and political circumstances. In Europe the major part of facilities is driven by biomass. Facility sizes range up to 2.2MW_{el}. In the US, the field of ORC is dominated by geothermal systems. The company of Ormat has constructed comparably large units which are mainly installed across the US (some in Africa and Oceania). These units have electrical outputs of up to 92MW. For the year 2012 the overall installed electric power by Ormat geothermal applications is estimated to 626MW [Ormat Technologies Reports 2013, Fourth Quarter and Year End Results]. Taking a look at Europe, ORC is mainly used in a CHP context. The grid access laws in many European countries demand a usage of the sink heat. In order to increase the primary energy efficiency the new version of the German EEG demands a heat usage ratio of more than 60% [18].

Table 1.2: number of ORC plants across Europe

-	biomass	geothermal	recovery	total
Germany	73	4	3	80
Italy	59	1	10	70
Austria	28	1	1	30
Latvia	12	-	-	12
Spain	7	-	-	7
Poland	7	-	-	7
Russia	2	-	3	5
Switzerland	4	-	-	4
UK	3	-	-	3
Belarus	3	-	-	3

Czech	3	-	-	3
France	1	1	-	2
Finland	1	-	1	2
Romania	1	-	1	2
Croatia	2	-	-	2
Slovakia	1	-	1	2
Turkey	1	-	1	2
Belgium	-	-	1	1
Denmark	1	-	-	1
Estonia	1	-	-	1
Sweden	1	-	-	1
Bulgaria	1	-	-	1
Netherlands	1	-	-	1
Slovenia	1	-	-	1
total	214	7	22	243

The biggest player in the European market is surely Turboden of Italy. They claim a total of 252, 218 are biomass driven. Nearly all of these units are feeding their rejected heat into a district heating or a heating system.

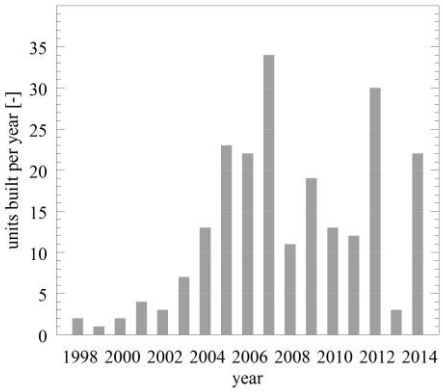

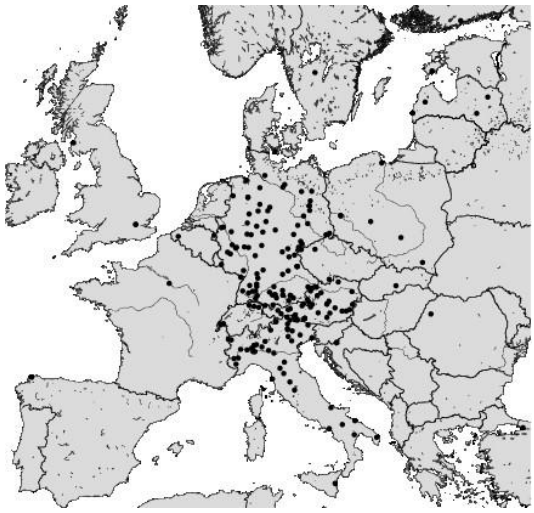

Figure 1.8: ORC units taken into oper- Figure 1.9: ORC power plants across ation in the years 1998 to 2014 Europe

Besides the field of biomass, heat recovery applications are on the second rank (26). In the next years the activities in this very versatile sector will certainly increase as many industrial branches demand for more efficiency and better overall process economy [21–23]. Geothermal applications (7) and solar play an inferior role in Europe. According to the Agency of Renewable Resources (FNR)

the installed electric power of biomass driven CHPs in Germany summed up to 1250MW_{el} by the end of 2011 [24]. For the plants shown in Figures 1.9 and 1.8 it should be mentioned that the data are based on own research, based mainly on the references of the major manufacturers (Adoratec, Maxxtec, Turboden, GMK, Ormat). For the sake of correctness it needs to be mentioned that full data are not available for all facilities mentioned above. Therefore the two listings are not fully coherent. However, Figure 1.8 shows some effects: a first peak of units is taken into operation between 2004 and 2007. This boost has been triggered by two facts: the biomass fuel was relatively cheap and the incentives by the Grid-Access-Act made this technology an appealing investment. The following reduction in the years of 2008 to 2011 may be explained by a market consolidation. The biomass prices rose, the technical standards for such power plant were adjusted after some severe accidents. Those experiences may have damped the market dynamic.

1.4 Water versus organic fluids

For high temperature applications organic matters with standard boiling points [1]up to 400 °C are employed. In the field of biomass conversion, different variants of systems come to use. Cycle designs including a recuperator are state of the art for medium and high temperature ORCs and increase the electric efficiency by 20% compared to a cycle with direct condensation. Additionally, some units are equipped with a split-system. In this case the input of two heat sources at different levels enables a better system control regarding pre-heating and recuperation ratio. This layout provides more variability in overall system design. Especially in biomass combustion low temperature levels in the exhaust ducts and economisers caused many corrosion damages in the past. Using an exhaust gas to thermal oil economiser at a higher temperature level avoids these problems and still increases efficiency. The following aspects have to be taken into consideration, when comparing steam cycles and organic cycles:

- In general lower evaporation pressures and temperatures. Savings in materials of pressurised parts of components.

[1] Standard Temperature and Pressure (STP) 101325Pa and 273.15K

- As most organic fluids expand retrograde into saturated vapour single-stage turbines without a bleeding system [1] can be utilised. This decreases the hardware investment costs drastically.
- Low pressure expansion ratios are not just favourable for single-stage turbines, but as well for the usage of alternative expanders
- For organics there is no need (or at least not to the same extent) for fluid treatment such as demineralisation and corrosion inside the system is very unlikely.

Putting a well engineered cycle into practice means essentially to find the perfect cycle fluid to close the gap between the heat source and the sink. Looking for a perfect fluid candidate for an organic cycle, the following properties have to be considered:

- Evaporation behaviour: high saturation pressure and low specific enthalpy of evaporation
- Condensation behaviour: isentropic or positive slope of dew curve
- Transport properties: low viscosity and high thermal conductivity, high specific heat capacity, high diffusivity[2]
- High pressure ratio
- Low molar mass
- High purity
- Long lasting, low reaction potential with oxygen and alloyed metals, no polymerisation potential
- Wide range stable temperature behaviour, low thermal decomposition rate
- Low inflammability or non-inflammable
- Possibly low toxicity for humans, animals and water organisms

[1] Steam taken from the middle section for reheating
[2] it must be noted that these criteria are contradictory

- Low CO_2-equivalent, both through emission and production
- High availability, competitive market and low price

Many scientists are investigating in cycle fluids for different kinds of applications: low temperature applications [25, 26], high temperature applications [27, 28], mixtures [29, 30], super-critical cycles [31], even working fluids for the use in space crafts [32]. Some approach the problem by analysis of practical experience, others focus on the prediction of chemical and thermodynamic properties [33]. Some even want to "design" new molecules with the reverse approach where the properties are defined first and corresponding molecules or molecule families are identified accordingly [34]. All the above listed constraints are a challenge. However, the variety of potential working fluids offers the opportunity to design a simple but still efficient cycle for many different conditions. In general, biomass fuelled high temperature ORCs can reach up to 20% electric efficiency. This is roughly 50% of their Carnot Efficiency. Under the same conditions and with a comparable level of complexity the ORC performs better than the Clausius Cycle. The following two Figures 1.10 and 1.11 show the two cycles in comparison. Under the same source and sink conditions (300 °C/80 °C) the simple Clausius Cycle has a theoretical expansion ratio[1] of 10, while the ORC reaches 120. The latent heat transferred into the steam cycle is larger than in the organic counter-part.

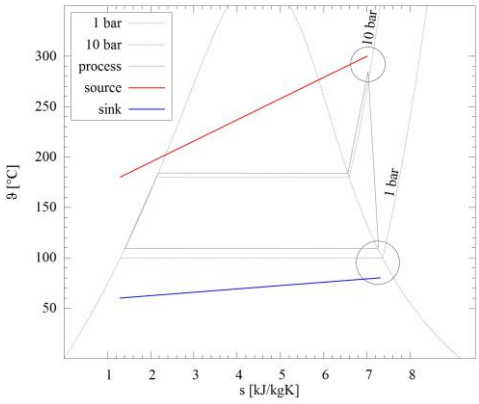

Figure 1.10: simple Clausius Rankine Cycle

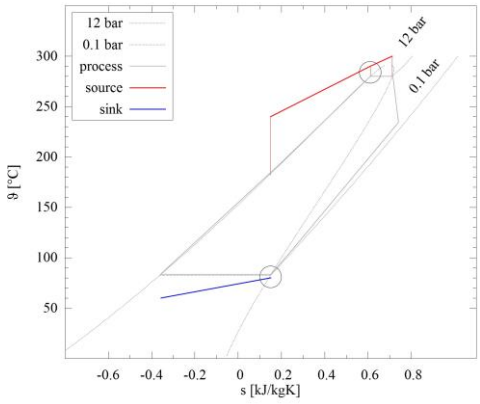

Figure 1.11: simple Organic Rankine Cycle

[1] expander inlet pressure divided by outlet pressure

Based on simplified assumptions the efficiency outcome of the above cycles layouts can be calculated. Taking a few of the most relevant cycle fluids the efficiency versus the input temperature level turns out to be as depicted in Figure 1.12.

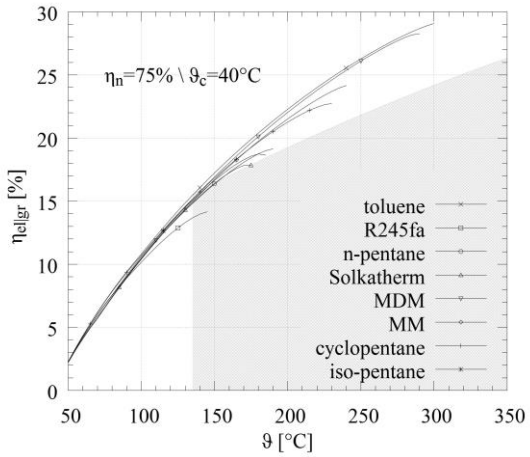

Figure 1.12: various fluids and electric cycle efficiencies in comparison to a steam cycle (gray)

It must be noted, that the above results are based upon the same sink conditions, with a temperature of 40 °C which may not always be the case of application in reality. Especially in biomass applications the heat sink is set to 80 °C/60 °C. The achievable efficiency declines accordingly. For the sake of comparability the cycle layouts are both single-stage turbines without a re-heating unit with the same isentropic efficiency η_n.

1.5 Economical aspects of ORCs

CHPs have a higher degree of freedom in terms of their economy. Whereas a standard power plant has one sort of revenues CHPs convert their fuel into two forms of energy and therefore sources of revenues. In most cases this would be electricity and heat. In some cases cold is provided as a third form of energy, for instance by thermal cooling machines running on heat. In the case of biomass power plants the recycling of ash can play a role as well, however the earnings from this source are rather negligible compared to those from power production. In the Scharnhauser Park case study (see Chapter 3) the heavy metal and noble metal fraction in the electro-static filter ash led to the consideration of recycling instead of disposal. Certainly the recycling or disposal of biomass ash contributes

to a cleaner environment. Particulate residues of tires, clutches and brakes usually precipitate at the sides of roadways. Landscape preservation measures in combination with biomass conversion can remove these residues. As in most power plant types, the specific costs can be expected to decrease with larger units, respectively larger design output. Basic costs (land, building, safety systems) are often not scalable. For small decentralised facilities this is a challenge. Many ORC-units in the small-scale range have to cope with that fact. As a consequence for the small and micro-scale sector, a competitive unit may be only feasible if there are synergistic effects such as waste heat process or improvement of the overall production process. In some cases backup, safety or reliability can be a reason to install an island ORC solution. The main cost factors for a biomass fuelled ORC power plant would be in the order of magnitude:

- Primary investment and annual debt service.
- Primary fuel for the main furnace, for instance: wood chips including charges for ash disposal.
- Secondary fuel for peak load boilers, for instance: natural gas, LPG, oil.
- Personnel expenses.
- Maintenance costs.
- Operating costs, for instance: auxiliary power, water, heating, lubricants, fluids.
- Insurance costs.

1.5.1 Investment costs

Regarding the overall investment costs, variation is very large. According to the local situation land prices may differ a lot. In many large projects the availability of customers and infrastructure is a chicken or egg dilemma. The development of a new residential quarter takes several years, where at the same time a supplier needs a return on investment within five years to establish the financing. This fact, especially during the initial phase of biomass based district heatings, leads to very low loads. As a consequence a low heat demand results in low turnover in heat sales. For heat-led systems this leads to a limitation of the electricity feed-in. In most projects the electric sales are the significantly more valuable part of the

business. In fact many suppliers consider their main business being electricity production, the resulting heat is a by-product, some would even say “waste heat” (while “wasted heat” is more appropriate). As a comparable basis for ORC prices, here only the module excluding all infrastructural or constructional measures are taken. The following Figure 1.13 gives an impression of the distribution of various system sizes, manufacturers and their prices. In Figure 1.14 the distribution of investment costs for units of Pratt& Whitney is depicted.

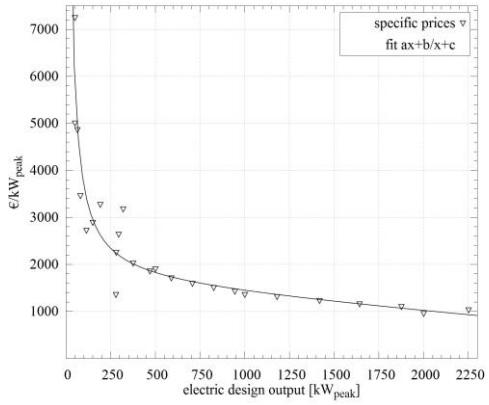

Figure 1.13: specific prices of various ORC modules (year 2012)[3–5]

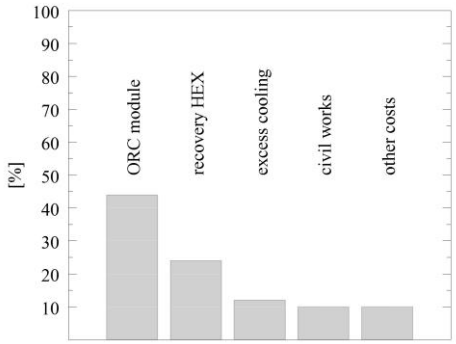

Figure 1.14: investment cost distribution [6]

1.5.2 Biomass prices

Table 1.3: regional German prices for wood chips according to moisture content (WG)[35]

-	-	LHV	increase	end energy
moisture class	e/t	e/MWh	2012-2013	e/MWh
WG 35 average	97.39	31.34	3.18%	25.072
WG 35 north	110.13	35.44	10.42%	28.352
WG 35 south	93.96	30.24	1.90%	24.192
WG 20 average	144.17	36.22	7.86%	28.976
WG 20 north	149.43	37.54	8.61%	30.032
WG 20 south	142.95	35.91	8.23%	28.728

Responding to the increasing demand of biomass fuels over the last ten years, the market prices adapted accordingly. For all types of wood based fuel, such as chips, logs, pellets and saw dust the market competition became more intensive. Based on the principle of sustainable cultivation the growth rates of biomass harvest are

strictly limited. Availability and price on the German market depend on the quality as well as the local situation. Therefore, northern and southern Germany have different biomass price indices. Beside the regional differences biomass has a seasonal variation, in quality as well as in availability and price. During the winter mainly stem wood is harvested and processed. During the summer period, landscape preservation residues are processed as well. In terms of thermal conversion, the quality of the latter tends to be worse. Especially the high foliage fraction can cause problems. High ash contents cause poor combustion and heating values and unfavourable exhaust gas values. Taking a look at the biomass statistic of this case study presented in Table 1.5, the heating value (LHV) of the material being processed is very poor. For the year 2012 the costs for fuel were fixed by contract to 17e per MWh of thermal energy in the heat transfer cycle. In the last column of Table 1.3 the prices are compared assuming an average process efficiency from fuel energy to useful heat of 80%. Regarding the minor quality of the fuel the price is appropriate.

1.5.3 Costs of cycle fluid

The average price of Octamethyltrisiloxane (MDM) has increased over the last years. In 2006 it was 15e per litre, in 2008 19e per litre and in 2012 and 2013 it rose to 22e per litre [SWE]. The entire cycle contains approximately 6000 litres. With regard to the experience in the case study, replacing 15% of loss per year has a remarkable influence on the running costs. Besides the direct primary costs, entailed costs for fluid quality management have to be considered. In general, the point of fluid ageing and the resulting cycle fluid treatment is often neglected in ORC applications [36]. The comparison with steam application plays a big role here. However, fluid quality management becomes a necessity with an increasing unit size and according filling volume. In technical applications a certain minimum leakage rate is unavoidable. Even if the feasibility of co-generation plant is based on incentives, such unexpected costs are fatal. Besides the loss through leakages in a system, contamination of cycle fluid is a critical point as well. For instance, the replacement of half of the working fluid filling can be necessary in the event of a lubricant leakage. The most contaminated part of the fluid is replaced by pure fluid. In this way additional costs are generated by the quality management of the cycle fluid. In order to re-use contaminated fluid high-boilers and low-boilers have to be removed. Low-boilers are contaminations in the working fluid that

evaporate at a temperature lower than the saturation temperature of the pure working fluid. High-boilers are still liquid when the main working fluid is fully evaporated. While low-boilers can be removed comparably easy and in a short while, high-boilers demand more effort. Slight heating under vacuum for a few minutes can remove most of the low-boilers (gases and short chain organics). In order to separate the high boilers, the MDM itself has to be extracted by evaporation. Running this process under atmospheric pressure takes a boiling temperature of more than 152 °C. For a 209l barrel this procedure takes almost 24h. The heat of vaporization at atmospheric pressure is 234kJ/kg. Therefore, a minimum of 32MJ of energy have to be "invested" for each barrel. If the recycling is not provided by an external supplier, the required apparatuses have to be installed on site. It must be remarked that the distillation of Siloxanes in contact with atmospheric oxygen can lead to unwanted cracking reactions [37]. Further information on this topic can be found in Section 1.6.5.

1.5.4 Personnel and administrative costs

Many authors claim the low personnel costs to be the major advantage of an ORC application [15]. This usually happens due to an over-simplification of the technology and the processes in a biomass facility. The main point for low personnel cost is unattended operation [38]. In steam applications a full automation is not possible as the attendance of a boiler engineer is required (according to boiler code). In ORC facilities this engineer is not required by law. However, this does not mean that the necessary maintenance works are less. In contrary due to the inhomogeneity of the fuel and the complexity of the process the observation of an experienced engineer or mechanic is even more required. A further point are administrative tasks such as quality control and fuel billing. With more competition in the fuel market stricter controls of the delivered biomass are unavoidable. In the case study described in Section 3 two persons are running the power plant.

1.6 Topologies of ORC in different application

There are various categories of ORCs. For each application purpose special variations have established in the market. According to the main degrees of freedom such as size and temperature levels, cycle layout and configuration can

differ a lot. In general, the flexibility of ORC concepts is larger than in other applications, as this technology combines numerous variations of cycle fluids, cycle layouts, heat sources and heat exchanger types.

1.6.1 Temperature ranges

Today's ORC market can be divided into three main fields of application: low, medium and high temperature applications. The low temperature field with temperature levels from 80 °C to 150 °C is dominated by geothermal heat sources and in some cases waste heat recovery. In the medium range the waste heat recovery is dominating. Up to 250 °C of source temperature various industrial, chemical and flue gas treatment processes deliver the heat for a bottoming cycle[1]. The high temperature systems, with source temperatures of 250 °C to 350 °C, are mainly based on biomass conversion. Above the three before mentioned temperature ranges steam cycles are well established.

1.6.2 Cycle scale

In order to categorize cycle type and scales within this work the following nomenclature will be used:

- Micro: less than 10kW$_{el}$
- Small: less than 100kW$_{el}$
- Medium: up to 500kW$_{el}$
- Large: 500kW$_{el}$ to 2.5MW$_{el}$

In order to classify ORC technology with respect to other energy conversion technologies, the two following Figures 1.15 and 1.16 depict the power range and the achievable efficiencies.

[1] Among combined cycles the one with the lowest temperature level

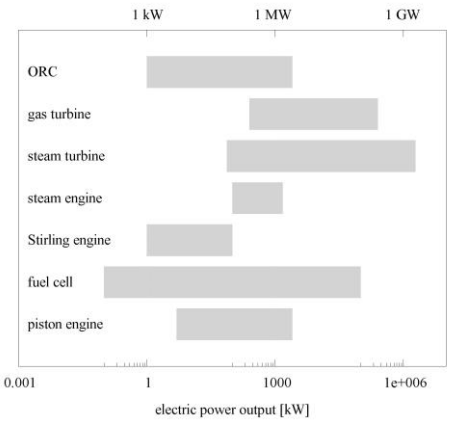

Figure 1.15: output power range of various conversion technologies

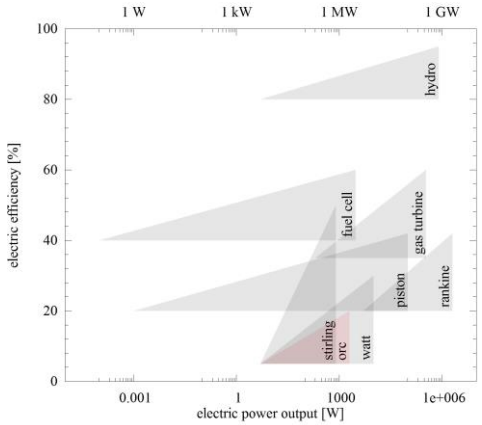

Figure 1.16: efficiencies of various conversion technologies

1.6.3 Cycle layouts

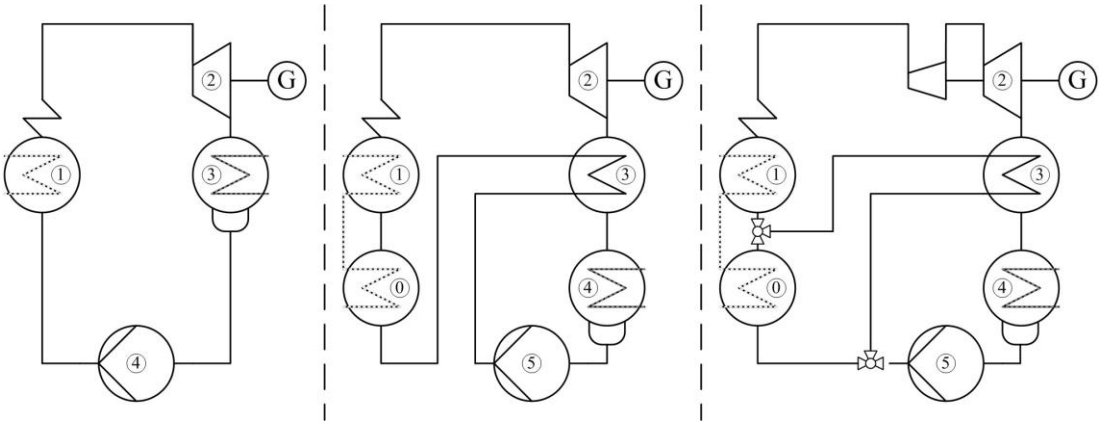

Figure 1.17: ORC layouts: simple, recuperated, split system with two-stage turbine

Due to the large number of applications and possible working fluids in an ORC, there are different cycle layout configurations. Each of these configurations may be favourable for its very purpose. The basic process taking place, can be described as follows:

- The heat source or topping cycle delivers heat into the ORC. Common heat sources are hot flue gas (direct heating) or a heat carrier (indirect heating). For the latter case pressurized water (low temperature source) or special thermal oils (high temperature source) can be used.

- The cooling cycle (sink) usually consists of pressurized water (district heating). It may contain a heat rejection unit and/or a heat storage tank. In some cases, where the temperature level is too low for further use (for instance geothermal cycle) the entire heat can be rejected with fan coolers.

- The liquid fluid is pressurized by a pump or compressor (quasi-adiabatic, polytropic compression). The temperature level of this sink depends on the type of application. In most cases this temperature level is between 30 °C and 90 °C.

- The pressurized liquid is heated, evaporated and super-heated to a state where the vapour is suitable for the expander. In case of a turbine this state is dry (single-phase vapour). In case of a volumetric expander it may be dry or wet (two-phase). The heating may occur in a single apparatus (evaporator 1 in Figure 1.17) or in multiple heat exchangers (recuperator, pre-heater, re-heater, evaporator) as depicted in the middle of Figure 1.17.

- In the next step the pressurized vapour is undergoing a poly-tropic expansion. This can takes place in a single or multi-stage (right scheme in Figure 1.17) expander.
- The vapour at the outlet of the expander is dry or wet and has to be cooled, condensed and sub-cooled in the next step. This can be done with a single heat (left scheme), a or with the combination of a recuperator and a condenser (middle and right scheme).
- Before the sub-cooled condensate is lead to the pump it is collected in a reservoir which is situated at bottom of the condenser unit.
- Auxiliary units such as filters, bypasses and start-up heaters are not shown in the above schemes for the reason of simplification.

Taking a look at the most simple layout (left) in Figure 1.17 a single loop with combined heating and evaporation and simple condenser may come to use. This configuration is robust, economic and compact. One would choose such a layout in cases with low expansion coefficients and small temperature differences between heat sink and heat source. Although this configuration has no recuperating unit it can be the most efficient design for isentropic or non-retrograde fluids or partial evaporation (wet evaporation). This would be the case in a low temperature application with a volumetric expander and methanol or ethanol as a working fluid. Depending on the fluid type it can be useful to design a lean cycle without recuperation, even with turbine expanders. Kaikko et al. have conducted a study on this issue [39]. The second layout in Figure 1.17 (middle) is the classical arrangement of a medium or large-scale application with large temperature spreads on the source side and between sink and source. As a consequence the expansion factor of the expander is larger and the downstream state of the turbine would lay wide in the saturated regime. Condensing directly from this state would cause an immense generation of entropy. Recuperation is economic in such a case, because the higher investment (into large heat exchange surfaces) is justified by the higher mechanical respectively electrical efficiency. The last configuration extends the before described layout by a splitter. The mass flow is divided after passing the feed pump. By doing so, low temperature fluid is fed into the pre-heater which enables the system to recover heat from a low temperature source. At the same time internal recuperation is done using the remaining mass flow. Both mass flows are reunited before entering the

evaporator. Such a configuration is useful if a high and a low temperature heat source is available, or the furnace system is equipped with a flue gas condensing unit.

1.6.4 Fluid types

Over many years engineers and scientists have tested new working fluids in order to improve generating cycles. The main objectives were efficiency, economy and operation improvement. They have been looking in all fields of chemistry to find better or more suitable fluids. In some cases, even metal vapours are used, for instance in Mercury-cycles. Another attempt for low temperature heat recovery is the Kalina-Cycle with its Ammonia-water mixture as a fluid. Since the time of the Naphtha Launches many classes of organic compounds came to use in ORCs. An overview of low-temperature working fluids, mainly for geothermal ORCs can be found in the work of Saleh et al. [26]. Heberle and Bru¨ggemann concentrated their fluid research on low-temperature second law efficiency of pentanes, butanes and some refrigerants [25]. Lai et al. [27] delivered an overview on different families of fluids (Siloxanes as well as alcanes and benzenes) and their potential for high-temperature applications (up to 300 ◦C). Further details in the field of working fluid research can be found in the publications of Drescher, Papadoupolous, Lakew, Chen, Wang, Yamada and Li. Table 1.4 shows families and classes of organics that are being used in ORCs:

Table 1.4: overview of some relevant ORC working fluids

class	name	CAS	MM	NBP	T_c	p_c	slope
-	-	x-x-x	[g/mol]	[◦C]	[◦C]	[bar]	- -/0/++
	Ammonia	7664-41-7	17.031	-33.327	132.25	113.33	- -
benzene	toluene	108-88-3	92.14	110.6	18.6	41.263	+
siloxanes	D4	541-05-9	296.62	175.35	313.35	13.32	++
	D5	556-67-2	370.77	210.9	346.00	11.60	++
	D6	541-02-6	444.92	244.96	372.63	9.61	++
	MD2M	141-62-8	310.69	194.36	326.25	12.27	++
	MD3M	141-63-9	384.84	229.87	355.21	9.45	++
	MD4M	107-52-8	458.99	260.75	380.05	8.77	++

	MDM	107-51-7	236.53	152.55	290.94	14.15	++
	MM	107-46-0	162.38	100.25	245.60	19.39	++
alcohols	ethanol	64-17-5	46.07	78.42	241.56	62.68	-
alkanes	n-butane	106-97-8	58.12	-0.49	151.98	37.96	+
	n-pentane	109-66-0	78.15	36.06	196.55	33.70	+
haloalkanes	R12	75-71-8	120.91	-29.752	111.97	41.36	0
HFC	R245fa	460-73-1	134.05	15.14	154.01	36.51	+
azetrope	SES36	-	178.42	36.7	175.04	29.17	+

The usage of chlorofluorocarbons (CFCs), hydrofluorocarbones (HFCs), hydrochlorofluorocarbons (HCFCs), and perfluorocarbons (PFCs) is critical in terms of ozone layer depletion and CO_2 equivalent. Their replacement fluids, the hydrofluoroethers (HFEs) are suitable for ORC applications as well.

1.6.4.1 Silicone oils as cycle fluid

In medium and large-scale ORC applications silicone oils play a large role. The term silicone oils is commonly used for all polymerized Siloxane chains. All compounds of this family are characterized by two Trimethylsilyl (TMS) groups at each end of the chain connected to each other by one or more Polydimethylsiloxy (PDMS) groups. Siloxanes have a wide range of application. PDMS are used as anti-foaming agent in medical treatment, as well as in food industry and cosmetics (lipstick, hairspray, deodorants, skin lotions). Due to their high electric resistivity Siloxanes are used in electronic industry. Their hydro-phobic character is used in water-repelling coatings for surfaces and fabrics. Many Siloxanes are classified as inflammable, however, they are more stable than their carbo-organic pendants. The bond energy of a siloxy group is significantly higher than the bond energy of a carbon chain [40]. The methyl-silane bonds in the TMS groups are more stable than the PDMS-PDMS connections, dissociation occurs here first. The properties that make Siloxanes interesting for power plant engineers are the relatively low flammability in combination with a low viscosity and a comparably good thermal conductivity. Therefore they can be used as heat transfer agents as well as working fluid in a cycle. Under normal operating conditions, without contaminants (oxygen, metals, acids) the commonly used silicone oils are long-term stable up to 300 °C, some even up to 400 °C.

1.6.4.2 Azeotropic mixtures

In science the discussion of fluid mixtures is en vogue. Potentials of mixtures are calculated and appropriate fluid couples are presented [29, 31]. Especially for low temperature sources overcoming the pinch point is very appealing. When the temperature profiles on two sides of a heat exchanger are parallel the entropy generation can be reduced and the useful temperature range in cycle can be increased. While parallel temperature profiles are impossible, a piecewise approximation can be achieved with mixtures. Chys et al. have shown with a simulation model for different classes of fluids, that efficiency improvements are possible. They state an improvement of 0.8%-points in efficiency from changing the MDM to a mixture of 80%/20% MDM-MM [29]. Chen et al. found an improvement of 10% and more for mixtures being used in super-critical low-temperature processes. However, one fact has to be kept in mind: the transport properties (thermal conductivity, viscosity) mostly become unfavourable for heat transport in mixtures, which then has to be compensated by larger transfer surfaces. This is expensive in investment and causes more pressure loss during operation. Furthermore the density can vary, this has to be respected in terms of the feed pump and the expanding unit. However, some authors, such as Qyewunmi et al. [30] have predicted that system component costs can be reduced with fluid mixture. Another very simple truth one has to bear in mind: these is no such thing as an absolutely pure fluid. This fact will be farther treated in the next sub-section.

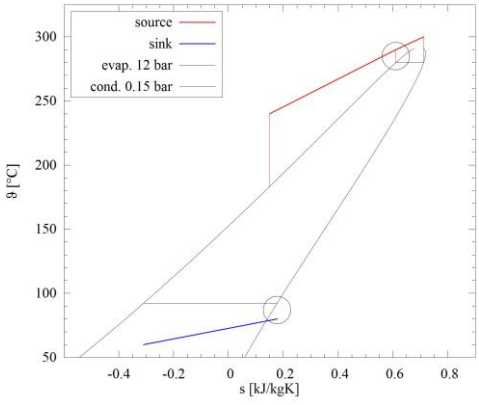

Figure 1.18: evaporation of pure MDM at 12bar

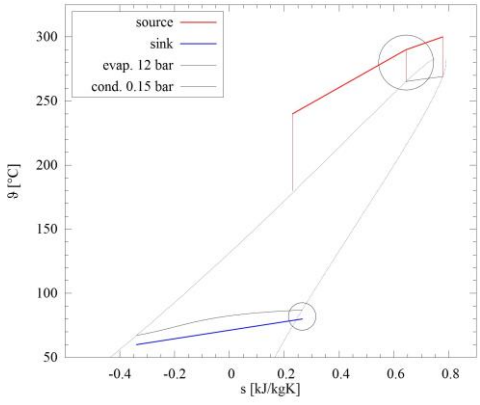

Figure 1.19: evaporation of 80%/20% MDM-MM mixture at 12bar

The two Figures 1.18 and 1.19 show the comparison of an ideal MDM process at

12bar evaporation level and 0.15bar condensation level with a 80%-20% mixture of MDM and MM under the same conditions. The conclusion that can be drawn from this simplistic example: the process can be enlarged by reducing the overall temperature difference between the heat source, the heat sink and the cycle.

1.6.5 Quality of the cycle fluid

Every power plant is designed according to the properties of the utilizes cycle fluid. Therefore, quality aspects as purity and stability are essential to reach the predicted performance, as well as keeping this performance over the life span of the facility. dd For steam cycles, de-aeration (removal of CO_2, N_2), desalination and acidity control (pH of more than 9) are the most important measures to keep the system clean and functional. In general all measures are meant to avoid corrosion and fouling. For ORC-systems corrosion is, with a few exceptions (Aluminium components and Ethanol as fluid), not of much interest. The chemical life span and purity of the cycle fluid, and thus its thermodynamical behaviour, are in the focus here. For the primary filling of the cycle a high purity of 98% or more are used. Dow Corning™claims a purity of more than 99% for OS-20 ®, R200(1cSt) ® respectively MDM [41]. However, over a longer period of operation the purity of the fluid decreases. Lubricants, inert gases and thermal oil can contaminate the system. If the turbine bearing lubrication is not provided by the cycle fluid, an additional lubricant is necessary. As the pressure in the lubrication system is higher than the pressure in the turbine stage (especially for impulse type engines), contamination is not avoidable. A similar scenario can be observed if leakages in the evaporator or pre-heater are not discovered in time. If a cold start is undertaken, the pressure in the Siloxane cycle is lower than the one in the source side. Under these conditions thermal oil is pressed into the cycle. Both agents have a similar density, therefore the thermal oil does not precipitate on the bottom of a vessel. As a consequence the feeding vapour going to the turbine may contain droplets, which may cause a turbine blade damage. The past operational experience of the project at hand has shown such problems. In order to prevent a loss of fluid and to save the environment from contamination, several attempts have been made to recycle the fluid. As a final result two system modifications have proven to be a real advancement: vacuum fluid recycling and fluid recycling from the bottom of the recuperator. For the first purpose the exhaust pipe of the

vacuum pump has been connected to a cold trap, condensing the remaining MDM from the gas mixture pumped from the condenser. If the reservoir is full the liquid is put back into the cycle. The second aggregate is a large vessel being placed on the flue gas economiser. By the heat of the economiser the lubricant MDM mixture is heated up while the MDM evaporates. In a second step the vapour is collected and condensed into replaceable barrels on the bottom of the system. With these measures the constant loss of cycle fluid could be drastically reduced. Where the annual loss before was approximately 10% to 15% nowadays the loss is almost negligible. Details on working fluid management can be found in the Chapter Results 8.2. While the loss of fluid is unpleasant and demands a certain investment into replacement fluid, degradation of the fluid is a far more serious problem. Several effects can trigger the decomposition of a cycle fluid:

- High temperatures, temperature hot spots (especially in evaporators)
- All kinds of strong oxidants [41]
- Oxygen: presence of oxygen increases decomposition significantly [37]
- Catalysts: some contaminates may act catalysing, such as Sulphur (flocculation from lubrication oil), or high-alloyed surfaces (Nickel-alloys)

Siloxy-bonds in Siloxanes are very strong (809kJ/mol), but compared to the Methyl-silane group it is the weaker link. The Methylsilane decomposition takes place above 400 °C. This means that all kinds of Siloxanes have a tendency to polymerise or oligomerise above 300 °C. The equilibrium of the polymerisation and the product configuration are depending on pressure and educt [1] configuration. During thermal decomposition formic acid may occur as product. In thermal conversion Siloxanes react to SiO_2, CO_2 and Hydrocarbon residues [41].

1.6.6 Connection to sink and source

The heat that is necessary to drive the cycle can be applied in various ways. In heat recovery applications of hot gas streams and industrial waste heat direct evaporators are used. If the purity and particle rate in the flue gas are appropriate hot gas evaporators can be used, without the danger of extensive abrasion or

[1] Educt, also known as reactant, is the precursor of a product in a chemical reaction [https://en.wikipedia.org/wiki/Educt]

fouling. In some cases direct heating is not possible due to local situation and a transfer cycle is needed. Especially if the production process that delivers the waste heat is well integrated the usage of a bottoming cycle has to done at the perimeter of the industrial area. Heat transfer cycle offer more versatility in operation. By-pass heat exchangers and heat storages are usually run with a transfer cycle (e.g. thermal oil, pressurised water). The downside of transfer cycles have to be mentioned at that point:

- Pressurised water has tight temperature levels, additionally if the transfer temperature exceeds 100 °C the pipes have to be certified according to boiler code. If the reason for using an ORC was avoidance of the 24/7 attendance, this is not an option.
- Thermal oil transfer cycles have shown unpleasant danger in the past. If the safety control unit is not operating properly, or all transfer pumps fail at the same time, spontaneous evaporations may happen. In some cases (as well in this case study) this lead to fires and explosions.
- The heat transfer with an additional cycle causes heat losses and additional parasitic energy demand.
- Revisions of the transfer cycle are a further point in the running costs of the facility. Cleaning, filtering and replacement of cycle fluid are costly.

The limits for thermal oil heat carriers are in a range of 250 °C to 400 °C [42]. Using, for instance, the thermal oil Therminol66 ® limits the temperature to a maximum of 355 °C. The manufacturer Solutia ® propagates this limit [42–44]. However, several years of operation of such cycles have shown, that a rigid fluid management is necessary to hold this limit. In the case study describe in the following chapter the temperature limit was set to 300 °C, following new regulations of the TÜV [1]. Essentially, the upper limit is determined by the heat transfer agent and the heat source. Using a biomass boiler limits the choice of the upper threshold. A boiler attached to a furnace deals with flue gas temperatures of about 950 °C. The size of heat transfer area and its convective heat transfer ability dominate the heat transfer from hot gas to transfer liquid. The U-value can reduce drastically in case of greater flocculation or coking than considered in the

[1] TÜV is a technical inspection authority for power plants in Germany

design safety margin. While the mass flow of the transfer agent remains almost constant a large temperature difference across the boiler wall has to be guaranteed. Increasing the hot gas temperature causes more exhaust losses and worse thermal conversion, including unfavourable pollutant values. Taking all these points together the feeding temperature of the thermal oil cycle is a practical constraint.

1.6.7 Operational mode

Depending on national legislation and the available temperature levels ORCs can be run in different modes: electricity-led or heat-led. For an optimal usage of resources as well as the decrease of CO_2 emissions combined heat and power is favourable. In this case a heat-led operation mode has to be chosen. However, the economic situation or the available temperature levels sometimes necessitate heat rejection. For instance, in geothermal applications it is not feasible to use the waste heat of the cycle. Temperatures below 30 °C to 40 °C are not usable for commercial applications (domestic water hygienic requirements to avoid Legionella Pnemophilia). Especially for small ORC-units under 100kW_{el} excess cooling to the ambient is the main heat rejection option.

1.6.8 Mobile applications

For sake of completeness the mobile sector has to mentioned as well in terms of ORC. Regulations on fleet emission, such as the EU introduced for automotive companies, have led to research in system efficiencies. Besides electric vehicles and hybrid technologies the common reciprocal engines are further developed to reach higher systems efficiencies. In individual traffic the ORC has not made its way into the market. Limited space and weight, the load characteristics and maintenance make it rather difficult to implement ORCs in cars. However, for road transport, the recovery of exhaust waste heat can reduce the system emissions. Long ranges and many operating hours can make recovery systems economic. In the naval transportation sector one should expect even better economic conditions. Large engines and an unlimited heat sink (sea water) are very appealing arguments, at least from a technical point of view. Unfortunately the financial view on this scenario reveals that the investment into such a high-technology drive is rather unattractive. The investor and the profiteer during operation of a ship are not the same party. Therefore there is no incentive to

construct a ship with higher overall efficiency. This scenario could change in future, if stricter regulations on fuel consumption (and fuel type) and environmental guidelines for container ships are mandatory on an international level.

1.6.9 Expanders

1.6.9.1 Turbines

Over several decades the range and abilities of turbines in industry have been enlarged. For super-critical Clausius-Rankine processes nowadays high alloyed steels with Rhodium and Nickel come to use. The demand for higher efficiencies comes along consequently with the increase of the life steam temperature. As a result the turbine materials have been steadily improved. However, the comparably low vapour temperatures of the feeding stream in ORC systems do not necessitate such high tensile strength. In general, turbine types can be categorised into two physical working principles: impulse and reaction.

- Impulse type: in one impulse stage a difference of pressure is entirely converted into acceleration of the flow. This happens in the nozzle section (stator or gate vane ring). In theory the absolute pressure in the blade section remains constant. In reality however, some slight changes in cross section may appear and cause small pressure fluctuations. In the blade section the gas flow is diverted. Meanwhile the mass flow applies a force on the blade causing a torque which results in rotation of the rotor.

- Reaction type: a gas flow crossing a reaction stage converts the applied pressure difference in both, stator and rotor. Reaction turbines are more sophisticated in design and the achievable stage efficiencies are higher in comparison to an impulse stage.

Besides the physical principle the flow configuration of the turbine plays an important role.

- Axial turbines are converting a flow velocity into a rotation while passing concentrically (or parallel in partial admission) through the engine's axis. The pressure difference between feed and drain is converted by the nozzle before the blades. Axial units are comparably simple constructions, blades are not necessarily warped. The forces in the system are well balanced, axial

forces are low. As the circumference of the rotor is larger than in radial system the rotational speeds are moderate. Therefore, many axial turbines are designed for direct synchronous operation, which saves gear losses. The simplicity of an axial turbine comes with the disadvantage of lower stage efficiencies.

- Radial turbines: radial turbines convert pressure differences by expanding while changing the main flow direction with respect to the axis. By employing the reaction principle, higher stage efficiencies can be achieved in comparison to axial units. The compact design leads to higher rotational frequencies in order to achieve the same inflow to rotation ratio. For grid feed-in operation a gear is necessary. The compactness of this principle makes it very suitable for micro or mobile applications [45]. The compactness and the sophisticated blade shaping result in higher engineering and construction costs.

1.6.9.2 Volumetric expanders

In the field of small-scale and micro-cycles a certain trend towards volumetric expanders can be seen. Taking a look at turn key prices of ORC modules in Figure 1.13 small cycles are suffering from the high basic engineering costs. Reducing these costs by using off-the-shelf (OTS) components, small cycles become more feasible. Being in the same range as power compressing units of air condition units or heat pumps can offer an alternative to newly developed expanders. Nevertheless, a certain amount of engineering is required to adapt a compressor unit to an ORC. Some companies have successfully done that in the past, such as BEP Europe.

- Scroll type or Lysholm type: widely used in air conditioning units. This engine type is comparably simple and therefore cheap. One disadvantage that comes with the principle is excessive wear at the sealing lips. It is required to adjust the sealing material and compressor tolerances to the properties of the fluid (acidity, solubility). Furthermore, the significantly higher operational temperatures have to be taken into account.

- Screw type: known as well from applications in the field of air conditioning, modified screw type compressors are being used as OR expanders. The working principle is very robust. Using it in reverse necessitates a

modification of the inlet gate valve. It is advantageous that the lubrication can be done from inside the cycle, which enables a hermetic and simple system. To achieve that, liquid working fluid has to be injected before the expander. This causes a lower specific enthalpy drop and increases the thermal efficiency of the cycle by means of reducing the electric efficiency. Ergo, a certain proportion of mass flow through the system (about 10%) has to be delivered without taking part in the conversion process. In some cases an adaptation of the lubrication flow to the load may be required.

- Roots type: often used as compressor for large two-stroke naval engines. The form of the rotor is somewhat simpler compared to the Lysholm type. The transport direction is perpendicular to the shaft. Based on the concept, thermal expansion can not be compensated as well as in a screw type engine. For that reason roots compressors are sensitive to particles in the flow, which can block the rotor. In comparison to scroll and screw types, roots engines are less costly in investment.

Two points have to be mentioned when volumetric expanders are used in ORC application:

- Taking OTS components from refrigeration systems requires adaptation to different operational conditions. Along with the lower temperature level in a refrigeration unit, the pressure ratios are lower as well. Useful expanders for ORC applications need to be modified accordingly.

- As volumetric expanders are designed for the before mentioned specific and comparably low pressure ratio, their part-load behaviour is comparably poor
[46].

1.6.9.3 Reciprocating engines

Piston engines are as well volumetric expanders, but here they deserve an own section. Coming from the automotive industry, modified Diesel- or Otto-engines can be used as a basis for an ORC expander. Again, the price of the components is a clear point for this engine type. Besides that, this engine type is interesting for special applications. When using low temperature differences between source and sink (e.g. around 100K) a piston expander can be used in an unrecuperated cycle. This layout keeps the investment costs low, as they are strongly depending

on heat transfer area. Additionally, this layout offers the possibility to evaporate the working fluid only partially and expand “wet vapour”. The wet vapour can reduce the necessary lubrication or even entirely replace the lubrication system. In contrary to impulse turbines, piston expanders are immune to droplet corrosion. The temperature range in which a common diesel engine is working is suitable for the use as expander. The pistons may even face lower wear compared to the explosion shocks by the ignition of fuel. A disadvantage of that technology may be the high noise level of the engine. Especially for micro CHP-units indoor operation (for instance boiler room in the cellar) may require special acoustic insulation.

1.7 Characteristics of biomass driven ORCs

The two degrees of freedom for a heat led ORC are: the heat source temperature level and heat sink cooling ability. Within these constraints, there is room for optimisation. Optimal operation for all load states during one heating season would be achieved by a combination of low super-heating in the evaporator, high feed vapour pressure, and low condensing pressure. As a consequence, the mass flow through the turbine reaches its maximum. To reach low condenser pressures, the sink temperature level must be kept as low as possible, while maintaining the capability to respond to a varying heat demand with smooth adaptation. These facts sound pretty trivial, but their mutual dependencies and dynamics make it rather complicated to give a simple advice for an optimisation.

1.7.1 Biomass as a fuel

The properties of untreated biomass fuels vary, in general, a lot more than industrially produced fuels. A biomass based power plant has to deal with seasonal fluctuations in quality. The main quality criteria for wood chips are: calorific value, water content, ash content, degree of granulation and contamination (for instance Sulphur and salt).

- Calorific value: the energy content of the material varies according to type or species. In general hardwood has a slightly higher LCV than softwood [47].

- Water content: fuel with a high water content converts more into latent heat while thermal conversion. The air demand for drying and burning the material causes more parasitic energy, see section Auxiliary power consumption. If the power plant has a flue gas condensation the largest part of the latent energy can be recovered before releasing the exhaust to the ambient.

- Ash content: with an increasing amount of ash, ergo non combustible material, the system has to process more fuel mass to achieve the same energy output. Meanwhile this causes more wear and tear on the transport systems and increases parasitic energy consumption in all sub-systems related with fuel and ash transport.

- Granulation: the size and granulation of the wood chips is essential for the transportation through the system and the chemical reactions while burning. Large pieces of wood can jam the system as well as dust can. A homogeneous distribution of size is important to assure a safe operation.

In Table 1.5 and Figure 1.20 the mean annual energy and ash content of the biomass fuel in the case study Scharnhauser Park are shown. The quality fluctuations, not only annually but as well from shipment to shipment, are a challenge for the operating engineers. In automatic operation (at night, during weekends) the system can not be adjusted. Therefore, a certain mismatch cannot be avoided.

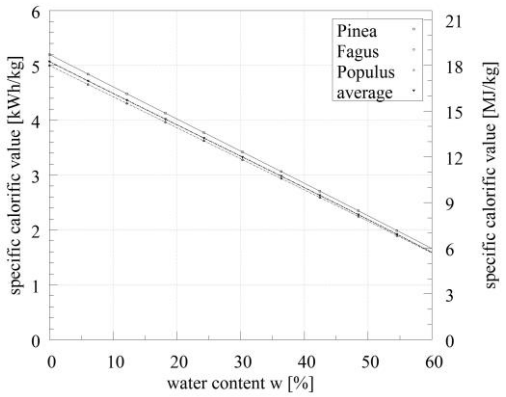

Figure 1.20: gravimetric LHV of various biomass species

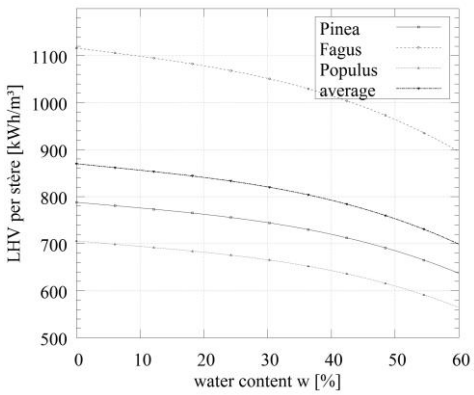

Figure 1.21: volumetric LHV of various biomass species

On average the energy content of of wood chips is given with values ranging from 0.679MWh/m³ to 1.022MWh/m³ [24]. In the case at hand the values are Table 1.5: measured fuel properties of the years 2004 to 2010

year	LCV	ash content
-	[MWh/m³]	[kg/kg]
2004	0.4788	0.93%
2005	0.6329	2.56%
2006	0.6359	11.41%
2007	0.4415	12.61%
2008	0.3638	9.39%
2009	0.6454	6.09%
2010	0.4721	8.12%
mean	0.5243	7.30%

rather low. The water content of the fuel being processed is 50% or more, the ash content at times reached 15%. To assess the fuel content the average consumption over the whole year can be compared with the energy output of the thermal system. For the combustion process an average degree of efficiency of 80% is assumed. Thus we receive energy contents as depicted in Table 1.5.

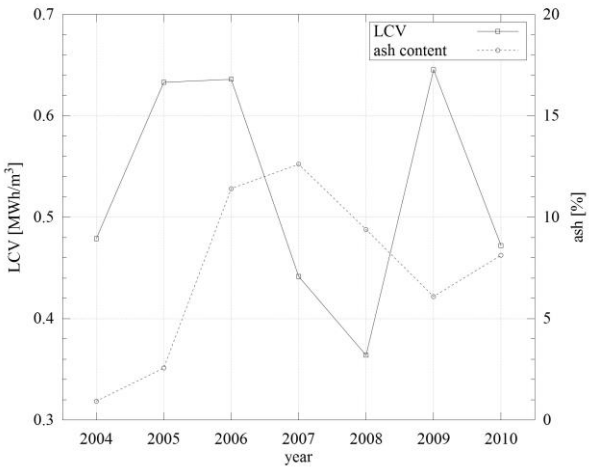

Figure 1.22: measured fuel properties of 2004 to 2010

1.8 Aim and motivation for this thesis

Observing the ORC market in Central Europe over several years, some major developments and trends could be seen. The deregulation of the energy market offered many opportunities for SMEs. Especially local suppliers began to enlarge their portfolios. Energy contracting, energy controlling and the operation of small, decentralised networks are such business operations. In this context many small suppliers, municipalities and companies in the timber industry decided to invest into ORC-based power stations fuelled by biomass. A lot of dynamics could be observed as well on the manufacturer side of the market. Small startups grew, some players failed and even big corporations (for instance: Bosch, Pratt&Whitney, GE, Mitsubishi) are nowadays involved in the ORC business. After years of subsidies for renewable energies, especially for systems with a high technological complexity, the economic situation has become harder. For existing power plants, especially in Germany and Austria, the increasing market prices for wood chips are a challenge. The operators of power plants that are connected to district heating systems have to fulfil their liabilities and supply customers with heat. While the heat prices in Germany are coupled to the gas prices, the wood chip prices are not regulated. For many suppliers this leads to an unprofitable operation of their CHPs. Taking a look at the large number of ORC units, built in the years 2004 to 2007 (Figure 1.8), that accomplished only half of their technical life span, the potential for improvement is huge. Taking a look at the following case study and the above introduction, the field of biomass based CHP offers great potential. In the case study examined in this thesis, an entire city quarter is supplied by an (almost) CO_2-neutral heat source. Meanwhile, the electric power demand of the city is, on average, covered by 50%. It seems as if this concept is a good solution, under the local conditions, to reduce CO_2-emissions. In a broader view, local biomass systems with their contribution to base load are the/one missing counter part for solar and wind energy. Especially the regional creation of value is one of the key aspects for a decentralized energy economy. Assuming a certain correlation in central Europe between space heating, domestic water and electricity demand, heat-led systems can cover at a great share of the these demands. Taking a look at the monitoring data of the years 2004 to 2013 there are multiple reasons to improve this power plant: the large proportion of excess cooling and the unpleasant operational behaviour. In addition, the personnel

costs, running cost and revision costs were higher than expected. Nevertheless,in the

ORC community, low maintenance and operating costs are one of the main proORC arguments. In the case of a biomass fuelled ORC-system considerable doubts have to be expressed. The way a power plant like the one at hand is designed, constructed and operated is never off the shelf. Therefore, the sub-systems have to be adjusted to each other, especially in terms of control systems. In many biomass power plant projects companies deliver a solitary work in their field. The interfaces to other crafts are either not sufficiently defined or necessary adjustments are just not done properly. Consequently, the power plant concept does not fully exploit its potential. Within this thesis, methods to analyse biomass power plants of this type shall be presented. A large amount of operational data has been measured and analysed in order to provide planners and engineers an access to validated models and comparative key figures. Many researchers contribute to the field of modelling. Often the models describe laboratory applications. When it comes to long-term experience of existing and market-relevant units, only little data is available. Quoilin, Lemort and Bru¨ggemann [38, 46, 48] have provided great simulations for heat-recovery, geothermal or micro applications. A holistic approach to biomass co-generation, including the districts heating and furnace behaviour in this power scale, is not available. The work hereinafter shall provide several modelling approaches for different questions concerning biomass fuelled ORC-units. Simple empirical modelling approaches as well as more complex thermal correlations and dynamical physical models. This thesis shall provide approaches for the improvement of a large number of already existing facilities. Along with theoretical approaches, the enhancement of day-to-day operation, practical improvements, working fluid management (and recycling) and design recommendations are as well in the focus of this work.

Chapter 2

Methodology

As a guide through this work this chapter describes the meta-methodology. In a second step, the according detailed methods for each analysis or modelling procedure can be found in the beginning of each modelling chapter. Models and their results have to be set into perspective to the questions that are described in the previous Section 1.8. The work procedure can be roughly described with the following points:

- Define the modelling scope according to the question.
- Define the model boundary and the according interfaces and connections.
- Data: define necessary data, set up metering hardware, meter, unify and post-process data. Refer to Chapter Data acquisition.
- Find the right modelling and simulation tools for each purpose. See in Chapter 5.2
- Find, integrate, adapt or develop property libraries for different tools and model types. See in Modelling of fluid properties and Modelling.
- Modelling: develop basic models, sub-component models, component models and finally system models (Modelling)
- Evaluation, calibration and validation: set up various test courses containing load cases of interest (Validation results).
- Develop relevant parametric studies of the entire ORC-unit and of relevant sub-systems.
- Evaluate parametric studies, compare performance (Simulation results and improved operation strategies).

- And finally: draw conclusions from the results (technically and economically), give design recommendations (Discussion of results - final conclusions).

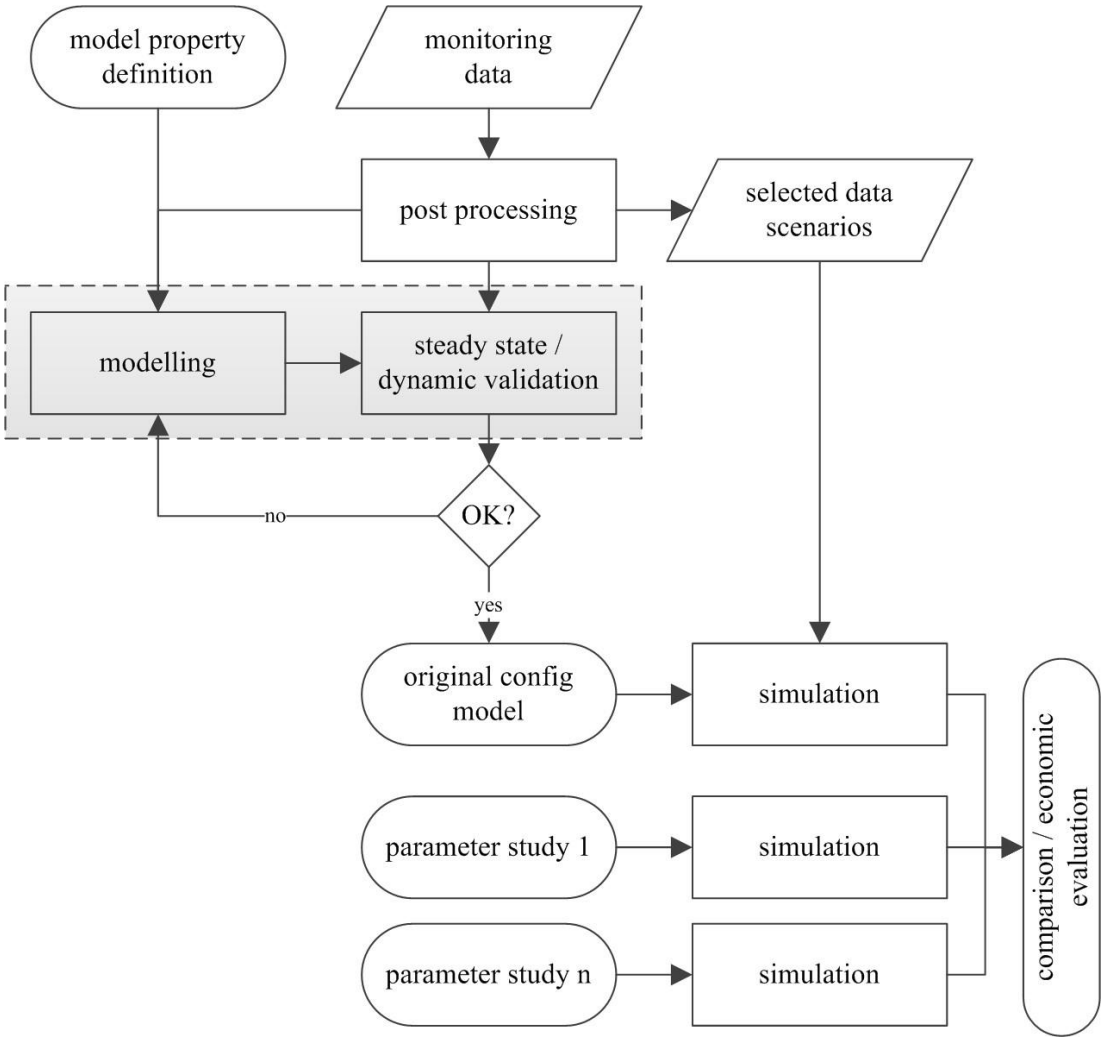

Figure 2.1: overall modelling process

In the above Figure 2.1 the entire modelling procedure is depicted. Although the steps seem trivial, the structure reveals what extend of results is expected of a model and what it is able to deliver. Sub-processes such as “modelling”, “calibration” or “validation” are explained in the course of this chapter.

2.1 Modelling scope

There are two main goals for this thesis: find the most relevant load scenarios for an existing system and test modifications on the system to predict future

scenarios. In order to find the most efficient way to operate the entire system, the behaviour of the system to reoccurring load situations has to be determined. Reoccurring situations would be for instance the step caused by many users in the morning taking a shower in a certain period of time. Based on given loads in the sink system (district heating) and defined supply data (furnace heat versus time) a model for appropriate representation of the real behaviour has to be found. For this purpose a purely empirical model is the method of choice as several years of monitored data exist. These data can provide a solid statistic basis. With a comparably small number of inputs and a low complexity, reliable prediction can be achieved. The above mentioned goals have to be elaborated under the consideration of non-thermodynamic effects as well. Wear on the system, as well as long term stability of the cycle fluid play a major role when it comes to the economy of the entire cycle. For instance the rather trivial measure to increase the source cycle temperature will increase the electric power output of the cycle, but it can lead to thermal decomposition of the working fluid. A further example: excessive use of the vacuum pump will certainly increase the condensing efficiency and result in higher pressure differences across the turbine. This short-term enhancement of the performance leads to an increased loss of cycle fluid. On the one hand side the replacement of working fluid is costly. On the other hand, a lower filling level of the cycle and the resulting super-heating leads to higher entropy generation in the low pressure section of the cycle. In some cases overheating may even result in a higher decomposition rate of the silicone oil. The optimisation of the cycle is a balancing act between all these constraints.

2.2 Model boundary and interfaces

The following Figure 2.2 depicts the modelling boundaries of the developed models. While the single units in the cycle (turbine, alternator, pump, HEXs, piping et cetera) are based on detailed physical, semi-physical or empirical correlations, the sink and source are given black boxes. Both black boxes are less of an active model, but only deliver data, in this case feed temperature and mass flow. The detailed behaviour of the furnace system and the district heating are not object of this work. The source control is assumed as an ideal source that delivered a feeding temperature chosen by the operator. The return temperature is set according to the specifications of the thermal oil boiler (around 240 °C). The mass flow modulation of the source systems acts according to the requested heat being

processed by the ORC. The “ORC physical” contains all components of the cycle and their parameters. It is embedded into the “control system” boundary. By separating these two systems parameter changes in the control system are easier.

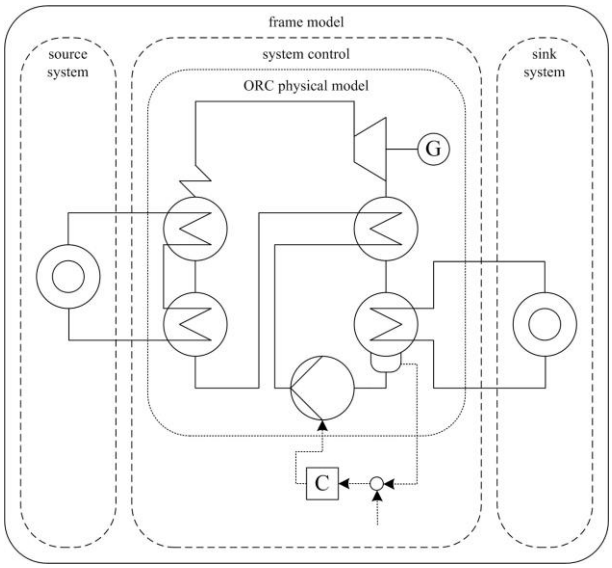

Figure 2.2: model boundaries for an ORC power plant including control, sink and source

2.3 Data acquisition and data post-processing

As a first step the before described model properties are defined (scope, boundary, et cetera). This choice influences the modelling process as well as the monitoring and data post-processing. Besides the set of required sensors, some operational scenarios may be of interest as well. Before the measured raw data can be used for validation and simulation, post-processing is required in many cases. Accordingly, the following measured have been undertaken:

- Concatenation of daily data sets to weekly and monthly data sets. By doing so, the operation of the plant can be set into a context and long-term load profiles (for instance weakly) of interest can be detected. Furthermore, interruptions and failed start-ups can be identified and filtered. In many cases systematic measuring errors can be detected (broken wire, leaking pressure gauge, processing error in the PLC).
- In order to use the data in calculation the formats (date, time) have to be adjusted. Such trivial changes as decimal separator and column separation character, are altered by using various scripts (ruby, VBA-macro).

- Data correction: for instance the state of each switch group for the heat rejection fans is noted during monitoring with a boolean “True” or “False”.

  For further usage these values are replaced by “1” respectively “0”. In order to increase the accuracy values obtained by a sensor in a Real format are first multiplied and then converted to Integers. Often this leads to inconsequential data formats or missing digits. In this data acquisition several examples are present (e.g. pressures, rotational frequency).

- The unification of time steps is a challenge, especially when various data sources have to be combined. In this case, the relevant data are recorded with respect to the same clock. However, for the inclusion of weather data, which are obtained by a separate system, this issue is relevant. Daylight saving time is accounted for in the database.

After consistent and unified data sets are created, they are used for the modelling and validation procedures. There are mainly two approaches for the separation of modelling and validation data sets. Alternating splitting of data into odd and even time steps is one way. For instance in automatic fitting tools (eurequa aka formulize) this approach is chosen [49]. When a predictive forward looking model is needed this approach may be elusive. The chance that consecutive data point (measured in a power plant) are lying near to each other is high. As a consequence, the validation might over-predict the statistical quality of the correlation. Therefore, modelling, calibration and validation data sets have been obtained from different days within a period of a week or month. Further detailed information on the modelling and validation are given in Subsection 2.5.2. At the end of the modelling process a satisfyingly validated partial model or component model results. The scenario predictions are done by various parameter studies that are based on the original model. The results of the simulation case studies can be found in Chapter 8.

2.4 Empirical modelling

2.4.1 Model description

Figure 2.3 depicts the concept of a simple black box model. The power plant model is represented by empirical correlations based on the statistics of monitored data.

In this simple version sink and source side of the power cycle receive a mass flow and a feed temperature as variable input. The corresponding outputs are generated power and the return temperatures of source and sink.

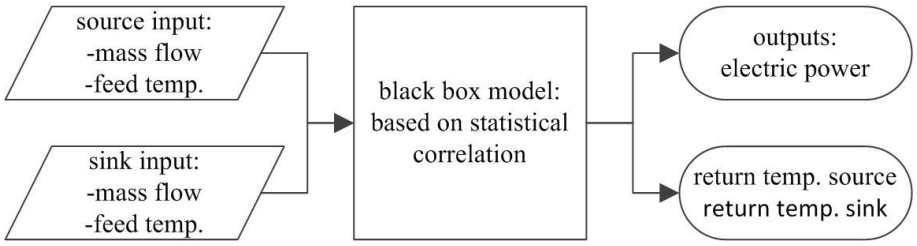

Figure 2.3: scheme of an empirical black box model

According to the purpose of the model, outputs and inputs to an empirical system may differ. Maintenance and diagnosis of an existing cycle was in the focus when the idea for this model came up. In most cases a company running a cycle has personnel observing the error messages of a power plant and engaging if a repair is required. For instance: wear level control of bearings and lubrication oil quality checks. Unfortunately, some operational states of an ORC-module may be well within the safety limits while at the same time the efficiency decreases. In cases of cycle fluid decomposition, fluid loss or fluid contamination the effects gradually increase, which makes it hard to discover them. Especially in systems where many variables influence the result a clear diagnosis is not trivial.

2.4.2 Empirical modelling process

An important part of modelling is the simplification of systems. No matter if a model is dynamic or steady-state. No matter if it is a Grey-Box or Black-Box, empirical correlations are often part of it. The following Figure 2.4 shows the modelling procedure that has been used for the empirical sub-models as well as for the Black-Box model (Chapter 5.1.1).

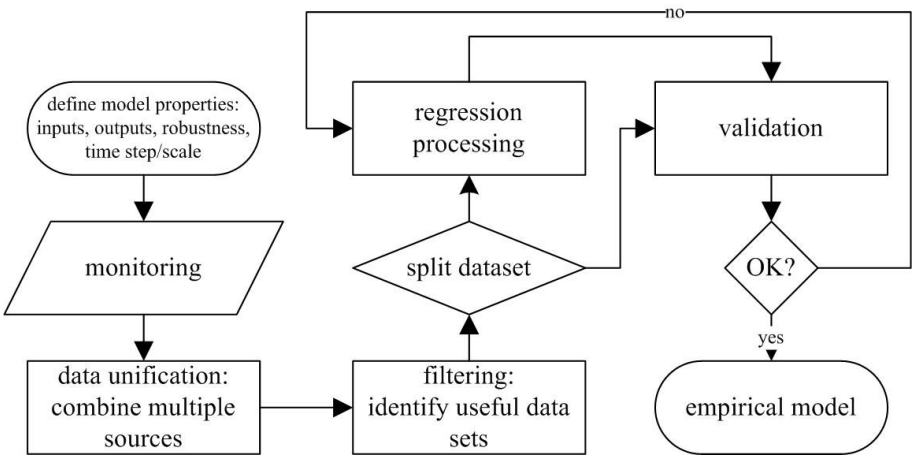

Figure 2.4: empirical modelling procedure

The Figure 2.4 depicts the procedure that is used for empirical modelling. It is applied for components models as well as for the empirical cycle model (as in Section 5). The sequence listed in detail:

- Data pre-processing: the monitored data are chosen via weekly plots. Interesting periods, for instance a day with a wide range of load changes, are chosen from a week with regular operation. Weeks with shut-downs or longer interruptions are not useful as the cycle need several days to recover after a full stop. Potentially useful days are then checked for data failures as described in Section 4.

- Useful daily data sets are processed via calculation scripts. For instance a Matlab (including a REFPROP function wrapper) routine calculates the states and transport properties for the heat transfer in a heat exchanger.

- The calculated properties are used as input for model sub-routines (e.g. heat transfer correlation). The sub-routines are fitted with a fitting algorithm (Matlab).

- Promising results for the parameters of the fitting procedure are forwarded to a validation routine. The validation can be achieved via two different strategies: alternating data splitting or en block validation. For the first option every even n (0 to 8640) is taken for fitting, every odd n (1 to 8439) is taken for validation. For the latter method one daily period is used for fitting and other days of the same week is used for validation. The first

method is faster but has a lower prediction quality. Therefore, in most cases the second method has been used.

- After several loops of iteration one receives a correlation with high prediction quality for the sub-routine. In a last step the correlation is embedded into the component model.

2.5 Dynamic physical modelling

2.5.1 Boundaries and interfaces

On the source side the inputs for a physical model (mass flow, feed temperature) can be defined either through measured data or a furnace model. The following parameters have to be defined to determine the input for power cycle:

- Source cycle fluid type, phase and composition: pressurized water, hot gas stream or thermal oil
- Density of source fluid
- Transport properties of source fluid: heat capacity, thermal conductivity, viscosity
- Geometric properties: heat transfer surface
- Flow configuration, surface shape
- Heat transfer model: according to geometric properties, shape and flow regime

2.5.2 Dynamic modelling process

The overall procedure from measured data and steady-state correlations to a complete cycle model is depicted in the following sketch in Figure 2.5:

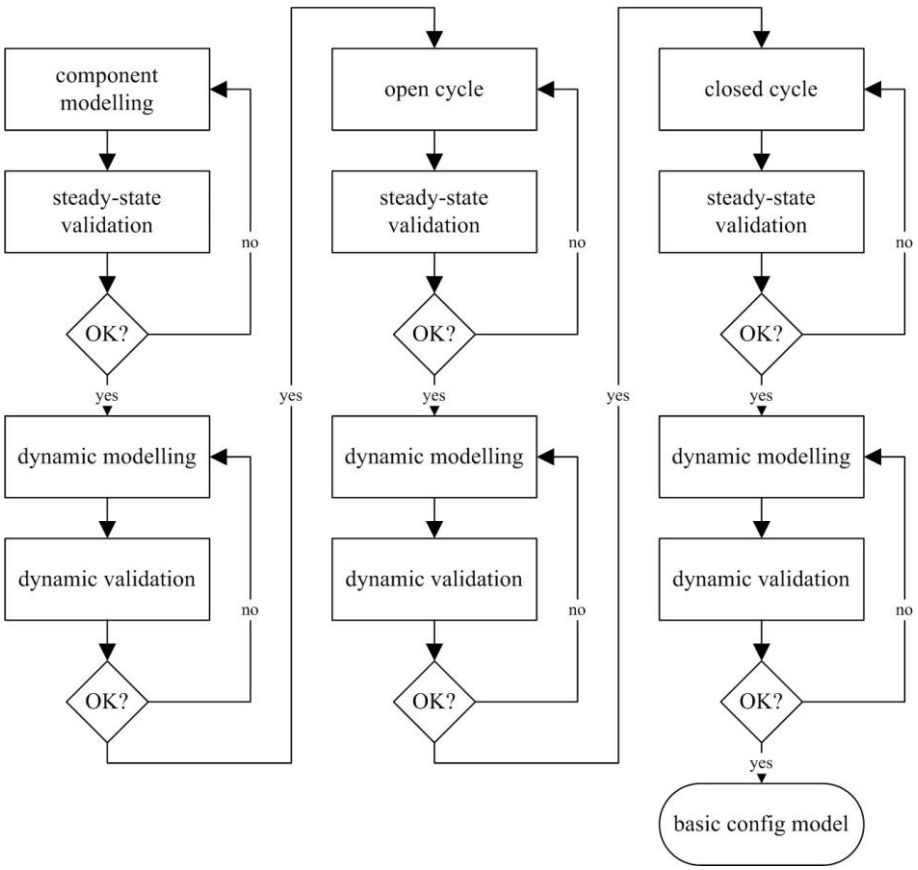

Figure 2.5: the modelling stages of dynamic modelling

The following Figure 2.6 shows two partial models of an open loop that are connected to a closed loop configuration in the last step:

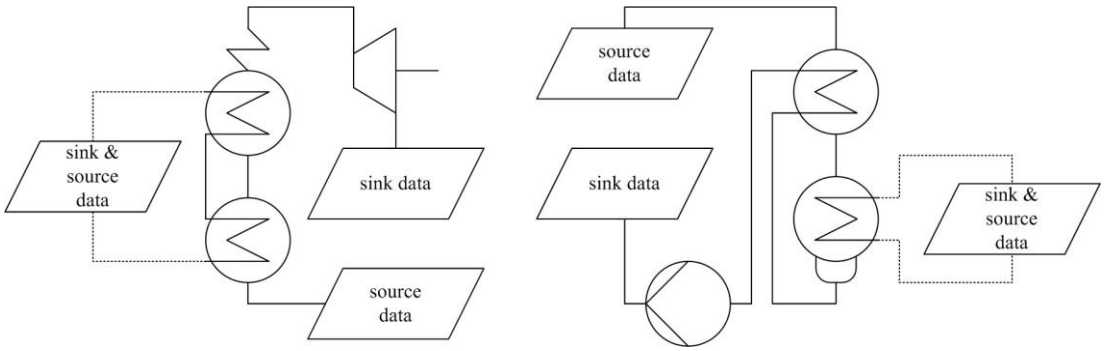

Figure 2.6: open loop partial models

This modelling procedure follows a bottom up strategy. The basis for all models is a single component model, with a steady-state approach. Measured data are used to find a correlation (for instance: single-phase heat transfer, two-phase heat transfer) and calibrated with measured mean data. The correlations are then validated with other data sets. In the next step, the correlations are implemented

in a dynamic component model (for instance the pre-heater). The dynamic model is tested versus mean values in order to evaluate its stability and deviation. This is done in an open loop, where sink and source are defined by measured data sets. If the result is satisfying, the same procedure is repeated with dynamic data. The response to the variation in the input data shows if the assumptions for the inertias are valid. At the end of the procedure the loop of the entire cycle model is closed. Again, the two steps of steady-state validation and dynamic validation are repeated.

2.6 Assessment criteria

2.6.1 Degrees of efficiency

Depending on the operation strategy and the feed-in tariffs different criteria for efficiency can be assessed. In order to have a clear definition to refer to, the efficiencies are explained hereinafter. First of all we remember the Carnot's definition of efficiency for a process converting heat into motion. For our case, under design conditions, we receive:

$$\eta_c = \frac{T_{source} - T_{sink}}{T_{source}} = \frac{573.15 - 333.15}{573.15} = 0.4187 \tag{2.1}$$

Under the given circumstances, the Carnot efficiency can be used as the reference for the exergetic efficiency. We assume a heat power cycle as reference and therefore neglect the chemical potential of the system. A more "down to earth" definition of the efficiency is the thermal efficiency. It defines how good thermal energy is transformed into motion or electricity. The expression "thermal" is a bit misleading in this context, therefore we rename it to "electric". For our system we receive:

$$\eta_{el,gr} = \frac{P_{el}}{\Phi_{in}} \tag{2.2}$$

which is the gross efficiency. Taking auxiliary power into account, the net thermal efficiency can be written as:

$$\eta_{el,nt} = \frac{P_{el} - \sum_i^n P_{i,aux}}{\Phi_{in}} \tag{2.3}$$

In order to judge the quality of a power plant process, the before introduced Carnot efficiency can be used as a reference. Consequently, we receive the gross exergy efficiency[1]:

$$\eta_{ex,gr} = \frac{\eta_{el,gr}}{\eta_c} \tag{2.4}$$

and finally the net exergy efficiency:

$$\eta_{ex,nt} = \frac{\eta_{el,nt}}{\eta_c} \tag{2.5}$$

As a key figure for the comparison of various CHP systems the heat-to-power ratio can be used. It does not necessarily say something about the quality of the conversion process (source or fuel energy is neglected), but it may help finding the right conversion application for a certain required end user heat-to-power profile.

$$HPR_{gr} = \frac{\Phi_{sink}}{P_{el}} \tag{2.6}$$

Accordingly to the net efficiency a net heat to power ratio can be defined:

$$HPR_{nt} = \frac{\Phi_{sink}}{P_{el} - \sum_i^n P_{i,aux}} \tag{2.7}$$

Depending on the constraints set by the feed-in tariff and the legislation of a location, the according criterion of a system has to be optimized. In the case at hand the power-to-heat ratio is not relevant, as the electric grid is not an island and the power generation is heat-led. The heat being fed into the ORC-system, can be seen as a simplified fuel equivalent with its according market price. Thus, the electric gross efficiency is the criterion to optimise the ORC-system for. For sake of completeness, we take a look at the total efficiency of the entire power plant concept. From the fuel production, transportation, conversion and distribution to the end user:

$$\eta_{el,total} = \eta_{fuel} \times \eta_{furn} \times \eta_{TO,loss} \times \eta_{el,nt} \times \eta_{grid,loss} \tag{2.8}$$

$$\eta_{th,total} = \eta_{fuel} \times \eta_{furn} \times \eta_{to,loss} \times (1 - \eta_{el,nt}) \times \eta_{DH,loss} \tag{2.9}$$

[1] This definition of the exergy or exergetic efficiency is only valid for the comparison of heat to power cycles. It is not valid for processes including chemical reactions

As all the above degrees of efficiency are just a snapshot for a certain moment and load state, a more meaningful criterion for economical evaluation is necessary. Based on the electric gross efficiency one can derive the annual electric efficiency[1]:

$$\bar{\eta}_{el,gr} = \frac{W_{el}}{Q_{in}} = \frac{\int_0^{8760} P_{el}(t)dt}{\int_0^{8760} \Phi_{in}(t)dt} \tag{2.10}$$

Finally, we take a look at the weighted degree of efficiency. In order to compare the annual performance of a system and its potential improvement or degradation, the single load ranges can be weighted (using X˙n) according to their temporal relevance. For each load state, for instance from 0.0 to 1.2 (with intervals of 0.1 or 0.2) this method can be applied. The load states can be derived from Figure 3.9 in Section 3.2.2):

$$\bar{\eta}_{el,an} = \bar{\eta}_{el,gr,1} \times X_1 + ...\bar{\eta}_{el,gr,n} \times X_n = \sum_{i=1}^{n} \bar{\eta}_{el,gr,i} \times X_i \tag{2.11}$$

The above efficiency represents the total improvement of a system on a yearly basis. It reveals the effect of an improvement of single load states on the overall economical performance. The effort to calculate this criterion is very high compared to determination of the mean annual electric efficiency in Equation 2.10.

2.6.2 Economic criteria

Improvements and optimisations on a technical system, finally have to show their economical impact. The economical analysis of this power plant case study is based on the following assumptions:

- The demand of wood chips for the furnace is covered by one contractor. Fortunately, the contract determines that the billing of the fuel is done via the heat meter of the thermal oil system. Therefore, losses in the heat transfer system can be neglected. The furnace conversion efficiency and the LHV of the fuel are irrelevant (for the fuel costs).

[1] Basically the reciprocal of the SEER

- The feed-in tariff for the generated electricity is fixed to 225e per MWh_{el} for the entire power range. There is no degradation as in the feed-in tariff of photovoltaic systems.
- Heat going into the district heating has an average loss of 11% (average measured over the observed years) and the end user pays 55e per MWh_{th}.
- Based on the data of the years 2007 to 2014, the auxiliary electric demand is set to an average of 2.5% across the whole load range. This value refers to the thermal input of the ORC. Including VAT, the price for this electricity (109.85e per MWh_{el}) is the long-term mean of seven years.

Excluding the personnel costs, administrative costs and debt service for the entire power plant, the specific EBIT[1] for the OR-system can be drawn as follows:

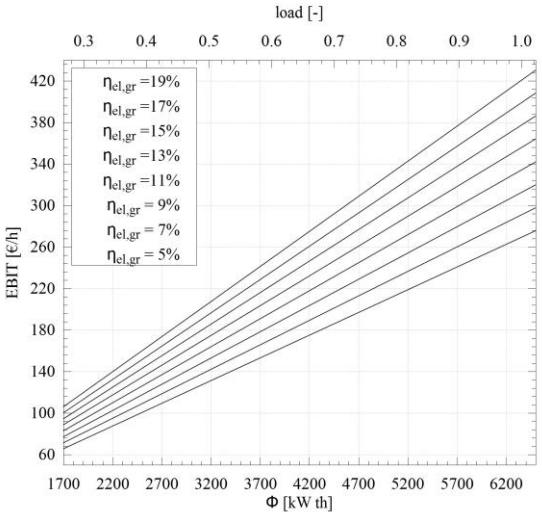

Figure 2.7: specific EBIT for various electric gross efficiencies of the ORC-module vs. thermal input

In Figure 2.7 each line represents a certain degree of electric gross efficiency. Based on the thermal input to the ORC-system the according specific EBIT can be taken from the graph.

[1] Earnings before interests and tax

Chapter 3

The case study Scharnhauser Park

From 2006 up to the year 2013 the quarter “Scharnhauser Park” a part of the city of Ostfildern, near Stuttgart has been scientifically observed. In various European and national research projects the development of this quarter has been accompanied, monitored and assessed. Until 2011 the location was part of the CONCERTO programme. Within the project POLYCITY all aspects of sustainable city development have been elaborated [7]. Scharnhauser park at that time was one of the three project sites. From 2010 to 2013 the data monitoring was supported by the ERA-SME project RecoORC. In the following section all relevant facets of the energy supply system are described.

3.1 Project site

In the early 1990s the energy supply system for Scharnhauser Park had been modernised on behalf of the US Government. The hard coal fired furnaces were replaced by gas boilers (11 MW and 5 MW) and the energy supply company Stadtwerke Esslingen (SWE) have been charged with the operation of the boilers. In 1993 SWE took over the energy systems of Nellingen Barracks from the US Military Forces; at that time the network was supplied with steam. The former infrastructure has been taken out of operation and was replaced by a new hot water network. The structure of the heating network was coordinated with the development plan of the road system in this area. The district heating consists of three major loops connecting several side branches with each other. The topology is not homogeneous and therefore various pump and valve stations in the network are necessary to maintain the operation. The following Figure 3.1 shows a 3Ddrawing of the biomass power plant. The storage and the furnace are shown in the front. The building in the background is the turbine house, where the gas boilers are situated as well. The scheme shows the biomass delivery zone (1), furnace (2), thermal oil boiler (3), economizer (4) and exhaust treatment (5).

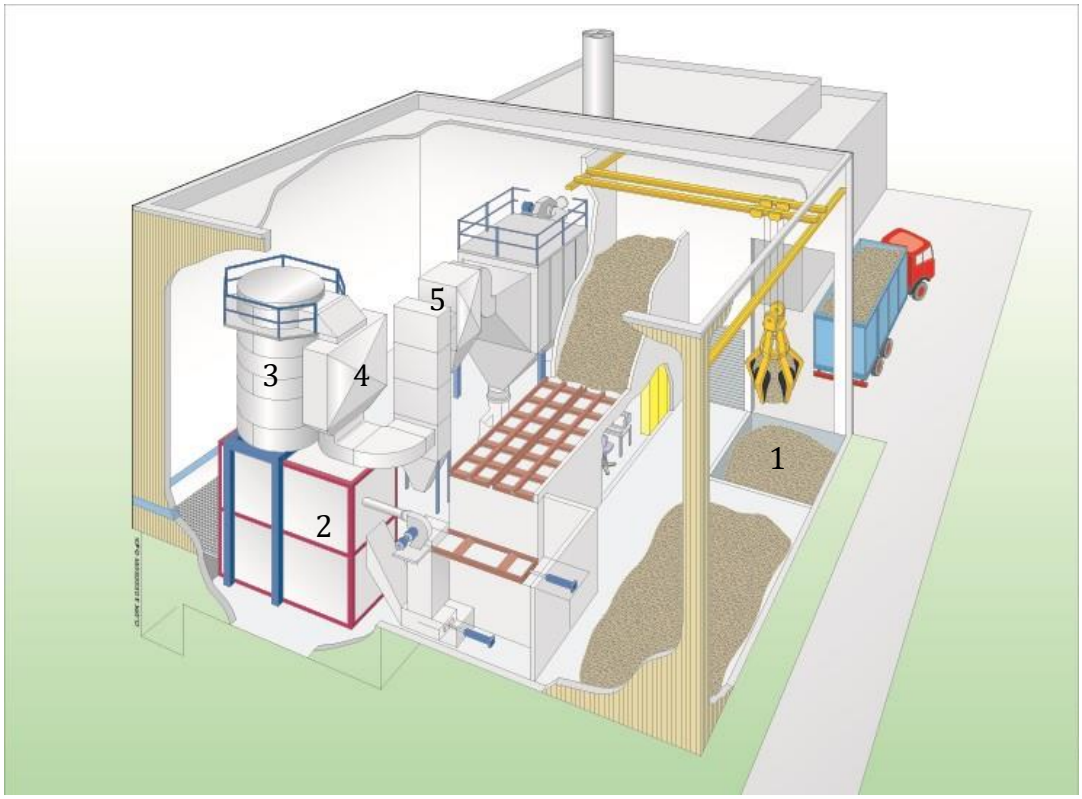

Figure 3.1: 3D-section through power plant [7] [courtesy SWE]

3.1.1 Location and climatic conditions

The Figure 3.2 depicts the climate conditions for the location of the case study. It shows the hourly temperature values of the year 2011. Furthermore, the long-term monthly means, minima and maxima are plotted. In Figure 3.3 the according heat demand for the local climate conditions is exemplarily depicted for three different years.

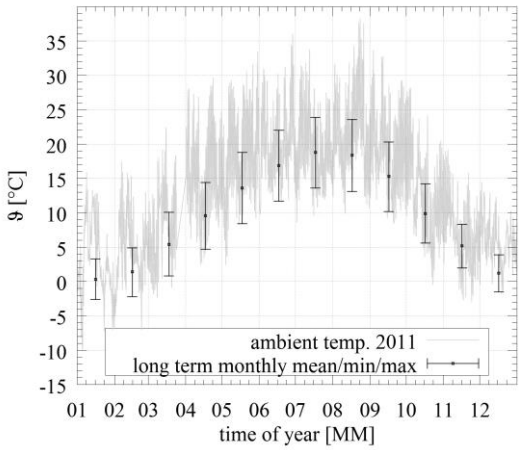

Figure 3.2: ambient temperature of year 2011

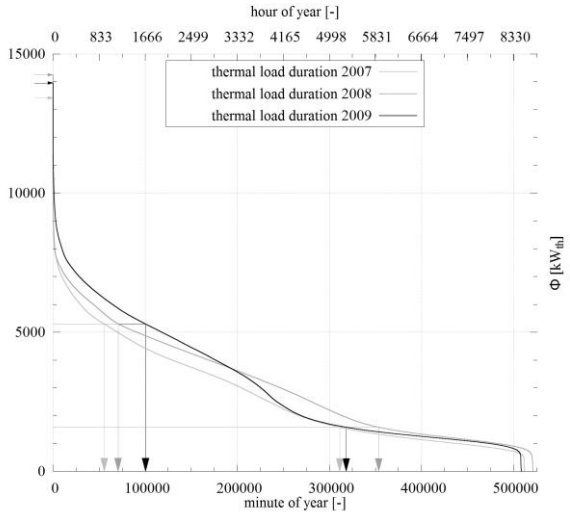

Figure 3.3: load durations of district heating heat rate of the years 2007-2009

The arrows in Figure 3.3 point out the maximum thermal output power of the ORC-unit. Thus, the full load hours, respectively minutes, can be derived from the intersection with the time axis. The arrows pointing to the ordinate mark the maximum power point of the single years. These basic analyses show, that in the first years of operation the system encountered a typical problem of many newly developed district heating systems: the sink demand is too low. The minimum load on the sink side, necessary to keep the ORC-system running (1.7MW$_{th}$), is below 5000 and 5800 hours per year. Consequently, the peak load systems have to cover the demand during 3000 to 4000 hours per year. While the load duration is a theoretical instrument, the real operating hours in co-generation mode are even less. During the summer period solely heat for domestic water is required. The revision periods of biomass fuelled systems are longer and less predictable compared to fossil fuel systems - in terms of extent and complexity. In comparison, large combustion engine CHPs have a fail prediction based on a wear measurement. The sheer number of motor CHP-units leads to more experience and a reliable statistical basis for such predictions. The number of parts and the complexity of classic combustion engines and a biomass furnace differ significantly. However, the 2000 hours of non-cogeneration mode due to low demand during the summer period are not that problematic when the revision takes place then.

3.1.2 General performance of the plant - key figures

Table 3.1 gives a short overview about the key figures of the facility. Under day-to-day operational conditions, these values may deviate. However, they give a rough impression about the energy flows of the system. The long-term monitoring provides more data, which are compared in the following chapters. Especially the observed auxiliary power consumption (Section 3.1.3) may be of interest for the design of such a type of power plants.

Table 3.1: design specifications of biomass plant

component	description	value	unit	reference
biomass furnace	thermal power	8000	kW	[manufacturer]
wood storage	capacity	1400	m_3	[manufacturer]
fuel consumption	design point	200	m^3/day	[manufacturer]
auxiliary power	electric	25	kWh_{el}/MWh_{th}	[manufacturer]
fuel consumption	average	43000	t/a	[SWE]
pri. energy saving	-	38000	MWh/a	[SWE]
CO_2-reduction	-	7000	t/a	[SWE]

Since the power plant has been taken into operation (year of 2004), the overall performance of the system was monitored. All heat-converting, respectively heattransferring sub-systems are equipped with ultra-sonic heat meters. They are used for real-time data acquisition as well as for monthly or annual balancing. The following Figure 3.4 depicts the overall thermal output to the district heating in comparison to the biomass based heat. To set this into scale, the degree days of the location and the population of the quarter are shown as well. The long-term mean of degree days (1970-2012) is 3761Kd. This means, that in the observed period of operation the climatic conditions were, with one exception in 2010, constantly warmer than expected. This means that this power plant, a heat-led type, has to work under warmer conditions than it has been designed for. For designers of such facilities this fact is very interesting. The relevant design and feasibility guide lines for CHP installations (for instance: DIN 18599, VDI 2067, VDI 3985 [50–52]) provide general information. Those are, up to now, not adapted to changing climate conditions.

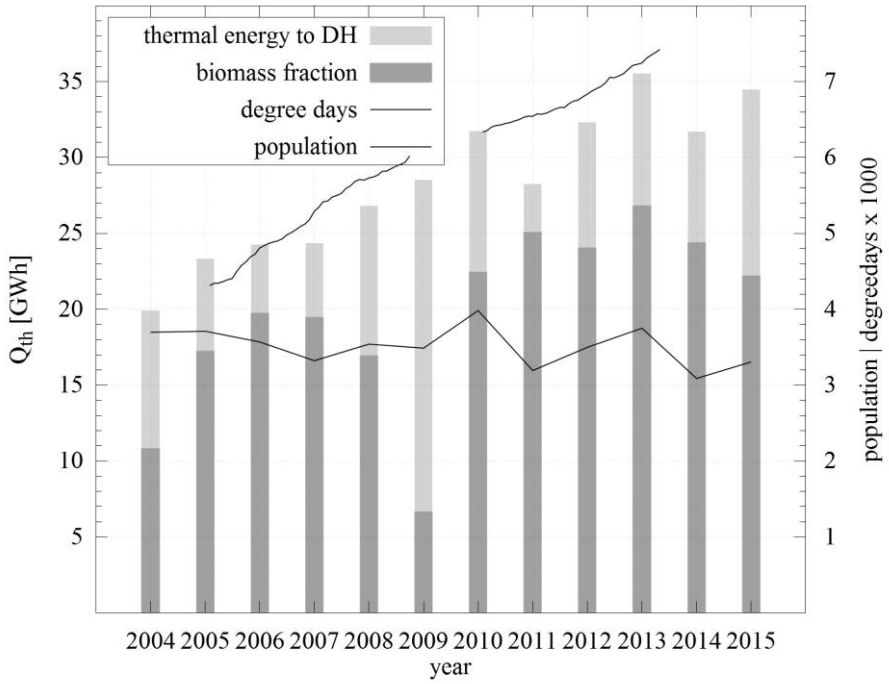

Figure 3.4: annual energy produced by biomass / delivered to district heating

3.1.3 Auxiliary power consumption

Auxiliary power consumption comprises the power consumption of all auxiliaries. At the CHP-plant Scharnhauser Park auxiliary energy is required to operate the following components of the system:

- Fuel-feeding system: conveyors, stoker, through chains, ash flaps
- Furnace fans: combustion air, exhaust fumes and exhaust gas recirculation
- Furnace cooling: grate cooling loops
- Thermal oil pumps, primary pumps and drainage respectively emergency pumps
- ORC-module: feed pump, vacuum pump, alternator cooling, alternator agitation, control system
- Heat rejection system, fans and pumps

- District heating network: circulation pumps for primary and secondary loop Due to the application of frequency converters to control the pumps operation the saving energy potential related to the optimisation of pumps operation is relatively low. There are some key points that influence the auxiliary energy demand in a power power plant as the system at hand. Fuel: besides many advantages biomass has its down sides as a fuel: heavily varying qualities are harder to handle in daily operation than gas or oil. The fuel composition regarding size, type of wood, ash content and water content influences the fuel feeding system and the combustion. Higher contents of water and ash demand more fuel to achieve the same output, hence the transportation energy for cranes, belts, and stokers rise accordingly. In this case the fuel has a higher density which results in even higher loads (and wear) for cranes. Along with a higher content of water, the primary air ventilators consume more power. The same happens with increasing ash contents for exhaust and recirculation ventilators. Excess cooling: in many facilities the operation strategy tries to maximise the electric output of the generator. Running a heat-led system means that excess heat has to be rejected to the ambient. During these periods the consumption for cooling pumps and fans adds on top of the auxiliary demand. Furthermore, many components of power plant need additional cooling when operating under summer conditions, for instance the alternator.

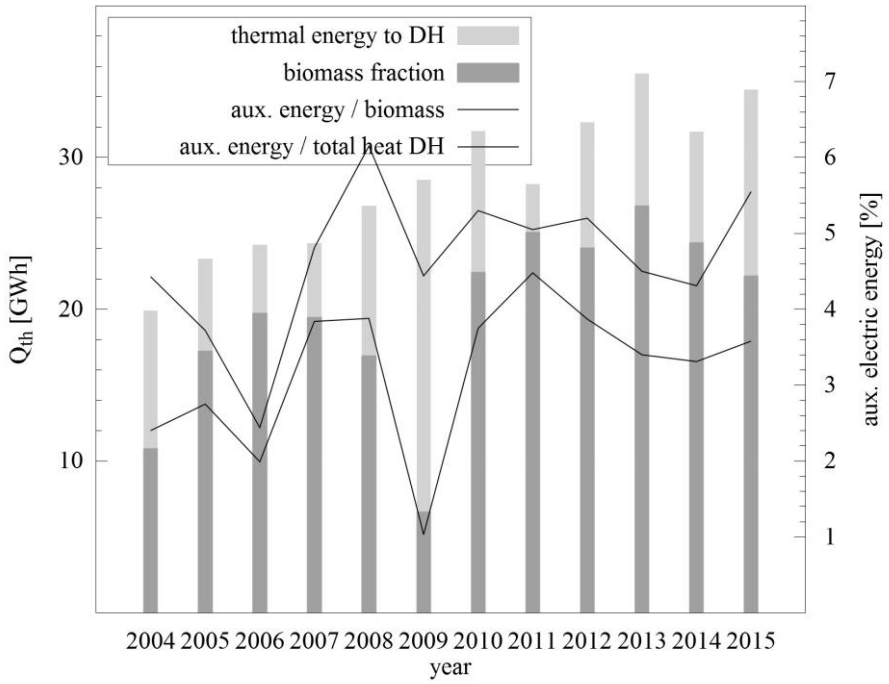

Figure 3.5: auxiliary power in correlation to converted heat (biomass and gas)
Table 3.2: auxiliary power consumption of the power plant system

item	P_{max}	emergency power	reference
-	[kW]	[-/x/opt][?]	-
biomass conversion	108.55	x	Table A.3
fuel and ash transportation	85.75	-	Table A.1
furnace cooling	2.20	x	Table A.6
thermal oil cycle	110.75	x	Table A.4
ORC	87.10	-	Table A.7
district heating (primary)	30.00	-	Table A.2
district heating (secondary)	5.50	-	Table A.2
heat rejection and others	-	-	-
total	429.85		

[?] always on / supplied during emergency power mode / optional

It must be noted that the above mentioned 5.5kW for the district heating are solely the secondary pumps for the condenser.

3.2 District heating network

The local district heating network in Scharnhauser Park is the backbone of the thermal energy supply. It supplies 557 customers (2009) with nominal heat rates of 10kW to 250kW. The network main pipes are 13.5km long, the overall length is 17.7km. As the city of Scharnhauser Park was not built from scratch the district heating system is heterogeneous. It consists of three closed rings and several small side branches. Several valve stations, located at nodes of the system, control the differential pressures to assure a reliable and equal distribution of the heat. As the topology of the network is rather complicated, the control system is not trivial. In total it contains 184.3m^3 of water. As a results the entire system has a thermal capacity of 774MJ/kg. If the systems heat supply is disrupted this capacity can deliver 4.3MWh before the the minimum threshold of 55 $^\circ$C is reached. A map of the quarter including the district heating pipes can be found in Figure 3.6. The power plant is on the very top centre of the map.

The water in the network is driven by three parallel circular pumps. Each of them can provide the necessary volume flow to cover the peak heat demand, if the temperature spread in the network is 20K. All three units are connected

Figure 3.6: map of the quarter including district heating [SWE]

to one frequency converter with a sequential control. If more than one pump is necessary, the first unit is set to 100% and the next one is regulated by the frequency converter. In terms of economy and redundancy this is a good operation mode. The pumps (KSB Etabloc GN 080-315) have an overall efficiency of around 75% over a range from 60% to 100% of load. Under nominal speed of 1470RPM, the power consumption of each pump ranges between 1.5kW_{el} and 10.5kW_{el}. As depicted in the Sankey chart in Figure 3.7, the heat into the district heating network can be categorized for three different purposes: private, commercial and network losses. During the year 2009 the amount of construction sites with heating demand was rather high (dehumidification). As this is included in the category of losses, it explains the high loss value of 16% in Figure 3.7. In the following years the network losses were in a range of 10% to 11%. In Table 3.3 the design specifications of the district heating system are concluded.

Table 3.3: design specifications of the district heating system

	item	value	unit
piping	pipe manufacturer	Isoplus, Logstor	[-]
	type	PJP, single ins.	[-]
	diameter	DN25 - DN300	[-]
	length main pipes	13.5	[km]
	total length	17.7	[km]
	volume	280	[m^3]
	connected customers	557	[-]
performance	annual work	35000	[MWh/a]
	max. load	16	[MW]
	mass flow	12 - 127	[kg/s]

	volume flow		43.5 - 460	[m³/h]
	network pumps	3 x 18.5 [		
	difference	0.7-1.1 [		
	feed		5-6	[bar]
	return		4-5	[bar]
	maintenance		3.5	[bar]
temperature	feed		70-90	[°C]
	return		55-65	[°C]
	mean difference		20-25	[K]

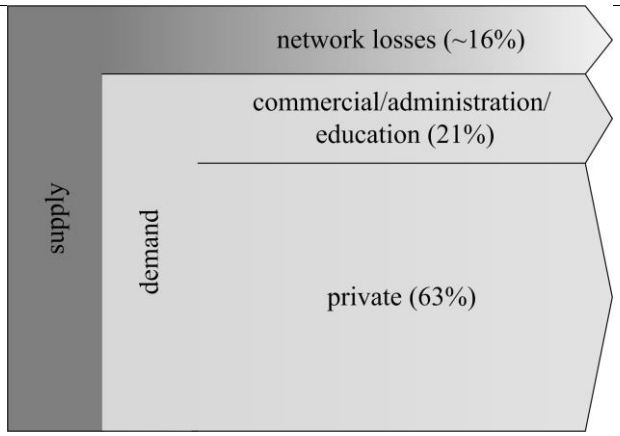

Figure 3.7: thermal energy flows of the district in 2009

3.2.1 District heating control

The district heating control is a multi-level system with manual and automatic control modes. The main system is based in the power plant. Here, the feed temperatures and the differential pressure control of the system are situated. In automatic mode, the feed temperature is defined as a function of the ambient temperature. Consequently, the return temperature is a result of the feed temperature, the demand and the mass flow. A temperature spread of 20K is regulated by adjusting the water mass flow via the main net pumps. As parameter of the automatic mode the heating curve gradient and off-set can be defined. Throughout the network many sub-systems are controlling the equal (or almost equal) distribution according to the demand in the side loops and branches. By

opening and closing the valves of the 566 transfer stations, each consumer in the network attempts to cover his demand.

3.2.2 Thermal demand

The power plant is the main source of power for the Scharnhauser Park. As there are no back-up systems the supplier has to provide heat to the customers at all times. Aiming on a low impact and feasible costs, a high proportion of biomass being processed is a major goal. However, due to foreseeable and unforeseeable incidences this is not always possible. The backup and peak-load gas boilers are taking over if the biomass system is out of order.

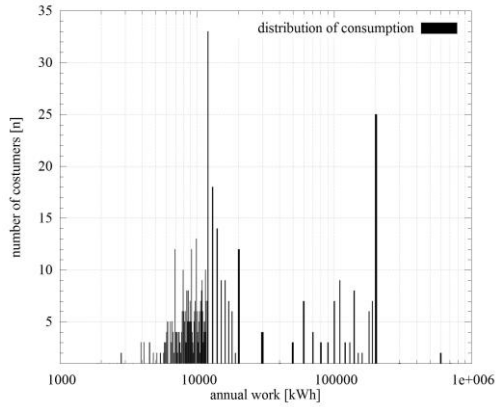

Figure 3.8: distribution of annual consumption of heat

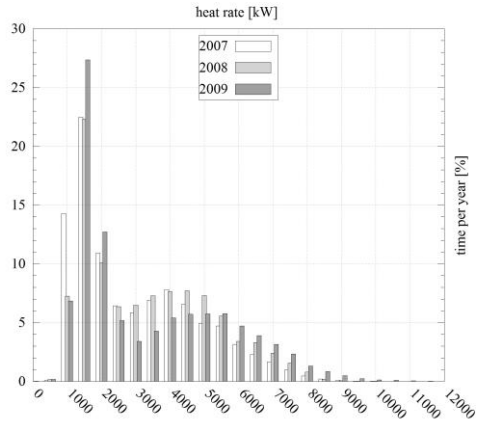

Figure 3.9: statistical distribution of thermal demand for three years

Figure 3.9 given an impression of the annual distribution of thermal demand over three years. One has to keep in mind, that the maximum design power at the ORC-unit's condenser is 5356kW$_{th}$ (see Figure 3.10). Assuming that the electric efficiency is not as high as designed, but the total efficiency remains stable this value may rise to 5500kW$_{th}$. The distribution shows two maxima: at 4500kW$_{th}$ and 1500kW$_{th}$. The lower maximum results from low energy consumption at night and low consumption during summer. Such load states can be only covered with the help of excess cooling. Even the second maximum is not optimal for this ORC-unit. A favourable load would be around 5300kW$_{th}$, the design value given by the manufacturer. With a look at the future development a larger overall demand could cause a deviation of the second maximum to higher values. As a further characterisation of the network the number of clients and their annual demand has to be taken into account. Figure 3.8 shows the statistical distribution

of annual consumption in classes. The majority of consumers are within a range of 6MWh and 11MWh. It can be assumed that these values represent the single houses, semi-detached and some multi-family homes.

3.3 Process description of the facility

The following sections will provide detailed descriptions of the energy conversion systems being used on the project site. All technical facets of the facility will be described to a useful level of detail in order to simulate the entire system. The constraints that are limiting the system will be listed and discussed. The following Figure 3.10 provides a graphical overview on the energy flows of the sub-processes.

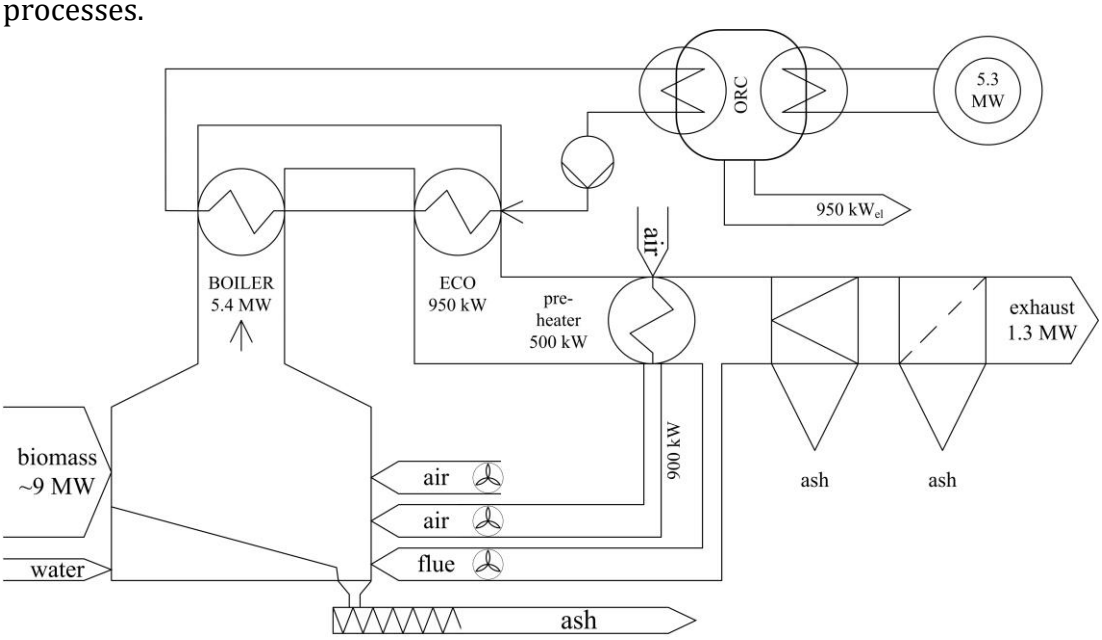

Figure 3.10: scheme of biomass based power and mass flows in the power plant

3.3.1 Thermal conversion

Biomass is widely used for energy purposes and it is believed that energetic utilisation of solid biomass will become the major contributor to the global energy balance among renewable energy sources. The system investigated here is based on this technology. Within the conversion technologies biomass combustion is the most mature and market-proven technology, which provides over 90% of the total energy generated from biomass. The main advantage of biomass combustion is the relatively high efficiency of modern furnaces and the economic feasibility of bio-energy projects. However, problems still occur due to changing fuel

properties and unstable operation of biomass combustion systems [53]. To meet the growing requirements for conversion efficiency, ease of operation and stability of the combustion process, it is necessary to continuously develop the biomass combustion systems. This development should be based on practical experience from existing biomass combustion plants.

3.3.2 The furnace

The corner stone of the Scharnhauser Park plant is a wood chip biomass grate furnace, which serves as the thermal energy source of the CHP and drives the ORC module, where electricity is generated. Under design conditions, the fire box can convert approximately up to 9MW of fuel energy into more than 6.3MW of thermal output into the heat transfer cycle (thermal oil). The characteristics, especially the geometry of the furnace, guarantee that fuel with a water content of up to 60% can be reliably converted. A stoker system feeds the unit with fuel, which is then transported via a moving grate through the furnace. To avoid bunker fires a back burning protection is integrated in the feeding system. At the end the thermal conversion process the ash is collected in a funnel and transported via a chain conveyor to the ash disposal container. For the necessary air supply to the conversion process five fans are installed for various purposes: drying, primary combustion air, two secondary air supplies, tertiary air supply and a flush fan. The entire system is equipped with fire clay and insulated from the outside. The combustion process takes place under moderate vacuum conditions.

3.3.3 Thermal oil boiler

On the top of the furnace the thermal oil boiler is situated. The spiral heat exchanger tubes are connected to the inner heat transfer surface. A flue gas stream of 20000m^3/h transfer approximately 5.3MW heat to the thermal oil in the pipes. The flue gas is cooled from a temperature in a range of 950 °C to 1000 °C down to 370 °C. At the same time the thermal oil is heated up from 250 °C to 300 °C. Biomass exhaust gases contain a large amount of ash and particulate matter that build up on the heat transfer surface. A compressed air cleaning system clears the heat transfer surface in adjustable intervals.

3.3.4 Thermal oil economiser

After passing the boiler, the flue gas is directed through the economiser. Here, another 950kW of heat are transferred into the thermal oil. The flue gas undergoes a temperature drop of 100K to 110K. On the cold side of the heat exchanger, the thermal oil returns from the district heating, respectively the ORC.

3.3.4.1 Combustion efficiency

In recent years, a great development of biomass combustion technology could be observed, which is still ongoing. The primary aim of this development is to maximize the conversion efficiency and thus the profitability of bioenergy projects. The conversion efficiency of biomass combustion plants depends mainly on two factors: the amount of unburned fuel components in exhaust fumes and ash as well as the excess oxygen content of exhaust fumes. The energy losses due to incomplete combustion in modern furnaces are negligible. The amount of unburned carbon in the ash is usually lower than 5% of the dry fuel mass and the CO content of exhaust fumes is in most cases lower than 250mg/Nm^3. In modern grate furnaces relevant energy losses are caused by a relatively high oxygen content in the exhaust fumes. This is necessary to have an excess air ratio of above one in order to ensure complete combustion of the fuel. High excess air ratios cause additional thermal losses of the hot flue gases related mainly to the heating of inert nitrogen in the air. The combustion efficiency is mainly determined by thermal losses and imperfections in conversion. Such conversion losses can be recognized by unburnt fuel residues in the ash. In this case such effects have not been observed. As a consequence those losses can be assumed to be negligible. Thermal losses can be calculated according to the following formulation [54, 55]:

$$\eta_{tc} = 1 - \frac{(\vartheta_{fg} - \vartheta_{amb})\left(1.39 + \frac{122}{CO_2+CO} + 0.02 \times u\right)}{LCV_{df} - 24.42 \times u} \tag{3.1}$$

Based on measured values of the flue gas sensors the thermal conversion efficiency can be calculated and plotted versus the thermal output of the system,

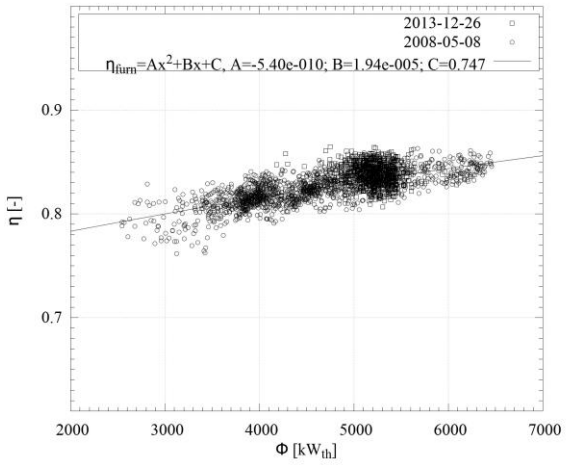

Figure 3.11: thermal conversion efficiency of the furnace versus the heat thermal power output

as depicted in Figure 3.11 (two days of data from 2008 and 2013, minutely means).

3.3.5 Exhaust gas treatment

The flue gas quality of biomass power plant has to comply with the Federal Immission Control Act (Bundes-Immissionsschutzgesetz, BImSchG). Therefore, several technical measures are necessary to clean flues gases and combustion residues of a biomass furnace. Besides the common emissions of a combustion, such as CO_2, CO, NO_X, H_2O, and unburned hydrocarbons, a relevant part of particulate matter has to be removed from the exhaust gas. The combustion of a solid fuel brings the disadvantage of particulates that are carried on the hot gas stream. Too low temperatures in the combustion chamber can lead to unburned residues of hydrocarbons, too high temperatures can cause NO_X-emissions and damage to the boiler surfaces. In order to control the flue gas properties primary and secondary measures are taken.

Primary measures:

- Moisture content: by drying or wetting the fuel, the appropriate water content is adjusted. In this way the proper ignition point in the furnace can be controlled. Dry fuel causes early ignition and may cause bunker fire by reverse burning.

- Combustion air pre-heating: by heating up combustion air, with an exhaust heat exchanger the efficiency of the furnace increases and at the same time the reaction with the combustible can be controlled in a better way.
- Exhaust re-circulation: in order to lower the degree of reaction and the temperature in the fire box, flue gases are diverted back to the furnace.
- Primary air supply: the primary air is added in the first combustion phase. Regulating the supply of air changes the quality of the chemical conversion.
- Secondary air supply: the secondary air is added in the last combustion phase. The completeness of the reaction can be controlled by changing this variable.

Secondary measures:

- Cyclone: larger particulates are removed from the flue gas stream.
- Electrostatic filter: remaining fine particles are electrically charged and filtered from the gas stream.

3.3.6 Heat transfer system

The transfer system circulates the heat carrier, Therminol66 ®, from the furnace to the district network heat exchangers and the ORC. With two circular pumps in parallel (KSB SYN 80-250) the transfer agent is delivered through the system. For safety reasons parallel pumps are necessary in this case. If the system is faulty and the circulation of thermal oil stops, the boiling of the oil can destroy the facility. Unfortunately such an accident happened during the observation period of this thesis. As a consequence one emergency pump has been installed, to provide the required mass flow for cooling the system after a shut-down. To avoid evaporation and cavitation through gases in the oil the entire cycle is pressurised.

3.3.7 Heat rejection system

The heat rejection system of the facility is located on the roof of the turbine house. The heat exchangers are dry cooler types with electric fans arranged in three groups of eight with an overall heat rate of 3.9MW_{th}. The entire system is divided by a heat exchanger (PHE) unit into a primary and secondary loops. The primary cycle is equipped with a heat meter, a circulation pump (5.5kVA) and a check-valve. The secondary loop contains one unit of the same pump type. In total the of fans have an electric design power of 19.2kVA.

3.3.8 Control systems

During the operation of a power plant cycle and its adjacent systems, control procedures for each phase of operation are necessary. For this case study the following control systems are in use (3.12).

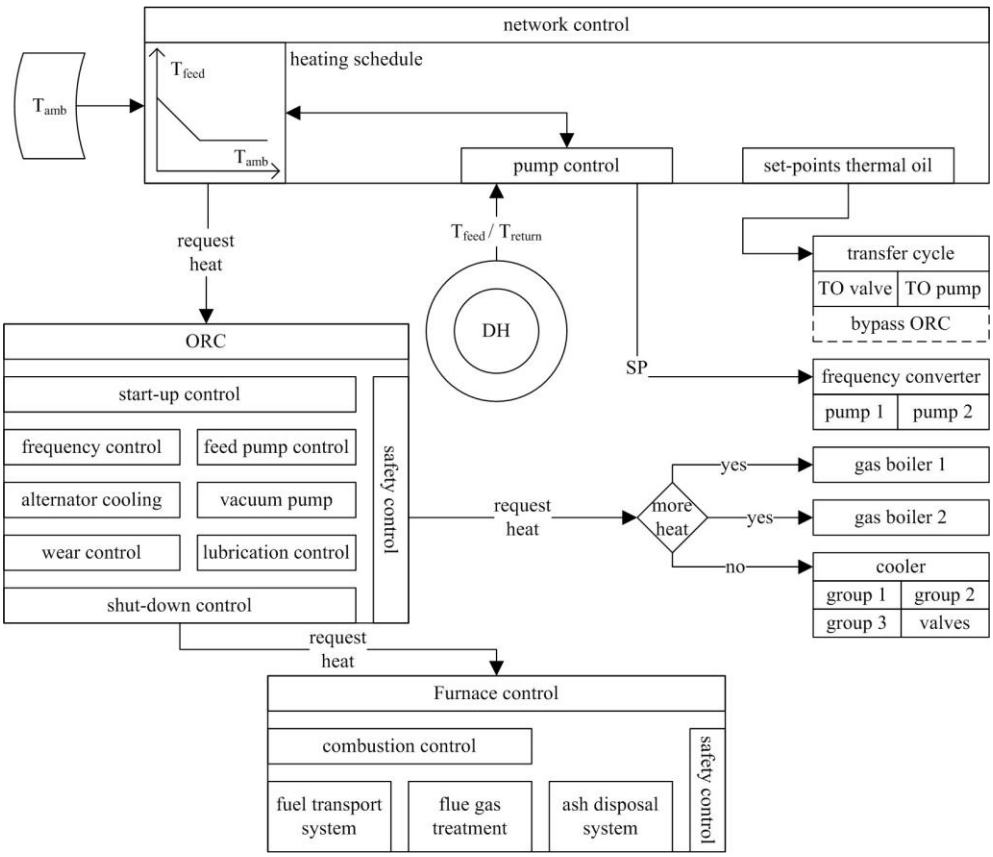

Figure 3.12: control scheme of energy supply system of case study Scharnhauser Park

- District heating control: the feed temperature of the network is defined by a temperature schedule function. In most cases the feed temperature would remain stable during summer and have a slope in winter. The temperature difference is used as an indicator for the consumption in the net. In case the return temperature falls below a certain value the mass flow of the network pump is increased while sending a heating request to the heat source, in our case the biomass furnace.
- The biomass furnace control: it contains many sub-systems, not all are explained here in detail, but the relevant ones to understand the process. If the furnace receives a heating request from the district heating system the fuel transport system is engaged. The crane control is requested to fill the cross conveyor. After doing so, the conveyor feeds the stoker, which then delivers the fuel into the combustion chamber.
- The conversion process control system: by adjusting the feed air parameters the combustion is regulated. For this purpose the fan controls

provide an appropriate amount of primary and secondary air and recirculated flue gas.
The furnace temperature sensors provide input signal for the control, the set-point is given by the operating engineer.

- The exhaust gas treatment: here the control checks the flue gas properties and the ash fraction in the multi-cyclone and the electrical precipitator. In this way the cleaning periods for the precipitator plates are controlled.

- Transfer system: to assure safe operation and good heat transfer in both furnace heat exchangers and ORC evaporator (and pre-heater) the feed and return temperatures have to be stable. The maximum feeding set-point is given by the operator. In most cases this value will not exceed 300 °C.

- Heat rejection system: in cases when the return temperature of the network exceeds the set-point the cooling unit is started.

3.3.9 Auxiliary boilers

In addition to the biomass furnace the facility has two large gas boilers. In 2003 the power plant was set up with one $9MW_{th}$ and a $5MW_{th}$ unit. In the year 2010 the smaller unit was replaced by another $9MW_{th}$ boiler. In its current configuration the power plant can deliver up to $24MW_{th}$ of thermal energy. Taking a look at the annual load distribution the old configuration would have been sufficient. Due to the fact that a gas boiler is a long-term investment, the current setting makes sense in terms of a future increase in demand. Assuming that a gas boiler has comparably good load behaviour this over-sizing has no negative effects, from a energetic point of view.

3.4 ORC-module

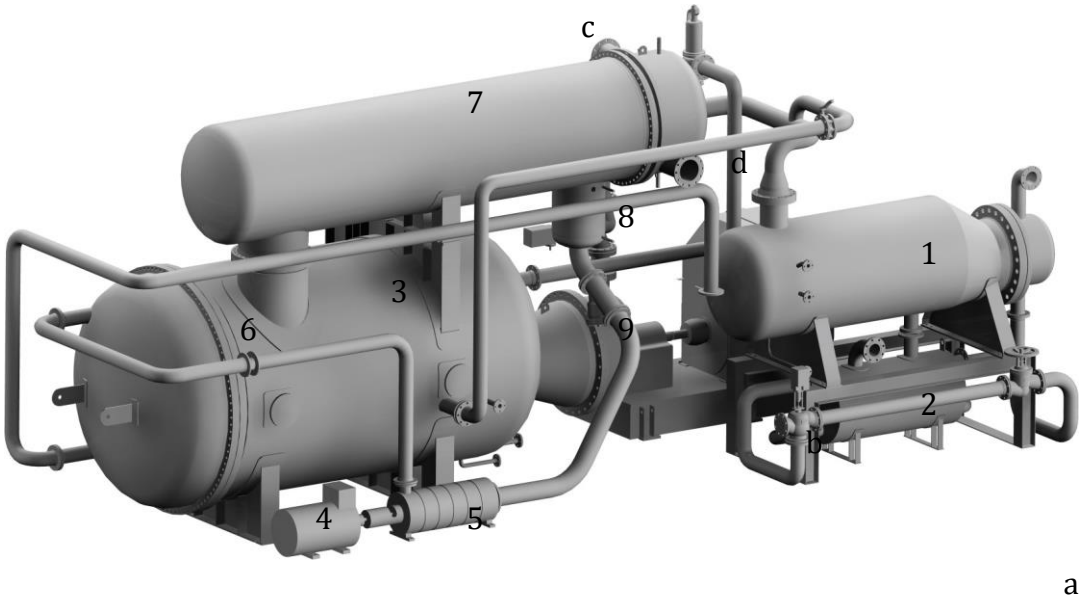

Figure 3.13: 3D-view of the case study ORC-module

1. evaporator, tube-shell kettle type
2. pre-heater, PHE type
3. recuperator, tube-shell with fins
4. feed-pump drive
5. feed-pump
6. volume-flow orifice
7. condenser, shell-tube type
8. hotwell, condensate reservoir
9. turbine and diffuser

a source: hot thermal oil feed b source: cold thermal oil return c sink: cold water feed d sink: hot water return

The above depicted ORC-module is in the focus of this work (Figure 3.13). In 2004 the local supplier SWE (water, heat, gas) decided to invest into a renewable co-generation unit. At that time the ORC technology in large-scale was about to mature. From today's point of view it can be said that the ORC market has

advanced significantly. At the time of its construction however, this engine was a prototype and the first one of its kind. Some competitors, such as Turboden, offered similar solutions. Over the years the cycle has been configured, modified and repaired. Through this time the engineers working on the machine learnt a lot. One intention of this thesis is the documentation and analysis of the modifications and advances, as well as the failures. The picture above shows already the second version of ORC engine after the first evaporator had been replaced. In 2005 the original apparatus leaked. Vibrations induced by bubble detachment led to metal fatigue in the plate stack welds. As a consequence the pre-heater had to be modified and the evaporator has been redesigned and replaced.

Table 3.4: design specification of the case study ORC-module

item	value	unit
Thermal input	6 356	[kW]
Electrical output (net)	950	[kVA]
Electrical output (gross)	1000	[kVA]
Thermal output (condenser)	5 300	[kW]
Electrical efficiency (net@100%)	0.15	[-]
Electrical efficiency (gross@100%)	0.16	[-]
Thermal efficiency	0.78	[-]
Electrical and thermal losses	156	[kW]
Temperature level source	300 / 240	[°C]
Temperature level sink	80 / 60	[°C]

3.4.1 Control systems of the ORC-unit

This chapter gives a brief introduction into the control systems and sub-systems within the ORC-module. In Figure 3.14 an overview of all control phases and their interconnection is depicted. In the following sections the single sub-procedures are explained in detail. To understand the entire system, one has to take a look into the control strategy. Under normal operating conditions the district heating network is set to a feeding temperature which is a function of the ambient temperature. As a consequence of a certain amount of demand in the network, the return temperature reaches an equivalent level. In most cases in such applications the feeding temperature would be around 80 °C and the return around 60 °C. The network pumps control variates the mass flow to achieve the desired return

temperature. Most buildings on the project site are low energy standard. Feeding temperatures of the heat system, such as floor heating (35 °C), are far below the delivered temperature level. However, for safe and hygienic operation of the domestic water systems across the whole network, feeding temperatures above 70 °C are necessary. By doing so, all reservoirs of hot domestic water in the households can be sterilized to avoid the spread of Legionella Pneumophila. The priority of the system is a reliable support with heat at all times. All other processes are a consequence of the above mentioned conditions. As soon as the consumers take more energy from the system as the plant feeds into it return temperature declines and triggers the ORC to deliver more heat. This leads to lower return temperatures in the thermal oil circuit. The threshold of 240 °C is under-run. As a corollary the biomass furnace receives a request for more output power. The fuel and air supply systems go to a higher load point. All the control cycles are part of one main control system communicating on one bus.

3.4.1.1 Start-up procedure

This section provides a brief introduction into the principles and control strategies of an ORC (or a Rankine cycle in general). While the total time a ORC is spending in start-up phase is (or at least should be) very short, it gives a good overview why cycles are not available just-in-time. Figure 3.14 depicts the control scheme for the ORC-system including start-up , default operation and the safety chain.

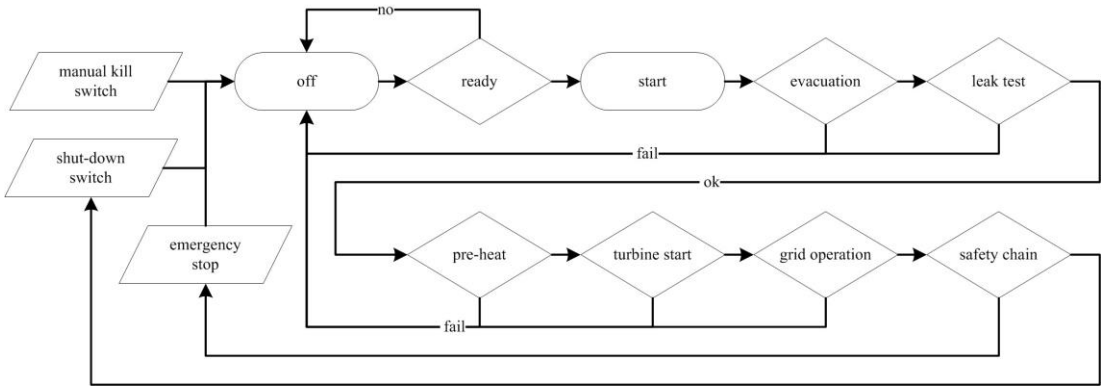

Figure 3.14: start-up, default operation an safety chain including stop-procedures

A cycle, such as the one at hands, contains 5000l to 6000l of cycle fluid and several tons of metal. Assuming that the source cycle (furnace or boiler) is already running, still the thermal inertia of the cycle has to be respected.

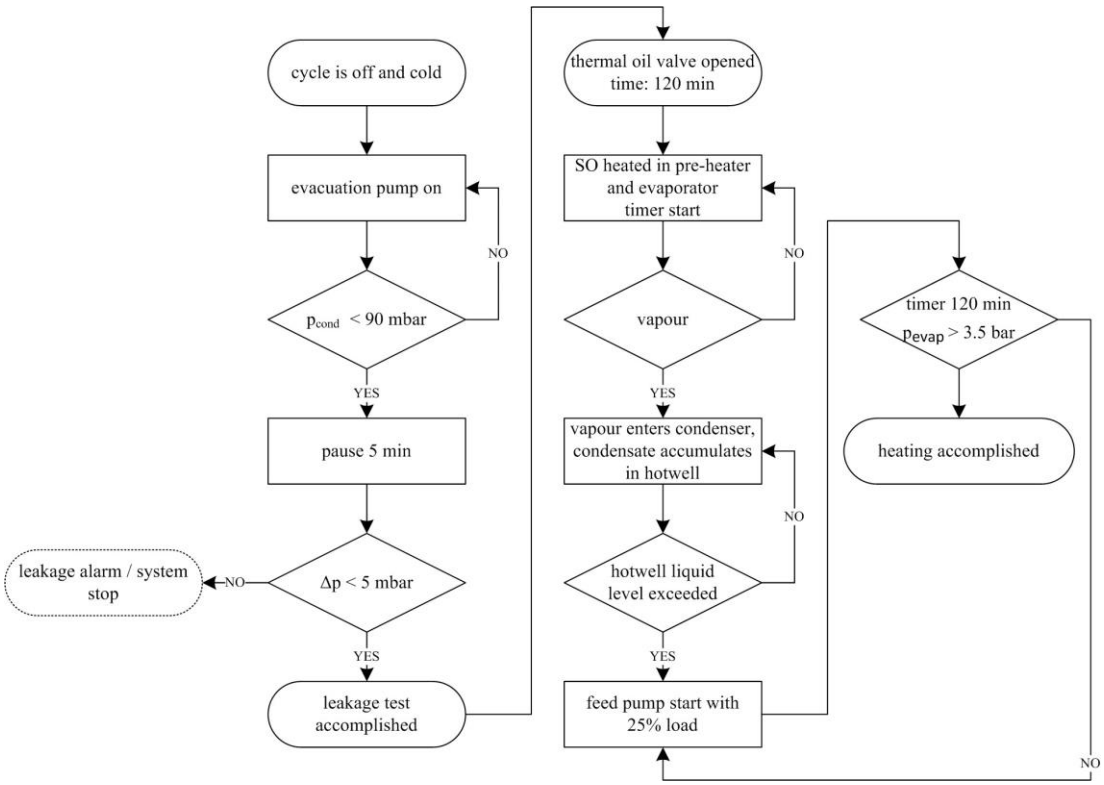

Figure 3.15: procedure for a cold start for the ORC-unit

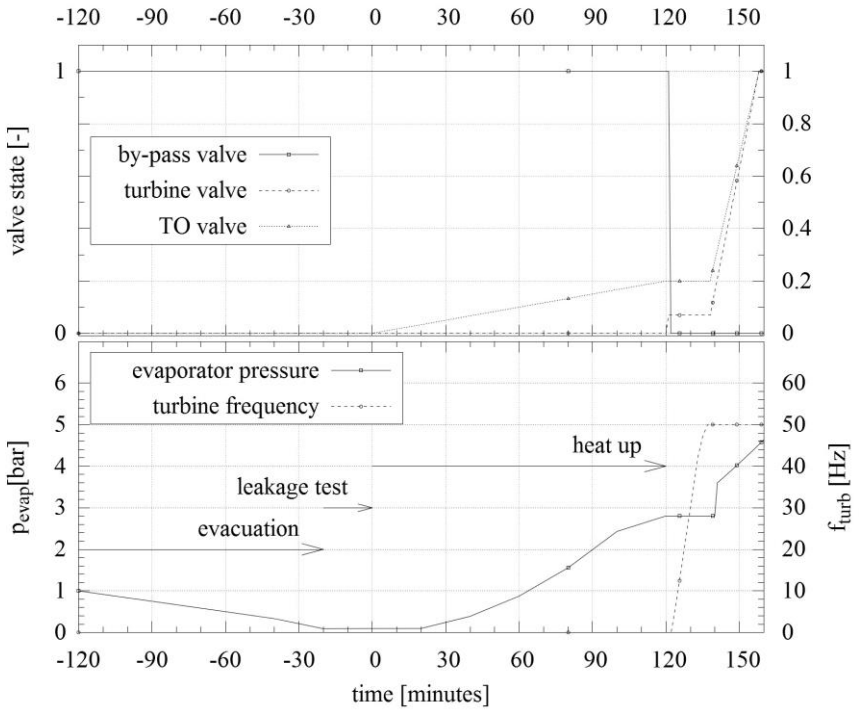

Figure 3.16: ORC-unit start-up in theory

Figure 3.15 shows the detailed cold start procedure for the ORC-module.

Figure 3.16 plots the theoretical states inside the cycle during an ideal start-up. Initialising the start of the cycle, an evacuation procedure starts. For 100 minutes the vacuum pump removes gases from the system. In the worst case, after a revision, the cycle is filled with air under ambient atmospheric pressure. After the evacuation the pressure level has to remain stable to proof there are no leakages in the system. If this test is passed, the heating of the cycle starts. While the turbine is by-passed, the feed-pump circulates the heated fluid until a evaporator pressure of 3.5bar is exceeded. At this point the bypass is closed and the turbine control valve is opened. Real measured start-ups can be found in Section 7.6.1. During the entire start-up procedure the thermal oil from the furnace is partially fed into the ORC, the remaining heat is transferred directly into the district heating via a bypass heat exchanger. The control valve's state is depicted in the upper diagram of Figure 3.16.

3.4.2 Standard operation

3.4.2.1 Alternator cooler

The alternator is equipped with a water cooled heat exchanger system. It is connected in parallel to the condenser of the district heating. Consequently, the measured heat across the secondary side heat meter of the ORC slightly deviates from the heat transferred solely through condensation. The overall effect can be neglected. Besides the water cooling the generator unit has an additional fan for emergency cooling (roughly 50kVA).

3.4.2.2 Level control

The dynamic adaptation of all heat and energy flows in the cycle is done by a condensate reservoir level control. Based on the filling level of the hotwell a frequency converter is set to drive the feed pump in order to reach the set-point level (300mm). The reservoir and the level control are in the main focus when it comes to high frequency dynamics in the cycle.

3.4.2.3 Stop-procedure

For the sake of completeness the stop procedure is explained in this paragraph. Many events necessitate a fast shut-down:

- Grid failure: without the guidance of the public electricity grid there is no control reference for the alternator. In some cases units may be equipped with an island control to maintain emergency power, but not in the case of this facility.
- Alternator failure: in case of a failure of the alternator or its sub-systems such as the cooling cycle a shut-down is initialized.
- Pressure alert: exceeding pressure thresholds in either of the heat exchangers causes a shut-down.
- Vacuum alert: if the cycle is not able to keep the level of vacuum in the condenser the cycle is stopped. This might be an indication for a leakage of the condenser tubes.
- Over-heating: when the demand in the district heating network is very low and the rejection unit is not able to keep the return temperature level beyond a certain value the cycle must be stopped.

In event of an emergency shut down the turbine valve closes and the bypass valve guides the hot vapour directly into the recuperator. If this procedure is not quick enough the turbine may speed up due to a loss of drag torque. Bearings and the rotor may be damaged by displacement or extensive wear in such a situation.

Chapter 4

Data acquisition

4.1 General comments on data acquisition

While analysing the monitoring data made available for the year 2009, the data acquisition system turned out to be inadequate for a comprehensive assessment. Until that time data have been monitored through the furnace control system. Only a few sensors of the ORC-system have been forwarded from the ORCmodule's Programmable Logic Controllers (PLC) to the main control bus. These data have been analysed until beginning of 2010. From 2010 on the analyses are based on the more detailed data of an OPC-system with high temporal resolution. The monitoring has been optimized until 2012. The number and location of the sensors was then adequate for a comprehensive analysis. Changes on the system turned out to be complicated as most works had to be done during stand still. Therefore, mainly the summer revisions have been used for this purpose. Several severe damages in 2005, 2006, 2008, 2012 and 2013 have caused long and costly modifications or even renovations. In 2005 and later in 2006 the evaporator started leaking. After a first repair the aggregate finally failed in 2006. The heat exchanger had to be completely replaced. Instead of a plate heat exchanger a shell tube evaporator came to use. The long off-line time in 2008 and 2009 has been caused by a fire. Due to malfunctioning controls the thermal oil temperature in the boiler exceeded its limit of 355 °C by 300K. The maximum pressure and volume exceeded the capacity of the systems pressure vessel and reservoirs. After being released to the atmosphere the thermal oil ignited and caused a fire. This resulted in a serious damage of the facility. Three storeys of the building had to be renovated and several technical appliances had to be replaced after this event. This incident lead to several changes in the system control. A new safety chain had to be applied. In cooperation with the technical inspection authority (here TUV) a new concept was put into practice. Fast emergency shut-downs are now¨ assured by the appropriate interaction of primary, secondary and recirculation ventilators. It has to be mentioned that the data of different periods

of operations are not fully comparable. Therefore, the useful amount of data for modelling and validation is restricted to a few month out of four years of full monitoring.

4.2 Monitoring concept

In order to receive comprehensive and coherent data sets, that provide enough information to describe the system entirely, various data sub-systems are being used. The entire plant is equipped with a PLC to measure and control the processes. The PLC is the basis for the data acquisition for this case study.

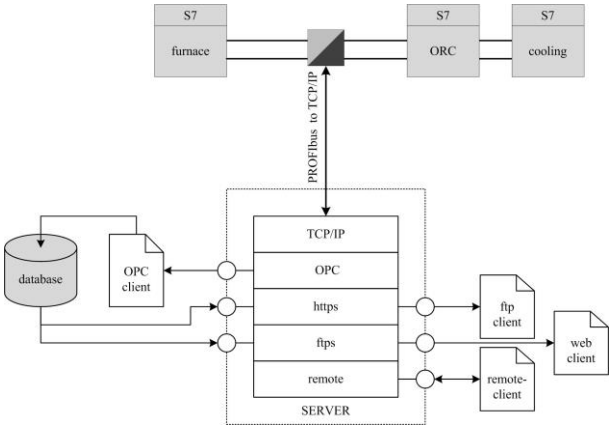

Figure 4.1: data acquisition structure, including PLC, Gateway and data management

4.3 Long-term monitoring

The main control computer in the power plant is using a software named Zenon by the company of Kohlbach, Austria. Data from the PCL components are connected to the main computer via a gateway (PROFIbus to RS-485). All values that are processed within the PCL can be accessed in this way. The standard monitoring of the power plant logs the process parameters with a time step of one minute and saves them in an internal database. Data can be exported to files in various formats such as dBase or CSV. In terms of validation for dynamic simulation the quantity and time step of this system is not appropriate. Furthermore sensors in the OR-cycle, which are in this case in the centre of interest, can not be accessed. As a result this monitoring system has to be combined with further systems and sensors to receive a complete view on the power plant.

4.4 Monitoring

4.4.1 Data acquisition system

4.4.1.1 OPC-protocol

OPC Unified Architecture (UA) is an industrial communication protocol. Since 2006 it is standardized in the current version. The following scheme illustrates the layer model of OPC-UA from the data source to the client and server operating system.

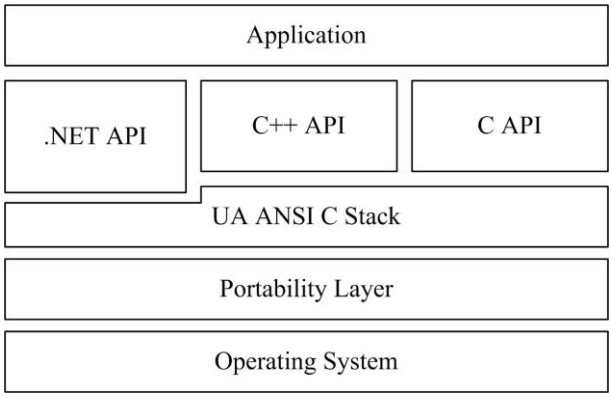

Figure 4.2: communication stack architecture of OPC-UA [8]

This communication layer structure provides the possibility to connect various data sources and receive a uniform and coherent data output. In this case M-Bus,
Modbus, Profibus and analogue signals are bundled and provided on one single OPC-server structure via TCP/IP.

4.4.1.2 PLC-Siemens Simatic

The control system of the ORC-system consists of the following components:

- S7-315-2AG10: Main CPU unit
- SM321: digital input module (32 channels)
- SM331: analogue input module (8 channels)
- SM322: digital output module (32 channels)
- SM332: analogue output module (8 channels)

- CP343-1 Lean: PROFIbus to Ethernet gateway

The control software contains 33 function modules and 24 database modules. The above mentioned gateway unit has been additionally installed and configured by the author in order to make the PLC data accessible via an OPC-network. The other components are part of the ORC-unit.

4.4.1.3 OPC-server configuration

The procedure of making the PLC data available via an OPC-Server, as put into practice by the author, is described in this section. In a first step the data points and their addresses have to be allocated and assigned. To do so, the service reads its configuration file (TcpIpH1.txt). Within this file the PLC functions, parameters and variables are allocated via the component name, the byte address and the data type:

```
 ORC(ALIASES) ]
EE 4622 51 FR=DB12,REAL48.0 EE 4622 51
FI=DB12,INT52.0
TE 4140 01 FR=DB12,REAL54.0
TE 4141 01 FR=DB12,REAL0.0
1 [
2
3
4
5
```

In total the server has been configured for 607 data points, but it must be mentioned that not all are of interest for the analysis. Some data points are doublets either by using two different aliases for one value or addressing one value in two different data types (for instance integer and double). With the next step the OPC-client is configured. Via a XML file the wanted addresses and properties (read interval, delimiter, file write mode) are assigned:

```
?xml version="1.0" encoding="utf 8 "?>
<OpcConfiguration xmlns:xsi="http: //www.w3. org/2001/XMLSchema instance" xmlns:xsd="http: //www.w3.
org/2001/XMLSchema">
<OpcServerURL>opcda:///INAT TcpIpH1 OPC
Server/{3DA28330 68CB 11D2 9 C65 0021 A0020009}</OpcServerURL> <Groups>
<OpcGroupConfiguration Name="ORC">
<Intervall>10000</ Intervall>
<OutputFileName>d:\DATA OPC\%Y%%M%%D% logfile ORC . txt</OutputFileName>
<AskBeforeOverwriteOutputFile>true</AskBeforeOverwriteOutputFile>
<OutputFileSplitMode>3</OutputFileSplitMode>
<WritingTriggerMode>1</WritingTriggerMode>
<Delimiter>;</Delimiter>
<DataMode>0</DataMode>
<Items>
<OpcItemConfiguration Name="ORC. EE 4622 51 FR"> - - -
<ShowQuality>false</ShowQuality>
</OpcItemConfiguration>
<OpcItemConfiguration Name="ORC. TE 4141 01 FR"> - - -
<ShowQuality>false</ShowQuality>
</OpcItemConfiguration>
<OpcItemConfiguration Name="ORC. TE 4140 01 FR"> - - -
<ShowQuality>false</ShowQuality>
</Items>
</OpcGroupConfiguration>
1
2

3

4
5
6
7
8
9
10
11
12
13
14
15
16
17
18
19
20
21
22

</Groups>
</OpcConfiguration>
23
24
25
```

The above example shows the definition of three data points. The measured electric alternator power is provided as integer and as real values but only initialized as a real. The two latter addresses are temperatures of the thermal oil cycle as real values.

4.4.2 Data selection

Within the process of monitoring the selection of data, especially the distinction between useful and useless data is crucial. Complete accuracy of data is not possible, hence we have to define an acceptable range of deviation and an

appropriate quality for the purpose. In the following paragraphs the data selection in this work is described. It is one aim in managing a CHP-plant to keep it running at full load. In reality, the modulation in load is needed. For the final aim, optimising dynamic load behaviour, comparable data have to be used as validation. In order to simulate and validate representative load situations, typical patterns have to be identified. Besides the validity of data a more important criterion has to be fulfilled: the availability. Changes on the system, shut-downs, sensor failures and many more reasons minimise the useful datasets.

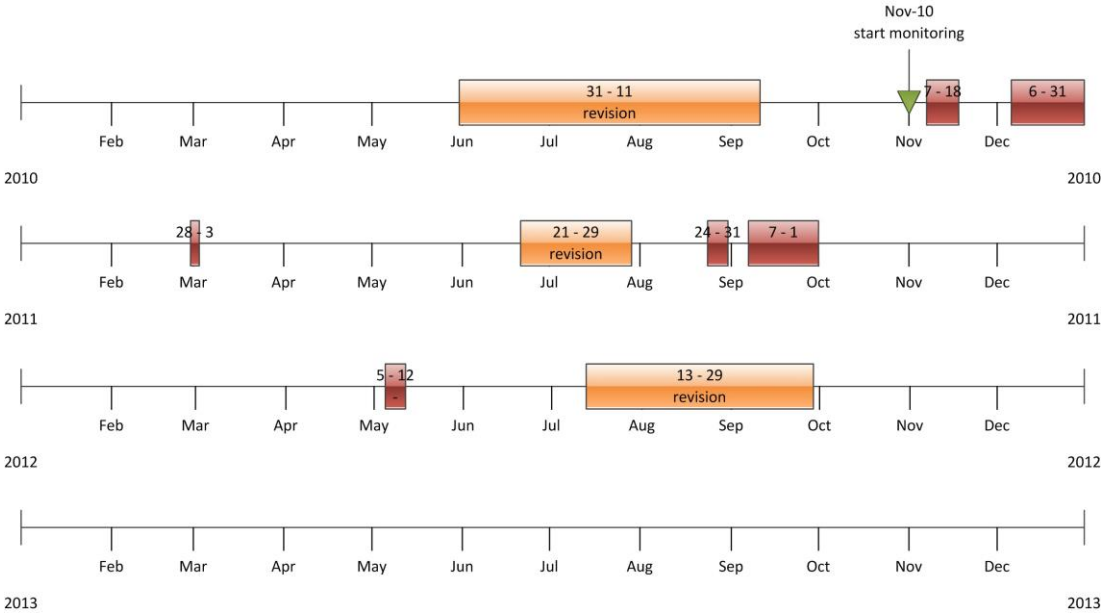

Figure 4.3: monitoring period including interruptions

In Figure 4.3 an overview on the the year of 2010 to 2014 is given. Light grey boxes represent planned revisions, dark grey boxes unexpected or unplanned downtimes of the OR-cycle.

4.5 Data quality

In the following section the sensors being used for monitoring are described; their position in the system, mounting situation and sensor type. Values from these sensors are processed by the control system via Profi-bus. In November 2009 a Profi-bus to TCP/IP interface was installed. Using the OPC-protocol the values can be provided by the OPC-server and recorded by an OPC-client. For this purpose, an OPC-client, based on the Softing [56] architecture was developed. For the analyses presented all sensors and relevant control parameters have been monitored with a time step of 10 seconds in datasets of 24 hours. The data are

written to CSV-files and then further processed. To derive the load characteristics of this cycle, data from the power plant and the ORC are unified according to both, time stamp and time-step length.

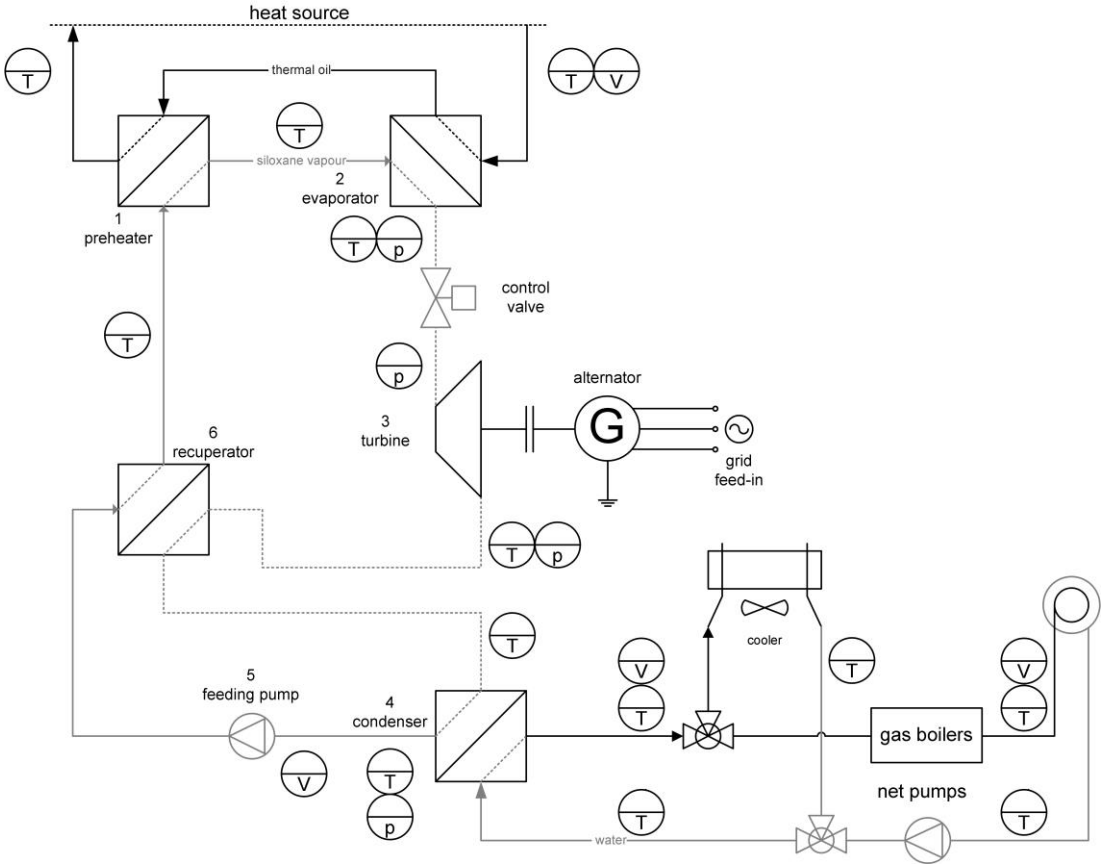

Figure 4.4: location of sensors in the OR-cycle

Figure 4.4 depicts a scheme of the most relevant sensors concerning the ORCmodule.

4.5.1 Temperature sensors

All temperature in the system are measured using PT-100 types. The sensors comply to IEC 60751:2008, Class B [57]. The accuracy of the sensors is given in the manufacturers manual with a maximum deviation according to the function in Equation 4.1.

$$\Delta T = \pm(0.3 + 0.005 \times \vartheta) \tag{4.1}$$

which then leads to an error for a measured temperature difference:

$$\epsilon[\%] = \pm\left(0.5 + \frac{3}{\Delta\vartheta}\right) \tag{4.2}$$

Table 4.1: deviation of PT-100 sensors according to standard IEC60751 Class B

temperature [°C]	deviation [K]
50	0.55
100	0.80
150	1.05
200	1.30
250	1.55
300	1.80
350	2.05

Temperature sensors are used in the cycle for various media and under very different circumstances. Five media are measured: Therminol66™, Octamethyltrisiloxane, turbine oil, water, and ambient air. Accuracy for this work is relevant for water, MDM and T66. The turbine lubrication system is interesting for revision planning and emergency shut down. However, it is not of interest for simulation.

The following types of sensors are used in the cycle:

Table 4.2: list of the most relevant temperature sensors in the OR-cycle

ID[?] -	type -	manufacturer -	range [°C]	accuracy -	location -
TE41-40	PT-100	PMA [58]	0 – 400	EN60751[??]	thermal oil feed
TE41-41	PT-100	PMA	0 – 400	EN60751	thermal oil return
TE42-40	PT-100	PMA	0 – 400	EN60751	turbine feed
TE42-41	PT-100	PMA	0 – 400	EN60751	turbine return
TE42-42	PT-100	PMA	0 – 120	EN60751	condenser in
TE42-43	PT-100	PMA	0 – 150	EN60751	condenser out
TE42-44	PT-100	PMA	0 – 200	EN60751	pre-heater feed
TE43-40	PT-100	PMA	0 – 120	EN60751	water feed
TE43-41	PT-100	PMA	0 – 120	EN60751	water return

TE45-40	PT-100	Electrotherm	0 – 120	EN60751	excess condensate

[?] the ID is equivalent to the sensor name in the S7 control [??] [57]

4.5.2 Pressure gauges

Pressure is measured by temperature compensated strain gauges. The P40 type sensors have an average characteristic deviation of ±0.3%. A maximum deviation of ±0.5% is given by the manufacturer [58]. In order to validate the pressure sensors, in every revision phase the sensors have been checked while the cycle was under atmospheric pressure. This proves that a sensor is functional and has no a relevant offset. More problematic than the actual accuracy of the sensors is the location of the pressure gauges. During the monitoring some unexpected deviations in pressure measuring have been detected. With increasing fluid velocity and uncertain flow vectors the interpretation of measured pressure value can become tricky.

- The vapour from the evaporator is flowing through a long pipe, under a very high pressure. The deviation by misalignment of the pressure sensor can be neglected.
- The feed pressure of the turbine is measured in the gate vane ring. The velocity is assumed to be very low and the pressure is high.
- The condenser pressure is measured via a radial tube on the middle axis. This location provides a mean pressure value. Despite the pressure level is very low the dynamic pressure influence is not significant due to the low fluid velocity.
- The most critical spot for pressure measurements is right after the turbine. High velocities, a low absolute pressure level and varying flow velocities and vectors are problematic.

Figure 4.5: pressure lines for inlet and outlet of turbine

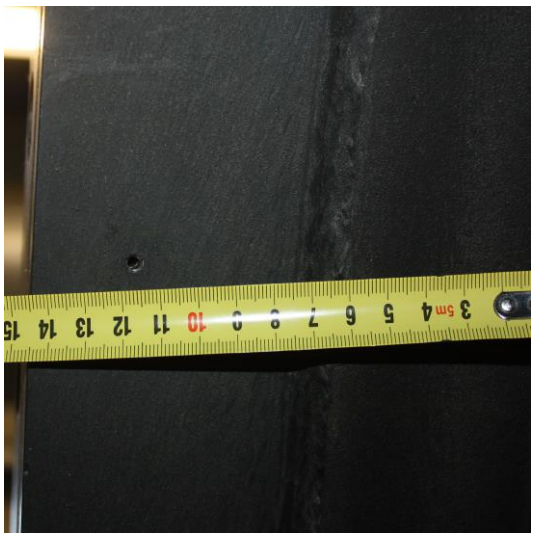

Figure 4.6: turbine drain pressure bore hole

Further information concerning the data quality of pressure can be found in Section 7. Figure 4.5 shows a picture of the turbine housing including the two pressure taps for feed and return pressure. During day-to-day operation, the unit and the pipes are covered by insulation and not accessible from the outside. The picture on the right (Figure 4.6) shows a close-up of the pressure port on the drain side of the turbine.

4.5.2.1 Pressure control sensors

For safe operation within the allowed pressure range the unit is equipped with various safety valves and pressure switches. The most important sensor is the one for evaporator pressure. It is set to a maximum value of 11.5bar. In case of overstepping this threshold, a full emergency stop is initialized. The thermal oil valve is completely closed and the thermal input into the cycle is bypassed to the backup heat exchanger (connected to the district heating). The excess cooler are enabled and cool the remaining thermal capacity in the cycle down to approximately 60 °C. The same procedure is carried out, if the recuperator hot side pressure goes below 0.3bar. This case may happen if the vacuum pump control fails. The sensors in this case are DSF 152 (evaporator) and DSF 125 (recuperator) produced by the company Sauter AG.

4.5.3 Frequency sensors

The rotational frequency of the drive train is measured with an optical pulser. Its impulses are transduced by a DA-converter to an output signal range of 4mA to 20mA. The signal is further processed via a current input of the PLC.

4.5.4 Flow meter

The volume flow of the liquid MDM is measured on the high pressure outlet of the feed pump. In this part of the cycle the deviation caused by temperature and two-phase effects are low. The fluctuation of temperature is in a range of 80 °C to 90 °C. The volume flow is measured according to the principle of differential pressures across a standard orifice. A ceramic pressure transducer returns a current signal of 4mA to 20mA for a differential pressure of 250mbar. The differential pressure difference is linearised and scaled to a volume flow of 0 to 120m^3/h. The manufacturer claims an accuracy of 0.1% (linearity) and ± 0.25% of noise in the output signal. While calculating the heat flows through the system, a discrepancy between the heat meters on the sink side, the source side and the internal mass flow appeared. A first guess was a wrong calibration of the orifice or a problem in the pressure taps of the differential pressure gauge. A deeper look into the specifications of the ORC-module revealed that an adaptation factor has been set wrong in the PLC. While the design pressure of the sensor was set to 25000Pa the conversion factor in the PLC register was set to 27648Pa. In order to determine the right value an ultrasonic flow measurement was conducted. A Portaflow-C by Fuji Electric has been used for that purpose. One week of data (10 seconds time step) have been taken, using a flow FSD22 flow detector type as depicted on the picture in Figure 4.7.

Figure 4.7: flow detector attached to pipe connection from feed-pump to recuperator

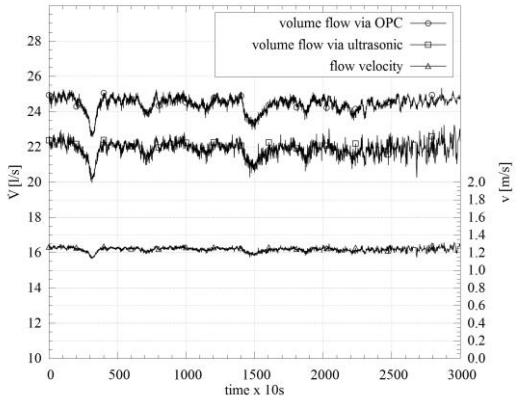

Figure 4.8: volume flow measured via ultrasonic and via PLC (30000 seconds)

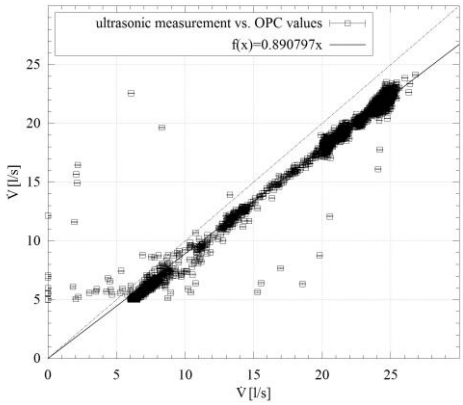

Figure 4.9: ultrasonic volume flow measurement versus PLC values

The results of the measurement in Figure 4.8 and 4.9 show clearly the deviation between the PLC values and the real values. Fuji claims an accuracy of ±1% for the Portaflow-C. For the measured range on velocity between 0m/s and 2m/s a dispersion of ±2m/s has to be expected. Therefore an accuracy of ±1.3% in the above depicted range is more realistic. Fortunately the measurement shows a linear behaviour between the two measurements. The data from the PLC can be easily corrected by using the factor 0.890797.

4.5.5 Heat meters

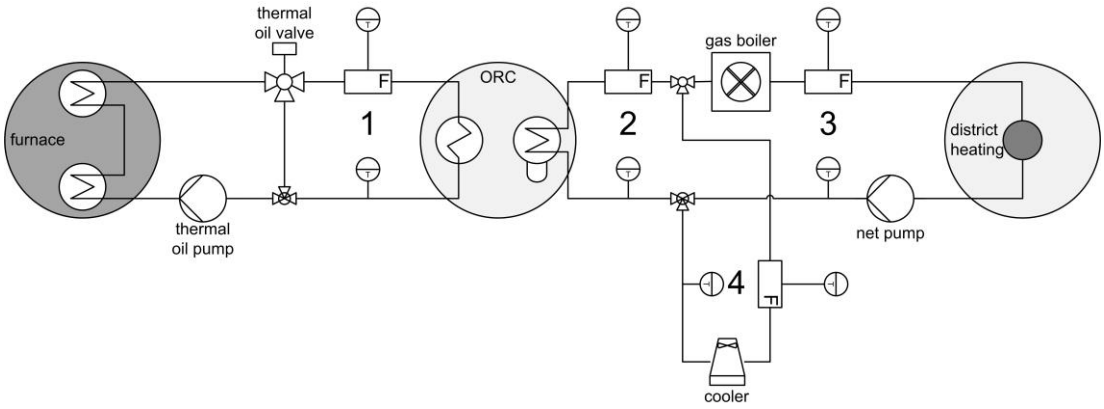

Figure 4.10: heat meters in the power plant

The district heating is monitored with a MAXICAL ® III type [59] heat meter. The manufacturer states an accuracy class of 0.2% for temperature spreads larger than 20 K. In the heat transfer system, the thermal oil is measured utilising a MAXICAL®401 [60]. All heat meters fulfil the requirements of an EN 1434-1 Class A device [61]. Therefore, less than ±2% deviation can be expected taking the sensor's and calculator's accuracy into account.

$$\epsilon = \pm \left(0.15 + \frac{2}{\Delta \vartheta} \right) \tag{4.3}$$

Across the relevant range of temperatures the deviation of the flow meter is as depicted in Figure 4.11. During the monitoring period, disturbances have been discovered in the district heating sensor. Outliers have been removed with a data filter.

4.5.5.1 Offset drifting

The use of heat and flow meters in practice comes along with systematic metering errors. Due to their complexity and the operation under rough conditions the accuracy of such sensors has to be checked regularly. Especially if the measured liquid tends to react with its surrounding materials this is the case. Long term studies such as the one conducted by Leitgen [62] show meta data of sensors being used in district heating systems. The author claims that the average deviation of measuring devices has not significantly improved since the 1980s. For the unfortunate effect of offset drifting multiple factors are responsible:

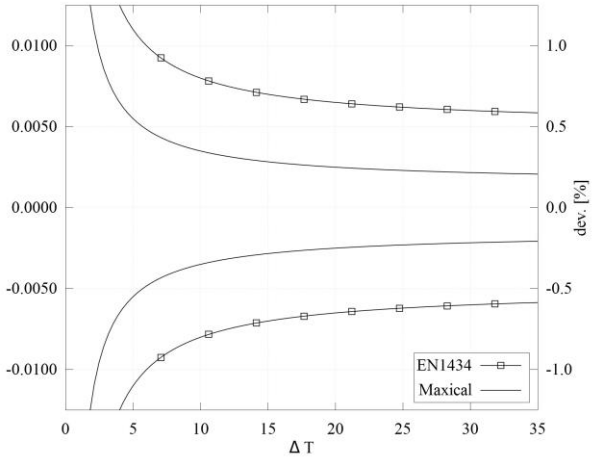

Figure 4.11: comparison of temperature sensor deviation in MAXICAL flow meter to EN1434 eClass-A

- In most cases the medium is water with varying compositions. Especially sediments of minerals, such as Magnetite can form a layer in pipes or rotors. through its damping ability the result the normally has an negative off-set.
- Corrosive processes on electric contacts (soldering) can cause a disturbance in the signal forwarding.
- The electronic and logic circuits in the processing unit or the transducer of the sensor can fail and cause offsets or even interruptions.

In our case the relevant heat meters for billing are regularly checked and calibrated, according to the regulations of the German heating billing standards. However, these check-ups are not obligatory for the primary sensors for thermal oil. This heat meter is only used for internal balancing. During the data acquisition of the heat meters discrepancies between the two sensors have been discovered.

4.5.5.2 Drift compensation

Unfortunately, the above described effects are dynamic. In order to receive reliable data sets of a longer period (e.g. 2 to 3 years) a frequent accuracy test and an according drift compensation is necessary. For the data hereinafter the compensation has been done once every week. For a data set of n = 8640 steps (time step of 10 seconds) the following algorithm has been used:

$$\sum_{i=1}^{n} \dot{Q}_{to,i} - \sum_{i=1}^{n} \dot{Q}_{dh,i} - \sum_{i=1}^{n} \dot{Q}_{loss,i} - \frac{\sum_{i=1}^{n} P_{el,i}}{\bar{\eta}_{el,gr}} = \sum_{i=1}^{n} \dot{Q}_{off,i} \tag{4.4}$$

furthermore the mean value of the offset can be calculated:

$$\frac{\sum_{i=1}^{n} \dot{Q}_{off,i}}{n} = \bar{\dot{Q}}_{off} \tag{4.5}$$

the off-set factor is then defined as:

$$\frac{\bar{\dot{Q}}_{off}}{\bar{\dot{Q}}_{to}} = f_{off} \tag{4.6}$$

In order to support the above calculations as a second method the secondary side of the evaporator and pre-heater have been measured. Over a long period of operation (e.g. one day) the accumulated enthalpy difference across evaporator and pre-heater has been set in correlation to the measured heat flow into the system. As a result it can be stated that the offset is negative. Applying this method to several days resulted in an average deviation of approximately −1%. In some cases the deviation can be up to −5%, if the re-heating loop (condensate evaporation) of the recuperator is running. For the further calculation in this work, such as the validation and simulation of the heat flow into the cycle this off-set calculation has been undertaken for each dataset being used.

4.5.5.3 Fluid sensors

For the sake of completeness, pressure sensors have to be mentioned here as well. They prevent dry running or damage to the cycle in case of extraordinary events, such as:

- Control errors in the hotwell level control.
- Pump failure due to blocking or electric failure.
- A Failure of differential pressure measurement.
- A leakage in the condenser with district heating water intruding in the cycle

The system is equipped with three level sensors: one each for maximum and minimum liquid level in the hotwell, one in the vacuum system. In case of hotwell dry run or overflow the emergency shut-down is enabled. Each sensor is connected via a four wire lead, two wires for the digital signal and two for diagnostics.

4.5.6 Filling level indication

The evaporator is equipped with a magnetic level indicator (Vaihinger, Type 75/111 PN40). A magnetic float in a glass tube triggers magnetic flaps. The flaps indicate the liquid level to the operator. The accuracy of the display is influenced by the weight of the float, the temperature of the apparatus and the liquid and of course by the density of the liquid. Varying consistences of the fluid may lead to an offset. Deviations can be expected if the liquid contains two phases. For this

type of gauge the precision of the measured values is larger than the size of the magnetic flaps. In this case one can expect a minimum deviation of ±1.5cm. The level indicator is a purely mechanic system, therefore a electronic acquisition of the measured values is not possible. The operators have tried to note the liquid level, as far as it was possible during the daily business in the power plant. All-in-all the results taken from the level gauge have to be taken as a rough estimation or indication and not as a precise measurement.

4.6 Data post-processing

4.6.1 Data analysis methods and tools

Besides the common tools and programmes to read, view and plot data custom made methods have been applied during this thesis. The amount of data and their format makes it necessary (220 million data points). Between the year 2010 and 2014 the power plant has been recorded with almost no interruption, at a time step of 10 seconds. Within this sheer amount of data useful datasets had to be identified. A first attempt to create a common local mySQL data base was not successful. The performance was poor. As a minimum requirement ASCII files with a CSV format were chosen. This way is versatile and compatible with all used programmes, such as MATLAB, MS Excel, EES, et cetera. The identification of appropriate data sets was undertaken using scripts of the language ruby in combination with GNUplot. However, the rising requirements for long term-data analysis (weeks, month, years) made a new strategy necessary. By introducing the server-based MS-SQL data base EMtool the performance issues could be resolved. Once the feeding process of the data base is accomplished, time series of absolute or mean values (custom periods) can be generated straightforward. EMtool is a software developed by the University of Applied Sciences Stuttgart. The author was part of the developer team of the software.

4.6.2 Data unification

In order to unify and conclude various data sources the database tool EMtool has been used. It is capable of reading data from different sources and combined them in one database, for instance weather data and OPC-data. The tool can generate time series of weighted means.

4.6.3 Data manipulation

The following methods have been applied in order to enhance datasets for calculation and simulation.

- Peaks: the data transfer over the PROFIbus causes errors at times. The most significant byte is transferred first (Big Endian) which leads to values that are multiple times higher than physically possible. Applying a filtering script that replaces every value that is more than twice the design value by a mean value of the two values before and after the error solves that problem.

- Freezes: when the data connection is lost due to a power failure on the bus or network error the last measured value remains in the buffer until a new value is sent. This problem appears usually during emergency shut-downs. It is not relevant for data sets that are used for calculation, simulation or validation.

- Smoothing: for the use of dynamic solvers such as DASSL in modelica input values have to be smooth. Therefore, data sets have to be splined to make them continuous for two derivatives. Within modelica this is done with the SplineData class.

- Time series: to handle large data sets and generate time series the before mentioned EMtool has been used.

4.6.4 Data storage

As the most versatile method to store the data the simplest form was chosen: ASCII in character separated text files. The OPC-client writes the data in text files with a comma as decimal separator and semicolon as column separator. The data format is double with three decimal places or integer. Boolean data formats, such as states of pumps or fans, are returned as “False” and “True”. The following replacements are made with a ruby script:

- each comma is replaced by point

- semicolons are replaced by a blank

- “True” and “False” are replaced by “1” respectively “0”

Chapter 5

Modelling

"...essentially, all models are wrong, but some are useful."
George Edward Pelham Box (*?*1919 †2013)

Whenever modelling is used to find a solution for a question, the first decision that has to be made is the level of detail. It determines complexity, computational time, input and output data in quality and quantity. The very purpose of the cycle simulation in this work is gathering more information about the interaction of the internal processes and correlations. The recommendations for a further optimisation are based upon this information. This chapter deals with several approaches to modelling. First of all the entire cycle is treated as a black box. For engineering tasks often simple and robust models are needed. In the first planning phase of a power plant project less complex modelling strategies are favourable in terms of computational time. In the layout process of a cycle steadystate calculations come to use. As the most sophisticated discipline the dynamic modelling provides the highest level of details. Dynamic models are useful in order to determine the interaction of the generating cycle and other connected systems, such as district heating and the heat source. For the design of the control system of a plant dynamic models are inevitable. It may be sufficient to set up an empirical black box model to estimate the electric performance of the cycle. In this case the model would be a projection of past experience into the future. As soon as the configuration of the plant changes the output data may be invalid. In Section 5.1.1 the mode of this work this empirical approach will be presented including some results.

A final remark has to be made to introduce into this chapter: many researchers are working on laboratory set-ups. This approach is appealing when it comes to data acquisition. Test runs can be done relatively easy. The external constraints can be set in a way to meet the desired operational points. Unsatisfactory runs can be repeated. Under the conditions of a real application, test runs are the result of

an enormous amount of data being filtered afterwards. A main disadvantage in this approach is the limited influence of the researcher on the system. During the period of this work, many necessary changes on the hardware have been put into practice. Often this led to incoherent data sets that are not comparable. As far as possible, the following models are based on coherent hardware settings. Besides this handicap the results obtained from a “real” system can be adapted straightforward as instruction for optimized operation.

5.1 Modelling approaches

5.1.1 Empirical modelling

The operation of a small CHP usually keeps the the maintenance of the system within acceptable boundaries. In a Diesel module, system components such as the cylinder heads, valves, gaskets or piston rings have assigned revision intervals. Those intervals are based on experiences gathered from a large number of units running under various conditions for a long time. In contrary, plant systems that are not “off the shelf” do not come with this advantage. The personnel has to diagnose defective parts and estimate the necessity for repairs. Some auxiliary diagnosis systems are of help for this purpose. For instance, the bearing wear control, displacement gauges and the turbine oil temperature sensors provide information about the state of the engine. However, the complexity of the system and the cost saving pressure collide here. A comparably simple and cost effective way for diagnostics is needed. Complex dynamic model, such as the ones in this work are not feasible for most operators of small power plants. A local supply company does not have the financial or personnel resources to do so. In this chapter a less complex way of finding a reliable model to diagnose wear and degradation on the system is proposed. In the case at hand the model helped finding a leakage in the recuperator. With a rising number of processes the modelling of a system might become complex to an extend where the capabilities of modelling are exceeded. For rather complex systems and sub-systems empirical models are able to describe the behaviour of a system at question in an adequate way. For empirical modelling no detailed information about the physical processes is necessary. This is the biggest advantage and, at the same time, the biggest disadvantage of this method. In terms of coherence and reversibility this is a down side.

5.1.1.1 Modelling procedure

In order to generate an empirical cycle model representative data sets containing the full load range are needed. For the most relevant load points the data has to be filtered. In the case at hand special events such as emergency shut-downs or heat up procedures have been neglected. These events are on the one hand not meaningful enough for every day operation in terms of diagnosis. On the other hand the modelling of such events is too complex for an empirical modelling approach. The following scheme (Figure 5.1) shows a possible black box model concept:

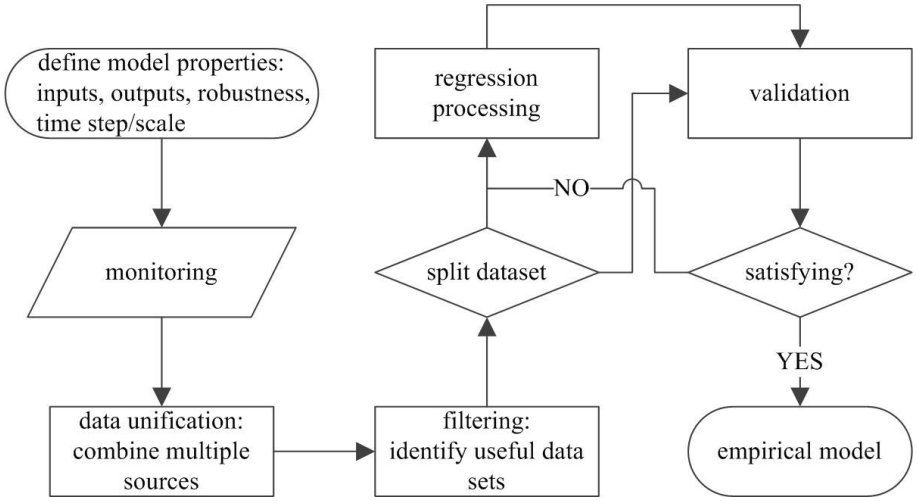

Figure 5.1: procedure of empirical modelling process

The following Table 5.1 shows possible inputs and outputs for an empirical approach. It should be noted that not all displayed combinations are necessarily useful. Another trap one may encounter is that a model does not follow the conservation of energy. To a certain extend this is acceptable and can be explained by dynamic effects. In cases where steady offsets are observed in the results, something obviously went wrong in the modelling process.

Table 5.1: potential empirical model variants

	INPUTS									OUTPUTS		
model	$\dot{Q}_{to}$	$\dot{m}_{to}$	T_{fto}	T_{rto}	ΔT_{in}	$\dot{Q}_{dh}$	$\dot{m}_{dh}$	T_{fdh}	T_{rdh}	η_{el}	P_{el}	T_{rdh}
1		x	x				x	x			x	
2		x	x			x	x			x	x	
3	x		x				x	x		x	x	

4			x				x	x	x		x	x	x
5		x	x				x	x	x		x	x	
6		x				x	x	x			x	x	
8			x	x			x	x		x	x	x	
12		x	x					x		x		x	

In order to find a useful and applicable empirical model the very purpose of the calculation has to be determined. For sure an empirical model cannot serve as basis for control optimisation. Taking a look at all degrading processes within an ORC a simple empirical model provides the opportunity to diagnose the process. Under the constraint that the hardware remains unchanged the behaviour can be predicted and compared with measured values. If the simulation deviates significantly, further checks on the system can be done. Especially in power plants unmanned operation this method can be used for diagnosis. Two different methods to obtain an empirical model can be used: a manual regression analysis based on physical estimations or an automatic genetic regression. The first procedure will be used in this section. The following assumptions are made for our case:

- The cycle is heat-led. Therefore, the dominating energy flow is the sink (district heating).
- The input to the cycle is defined by the temperature spread and the mass flow of the thermal oil.
- The return temperature remains stable, as it is the control variable of the thermal oil valve controller.
- Extremely low load states, start-ups and stops can not be modelled.

The entire potential of a given cycle can be expressed in terms of the Carnot efficiency. Extending the Carnot efficiency with some estimated multiplicands, a first approximation for maximum mechanical efficiency is obtained:

$$\eta_{el,max} = \frac{T_{TO,feed} - T_{DH,ret}}{T_{TO,feed}} \times \eta_{mech} \times \eta_s \times a \tag{5.1}$$

Based on the calculation in Chapter 2.6, this ORC unit reaches about 50% of its Carnot efficiency (a = 0.5). Furthermore, one can assume a mechanical loss in the

drive train of 2%, ergo the mechanical efficiency η_{mech} is 0.98[1]. According to the nominal isentropic efficiency given by the manufacturer, the turbine can convert 78% of the nozzle energy into mechanical energy. Through scaling effects and constant parasitics the cycle efficiency decreases with lower load. One variable representing this lower load is the mass flow of the sink with its exponent c (for instance: 0.25). Multiplying the load dependency factor with the maximum electric efficiency and the other components, it leads us to the electric (gross) power output of the cycle:

$$P_{el,gr} = \Phi_{in} \times \eta_{el,max} \times \left(\frac{\dot{m}_{sink}}{\dot{m}_{sink,nom}} \right)^{c} + d \tag{5.2}$$

The following two plots in the Figures 5.2 and 5.3 depict the simulation results (one day, ten second time steps). Further results and the validation can be found in Chapter 8.

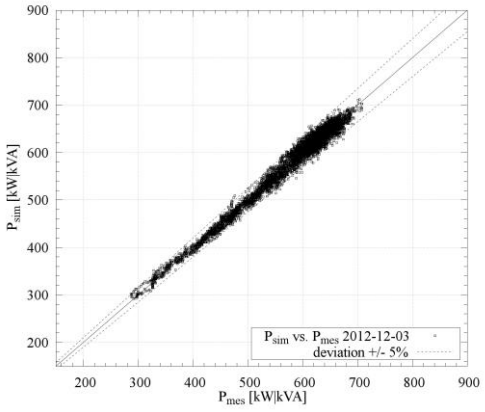

Figure 5.2: simulated vs. measured

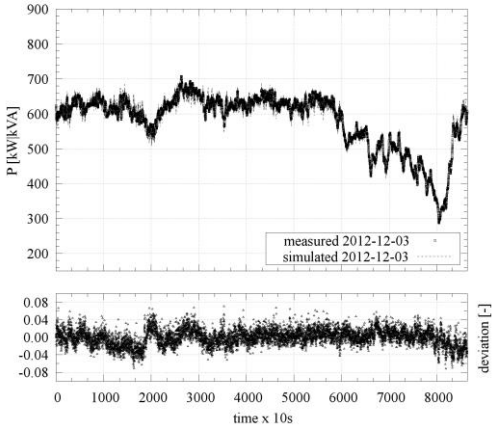

Figure 5.3: simulated and measured electrical output of ORC-unit electrical output and deviation of ORCunit vs. time

Table 5.2: fitting results for empirical cycle correlation

coefficient	a	η_s	c		η_{mech}	$\dot{m}_{sink,nom}$
value	0.5	0.78	0.25		0.98	63kg/s
	$P_{mes,mean}$	515.35KVA				
	$P_{sim,mean}$	509.58KVA				
	PPMCC	adj. R^2	$\epsilon_{min,rel}$	$\epsilon_{max,rel}$		ϵ_{mean}

[1] For a constant speed drive train, the mechanical loss could be set to a fixed value across the whole load range, for instance 20kW.

0.9884	0.9678	+7.71%	-37.81%	-1.12%

5.1.2 Steady-state modelling

For many engineering related questions a steady-state model is sufficient to give an answer. In early planning phase of a power plant as well as in the calculation and design of single components (heat exchangers, pipes) this model type comes to use. When a medium sized co-generation power station is developed, a classic top down approach is applied. The annual heat demand of the users is estimated either by existing energy bills or by building simulation. Based on (mostly) hourly climate time series of the location the load distribution is deduced. In most cases this would be the basis for the design of the furnace and co-generation unit. Based on mean source and sink temperatures the energy conversion potential of a cycle type can be derived. The degree of detail of such hourly calculation cannot deliver system control parameters with a satisfying quality. The common calculation methods for steady-state, such as NTU or LMTD, are shown in standard literature [63].

5.1.3 Dynamic modelling

The main focus of this work is on the dynamic modelling of the ORC. It provides the opportunity to take the transient behaviour of complex systems into account. The strategies and techniques are described in the following sections.

5.2 Modelling software

This section provides an overview on the used modelling techniques and software packages that have been used during the course of this thesis.

5.2.1 MATLAB

During the modelling process MATLAB of MathWorks has been used. In order to find correlations for the heat transfer processes as well as for the mechanical components. First of all code to access the REFPROP-Library has been implemented. With a package provided by NIST the property functions provided by the REPPROP.DLL can be accessed. In its original version the functions have been processed in the original Fortran code. For more compatibility and better performance the code has been translated to native MATLAB code by Wait in 2011. The bus-routines are called via the function refprop.m with relays the

request to rp proto.m . Here the calls are assigned to the .DLL via a standard call. The requested properties of a single, unmixed fluid can be computed with a command as the following:

```
result=refpropm ( prop_req ,  spec1 ,  value1 ,  spec2 ,  value2 ,  substance1 ) ;
```

The requested property can be chosen out of 36 available. As syntax the function demands strings for the property, spec1, spec2 and substance. For instance, an enthalpy calculation for MDM at a pressure of 1bar and 298.15K would be the following command:

```
enthalpy (: ,1)=refpropm ("H" ,"P" ,100 ,"T" ,298.15 ,"MDM") ;
```

By using this package all relevant properties for heat transfer calculations can be processed. For the modelled aggregates of the cycle this procedure has been used with monitored data sets. After calculating a set of fluid properties for each day of monitored data the files have been used for modelling, fitting, calibration and validation.

5.2.2 EES

For the calculation of linear systems the Engineering Equation Solver (EES) has been used. The necessary fluid calculations have been implemented using an external DLL. The DLL contains an implementation of the REFPROP-library for Siloxanes and water as well as custom equations for thermal oil.

5.2.3 modelica

Modelica is a non-proprietary, object-oriented, equation based programming language. It was designed to model complex physical systems containing mechanical, electrical, electronic, hydraulic and thermal systems. The modelica design effort was initiated in September 1996 by Hilding Elmqvist. One goal was the development an object-oriented language for modelling dynamic technical systems in order to reuse, extend and exchange models in a standardized format. The following basic concepts are part of the modelica language:

- Physical systems are interconnected via interfaces that imitate the real physical connection. For instance a pipe has three connectors to transport

its information (temperature, pressure, mass flow or pressure, enthalpy, mass flow)

- The definition of models in an a-casual form, permitting reuse, abstraction and unconditional connection.
- The mutual independence of the model interface and its internal description.

Modelica is a very universal approach to computational modelling and simulation, by being able to represent a range of application areas and providing general notation as well as powerful abstractions and efficient implementations. While modelica resembles object-oriented programming languages, such as C++ or Java, it differs in two important aspects: first, modelica is rather a modelling language than a conventional programming language. Modelica classes are not compiled in the usual sense, but are translated into objects that are then exercised by the simulation engine. The modelica view on object-orientation is different as the modelica language emphasizes structured mathematical modelling. A modelica model is primarily a declarative mathematical description, which simplifies further analysis. Dynamic system properties are expressed in a declarative way through equations [64]. For the usage as wide range modelling environment, modelica has some features that support dynamic modelling by nature. Such as:

- A-causal, declarative modelling: each component model is described by a set of algebraic, differential, and event-triggered equations, which describes how the modelled object behaves. The boundary conditions (pressures, temperatures, flow rates) are not necessarily declared a-priori as input or outputs. This is essential, to achieve truly object-oriented modelling of physical systems, since the model of a physical system is always the same, no matter how the adjacent system look like.
- Code transparency: instead of closed models, the declarative approach allows the model code to be written in away that equations are written on paper, without bothering how the equations will eventually be solved.
- Encapsulation: the models of system components are connected through pre-defined interfaces or connectors (for instance: fluid connectors with pressure, flow rate, and enthalpy).

- Inheritance: as a hierarchical structure, complex models can be obtained by extending the behaviour and properties of an existing class. It is then possible to reuse the variable declarations, equations and other contents of a family of base components (e.g. pumps or valves) in a derived class.

- Re-usability. At the component level, it is often possible to re-use models provided by standard libraries, by simply developing a few specific components with ad-hoc modelling if needed. At the system level it is possible to easily manage a family of models with different accuracy and simulation speeds. This allows for a straightforward system for model construction out of re-usable components, just by replacing and reconnecting individual components using uncomplicated re-configurations.

- Flexibility: models of power plant components can have a widely varying complexity, depending on the desired degree of detail. On the other hand, their boundary connections essentially fall under three categories: fluid flange connections, thermal transfer between zero or one-dimensional objects, and mechanical flanges. Therefore, it is possible to define standard connectors for these types of interfaces, or even to re-use pre-defined interfaces.

- Modularity: for the development of the single components of a system, it is possible to build the model of a plant unit by connecting the models of its physical components in any way that makes physical sense and with an arbitrary number of hierarchical levels.

5.3 Applied modelling strategies

5.3.1 Scope

The scope of the models developed in this work:

- Generate single component models that are suitable for parametric studies.

- Setup of partial models, such as the hot side and the cold side of the plant, in order to validate.

- Setup entire model of a cycle to improve in terms of: electric efficiency, thermal efficiency, control behaviour.

The desired output variables for an economical and technical assessment are:

- Mechanical power of the turbine.
- Electric gross and net output of the alternator unit.
- Auxiliary power demand related with the feed-pump.

It is inefficient to set-up a model with a higher degree of detail than necessary to answer the question the model was indented for. The proper degree of detail is achieved as soon as the actual questioning can be answered. However, within this work some details are already included as a basis for further development. For instance, the variation in the rotation frequency of the electric grid is set as a constant parameter. It can be used as a variable input in order to take the variation of the grid frequency (including rotational dynamics) into consideration.

5.3.2 Boundaries

In the focus of this work is the optimisation of a certain type the ORC-unit. Therefore the control and demand of the district heating are given. Furthermore, the detailed behaviour of the biomass furnace is not part of the model. The interaction of the cycle with its ambient is not taken into account (for instance: temperature in the turbine house). The frequency control of the alternator is assumed to be given as well.

5.3.3 Time-scales and time-steps

A basic criterion for all modelling activities are step size and simulation duration. As a compromise between validation data and the necessities for dynamic simulation the data time step has been (mainly) set to 10 seconds. A useful duration for a dynamic model for the case at hand would be in the range of one hour to a week. For many questions concerning user behaviour and demand profiles a duration of one day can be sufficient as well.

5.4 Modelling of solid material properties

5.4.1 Steel

As in most large engineering applications steel plays an import role in the ORCSystem. The major parts of the heat exchange surfaces and vessel material are manufactured from steel sheets and pipes of the types P235GH, P265GH and St 35.8 I (DIN 17175). Those steel classes are generally known as boiler steels. Alloyed steel has advantages in the field of corrosion, but due to the high prices such materials are only applicable in small ORC-units. In serial production of medium and large units the material price is the most dominant cost factor for heat exchangers. In this case study the module mainly consists of boiler steel. For the calculation of embedded metal masses in heat transfer processes a material density of steel of 7850kg/m^3 has been used. However, more interesting are the thermal properties of the material:

Table 5.3: thermal properties of various steel categories

DIN Code	Name	20 °C	100 °C	200 °C	300 °C	400 °C
-	-	[W/mK]	[W/mK]	[W/mK]	[W/mK]	[W/mK]
1.0305	St35.8	57	57	54	50	45
1.0315	St37.8	57	57	54	50	45
1.0345	P235 GH	55	55	51	48	44
1.0402	C22	55-61	-	-	-	-
1.0425	P265 GH	55	55	51	48	44

Based on those values polynomials have been fitted and integrated into VBA for MS Excel, MatLab and modelica sub-routines. The source code can be found in the Appendix A under Solids properties.

5.4.2 Aluminium

Aluminium and its alloys play an inferior role for structurally relevant parts. For industrial applications weight saving is mostly not important. In the naval or mobile sector this may be more of interest. However, the good heat conduction of aluminium is used for surface enhancements in heat exchangers, such as baffles and fins. In the case at hands the finning of the recuperator tubes is made of aluminium Al 99.5 (EW AW-1050 / 1200). The used properties of aluminium are:

Table 5.4: thermal conductivity of AL99.5

DIN Code	Name	th. conductivity	heat capacity	density
-	-	[W/mK]	[J/kgK]	[kg/m^3]
3.0255	EN- AW-1050A	220	900	2700

5.5 Modelling of fluid properties

5.5.1 Equations of state (EOS)

In chemical and energy engineering, design and simulation of fluid properties has become a indispensable part. From simple correlations to sophisticated physical energy and transport models, an wide range of methods is available. It is up to the user (engineer), to find an appropriate fluid computation method. One has to define the constraints such as the desired properties and flexibility and make a compromise with accuracy, availability and complexity. Over more than 100 years, various different and more or less related approaches to EOS have been developed. An assortment of different approaches and their development and interrelation is depicted in Figure 5.4. The general answer to the question which approach is the best is not possible. Many reasons, not only technical ones, have led to this variety in EOS. Wei and Sadus [9] attribute this to the fact that inter-EOS comparisons are rare and many scientist may be blinkered and focused on the EOS they are familiar with. For this work the criteria are: availability of an implementation, accuracy, consistency and computational speed. Nowadays, with powerful computer systems, the accuracy of EOSes has become less of a problem.

Since Emile Clapeyron in 1834 concluded the Boyle-Mariotte law and Charles'' law of volumes to the Ideal Gas Law scientists have consequently improved the understanding of fluids. Johannes Diderik van der Waals, in his doctoral thesis (published in 1873), came up with the interaction of attraction forces of molecules. This resulted in the first EOS predicting the coexistence of liquid and vapour [9]. His Real Gas Equation is the basis for many following equations of state.

$$R \times T = \left(p + \frac{a}{V_m^2}\right) \times (V_m - b) \tag{5.3}$$

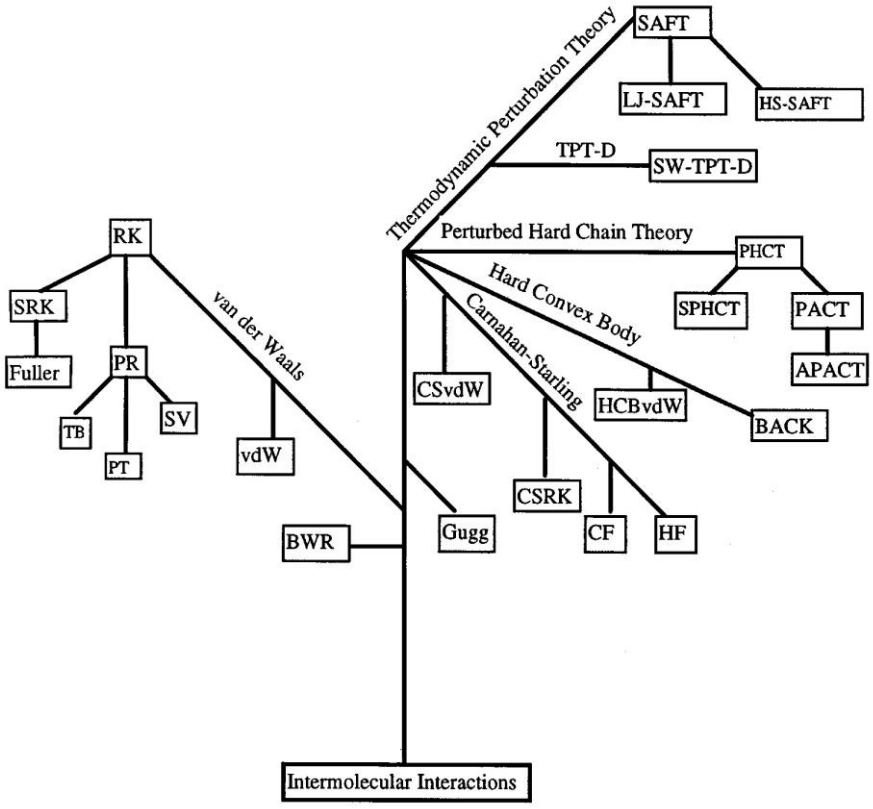

Figure 5.4: development and inter-relation of EOS [9]

The idea of relating the EOS to several physical parameters of a fluid was introduced. The molar mass, the critical pressure and critical temperature could be reasonably well measured for each fluid. However, this equation gives only good results for non-polar fluids in a low temperature range.

$$a = \frac{27 \times R^2 \times T_c^2}{64 \times p_c}; b = \frac{R^2 \times T_c^2}{8 \times p_c} \tag{5.4}$$

The two parameters a (attraction parameter or cohesive pressure) and b (the co-volume, as well called excluded volume) represent the inter-molecular behaviour. For quite a long time this EOS was the state of the art.

5.5.1.1 Virial EOSes (Benedict-Webb-Rubin)

Virial equations of state are based on a larger number of parameters than cubic EOS. In the development of EOS from van der Waals on to today two strategies have been followed: reasonable complexity and reasonable accuracy versus higher complexity and higher accuracy. Onnes [65] expressed the ideal gas law using the virial theorem. It is based upon statistic mechanics, where kinetic

energy of a number of atoms or molecules corresponds to temperature. The virial equations are composed from different terms of interactions. This idea is base on perturbation theory. With increasing complexity (orders of n) the equation of state becomes more accurate. Benedict, Webb and Rubin worked at the improvement of this theory. By altering and extending the Beattie-Bridgeman equation they found a very accurate EOS for several hydro-carbons [66].

$$p = RT \times \rho + f_1(R,T) \times \rho^2 + f_2(R,T) \times \rho^3 + f_3(\alpha,a) \times \rho^6 + f_4(p_c,T) \times \rho^3 \tag{5.5}$$

This original equation has been modified and extended by many others. From the former eight parameter equation nowadays versions with 30 or more parameters can be found in literature. The results of virial EOS are usually of good quality at low and medium densities and low pressures.

5.5.1.2 Soave-Redlich-Kwong (SRK)

In the field of cubic EOS Redlich and Kwong developed their formula with a few parameters less compared to the virial approach. With just two empirical parameters that can be fitted from measured data, this formulation achieves a reasonable accuracy if the reduced pressure is less than half of the according reduces temperature of the calculated state.

$$p = \frac{R \times T}{V_m - b} - \frac{a}{\sqrt{T} \times V_m\,(v_m + b)} \tag{5.6}$$

In 1972, Soave [67] improved the above theory by introducing an additional term which contains the Acentric Factor α as a function of the temperature. This factor accounts for the non-spherical characteristics of larger molecules.

$$p = \frac{R \times T}{V_m - b} - \frac{a \times \alpha}{V_m\,(v_m + b)} \tag{5.7}$$

5.5.1.3 Peng-Robinson (PR)

The Peng-Robinson EOS (PR) performs similar to SRK-EOS, except for the calculation of the density of non-polar compounds which is a real advantage when it comes to Siloxanes. Just four years after Soave, Peng and Robinson [68] came up with their EOS. Taking the suggestion of Soave and extending his approach by

a quadratic term, they received an expression with even higher accuracy. In case of non-polar fluids, such as many organics, the density results are fairly better.

$$p = \frac{R \times T}{V_m - b} - \frac{a \times \alpha}{V_m^2 + 2 \times b \times V_m - b^2} \tag{5.8}$$

where

$$a = \frac{0.457235 \times R^2 \times T_c^2}{p_c}$$
$$b = \frac{0.457235 \times R \times T_c}{p_c}$$
$$\alpha = \left(1 + \kappa\left(1 - \sqrt{T_r}\right)\right)^2$$
$$\kappa = 0.37464 + 1.54226 \times \omega - 0.26992 \times \omega^2$$

5.5.1.4 Peng-Robinson-Stryjek-Vera (PR-SV)

As well as other EOS, the PR-EOS has been steadily improved. Ten years after Peng and Robinson, Stryjek and Vera [69] extended the definition of κ. The original κ of PR was now redefined as a polynomial of third order (instead of two). Furthermore, a second κ-function was introduced. With this, so called "pure component parameter", a more realistic behaviour could be modelled for many fluids. For the sake of completeness, the final stage of development has to be mentioned as well. In order to improve accuracy in the two-phase region two more κ_i parameters where added to the κ definition. In comparison to experimental data these formations perform within a deviation of 2% [70].

$$\kappa = \kappa_0 + \kappa_1 \times \left(1 + \sqrt{T_r}\right)(0.7 - T_r) \tag{5.9}$$

and finally and most complex version of the PRSV-EOS:

$$\kappa = \kappa_0 + \left[\kappa_1 + \kappa_2 \times (\kappa_3 - T_r) \times \left(1 - \sqrt{T_r}\right)\right] \times \left(1 + \sqrt{T_r}\right)(0.7 - T_r) \tag{5.10}$$

where for both versions κ_0 is defined by a polynomial function of the Acentric Factor ω:

$$\kappa_0 = 0.378893 + 1.4897153 \times \omega - 0.17131848 \times \omega^2 + 0.0196553 \times \omega^3 \tag{5.11}$$

5.5.2 Multi-parameter equations of state

In order to reach higher accuracies and set up coherent and arithmetically stable EOS, large advances have been made over the last years. Most of the above

introduced correlations deliver fairly good results, that are sufficient for the most engineering tasks. However, dynamical simulations demand better properties quality. Stability of equations becomes important when the number of iterations increase. Many multi-parameter EOS are based on the Helmholtz Energy, describing the total energy potential in a fluid in equilibrium with its ambient. The Span and Wagner formulation [71, 72] for a fluid under thermodynamic conditions (no electric or magnetic energy involved) divides the total Helmholtz Energy into an ideal gas term and a real gas term (residual energy):

$$\frac{E(T,\rho)}{RT} = E^0(T_r,\rho_r) + E^r(T_r,\rho_r) \tag{5.12}$$

Where the ideal Helmholtz Energy is defined as a function of the ideal heat capacity. The total ideal enthalpy is the sum of the reference state (h_0,s_0, et cetera) and integral of the ideal heat capacity with respect to the temperature:

$$\begin{aligned} E^0 = {} & \frac{h_0 \times T_r}{R \times T_c} - \frac{s_0}{R} - 1 + ln\left(\frac{T_{r,0} \times \rho}{\rho_0 \times T_r}\right) \\ & - \frac{T_r}{R} \times \int_{T_r,0}^{T_r} \frac{c_p}{T_r^2} dT_r \frac{1}{R} \times \int_{T_r,0}^{T_r} \frac{c_p}{T_r} dT_r \end{aligned} \tag{5.13}$$

5.5.2.1 BACKONE-EOS

BACKONE is an physically based implementation of the Helmholtz Energy. Molecular interactions are expressed by a sum of contributors each standing for a characteristic type of interaction. In this case the interactions are categorized in hard-body, polar and attractive dispersion forces. Low number of coefficients,and therefore fast computation make it interesting for long term simulations.

$$F = F_H + F_A + F_{pol} \tag{5.14}$$

For sake of completeness, it has to be mentioned that BACKONE is the latest in a row of BACK-type EOS (MOBACK, DIBACK, QUABACK). Detailed information on this topic are given by Weingerl, Wendland, Fischer [73], Mueller and Winkelmann [74].

5.5.2.2 SAFT-EOS

The Statistical Associating Fluid Theory (SAFT) proposes a model consisting of an ideal term and a residual term expressed as reduced Helmholtz Energy. The residual term accounts for different class of inter-molecular forces expressed in

three terms of interaction: segmental interaction, chain formation and association interactions.

$$\frac{A}{N \times k \times T} = \frac{A^{id}}{N \times k \times T} + \frac{A^{seg}}{N \times k \times T} + \frac{A^{chn}}{N \times k \times T} + \frac{A^{ass}}{N \times k \times T} \qquad (5.15)$$

This formulation uses the chemical nomenclature for the Helmholtz Energy which is A instead of F. Details on SAFT as an EOS can be taken from the publications of Chapman et al. [75–77] or Wei et al. [9]. Huang and Radosz have worked on modified versions. The according parameters for Siloxane compounds have been determined by Lai, Wendland and Fischer [27, 78]. The basis of measured values (for instance Lindley and Hershey) they used in their work is mainly the same as Nannan et al. [79] have used for their EOS for Siloxanes. Oyewunmi et al. [30] have used the SAFT method to predict and assess the potential of fluid mixtures in waste heat recovery ORC applications.

5.5.3 Cycle fluid

In the facility in Scharnhauser Park the medium R200(1cSt)^{R}, produced by Dow Corning, is used as working fluid in the vapour process. The chemical term for this, approximately (and hopefully) 100% pure substance, is Octamethyltrisiloxane or abbreviated MDM (respectively OMTS).

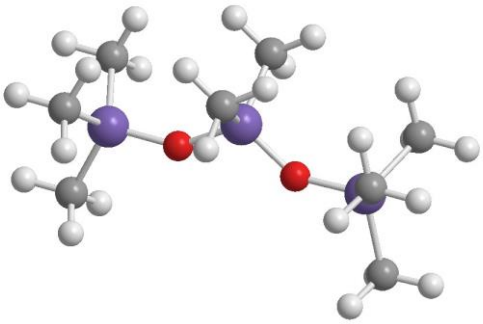

Figure 5.5: ball-and-stick model of MDM-molecule

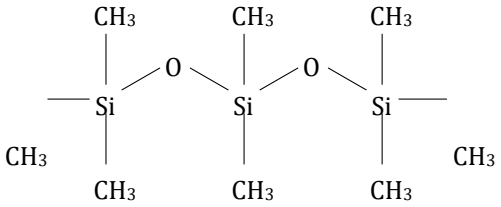

Figure 5.6: 2D molecular structure of MDM

MDM is a non-polar chain of three siloxy-groups saturated by eight methylgroups. The substance has a quite low surface tension and tends to evaporate quickly. MDM is hydrophobic. In a temperature range above 300 °C the material is likely to start a chemical decomposition process. However, in the temperature range below it is fairly stable. For humans MDM is almost non-

toxic, it is widely used as solvent and matrix in cosmetic products like deodorants and lipsticks. Some report a tendency to form formaldehyde in contact with air at temperatures above 150 °C [80]. If water is present the formaldehyde can react to to formic acid. MDM is weakly inflammable (category R10) and may form explosive gases (category H226). The flashpoint temperature is 29 °C. The critical state of MDM is relatively low in comparison to other fluids used in vapour cycles. Flannigan reports a critical temperature of 564.4K and a critical pressure of 14.4bar. These values are reported by DIPPR [81] with reference to Dickinson et al. [82], the values have been widely accepted for a long time. Colonna, Nannan, Guardone and Lemmon [83] proofed that Lindsey and Hershey's measured values have the best accuracy. Despite the fact that the purity of their measuring samples was not fully clear, the amount and distribution of the data seemed favourable. Their EOS based on the short Helmholtz EOS is accepted by REFPROP [84]. Based on that, a critical point of 14.15bar and 564.09K is used in this work. The molar mass of MDM, with a value of 236.534g/mol [85], is more than 13 times higher than the molar mass of water. The enclosed table shows the most important constants of MDM:

Table 5.5: properties of MDM

property	symbol	value	unit	reference
critical pressure	p_c	14.15	bar	[70, 84]
critical temperature	T_c	564.09	K	[70, 84]
critical volume	V_c	3.895	l/kg	[70, 84]
acentric factor	ω	0.532783	-	[81]
critical density	ρ_c	256.74	kg/m³	[70, 84]
critical compressibility	Z_c	0.266	-	[81]
normal boiling point	T_{b0}	425.66	K	[70, 84]
melting point	T_m^0	187.2	K	[70, 84]

Further properties data can be found in the Appendix A and in Chapter 5.5.1.

5.5.3.1 Vapour pressure

Within the latest version of REFPROP the Wagner-Ambrose-Equation is being used as follows:

$$ln\left(p_{sat,r}\right) = \frac{a \times \Theta + b \times \Theta^{1.5} + c \times \Theta^{2.5} + d \times \Theta^{5}}{T_r} \tag{5.16}$$

$\Theta = 1 - T_r$ is the complementary reduced temperature.

Table 5.6: Wagner-Ambrose parameters for MDM

fluid	a	b	c	d
MDM	-8.6693	2.2965	-4.4658	-8.4529

? further parameters can be found in Colonna et al. [70]

5.5.3.2 Surface tension

In order to find correlations for boiling and condensation the bubble and droplet parameters are crucial. For an accurate computation surface tension is necessary. The measured values in a higher range are rare, as the main interest in those values are production and product behaviour in chemical and pharmaceutical industry. However a few values in the range of 293K to 363K could be obtained. The results are shown in Figure 5.7. The values have been contributed by various authors over many years [86–93].

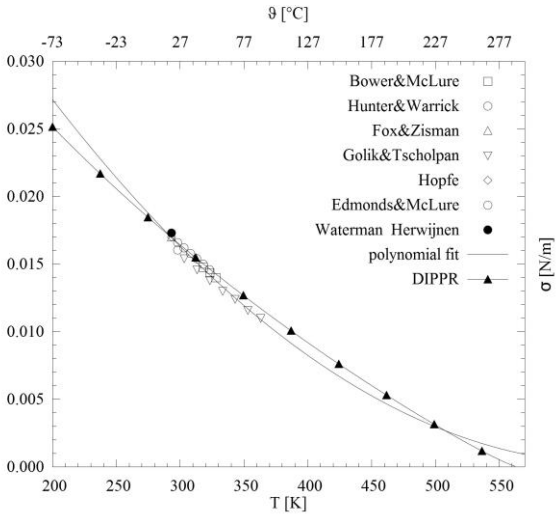

Figure 5.7: surface tension of liquid MDM

Equation 5.17 shows the polynomial used in the above diagram. For the calculations of boiling and condensation heat transfer this polynomial equation has been used.

$$\sigma(T[K]) = 0.0572338 - T \times 0.000178179 + T^2 \times 1.39317e^{-7} \tag{5.17}$$

5.5.4 Thermal oil

As a heat transfer agent between furnace and ORC-module a thermal oil is used. Consisting of a mixture of various Therphenyl compounds the matter has a widely stable temperature behaviour. In this case the mixture called Therminol66™ by the company of Solutia guarantees safe operation up to 355 °C [42]. The common operation range within this power plant is 200 °C to 300 °C (feed evaporator). In detail the fluid consists mainly of hydrogenated Terphenyl (CAS 61788-32-7, 74% to 87%), as well as partially hydrogenated Quarterphenyls and Polyphenyls (CAS
68956-74-1, up to 18%). The smallest share is pure Terphenyl (CAS 26140-60-3, 3% to 8%). The average molar mass of the mixture is 252g/mol [44]. Thermal oils are usually inflammable, which leads to a certain danger in case of leakage or pipe rupture. Hot spots due to temperature peaks, respectively a loss of pump power, can lead to evaporation. Being released in gaseous state to ambient atmosphere leads to self-ignition. Based upon the specifications and measured values of the manufacturer, functions for the use in VBA, MatLab and as DLL (used in EES) have been fitted. Furthermore, look-up tables have been created, which have been implemented in modelica. In this chapter the procedure and approaches are explained. One of the basic requirements for thermal simulations is the heat capacity of a matter. In an ideal approach the specific heat capacity would be computed as a function of the temperature and the applied pressure. In this case however, the system can be simplified. During the operation of a heat carrier evaporation as such must never occur (if so, an explosion would be the consequence). The simulation range is within the specifications of the manufacturer.

- Specific ideal heat capacity: The pressure in the transfer cycle remains almost stable on a certain level, no change of phase occurs. Real-gas deviations in heat capacity are not relevant.
- Density
- Ideal specific enthalpy: integration of the ideal heat capacity function over the domain of temperature.
- Thermal conductivity
- Viscosity

With the above properties the fluid is fully defined and Reynolds and Prandtl numbers can be derived as well.

5.5.4.1 Density

According to the specifications of the manufacturer the density of Therminol66 ® is described by a third degree polynomial.

$$\rho[kg/m^3] = a + b \times \vartheta + c \times \vartheta^2 \tag{5.18}$$

coefficient	a	b	c
value	1020.4	-0.619	-0.0003

5.5.4.2 Specific heat capacity and specific enthalpy

The specific enthalpy is required if a fluid is used in the class context of modelica. Solely using the specific heat capacity is not sufficient. As there was no library available in modelica, property look-up tables have been created as instance of the class “Modelica.Media.Incompressible.Table”. The following table shows the results of the validation of the Therminol66 ® library:

Table 5.7: calculated and given enthalpy values for Therminol66 ®

ϑ °C	h_{sim} [J/kg]	h [J/kg]	deviation [%]
120	204102	203891	0.103%
140	242943	242729	0.088%
160	283209	282992	0.077%
180	324916	324695	0.068%
200	368078	367853	0.061%
220	412708	412480	0.055%
240	458822	458589	0.051%
260	506433	506196	0.047%

280	555557	555315	0.044%
300	606206	605960	0.041%
320	658397	658146	0.038%

$$c_p[kJ/kg] = a + b \times \vartheta + c \times \vartheta^2 \tag{5.19}$$

coefficient	a	b	c
value	1.496005	$3.313e^{-3}$	$-0.8970785e^{-6}$

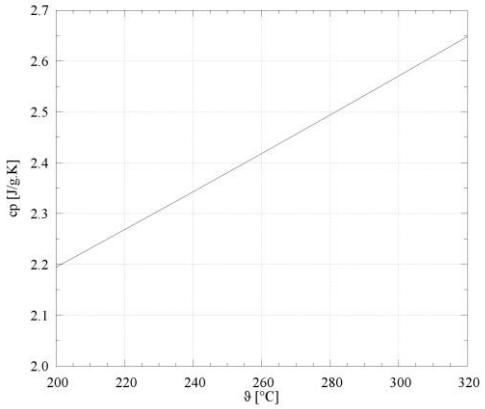

Figure 5.8: specific ideal heat capacity of T66

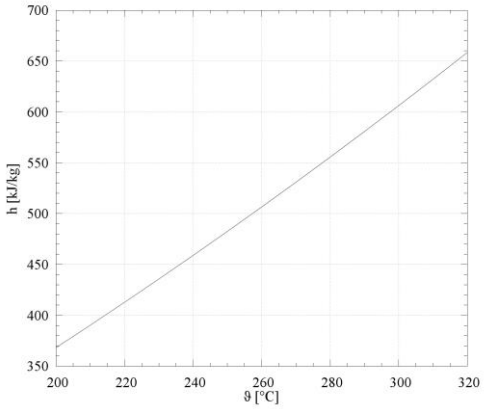

Figure 5.9: specific ideal enthalpy of T66

5.5.4.3 Transport properties

To obtain the behaviour of a fluid regarding friction and heat transfer the property of viscosity plays an important role. According to the Therminol66 ᴿ Bulletins [42–44, 94] kinematic and dynamic viscosities have been derived as follows:

$$\nu[Pas] = \mu[cSt] \times \rho^{-1} = e^{\frac{a}{b+\vartheta}+c} \times \rho^{-1} \tag{5.20}$$

coefficient	a	b	c
value	586.375	62.5	-2.2809

For further characterisation of the fluid the thermal conductivity has to be introduced as a scale for the heat transport ability of a bulk of fluid apart from the convective layer. According to data of the manufacturer the ability to transport heat can be described with a polynomial:

$$\lambda[W/mK] = a + b \times \vartheta + c \times \vartheta^2 \tag{5.21}$$

coefficient	a	b	c
value	0.118294	$-3.3e^{-5}$	$1.5e^{-7}$

The following two Figures 5.10 and 5.11 show the viscosities and the thermal conductivity of the thermal oil across the relevant temperature range.

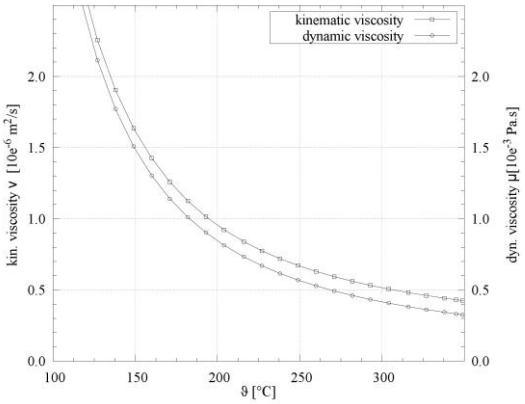

Figure 5.10: viscosities of liquid T66 vs. temperature

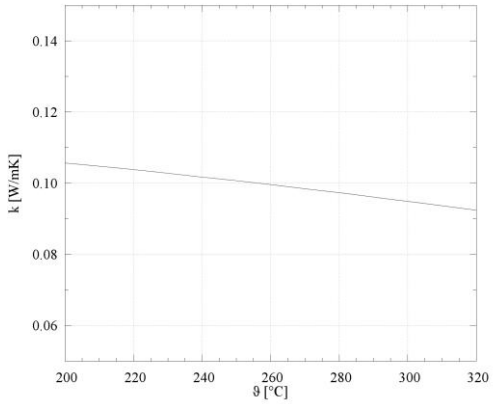

Figure 5.11: thermal conductivity of liquid T66 vs. temperature

Based on the above depicted transport properties, the Figures 5.12 and 5.13 return the Reynolds numbers and Darcy-Weisbach friction factor for a DN16 tube flow. Four different friction correlations are compared.

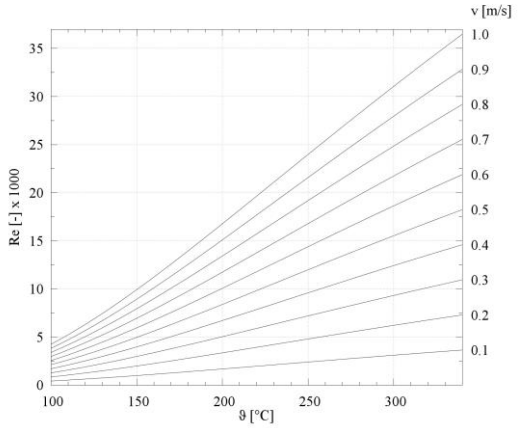

Figure 5.12: Reynolds numbers of T66 vs. temperature

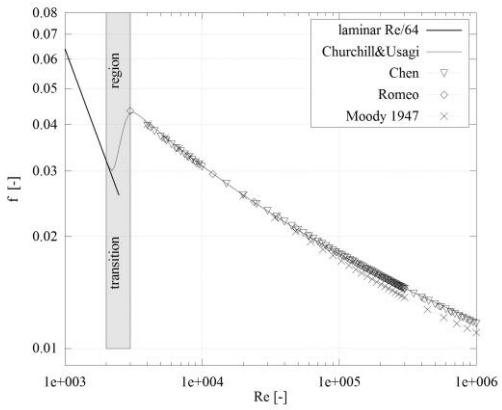

Figure 5.13: Darcy-Weisbach friction factor of T66 in a DN16 tube vs. Re

5.5.5 Water

For the calculation of the sink system, properties of water are required. Within this work the IAPWS Formulations are used (release of 1995). This most recent formulation for water is based on a multi-parameter EOS. Wagner and Pruss [95] released the latest update for most properties. The accuracy is outstanding, compared to other fluid property models. The thermal conductivity of water is given by the 2011 update of IAPWS as described in [96] by Huber et al. Viscosity values are based on the 2008 update [97].

5.6 Fluid properties for dynamic simulation

5.6.1 Cycle fluid and implementation of fluid data

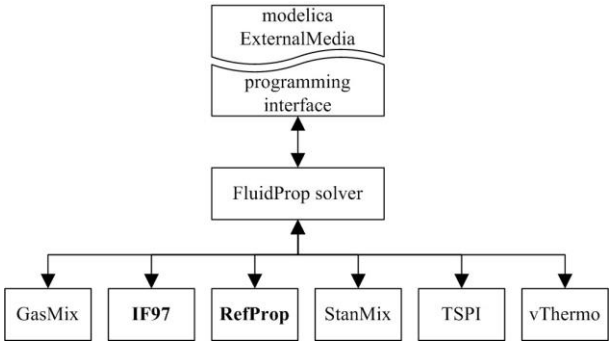

Figure 5.14: data structure of thermodynamic library [FluidProp]

The ExternalMedia library by Richter, Casella et al. [98] offers a broad spectrum of thermodynamic properties by implementing external data sources.

ExternalMedia is a quasi-standard. According to the modelica language specifications and class structure other media than the ones that are built in by default can be used. The library, as depicted in Figure 5.14, can be connected to the FluidProp solver which has been developed by Colonna, van der Stelt et al. [99]. This solver comprises different sub-programs and data bases and offers a similar programming interface for various code languages and dialects such as:

- Microsoft Excel: implementation as Add-in “Fluidprop.xla”, current version 2.4.0.51
- MATLAB and Simulink of Mathworks, programmed by Lux [100]
- Fortran: Intel Visual Fortran, Compaq Visual Fortran
- c++: Microsoft Visual c++, Borland c++

Besides the wide range of fluids and mixtures the package offers the use of the same basic code and library across many platforms and programs. Therefore inconsistencies of calculations are practically not existing. At the same time a dynamic model and a steady-state model could be calculated and compared using for instance modelica, MATLAB, MS Excel or CycleTempo. The following code snippet shows the implementation of MDM in modelica via the ExternalMedia library.

```
package MDM extends Externalmedia.media.ExternalTwoPhasemedium
   ( mediumName = "MDM" ,
      libraryName = "FluidProp.RefProp" , substanceNames = {"MDM"})
      ;

// These functions will not be used due to model settings ,
// but need to be defined in order to avoid compiler errors redeclare function extends
    density pT der algorithm assert ( false , "Error : MDM.density pT der is not
    implemented") ; d_der := 0;
    end density pT der ; end
MDM;
```

5.6.2 Other fluid computation approaches

Besides the commercial or semi-commercial applications REFPROP and FluidProp, other developers are working on fluid data for simulation programs. In this context the Tilmedia and CoolProp package have to be mentioned. Tilmedia provides working fluids and solid materials. CoolProp is the attempt to offer an OpenSource package. It includes the approach of pre-compiled data sets, that are written into memory as a table and interpolated by a search algorithm. Bell, Wronski and Quoilin [101] have shown that a dynamic bezier solver is more efficient than the classic approach of calculating single states for each time step in terms of CPU power and calculation time.

5.7 Modelling strategy of heat transfer into the cycle

During this work two possible approaches for the heat transfer into the ORC have been investigated. Again, the level of detail is crucial for the relevance of the results. In case of the pre-heater and evaporator two possible strategies with different outcomes can be applied: in order to obtain single discrete models, both evaporator and pre-heater are observed separately. This strategy offers the possibility to have a detailed look at the behaviour of both components. In this way, physical changes to one of the heat exchangers can be calculated and predicted. The various regimes of heat transfer and phase change can be calculated and correlated separately. On the other hand, the calculation is more complex and for validation more sensors are needed. In the case at hand, the states of the working fluid before the pre-heater and after the evaporator are fully determined. Furthermore, a temperature sensor between pre-heater and evaporator has been added in the course of the monitoring. Unfortunately, on the

source side only two sensors for feed and return temperature are available. A third one for the temperature between pre-heater and evaporator could not be installed. In order to obtain a calculation and a validation data set for the two aggregates the missing state had to be computed using the energy balance. The use of this synthetic data set might cause additional deviations. One way to avoid this case is a monolithic model of the two components. For the entire cycle calculation the internal processes in the heat exchangers are not relevant, solely the resulting state. On more point for this approach is the fact that the mass flows through the two components are equal. As a consequence pre-heater and evaporator could be seen as one component. By doing so, the comparability with other models, especially heat transfer correlations, in literature gets lost. For the sake of completeness one fact has to be mentioned in this section: besides the two above heat exchangers the cycle is equipped with a so called "condensate evaporator". As the recuperator is a rather large vessel and cumulations of liquid MDM can not be avoided in such voluminous systems, this additional heat exchanger has been installed. Liquid cycle fluid that collects in the very bottom of the recuperator shell is evaporated at turbine outlet pressure. A loop of one inch tubes is situated at the bottom of the vessel. The hot side (inside) of the tubes is connected to the return of the thermal oil (roughly 240 °C). In this way more fluid takes part in the process, the void portion of working fluid is reduced. The amount of heat being transferred into the cycle has been estimated to 150kW.

5.8 Heat transfer inside the cycle

Within the ORC-unit the following heat transfer processes take place:

- Recuperator: heat transfer from gas to liquid without phase change. The cold side is a regular, turbulent pipe flow (smooth surface). The hot side is a turbulent tube array flow with surface enhancement (aluminium fins). The heat is conducted through two materials, from the fins to the tube material (steel) they are attached to.

- Pre-heater: heat transfer from liquid to liquid without phase change in a PHE. In the pre-heater the heat is transferred from the hot side through thermal oil convection in a uniform flow channel. Conduction goes through the uniform constant steel wall. On the cold side the convection is identical to the hot side (except the fluid).

- Evaporator: heat transfer from liquid to liquid with phase change. On the hot side the convection can be described through a turbulent smooth pipe flow, for both boiling and super-heating section. The heat conduction through the surface material is tubular (steel tubes). On the cold side the transfer process can be described by a boiling and evaporation process for the liquid wetted part of the bundle. In the upper, non-wetted, tube rows a cross convection through a tube array takes place.
- Condenser: heat transfer from gas with phase change to a liquid. On the hot side partially turbulent film convection takes place. The conduction goes through a single material wall (steel). On the cold side of the tubes, again convection in turbulent pipe flow regime happens.
- Surfaces of vessels and tubing: heat transfer from gas or liquid to ambient through the conduction of the vessel material and the applied insulation material.

5.8.1 One-dimensional heat transfer

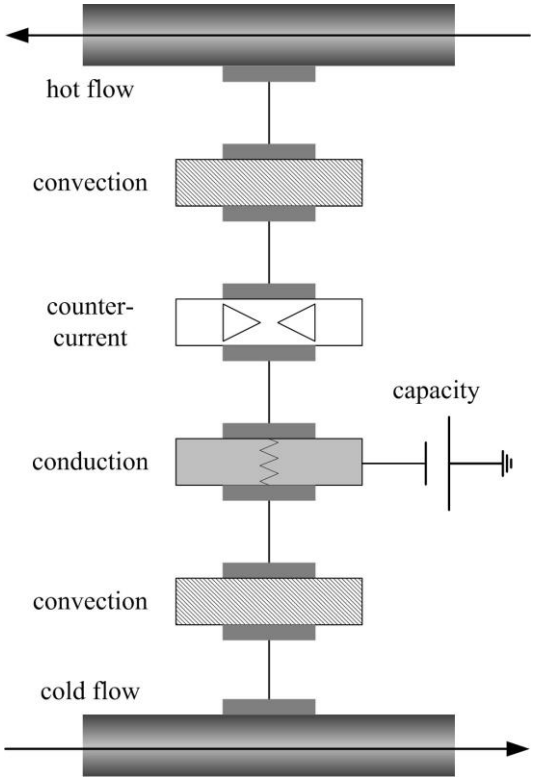

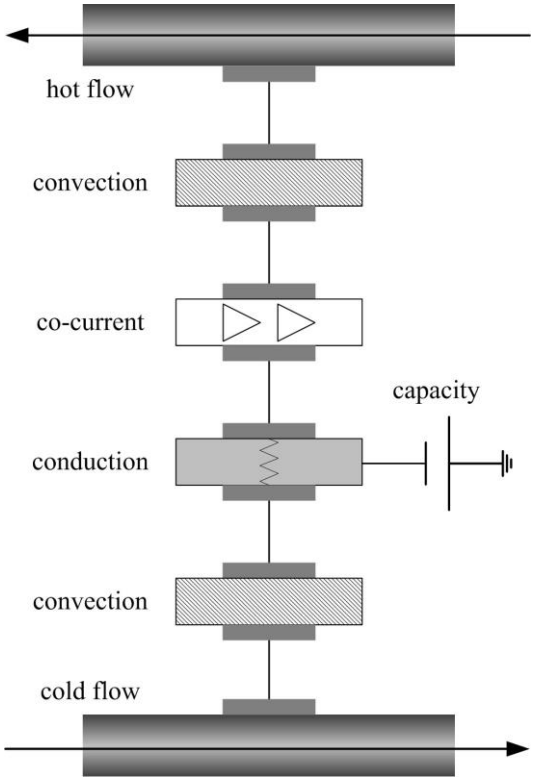

Figure 5.15: heat transfer model for 1D counter-current heat transfer

Figure 5.16: heat transfer model for 1D co-current heat transfer

Within the following sections the various heat transfer processes in the cycle will be dealt with. The fundamental model for all heat transfers is defined in the modelica 1D-HT class. It is based on the following assumptions:

- Hot and cold flow transport properties are independent from variations due to pressure changes.
- The only thermal inertia of the heat exchanger is concentrated in one node in the heat class. If not added externally, the capacity of shells is not respected. • In each node of the heat exchanger only single-phase heat exchange occurs.

hot/cold flow: the hot/cold flow classes define the geometrical and arithmetic properties of the hot side fluid. Characteristic length, surface, perimeter are defined. Furthermore, the modes for pressure drop and heat transfer calculation can be chosen or assigned to an external parameter.

convection: the convection classes reverse the heat flux for each node and serve as connectors.

current type: the current class swaps the heat flux of each node accordingly to the flow configuration. Flux 1 becomes flux n, flux n becomes flux n-1 and so forth. More details can be found in the documentation of modelica [102, 103].

conduction: the metal wall class arranges the thermal inertia of the heat exchanger. The difference of internal and external heat transfer surfaces can be respected within this class.

5.8.2 Pre-heater

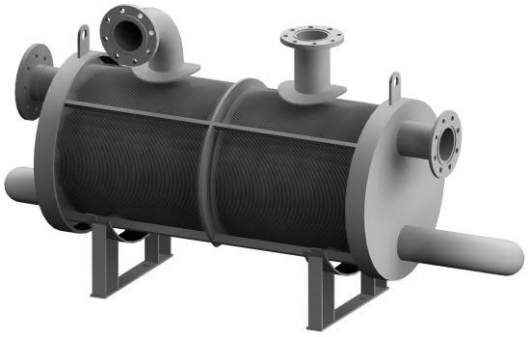

Figure 5.17: 3D-section view of the pre- heater (cutaway of shell)

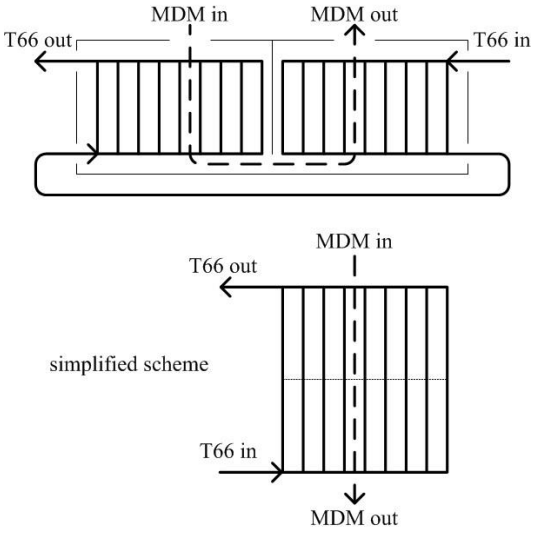

Figure 5.18: geometric simplification of heat transfer arrangement in pre-heater

The pre-heater is a compact, fully welded plate type (PSHE/HH476/2/2). All relevant properties of the unit are described in Table 5.8. The plate type counter flow characteristic of this unit provides a comparably high heat transfer density. Taking a look at the recuperator, approximately the same heat rate is transferred. The total volume of the pre-heater is approximately $1m^3$, while the recuperator sums up to more than $24m^3$. In the original design of the cycle the evaporator was a staggered two stage plate heat exchanger. One problem that comes with plate heat exchangers is sensitivity to vibrations. While liquid is boiling on a hot surface the vapour forms growing bubbles until the detachment diameter is reached. Consequently, the bubble flows reversal to gravity. On its way it collides with other bubbles that are still connected to the heated surface. A domino effect of

detaching bubbles starts. This effect is also called “galloping”. During this effect the plates are mechanically stressed. Welded plate stacks tend to crack when dynamic stress is applied: the plate stacks starts leaking. This effect is most likely when the plate distance is approximately one to three times the detachment diameter. In the case of MDM a plate heat pre-heater combined with a shell-and-tube type evaporator is the more robust design, but with a trade-off in module volume. An overview of all relevant design properties of the vessel is listed in Table 5.8. The values are either given by the manufacturer or based on calculations of the author.

Table 5.8: specifications of pre-heater

symbol	value	unit	description
Φ_{nom}	4115	kW	nom. heat rate
Δp_1	0.369	bar	nom. pressure loss, hot side
Δp_2	0.241	bar	nom. pressure loss, cold side
u_{nom}	642	W/m²K	design heat transfer coefficient
connector 1	DN150	-	flange hot side
connector 2	DN150	-	flange cold side
V_1	0.2537	m3	hot volume
V_2	0.3343	m3	cold volume
m_{dry}	3560	kg	weight net, dry
A_{trans}	212.1	m2	heat transfer area
k_f	0.000617	m²K/W	fouling factor
D_{out}	0.860	m	outer diameter of shell
L_{out}	1.734	m	length of shell
$\dot{m}_1$	40.91	kg/s	nom. mass flow hot side
$\dot{m}_2$	23.35	kg/s	nom. mass flow cold side

5.8.2.1 Heat transfer

As mentioned before the heat transfer area in the pre-heater is arranged as a stacks of welded disks. It is the only unit in the cycle that is not based on tubular heat exchanger surfaces. Due to that, there is a necessity for an other heat transfer calculation approach. In anticipation of the next chapter, no tube flow theories as Gnielinsky, Pethukov or Chen come to use. Furthermore, the HTRI correlation for

tubular boilers (recommended by the manufacturer of the thermal oil) cannot be used. The geometric arrangement of the unit is very particular. The tube contains two plate stacks connected from each of the outer sides. Thus, the unit basically consists of two heat exchangers. This is relevant in terms of thermal and pressure losses as the connection between the two stacks is longer than one large heat exchanger would be. However, for the calculation this plays an inferior role. In a first step the flow velocity on the primary side (thermal oil) has to be determined. Two constructive facts complicate this: the plate pattern and the flow pattern. From feed to the return the liquid will make its way with a certain statistical distribution across the plate. As a simplification a flow pattern, direction and mean velocity have to be defined. The velocity is based on the following assumptions:

- 50% of the plate stack volume are occupied by one fluid.
- 476 plates form two stacks of plates with 116 channels each. The stacks are impinged by the total mass flow for the thermal oil on the hot side.
- On the silicone oil side, the total mass flow goes through two serial volumes, each divided into 116 channels.
- The velocity is equally distributed across the width of the entire plate, therefore a mean velocity is used for calculation.
- The channel size on both sides of the heat exchanger is 5mm.
- The geometrical attribute for the Reynolds number is twice the channel height, ergo 10mm.
- The cross flow arrangement around the supply tubes is neglected, a pure counter-flow configuration is assumed.

One common approach to define the heat transfer coefficients in plate heat exchangers is based on the theory of channels. It is possible to compute the behaviour of a PHE to a great level of detail, for instance with CFD calculations like ANSYS CFX [104]. In this case a robust approach is needed to keep computational time to an acceptable amount, as before displayed in Chapter Modelling approaches. The approach chosen for the system in question is based on Nusselt's theory of similarity. For both sides of the heat exchanger coefficients for common

configurations and vessel types can be found. As a first approach the following formulation for a PHE can be taken for the two sides:

$$Nu_i = C \times Re^m \times Pr^n \left(\frac{\mu}{\mu_{wall}}\right)^x \tag{5.22}$$

where Nu is

$$Nu_i = \frac{\alpha_i \times L}{\lambda_i} \tag{5.23}$$

It can be assumed that the last term of the Equation 5.22 is approximately equal to unity. For instance the film heat transfer correlation, recommended by the manufacturer of the thermal oil [105], respects the influence of transport properties from wall to bulk for a temperature difference of 30K with the value 1.023. This factor can be included in the factor *C*. The overall heat transfer can be expressed merging the equations for both convection processes.

$$U = \left(\frac{1}{\alpha_1} + \frac{1}{\alpha_2} + \sum R_f + \frac{s}{\lambda}\right)^{-1} \tag{5.24}$$

Explicitly written:

$$U = \left(\frac{L_1}{C_1 \times Re_1^{m_1} \times Pr_1^{n_1} \times \lambda_1} + \frac{L_2}{C_2 \times Re_2^{m_2} \times Pr_2^{n_2} \times \lambda_2} + \sum R_f + \frac{s}{\lambda}\right)^{-1} \tag{5.25}$$

where s is the thickness of the heat transfer surface and R_f is the fouling factor. L_1 and L_2 are the geometric reference of each side.

5.8.2.2 Hot side - heat transfer

For the hot side convective heat transfer coefficient the following formulation given by the manufacturer for PSHE has been applied:

$$Nu_{hot} = 0.2 \times Re_{0.65} \times Pr_{1/3} \tag{5.26}$$

The coefficients are based on the assumption that the unit is an average counterflow PHE. A pressure adaptation factor can be neglected as the pressure drop is comparably small and the pressure level remains almost constant during operation. The mass flow on the hot side is approximately twice as high as on the cold side. The hot side Reynolds numbers and consequently the convection coefficient will certainly exceed the ones on the cold side. The two latter points lead to a simplification of the correlation.

$$\alpha_{hot} = \alpha_0 \times \left(\frac{\dot{m}}{\dot{m}_0}\right)^k \tag{5.27}$$

where α_0 is 678W/m²K, m_0 is 20kg/s and k = 0.95.

5.8.2.3 Cold side - heat transfer

On the cold side of the pre-heater the convective heat transfer follows the same principles as on the hot side. Both sides are operating in the turbulent regime (Re ranging from 4000 to 5000), but the cold side's range of mass flows is roughly half of the hot sides mass flow. Consequently, lower Reynolds numbers can be expected. In dynamic simulation the cold side is more relevant. Not just due to the fact, that the heat transfer coefficients are lower, but as well the modulation of mass flow is significantly higher. The fluctuation in pressure has to be considered as well. Taking these points into consideration, the cold side correlation has to be somewhat more sophisticated. Starting with a simple formulation for convective coefficient α[1] as the following:

$$\alpha_{cold} = C \times Re^m \times Pr^n \tag{5.28}$$

Within the ranges for C, m and n, that can be found in literature, this correlation does not converge well in this case. This led to the decision to set up an own correlation for this specific case. To account for the influence of the operational point (besides the influence of the Reynolds number) a mass flow factor was introduced. Reynolds numbers here are based on the assumption of full and homogeneous flow admission. With the flow configuration of the pre-heater this assumption is optimistic.

$$\alpha_{cold} = C \times Re^m \times Pr^n \times \left(\frac{\dot{m}}{\dot{m}_0}\right)^l \tag{5.29}$$

The above formulation (correlation type 2) correlates fairly good with the measured values (Table 5.9.

Table 5.9: fitting results for pre-heater correlation, type 2

coefficient	C	n	m	l

[1] by chance thermal conductivity and geometric attribute make Nu number and α similar in this case

value	0.3	0.7944	0.88	0.6925	

PPMCC	adj.	$\epsilon_{max,rel}$	ϵ_{mean}
0.9928	0.9856	+7.71%	-7.28%	+1.40%

The next correlation (type 3) that has been tested is:

$$\alpha_{cold} = C \times Re^m \times Pr^n \times p_r^q \quad (5.30)$$

In order to improve the above correlation a further factor is introduced. It represents the influence of the pressure. In cases where contaminations in the cycle fluid are expected this method can account for non-ideal effects. Correlation 4 combines the two correlations before and is a function of the reduced pressure and the relative mass flow rate.

$$\alpha_{cold} = C \times Re^m \times Pr^n \times \left(\frac{\dot{m}}{\dot{m}_0}\right)^l \times p_r^q \quad (5.31)$$

Running the model versus measured values the model behaves as depicted in Figures 5.19 and 5.20. In order to obtain the cold side heat transfer coefficient the heat rate has been calculated from the measured temperature difference of MDM across the apparatus and the mass flow measured in the cycle. For each daily data set of December 2012 the Reynolds and Nusselt values have been computed and written to files. In the next step these files have been processed by a MATLAB script fitting the coefficients of the model via a trust-region-reflective algorithm.

The overall model for the pre-heater is a combination of the mass flow dependent correlation for the hot side and the type 3 correlation for the cold side. The Figures 5.21 and 5.22 show the calculation versus the measured data of on day
(2012-12-03).

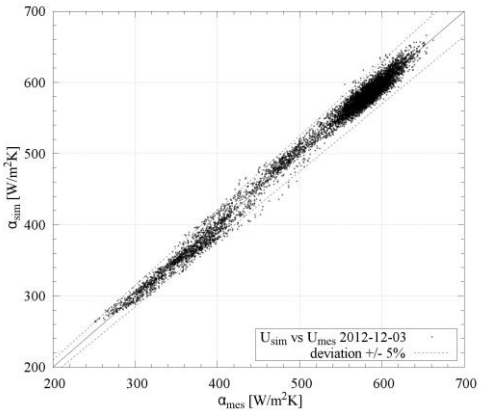

Figure 5.19: pre-heater cold side heat transfer simulated vs. measured

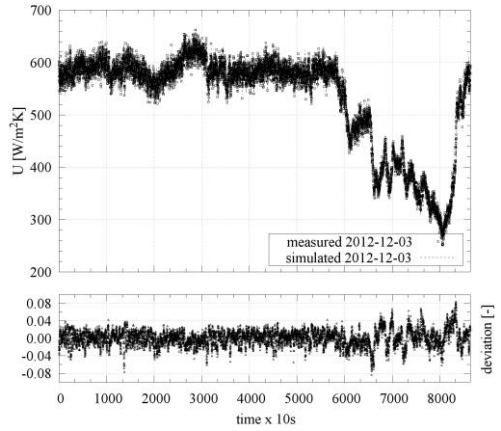

Figure 5.20: pre-heater cold side heat transfer simulated and deviation vs. time

coefficient	α_0	m_1	C_2	n_2	m_2	q_2
value	677.7	0.95	0.1025	0.8	0.42	1.25

PPMCC	adj.	$\epsilon_{max,rel}$		ϵ_{mean}
0.9959	0.9918	-3.58%	+3.93%	-0.0067%

U_{mean} 307.95W/m²K

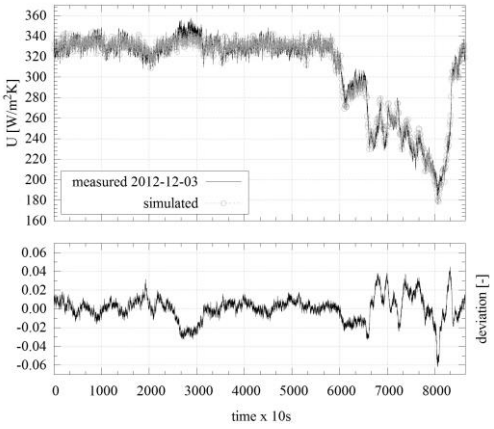

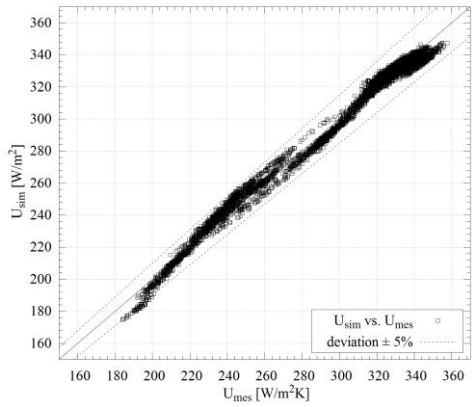

Figure 5.21: measured and simulated U-value of the pre-heater and deviations vs. time

Figure 5.22: measured vs. simulated U- value of the pre-heater

The correlation and its statistical results are shown in Table 5.10.

Table 5.10: fitting results for pre-heater correlation, type 4

coefficient	C	n	m	l	q
value	0.15	0.6841	0.1761	0.07	0.8825

	PPMCC	adj.	$\epsilon_{max,rel}$	ϵ_{mean}	
	0.9930	0.9998	-7.29% +7.62%		0.83%
α_{mean}	530.9W/m²K				

The model shows a good mean correlation in the range of ±1%. Most values are within ±7%. For a heat transfer model the deviation is fairly good. The validation of the results can be found in Section 6.3.4.

5.8.2.4 Cold side - Pressure characteristics

The nominal pressure loss is given by the manufacturer. While accuracy for the hot side (T66) is not too relevant, the cold side pressure characteristics have great influence on the entire cycle. The evaporation temperature, super-heating and finally the turbine behaviour are directly depending on that value. During validation the calculated pressure drop has to be checked and most probably adjusted. Under the assumption that the friction correlates quadratically with the flow velocity, the following simple Equation 5.32 can be used for the calculation. This includes the operation within a certain range of the turbulent regime. Laminar flows can not be covered with that approach. The primary side pressure loss for thermal oil is correlated according to the dynamic component of the Bernoulli Equation:

$$\Delta p = \Delta p_{nom} \left(\frac{\dot{m}}{\dot{m}_{nom}} \times \frac{\rho}{\rho_{nom}} \right)^2 \tag{5.32}$$

where the nominal pressure loss values can be found in Table 5.8.

5.8.2.5 Influence of transport properties

The following Figures 5.23 and 5.24 depict the variation of transport properties across the pre-heater. With an increasing temperature range between inlet and outlet the thermal behaviour of the fluid differs significantly. The number of sections or nodes for the calculation in the heat exchanger has to be chosen accordingly.

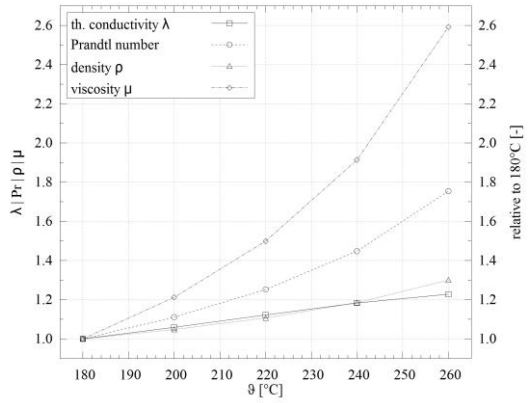

Figure 5.23: transport property vari- ation on cold side of pre-heater

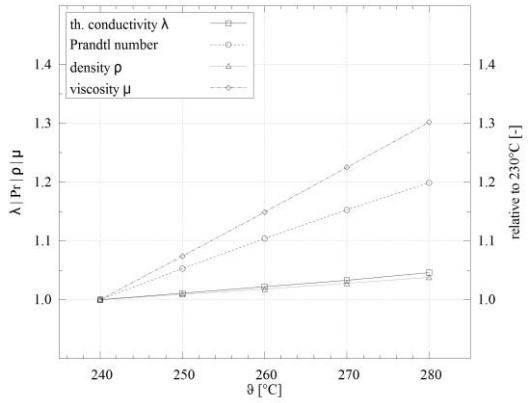

Figure 5.24: transport property variation on hot side of pre-heater

5.8.3 Recuperator (V1)

Remark: The following section describes the recuperator unit (V1), that has been used from 2004 to 2013. In the course if this work (2012) the monitoring results began to show erroneous results. After a diagnosis based on the measured data and the empirical model presented in Section 5.1.1 a leakage in the tube bundle was discovered. Thermal expansion and mechanical stress have led to a damage of the heat transfer tubes. The leakage was revised by sealing brackets. Unfortunately, this counter-measure was only temporarily successful. During the revision in summer 2013 the heat recuperator bundle was completely replaced. The new bundle (V2) is described in the next section.

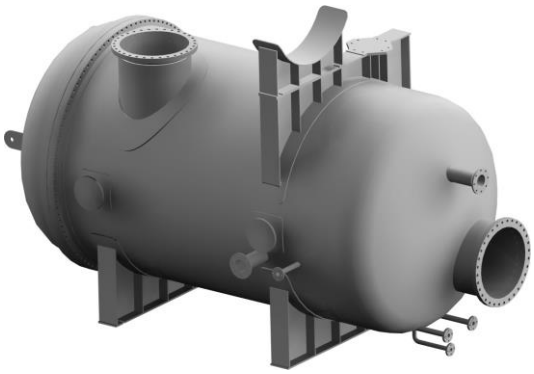

Figure 5.25: 3D-view of the recuperator (V1)

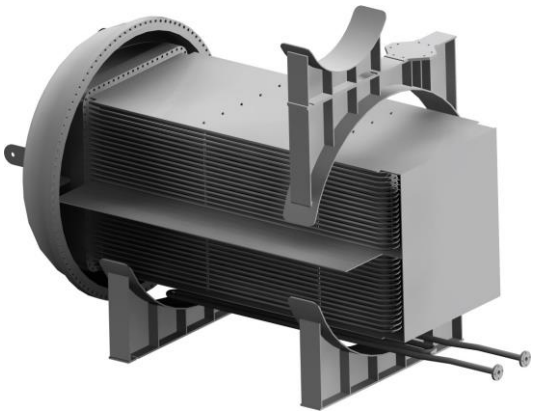

Figure 5.26: 3D-view of the tube bundle (V1)

The largest heat exchanger in terms of volume, transfer surface and heat transfer in the cycle system is the recuperator. It consists of a circular shell containing a square array of 480 u-tubes (St35.8/DIN17175). Each of the ten tiers

has 3 rows with 16 tubes. All tube legs (total length of 3.7 m) are finned over a length of 3.5 m with eleven fins per inch. Regarding the direct influence of the condenser to the drain side of the turbine the friction loss across the tube array has to be determined by measurement. A total pressure loss of 100mbar to 270mbar between turbine output, across the recuperator, to the condenser can be derived from the data in the chapter Monitoring. Compared to the pre-heater and evaporator the flow configuration of this unit is rather complicated. The unusual concept of using a squared tube array has a few interesting aspects. In order to increase the geodetic difference between the condenser and the suction side of the feed-pump the condenser is situated on top of the recuperator. The hot gas flow from the turbine drain enters the unit at the bottom, makes its way through the tube array and finally exits through a DN800 tube on the top of it. The squared array is concluded by a sheet cage, serving as retainer as well as deflecting sheets. The entire cage is set on L-shaped bearings (L-beam) that serves as a rail system when pulling the cage out of the vessel in case of maintenance.
Table 5.11: specifications of recuperator (V1)

symbol	value	unit	description
Φ_{nom}	4780	kW	nom. heat rate
Δp_1	n.n.	bar	nominal pressure loss hot side
Δp_2	n.n.	bar	nominal pressure loss cold side
$U_{nom,cold}$	410	W/m²K	heat transfer coefficient
connector 1	800	DN	flange hot side
connector 2	150	DN	flange cold side
V_1	21	m3	hot vapour volume
V_2	1.45	m3	cold liquid volume
m_{dry}	34000	kg	weight net, dry
$A_{tube,hot,gr}$	293.9	m2	outer heat transfer surface (gross)
$A_{tube,hot,net}$	268.4	m2	outer heat transfer surface (net)
$A_{fin,hot}$	4422	m2	heat transfer surface of fins
$A_{tube,cold}$	259	m2	inner heat transfer surface of tubes
N_{fin}	3030	[-]	fins per u-tube

$N_{u-tubes}$	480	[-]	number of u-tubes
D_{out}	2.70	m	outer diameter of shell
L_{out}	6	m	length of shell
L_{tub}	3.7	m	length of tubes
L_{finned}	3.5	m	finned length of tubes
$\dot{m}_1$	23.35	kg/s	nominal mass flow hot side
$\dot{m}_2$	23.35	kg/s	nominal mass flow cold side
V_{dis}	3.52	m^3	bundle displacement
m_{tube}	2970	kg	metal mass of tubes
m_{fins}	3214	kg	metal mass of fins
$D_{tube,out}/d_{tube,in}$	25.4/22.4	mm	outer/inner diameter of tube

5.8.3.1 Influence of transport properties

The following Figures 5.27 and 5.28 depict the variation of transport properties across the recuperator. With an increasing temperature range between inlet and outlet the thermal behaviour of the fluid can differs significantly. Again, the number of sections or nodes for the calculation in the heat exchanger has to be chosen accordingly. While the Prandtl number on the cold side differs significantly, it remains almost constant on the hot side.

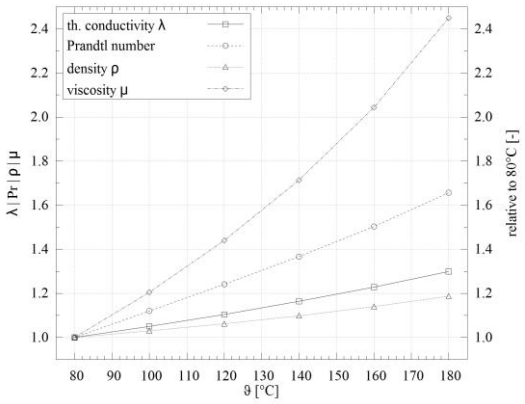

Figure 5.27: transport properties variation on cold side of recuperator

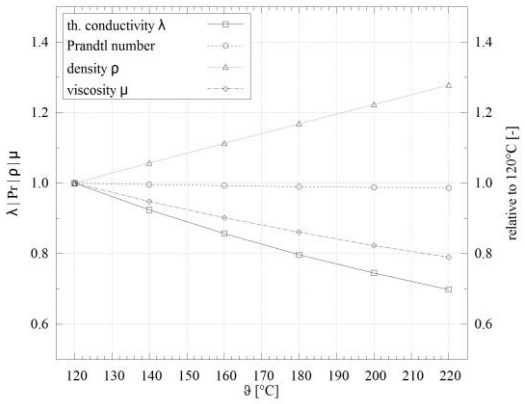

Figure 5.28: transport properties variation on hot side of recuperator

5.8.3.2 Cold side - pressure characteristic

The cold liquid fluid flow enters the head of the recuperator through a DN150 pipe and is released into a rectangular cross section (16cm x 80cm). From this chamber the flow is (equally) fed into 48 parallel tubes. After passing the first tube tier, the flow enters the next chamber (32cm x 80cm). In total the arrangement counts one entering volume, followed by four large volumes, one volume connecting the lower and the higher row, again followed by four volumes and finally ending in one small volume. The illustration of the flow configuration can be found in Figure 5.29. The Figure shows how the hot flow is going through one of the two layers.

The pressure drop across the liquid (cold) side of the unit consists of a sequence of concatenated pressure drops. The sum of all pressure differences can be written as:

$$\Delta p_{recu,hot} = \Delta p_0 + \Delta p_{tube,1a} + \Delta p_{bend,1} + \Delta p_{tube,1b} + \Delta p_0 + (5.33) \ldots + \Delta p_{tube,9a} + \Delta p_{bend,9} + \Delta p_{tube,9b} + \Delta p_{10}$$

where the fluid in each tier undergoes three pressure drops and one Carnot shock loss (abrupt discontinuity of flow field) by entering a significantly smaller or larger volume respectively cross-section. In addition, the feed and drain connections add one more shock loss.

$$\zeta = \left(1 - \frac{A_1}{A_2}\right)^2 \tag{5.34}$$

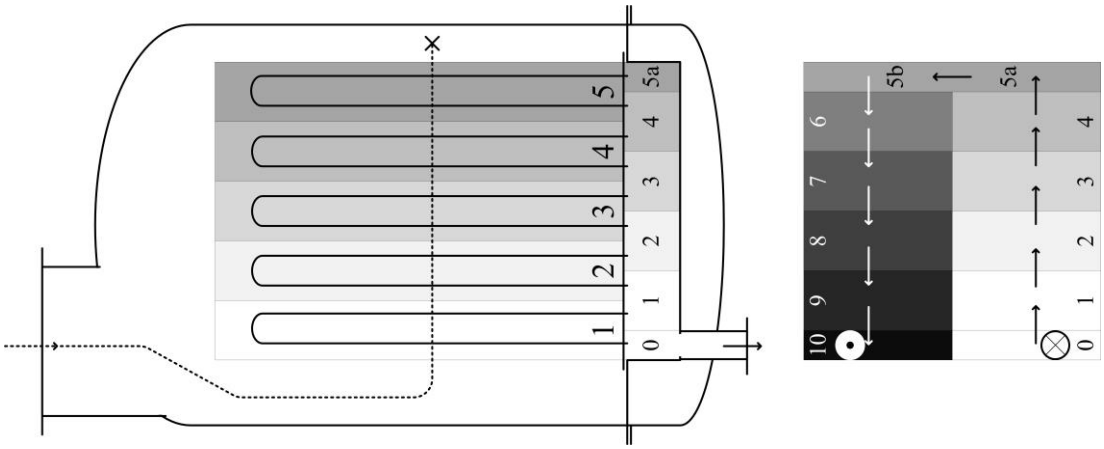

Figure 5.29: simplified scheme of recuperators hot side volumes and flow pattern

With the geometric attributes of the single chambers and tube tiers we receive the following list (Table 5.12) of shock losses:

Table 5.12: list of pressure losses in the tube array of the recuperator (cold side)

from	to	A_1	A_2	ζ
-	-	[m²]	[m²]	-
flange cold	chamber 0	0.0353	0.128	0.5240
tier 1	chamber 1	0.0378	0.256	0.7263
...	...	...	...	...
tier 5	chamber 5	0.0378	0.128	0.4962
tier 6	chamber 6	0.0378	0.256	0.7263
...	...	...	...	...
tier 9	chamber 9	0.0378	0.256	0.7263
tier 10	chamber 10	0.0378	0.128	0.4962
P				7.368

With these numerous pressure drops the physical computation becomes complicated. If each segment in heat transfer calculation has its own partial pressure drop it certainly increases the CPU load. Therefore one strategy to simplify the system is a lumped pressure drop. As moderate pressure differences have no severe influence on transport properties, the entire apparatus can be separated into one heat transfer calculation and one pressure calculation. However, the simplified form of the calculation has to be validated by a physical model and the empirical date of the unit. We first estimate the tube flow friction component.

We can assume a transition or turbulent regime inside the tubes, but in prospect to the dynamic solver a steady function is favourable. With the classic methods, such as Moody [106], Churchill et al., Jain, Chen or Haaland the Darcy-Weisbach friction factors for pipe flows can be determined accurately. The aforementioned equations differ in form (implicit/explicit), calculation regime, complexity, and CPU-load (number of iterations). These criteria play a role when implementing into a simulation. Romeo and Royo [107] have concluded the different aspects of pipe friction calculation. They propose a model with less than 0.05% deviation, which comes to use in the steady-state calculations in this work:

$$f_{DW}^{-0.5} = -a_0 \times log\left(\frac{\epsilon}{D \times a_1} - \frac{a_2}{Re} \times log\left(\frac{\epsilon}{D \times a_3} - \frac{a_4}{Re} \times log\left(\left(\frac{\epsilon}{D \times a_5}\right)^{n_1} + \left(\frac{a_6}{a_7 + Re}\right)^{n_2}\right)\right)\right) \tag{5.35}$$

coefficient	a_0	a_1	a_2	a_3	a_4	a_5
value	2.0	3.7065	5.0272	3.8270	4.5670	7.7918
coefficient	a_6	a_7	n_1	n_2		
value	5.3326	208.815	0.9924	0.9345		

In terms of dynamic simulation, this approach is not suitable. As an alternative, Churchill based on his earlier work with Usagi [108] found an equation that is valid for all flow regimes and delivers a steady result [109]:

$$f_{DW}^{-0.5} = 8 \times \left(\left(\frac{8}{Re} \right)^{12} + (A+B)^{-2/3} \right)^{1/12} \tag{5.36}$$

where the terms A (turbulent) and B (transition) are defined as follows:

$$A = \left(-2 \times log \left(\frac{\epsilon}{3.7D} + \left(\frac{7}{Re} \right)^{0.9} \right) \right)^{16} \tag{5.37}$$

$$B = \left(\frac{37530}{Re} \right)^{16} \tag{5.38}$$

Based on the above friction factors and the fluid's Prandtl-number the Nusseltnumber for the tube heat transfer can be calculated using the Gnielinsky solution for the Colebrook equation with high accuracy [110]:

$$Nu = \frac{(f_{DW}/8) \times (Re - 1000) \times Pr}{1 + 12.7 \times \sqrt{f_{DW}/8} \times (Pr^{2/3} - 1)} \tag{5.39}$$

Concluding the Carnot shock loss and the turbulent pipe friction one receives a formulation for the nominal pressure loss across the apparatus at mean nominal temperature and pressure (130 °C and 7bar).

$$\Delta p_{recu,cold} = 68375\text{Pa} \left(\frac{\dot{m}}{20\,\text{kg/s}} \times \frac{\rho(p,T)}{705.5\,\text{kg/m}^3} \right)^2 \tag{5.40}$$

5.8.3.3 Hot side - pressure characteristic

Due to lack of information about the flow pattern and the detailed topography of the vapour side of the recuperator a rather robust approach for the pressure characteristics is needed. Therefore, the nominal pressure loss of 7000Pa at a nominal flow rate of 20kg/s was taken as a first guess. The data measured during operation drew a totally different picture of the flow conditions. Similar to the

other heat exchangers the formulation for the pressure drop can be expressed as a law of similarity based on the Darcy-Weisbach equation:

$$\Delta p_{recu,hot} = 28\,476\,\mathrm{Pa}\left(\frac{\dot{m}}{20\,\mathrm{kg/s}} \times \frac{\rho(p,T)}{1.6017\,\mathrm{kg/m^3}}\right)^2 \tag{5.41}$$

The nominal density (1.6017kg/m^3) is calculated via the mean design temperature and pressure (177 °C and 0.278bar). If the pressure loss is related to the inlet conditions the reference density is 1.996kg/m^3 and the nominal temperature 228 °C. Reasons for the large deviation between the design value and the measured value are the complicated flow pattern on the hot side, a deflector sheet after the turbine and the surface enhancement (fins).

5.8.3.4 Hot side - heat transfer

Taking a look at the hot side of the recuperator, we find a tube bundle consisting of ten tiers with 48 parallel u-tubes each. The bundle configuration is staggered and circular fins serve as heat transfer surface enhancement. In order to give an estimation of the gaseous heat transfer the flow pattern has to be determined. Furthermore, the flow path and the resulting flow velocities have to be elaborated. In the case at hand the tube bank is impinged in cross-flow, the total configuration is a counter-cross-flow with ten nodes.

The following assumptions and simplifications are applied to the model:

- All tubes in the bundle are equally impinged by the gas flow.
- The u-bends do not take part in the heat transfer process.
- There are no by-passes and the velocity profile is uniform across the height of the arrangement.
- The flow distribution across all parallel tubes in one tier is equal. Therefore, the surface temperature of the tubes in one tier is equal as well.

The theory of heat transfer through tube arrangements is based on the theory of single tube forced convection. In a second step rows of single tubes are concluded. For a large number of serial tube rows an entire, mean heat transfer behaviour is calculated. The main question in vapour flows through tube arrangements is the issue of preferred flow lanes. During quasi-steady conditions certain flow patterns are formed in a bundle. These flow patterns

depend on the ratio of tubes and void space as well as the geometric arrangement. It is assumed that the first rows in a grid of tubes serve as a turbulence generator. After passing a larger number of tube rows in a regular pattern a uniform flow pattern evolves. It can be assumed that aligned tube patterns have larger preferred flow lanes and less turbulence due to a lower number of obstacles in the flow path. In this case the heat exchanger has a staggered arrangement. As a first step the flow path has to be determined. For a staggered arrangement the applied cross sections between the tubes have to be evaluated to receive the maximum flow velocity. This maximum velocity is responsible for the turbulence generation in the bundle and therefore influences the overall average heat transfer coefficient.

$$2 \times (S_{dia} - D_{tube}) < (S_{trans} - D_{tube}) \tag{5.42}$$

In the case at hand, this condition is false as the double diagonal distance is not less than the transversal distance. As a consequence the following expression is valid for our scenario [111]:

$$v_{max} = \frac{S_{trans}}{2\,(S_{dia} - D_{tube})} \times v_0 \tag{5.43}$$

From the above term, we receive an velocity factor of 1.8881. The velocity of the flow before the bundle has to be multiplied with this value to get the maximum velocity occurring between the tubes. At this point it has to be noted that the factor is only valid for bare tubes. In case of a finned tube bundle the velocity rises accordingly to the cross section being occupied by the fin material. Taking the displacement by the fin material into account the above velocity increases by another 8.7%. The according Reynolds-numbers for the bundle flow are calculated under the assumption that the velocity v_{max} is the criterion. A first rough estimation for our case can be done using the criterion correlation of Zukauskas et al. [112].

$$\bar{N}u_D = C_1 \times C_2 \times Re_{max}^{m} \times \bar{P}r^{0.36} \times \left(\frac{\bar{P}r}{Pr_{tube}}\right)^{0.25} \tag{5.44}$$

coefficient	C_1	C_2	m
value	1	0.36	0.6

It has to be noted, that the above equation is based on the mean temperature on the hot side. An adjustment for the temperature related changes in transport properties is applied by using the last fraction term. The correction factor C_2 can be neglected in cases where more than 20 tube rows are calculated (here: 60 tube rows). As a first result we receive convective heat transfer values on the hot side of 180W/m²K to 200W/m²K under design conditions (related to the bare tube area). After this basic calculation according to the commonly accepted theory, a few modifications are necessary. The finning of the tube bundle is assembled by roll cladding. Unfortunately, material expansion, mechanical and flow stress often lead to loose fins. In this case this failure has been discovered during revisions. Due to design reasons the bundle cannot be disassembled to a point where the fins could be reattached. As a result the heat exchanger performs worse and in terms of modelling an adaptation is required. Taking the surface enhancements of a tube bundle into account a comparison between regular tubes and enhanced tubes has to be done. Therefore, a comparative factor, the fin efficiency η_f is introduced. It characterizes the ratio between the total surface of the fin and the reduced surface due to the declining temperature gradient:

$$\eta_{fins} = \frac{\Phi_{fins}}{\Phi_{max}} = \frac{\vartheta_{fins} - \vartheta_{\infty}}{\vartheta_{tub} - \vartheta_{\infty}} \tag{5.45}$$

with a number of N fins we receive

$$\Phi_{trans} = h_{dN} \times ((A_{tot} - N \times A_{fin}) + \eta_{fin} \times A_{fin} \times N) \times (\vartheta_{tub} - \vartheta_{\infty}) \tag{5.46}$$

where A_{tot} represents the total surface consisting of the uncovered tube bundle surface and the surface of all fins.

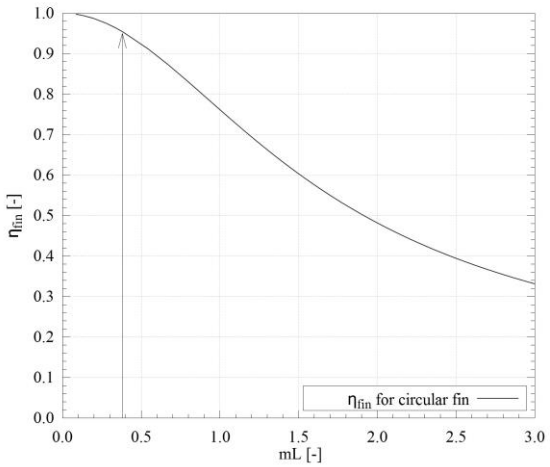

Figure 5.30: fin efficiency of the recuperator versus the shape criterion

In Figure 5.30 the efficiency for the geometric constellation is plotted. For an average heat transfer rate of 20W/m²K and the given circular geometry the fin efficiency is 0.95. Additionally the contact resistance at the bottom of the fin has to be taken into account. In this case a value of 0.001m²/WK is assumed. Based on the above theory of turbulence generation and the design data of the recuperator, various heat transfer correlations have been tested on measured data sets.

$$Nu_{recu,hot} = C_1 \times Re_{max}^{a} \times Pr^{b} \tag{5.47}$$

coefficient	C_1	a	b	
value	0.003874	0.8956	0.33	
	PPMCC	adj. R^2	RSME	SSE
	0.9793	0.9590	1.004	4041

A simplified correlation, neglecting the change in transport properties:

$$Nu_{recu,hot} = C_1 \times Re_{max}^{a} \tag{5.48}$$

coefficient	C_1	a		
value	0.00371	0.8956		
	PPMCC	adj. R^2	RSME	SSE
	0.9781	0.9567	0.9895	3912

The correlations are based on the Reynolds number calculated via v_{max} and the outer tube diameter as geometrical dimension. Validation results of the above equation can be found in Chapter 6. The results show, that the correlation using solely the Reynolds term performs very well. The Prandtl numbers have almost no influence as depicted in the previous Section 5.8.3.1.

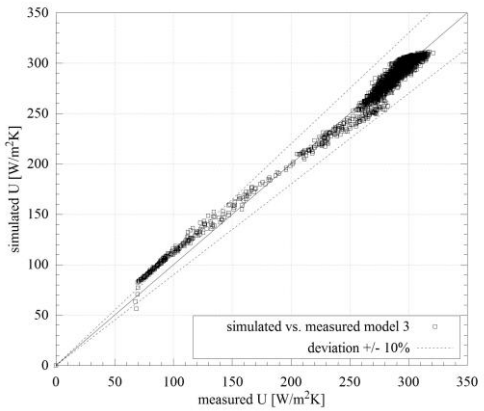

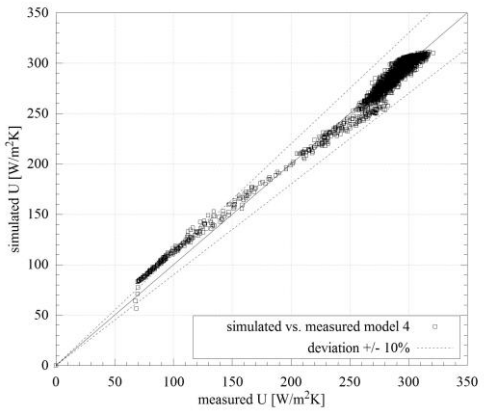

Figure 5.31: simulated vs. measured U-values of recuperator (model 3)

Figure 5.32: simulated vs. measured U-values of recuperator (model 4)

Both above depicted scatter plots (Figures 5.31 and 5.32) show a good model prediction quality within ±10% in the relevant load range (200W/m²K to 325W/m²K). Below 150W/m²K the model over-predicts as the flow is not fully turbulent during start-up of the engine. This deviation during low-load states is not relevant.

5.8.3.5 Dynamic modelling of recuperator

The dynamic model of the recuperator is based on the modelica Flow1D class. It accounts for the thermal inertia of the tube array including the mass of the fins. The effect of the shell mass and the auxiliary parts (retainer etc.) are neglected here. The dynamic model of the recuperator consists of the following modelica classes:

- Flow1DRCC: extended Flow1D class with variable heat transfer calculation according to Gnielinski's turbulent tube flow.
- MetalTube: tubular conduction ,including thermal inertia, through a metal tube with one radial node and N axial nodes.
- ConvHThtc: heat transfer connector between variable and constant heat transfer coefficient, one each for cold and hot side.
- CounterCurrent: swap function for temperature and flux vectors.
- Flow1DRCH: extended Flow1D class with variable heat transfer using an empirical equation.

5.8.4 Recuperator (V2)

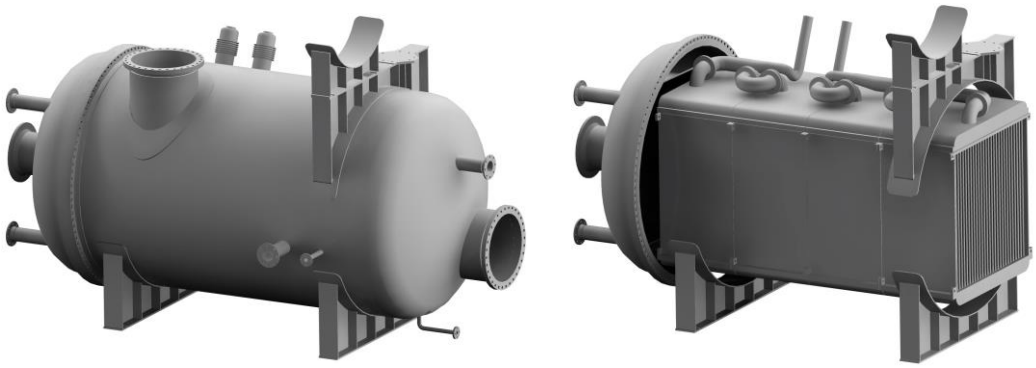

Figure 5.33: 3D-view of the recuperator (V2)

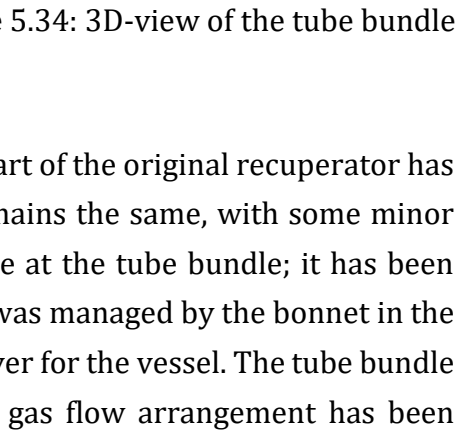

Figure 5.34: 3D-view of the tube bundle (V2)

As mentioned in the previous chapter, a large part of the original recuperator has been replaced in the year 2013. The vessel remains the same, with some minor modifications. Greater changes have been made at the tube bundle; it has been entirely replaced. While the flow arrangement was managed by the bonnet in the first version, in the second version it is just a cover for the vessel. The tube bundle is fed by direct tubing through the shell. The gas flow arrangement has been completely redesigned. This section shows the main differences and technical specifications of the new apparatus.

Table 5.13: specifications of recuperator V2

symbol	value	unit	description
Φ_{nom}	4600	kW	nom. heat rate
Δp_1	n.n.	bar	nominal pressure loss hot side
Δp_2	n.n.	bar	nominal pressure loss cold side
$u_{nom,cold}$	653	W/m²K	heat transfer coefficient
connector 1	800	DN	flange hot side
connector 2	150	DN	flange cold side
V_1	21	m3	hot vapour volume
V_2	2.328	m3	cold liquid volume
m_{dry}	34000	kg	weight net, dry
$A_{tube,hot}$	202.7	m2	outer heat transfer area of tubes
$A_{fin,hot}$	5420	m2	heat transfer area of fins
$A_{tube,cold}$	186	m2	inner heat transfer area of tubes
N_{fin}	740	[-]	fins per tube factor
$N_{u-tubes}$	1792	[-]	number of u-tubes
D_{out}	2.70	m	outer diameter of shell
L_{out}	6	m	length of shell
L_{tub}	1.7	m	length of tubes
$\dot{m}_1$	23.35	kg/s	nominal mass flow hot side
$\dot{m}_2$	23.35	kg/s	nominal mass flow cold side

m_{tube}	3692	kg	metal mass of tubes
m_{fins}	2930	kg	metal mass of fins
D_{tube}	25.4	mm	outer diameter of tube
V_{dis}	2.628	m^3	bundle displacement

5.8.5 Evaporator

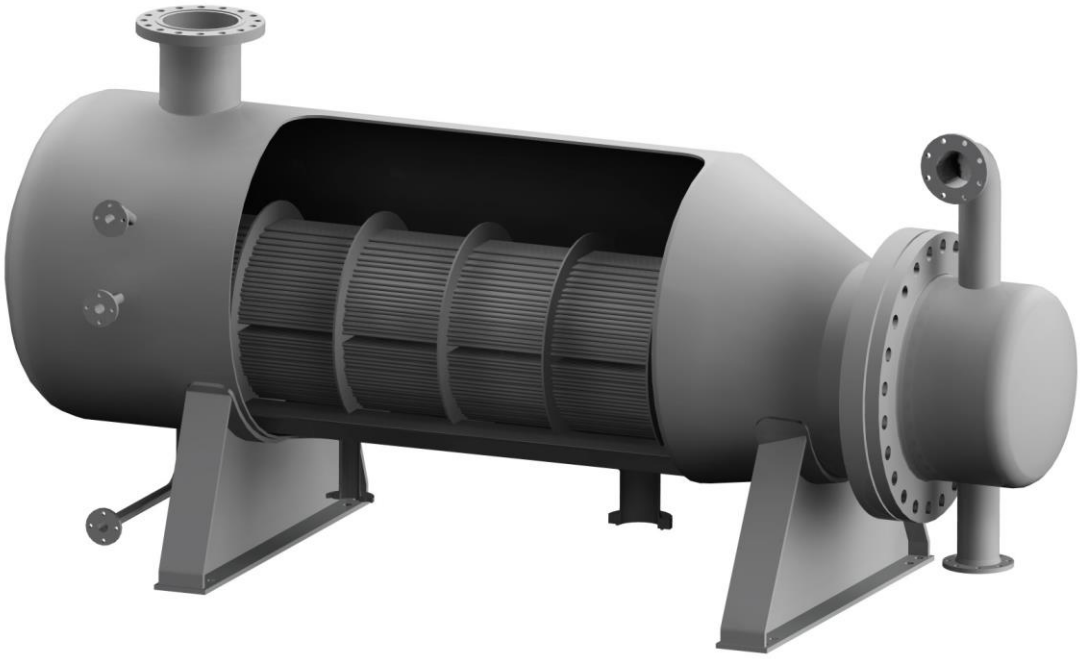

Figure 5.35: 3D-section view of evaporator

In Figure 5.35 a 3D-view of the evaporator with a cutaway section through the shell is depicted. The bent inlet on the top of the bonnet is the hot intlet of thermal oil. The vapour is leaving the apparatus through the large tube on the left top of the picture. The cold MDM is entering the vessel through the tube on the bottom (here half sectioned). The smaller tubes on the left side are the connectors for the level gauge and the pressure sensor.
The arrangement of the apparatus is pretty ordinary. The U-tube bundle, supported and divided by baffle sheets is inserted into the vessel. The discharge of the heat carrier into the tube bundle is done by a sheet separated bonnet. From the top the hot thermal oil flows through the 512 U-Tubes into the lower part of the bonnet. The liquid MDM is flowing into the vessel from the bottom, covering the main part of it with liquid. The upper part (approximately 200mm) is not wetted. The following drawing (Figure 5.36) depicts a simplified scheme of the evaporator.

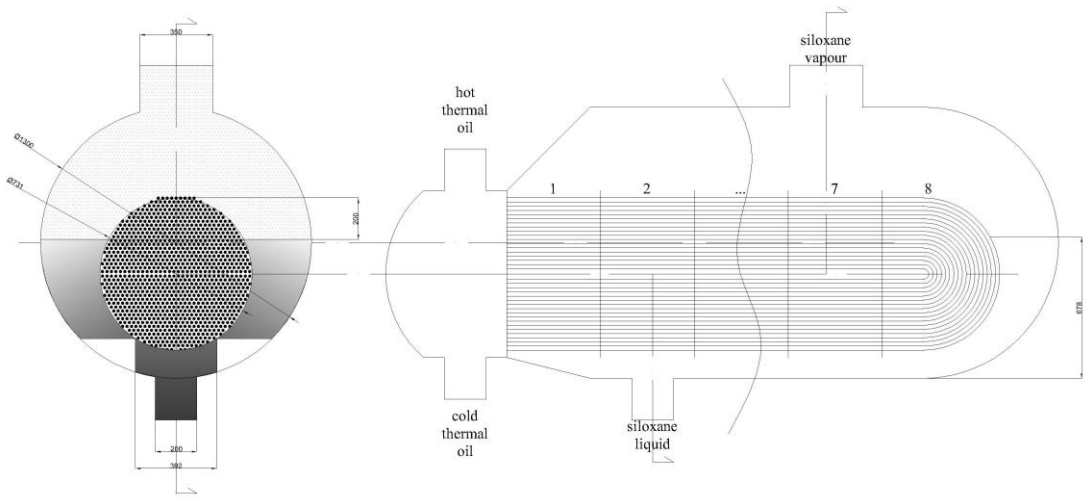

Figure 5.36: evaporator cross sections

In industrial application shell-and-tube type (STT) heat exchangers are popular. Their versatility and robustness is highly estimated. Many points argue for the shell-tube types:

- Circular shape and spherical surfaces provide enable smooth flows. In terms of pressure stress, the round shape of the vessel is advantageous and easy to produce.
- The pipe flow on the hot side is well understood. Various theories for forced convection in tubes with different complexity and accuracy are available.
- Using a head flange provides the opportunity to revise during inspection and clean by removing the bundle.
- Leaking tubes can be replaced, while defective sheets in plate heat exchangers are usually a death-sentence for the apparatus or at least for the plate stack.
- The form of the vessel is linearly scalable. In case more heat transfer is required the design can be simply increased in length.
- In many heat exchangers, such as plate types, thermal expansion leads to high mechanical stress at welds and solderings. The tube bundle in a STT has a under-determined bearing, therefore expansion is possible.
- Tubes are a cheap wrought material, with a high availability in various materials and sizes.

- STTs are versatile concerning flow patterns. The passes through the single tube tiers can be arranged by separator sheets in the bonnet.

This apparatus type comes with a few disadvantage as well:

- STT have lower U-values than PHE, especially if the outer flow is gaseous.
- To compensate for the lower specific heat transfer, STT are less compact [63].
- If the head flange is sealed, the sealing has to be compatible with the operation conditions, especially the hot side fluid.

The following Table 5.14 gives all relevant data for the calculation of the evaporator.

Table 5.14: specifications of the evaporator

symbol	value	unit	description
Φ_{nom}	2037	kW	nominal heat rate
Δp_1	0.06	bar	nominal pressure loss hot side
Δp_2	0.2	bar	nominal pressure loss cold side
U_{nom}	578	W/m²K	heat transfer coefficient
connector 1	200	DN	flange hot side
connector 2	150/350	DN	flange cold side
$V_{hot,liq}$	0.727	m3	hot volume
$V_{cold,gr}$	4.609	m3	cold gross volume
$V_{cold,net}$	3.472	m3	cold net volume
$V_{cold,liq}$	2.160	m3	cold liquid volume
m_{tub}	2498	kg	tube mass between both fluids
$A_{trans,1}$	136.4/161.4	m2	heat transfer area (inner/mean)
$A_{trans,2}$	185.8	m2	outer gross heat transfer area
k_f	0.0002	m²K/W	fouling factor
D_{out}	1.321	m	outer diameter of shell

L_{out}	4.459	m	length of shell
L_{tub}	3.335	m	length of tubes
$\dot{m}_1$	40.91	kg/s	nominal mass flow hot side
$\dot{m}_2$	23.35	kg/s	nominal mass flow cold side
D_{tub}	16	mm	outer tube diameter
d_{tub}	12	mm	inner tube diameter
S_1/S_2	18.4/21.4	mm	vertical/horizontal pitch

The total heat transfer area of the heat exchanger can be derived from its geometrical properties. In general one would design an evaporator such as this kettle type with an entirely floating heat transfer bundle. As it can be seen from the drawings: the top of the tube array is the largest cross-section in the vessel. Designing a unit like that, assures that the departure velocity reaches a minimum and the surface of the boiling fluid stays as calm as possible. The very aim is the avoidance of droplets being torn into the hot vapour stream. However, the kettle is not entire filled to the top of the bundle. Unfortunately, this makes the determination of heat transfer surfaces more complicated. In complex volumes obstacles (baffle sheets, separators, et cetera) result in very inhomogeneous flow patterns. Consequently, the calculation of local heat transfer is not trivial. In order to avoid a large number of iterations one approach for phase changes is the division of the total surface into sub-zones. In the case at hand the the according geometric parameter is the average filling level in the evaporator vessel. In case the tubes are dispersed equally, or more precisely, symmetrically across the flange plane the effective wetted tube surface ratio can be calculated as follows:

$$A_{seg} = r^2 \times arccos\left(1 - \frac{z_{bun}}{r_{bun}}\right) - \sqrt{2 \times r_{bun} \times z_{bun} - h^2} \times (r_{bun} - z_{bun}) \quad (5.49)$$

where z_{bun} is the non-wetted bundle segment height and r_{bun} denotes the radius of the tube bundle. In our case, with z_{bun} = 0.2m this leads to a surface coverage factor of:

$$A^* = \frac{A_{tot} - A_{seg}}{A_{tot}} = \frac{0.4199 - 0.1081}{0.4199} = 0.7425 \quad (5.50)$$

With this formulation we receive an apparatus with two different zones. In order to determine the flow pattern in the vessel and bundle arrangement some geometric parameters have to be calculated. In cases where a large number of tubes is combined in an array the theory of similarity can refer to the entire array

instead a single tube. Taking a look at the HEX at hand the 512 u-tubes are arranged in a diagonally staggered pattern. Via the vertical and horizontal pitch the void fraction in the array can be determined [63][Gh2]:

$$a = \frac{s_1}{D_a} \tag{5.51}$$

$$b = \frac{s_2}{D_a} \tag{5.52}$$

In our case the vertical fraction is larger than one. Therefore, it is negligible in the further calculations. With the horizontal distance the void fraction turns out to be:

$$\Psi = 1 - \frac{\pi}{4 \times a} \tag{5.53}$$

For this case Ψ is 0.429.

5.8.5.1 Boiling and evaporation

Having a look at the results of the Chapter 5.1.1 about empirical modelling the description of the heat source side is somewhat more important for the dynamics of the cycle than the sink. Therefore, a good overall model for a cycle needs a reliable and robust evaporation model. In literature the evaporation of water is widely discussed. For rather rarely used fluids, such as Siloxanes, the situation becomes more complicated. Many boiling correlations are aiming on refrigerants, alkanes or alcohols due to their relevance in chemical industry in terms of separating liquid matter. There is a large number of approaches to boiling and especially pool boiling. Unfortunately, up to now there is no mathematical model or theory that is able to describe and predict the complex processes of boiling as a whole. Hence, all approaches in today's literature are empirical to a certain extend [63] [Hab4]. In this chapter several common boiling correlations will be introduced and discussed. The main parameters of the heat exchanger and the fluid have to be identified and quantified. By doing so, finally, the most suitable solution in terms of accuracy, complexity and robustness can be found. It will be elaborated and applied to the entire model and if necessary adjusted accordingly.

5.8.5.2 Regimes of boiling

In order to understand the process going on in the pre-heater and evaporator a little overview about boiling shall be given. Since Nukiyama and Kutateladze described the process of boiling and its regimes, a number of empirical equations

has been found to approximate this rather complex relation. In a vessel with a heated surface and a liquid approaching the saturation temperature boiling begins with convection. Buoyant forces lift the hotter liquid. This regime is called free convection.

From a certain temperature difference of several Kelvin between the heating surface and the liquid single, isolated bubbles appear on the surface. Appearance, size and number are determined by geometric parameters such as the surface shape, material and arrangement and its roughness. In addition, the liquid being boiled and its state influence the boiling characteristics. By increasing the temperature difference the bubbles become more numerous and larger to a point where several bubbles are attached to each other and form configurations called jets and columns. By detaching from the surface the vapour bubble accelerates, including the liquid surrounding it. In some fields of research even the single shape and deformations of bubbles and their statistical relevance are studied to understand the heat transfer process [113]. For an engineering approach, this may lead way too far. During the process of nucleate boiling, the heat transfer coefficient from the surface to the liquid increases enormously, up to the point of the critical heat flux. From here on, the unsteady pattern of bubbles and the short contact time have a negative influence on the heat transfer. Above a certain temperature difference (100K), the boiled matter no longer wets the heating surface, but forms a stable vapour layer. The vapour bubbles are hovering on the vapour cushion. One share of the heat transfer in this regime is radiative. The last two regimes, transition boiling and film boiling are very interesting physical effects, but in our case not relevant for the description of the system.

5.8.5.3 Convective heat transfer

Before the nucleate boiling process with its obvious bubbles starts the first row of tubes being charged with liquid will transfer heat via convection. To which extend, or more frankly up to with row of tubes, this occurs is another question, mostly determined by the flow configuration and the temperatures in the process. However, for the low temperature differences of the boiling fluid to the heating tube surface, this regime of boiling can be expressed by the following formulation [114]:

$$\bar{Nu} = 0.54 \times Ra^{1/4} \tag{5.54}$$

for Rayleigh numbers up to 10^7 and for the regime of $10^7 < Ra < 10^11$

$$\bar{Nu} = 0.15 \times Ra^{1/3} \tag{5.55}$$

Taking a look at the heat transfer in tube arrangements, the calculation is based on a Prandtl-Grasshof-correlation [63][Hab3] that are pretty similar to the ones above. In fact, the explicit format comes with the advantage, that geometric and thermal parameters are separated. The Grashof number depends on the local temperature spread and the geometric parameter.

$$Nu_{lam} = 0.60 \times (Gr \times Pr)^{1/4} \tag{5.56}$$

and

$$Nu_{tur} = 0.15 \times (Gr \times Pr)^{1/3} \tag{5.57}$$

Many authors have contributed parameters for this type of correlation for various ranges of Prandtl and Grashof numbers (for instance: Saunders, Schmidt, Beckmann, Schuh). More important is Kirscher's average function, integrating both laminar and turbulent behaviour into one curve [63][Hab3] over a large range.
The convective regime ends at the on-set point of nucleate boiling (ONB).

5.8.5.4 Nucleate boiling

With increasing temperature differences between fluid and surface the boiling liquid will form vapour bubbles. First small isolated ones, later groups and clusters of bubbles forming jets and vapour columns. The major part of our boiling heat transfer occurs within this regime. As geometric criteria for the use of analogy theorems the bubble diameter is necessary. This diameter becomes a parameter for the Reynold number of a boiling fluid. When departing from the origin (most likely the heat transfer surface) the bubble leaves with a size defined as the detachment diameter. Depending on surface shape and roughness as well as thermo-physical properties of the material combinations this diameter varies. A simple approach is given by VDI [63]:

$$D_0 = 0.0149 \times \beta \times \left(\frac{2 \times \sigma}{g \times (\rho_{liq} - \rho_{vap})} \right) \tag{5.58}$$

where β is the detachment angle (as radians), and σ is the surface tension of the liquid. The final bubble diameter can be written as:

$$D_{bub} = \sqrt{\frac{\sigma}{g \times (\rho_{liq} - \rho_{vap})}} \tag{5.59}$$

5.8.5.5 Pool boiling correlations

Most authors agree upon the fact that organic fluid behave different from water during the process of boiling. To account for the non-polar behaviour and bubble departure characteristic of Siloxanes a specialized correlation is necessary. Mostinski's correlation [115, 116] is one candidate for the predictions of organic pool boiling. In the following part, several possible candidates for the case at hand are described. One of the first attempts to find a correlation for nucleate boiling was given by Rohsenow [117, 118]. He assumed, that the heat transfer is mainly determined by the liquid phase convection and the bubble agitation.

Later, based on this work, Bergles and Rohsenow [119] extended this theory. As a characteristic dimension he chose the maximum departure diameter of bubbles. Then nucleate boiling can be described by the following formulation:

$$Nu_{nb} = f\,(Re_{bub}; Pr_{liq}) = C_{surf} \times Re_{xbub} \times Pr_{liqy} \tag{5.60}$$

To account for the the boilers surface and liquid combination the adjustment factor C_{surf} is introduced. In the explicit form with the liquid dynamic viscosity and, the surface tension and the heat flux the Reynolds number for bubbles can be written as:

$$Re_b = \frac{\Phi}{h_{evap} \times \mu_{liq}} \times \sqrt{\frac{\sigma}{g(\rho_{liq} - \rho_{vap})}} \tag{5.61}$$

The Nusselt number can be calculated for this case:

$$Nu_{nb} = \frac{\Phi \times D_{bub}}{\Delta T \times k_{liq}} \tag{5.62}$$

Combining the expressions above we receive the following formulation:

$$\Phi = \mu_l \times h_{f,g} \times \sqrt{\frac{g(\rho_{liq} - \rho_{vap})}{\sigma}} \times \left(\frac{c_{p,liq} \times \Delta T}{C_{surf} \times h_{f,g} \times Pr_{liq}^{1.7}} \right)^3 \tag{5.63}$$

The above equation can return an rough approximation. Thome calls the role of this correlation “historical” [120], as the results are way too far off, compared to the number of parameters that are required.
One year later, Mostinski came up with a new approach [115, 116]. In his theory, applying the corresponding states, the combination of surface and liquid is neglected. The heat transfer coefficient is depending on two variables, the heat flux Φ and the pressure. As a further parameter the critical pressure is used to account for the fluids thermodynamic behaviour:

$$\alpha = 0.00417 \times \Phi^{0.7} \times p_c^{0.69} \times F_p \tag{5.64}$$

where F_p is the the non-dimensional factor to include pressure effects of the fluid on the process.

$$F_p = 1.8 \times p_r^{0.17} + 4 \times p_r^{1.2} + 10 \times p_r^{10} \tag{5.65}$$

In literature this method is said to be rather accurate concerning organic fluids, while the simplicity is very attractive in terms of CPU cost. With this method, it is necessary to run recursive calculations. A further method that needs to be mentioned in this chapter is the one of Stephan and Abdelsalam [121]. Based on statistical regression this method is reported to be reliable across different kinds of fluids, including organics and refrigerants. Collier and Thome [122] recommend this method for organic fluids.

$$Nu = 0.0546 \times \left[\sqrt{\frac{\rho_{vap}}{\rho_{liq}}} \times \left(\frac{\dot{q} D_{bub}}{k_{liq} T_{sat}}\right)\right]^{0.67} \times \left(\frac{h_{evap}}{D_{bub}^2}\right)^{0.248} \times \left(\frac{\rho_{liq} - \rho_{vap}}{\rho_{liq}}\right)^{-4.33} \tag{5.66}$$

In 1984 Cooper proposed an approach that included the roughness of the surface. The simplicity of the equation is appealing and well suitable as a base for fitting experimental data.

$$\alpha = (-0.4343 \times ln(p_r))^{-0.55} \times 55 \times p_r^{0.12 - 0.4343 \times ln(R_p)} \times \frac{1}{\sqrt{m}} \times \Phi^{0.67} \tag{5.67}$$

He recommended his correlation for a range of reduced pressures between 0.001 and 0.9 which meets the criteria of the validation system. Unfortunately, the molecular weight of MDM (and most other Siloxanes) [85] exceeds Cooper’s recommended range from 2g/mol to 200g/mol. Rao and Balakrishnan [123] have

presented results that show high accuracy for Acetone and Acetone ternary mixtures. This was a motivation to have a look into the correlations, despite Siloxanes and Acetone are chemically not too similar. Gorenflo's approach, based on a similar strategy as Mostinski, has the reputation of being the most accurate one. Literature reports an dispersion of ±30% for this correlation [63].

$$\alpha_{boil} = \alpha_0 \times F_p \times \left(\frac{\Phi}{\Phi_0}\right)^n \times \left(\frac{R_p}{R_{p0}}\right)^{0.133} \tag{5.68}$$

Similar to Mostinski's approach, the pressure correction factor is defined as:

$$F_p = 1.2 \times p_r^{0.27} + 2.5 \times p_r + \frac{p_r}{1 - p_r} \tag{5.69}$$

and the exponent for the relative heat rate:

$$n = 0.9 - 0.3 \times p_r^{0.3} \tag{5.70}$$

Another potential candidate for a boiling correlation would be the one of Ribatski-Siaz and Jabardo. Alavi Fazel [124] has compared ten correlations and developed an own correlation. The table shows his results, accuracy of the correlations is indicated.

Table 5.15: accuracy of various boiling correlations for different fluids [124]

model -	2-Propanol [%]	Ethanol [%]	Methanol [%]	Water [%]	Acetone [%]
Mostinski	24	34	70	⋆	⋆
McNelly	38	61	88	71	36
Boyko&Kruzhiline	66	66	67	79	53
Stephan&Abdelsalam	28	63	*?*	83	70
Gorenflo	21	21	12	15	15
Nishikawa	23	52	79	66	64
Fujita	*?*	*?*	*?*	*?*	53
Labantsov	93	93	92	94	*?*
Jung	52	*?*	*?*	*?*	93
Cooper	39	77	*?*	*?*	66

? deviation very off

Further work on this topic has been conducted by Hsieh et al. [125], Quoilin [48], and Garcia et al. [126]. Hsieh et al. have delivered a correlation that is worth looking into it. Despite it has been created to estimate vertical plate evaporation, one should consider it. Taking a look into Gnielinsky's widely accepted approach for condensation on a tube bundle, one will realize that plate and tube heat exchangers solely differ by a simple characteristic factor. Quoilin [48] has deduced a correlation based on Hsiehs [125] results. It extends the convective heat transfer by a factor and the Boiling number.

$$h = C \times \alpha_{conv} \times Bo_{0.5} \tag{5.71}$$

where

$$Bo = \frac{\Phi}{A_{trans} \times g \times h_{gf}}$$

Containing the heat rate, this equation requires again a recursive calculation. The above results gave the motivation to look deeper into several more or less complex correlations: Mostinski, Gorenflo, Stephan and Hsieh. The following section will provide results for this specific case, deciding which correlation is most suitable for tube-shell-evaporators that are evaporating Siloxanes on a steel surface.

5.8.5.6 Comparison of boiling correlations

The above listed boiling correlations have been investigated according to their accuracy and precision for siloxane fluids. Monitored data of average operation days have been used for calibration. From these data the heat transfer coefficients of the evaporator are calculated and compared to the predictions of the different models. The data set contains low, mid and almost full load of the cycle, in order to account for all regimes that might occur. In order to make the boiling correlations comparable, surface effects have to be cancelled. For Mostinski and Gorenflo the roughness and the reference roughness are set to the same value. When calculating the correlation the offsets to the measured values vary from +95% (Mostinski) up to +490% (Cooper, Gorenflo, Collier). In order to get a qualitative view, the correlations are normalized with respect to the according mean value.

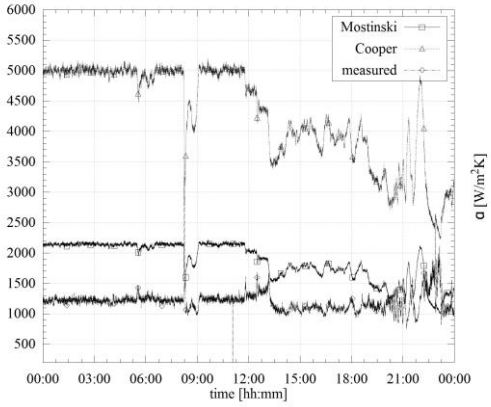

Figure 5.37: comparison of boiling correlations (Mostinski and Cooper) vs. measured values

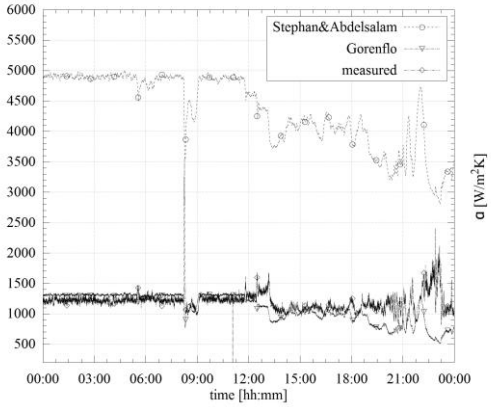

Figure 5.38: comparison of boiling correlations (Stephane& Abdelsalam and Gorenflo) vs. measured values

The above correlation are all deviating far from the measured results. However, their derivatives are well correlating with the monitoring data. This fact led to the decision to modify these formulations under the following conditions:

- The surface roughness is not known. Hence, the roughness factors are eliminated, respectively included.
- If reference values, such as α_0 and Φ_0, are required the design values are chosen (1325W/m²K and 20000W/m²).
- In a first attempt the correlations will be fitted by just one multiplicand.
- Furthermore, the exponents will be adjusted.
- Finally an own, modified formulation will be fitted.

Mostinski's adjusted formulation by a multiplicand (correlation 1):

$$\alpha = C \times 0.00417 \times \Phi^{0.7} \times p_c^{0.69} \times F_p \tag{5.72}$$

and fitting a custom exponent for the specific heat rate term (correlation 3):

$$\alpha = C \times F_p \times \Phi^n \tag{5.73}$$

Gorenflo's correlation in a modified version (correlation 4):

$$\alpha = C \times \alpha_0 \times F_p \times \left(\frac{\Phi}{\Phi_0}\right)^n \tag{5.74}$$

and finally one approach neglecting the heat rate and concentrating on the mass flow factor (correlation 2):

$$\alpha = C \times \alpha_0 \times F_p \times \left(\frac{\dot{m}}{\dot{m}_0}\right)^n \tag{5.75}$$

where the pressure correlation F_p is calculated according to Equation 5.65 and $\dot{m}_0$ is 20kg/s.

Table 5.16: fitting results for evaporator correlations

correlation	C	n	PPMCC	$R2$
1	0.0031	0.6809	99.049%	0.9811
2	0.2352	0.3740	98.790%	0.9759
3	0.5290	-	99.050%	0.9811
4	315.93	-	98.610%	0.9724

The correlation being used in the final evaporator model is number two. During validation it has shown the most favourable overall results among the four candidates (mean deviation, minimum/maximum deviation).

5.8.5.7 Modelling assumption for the evaporator

The following assumption have been made to simplify the physical process to a model-able complexity.

- Hot side, thermal oil feed: the flow distribution is uniform, the mass flow entering through the flange is equally distributed across all tubes of the bundle. Therefore, the flow velocity and heat transfer coefficient of in all tubes is equal.
- Tube bundle: instead of several groups of u-tubes with slightly differing length, all tubes are calculated with the mean length. Consequently, the pressure drop across the u-tubes is uniform.
- Actually not worth mentioning: the relative roughness of the inner surface is equal across all tubes.

- Cold side, the Siloxane feed: the MDM flow enters the vessel in a non-boiling state.
- The flow entering through the DN200 tube spreads equally in the vessel and creates an homogeneous state before the heat transfer is initialized.
- Furthermore, the flow spreads equally across the sections separated by the baffles. One receives eight sections of equal size and equal pressure conditions.
- Isobaric evaporation is a myth. However, the rather small pressure decrease in the end zone of the evaporator causes a slight decline in saturation temperature. Assuming a pressure difference of 0.07bar the difference in saturation temperature is 0.6K. This effect is neglected.

5.8.5.8 Vapour convection

While the heat transfer in the wetted evaporator bundle is determined by the pool boiling correlation, the part of the bundle above the liquid level needs another calculation. Vapour is rising as bubbles from the pool and accelerates towards the vapour outlet. By expanding during the evaporation process the Reynolds numbers and Prandlt numbers differ significantly from those of liquid MDM. Gnielinsky and Gaddis propose the following, widely accepted method [63], chapter [Gh1]:

$$Nu_{bun} = f_A \times f_N \times f_B \times Nu_{tub} = f_A \times \sqrt{Nu_{2lam} + Nu_{2tur}} \tag{5.76}$$

Matching coefficients are widely used in order to account for effects as by-passing the bundle, inhomogeneous flow contributions (preferred lanes) and the effects of baffles in the bundle. In this case, the flow pattern is cross-flow and no baffles are diverting the flow. Therefore, one coefficient is required to characterize the flow through the tube arrangement (f_A), one for the influence of the number of tube rows (f_N) and one for the bypass between shell and the array (f_B). The laminar contribution to the bundle heat transfer value is [63][Gh1]:

$$Nu_{lam} = 0.664 \times Re_{\Phi} \times \sqrt[3]{Pr} \tag{5.77}$$

the formulation for the turbulent layer can be written as follows [63][Gh1]:

$$Nu_{tur} = \frac{0.037 \times Re_{\Phi}^{0.8} \times Pr}{1 + 2.443 \times Re_{\Phi}^{-0.1} \times (Pr^{2/3} - 1)} \tag{5.78}$$

For the given geometrical attributes of the evaporator with its staggered tube pattern (pitch: 21.4mm/18.5mm/60°) one receives a vertical pitch ratio b of 1.158 and a horizontal pitch ratio a of 1.338. For ratios of b that are larger than one the void volume ratio is defined as:

$$\Psi = 1 - \frac{\pi \times D}{4 \times S_1} \tag{5.79}$$

For the given geometry Ψ is 0.429. Consequently, the geometric adjustment factor can be calculated for a staggered arrangement as follows:

$$f_A = 1 + \frac{2}{3 \times b} = 1.576 \tag{5.80}$$

The Reynolds number for this fluid flow is calculated dividing the Reynolds number in the cross section before entering the bundle by the according Ψ. The evaporating surface area of the fluid, at the given level of 200mm below the bundle top, is 4.8m². Certainly these geometric attributes are just a rough estimation, as the level differs slightly and the boiling surface is very wavy.

5.8.6 Condenser

Figure 5.39 shows a 3D model (including a cutaway) of the condenser. Saturated working fluid vapour is entering the vessel through the DN800 flange on the bottom left. From there, the vapour is routed to the top of the vessel. The vapour wets the tube bundle, droplets appear on the cold surface and flow to the bottom of the bundle. The entire condensing liquid film is collected in the bottom of the shell and directed to the hotwell.

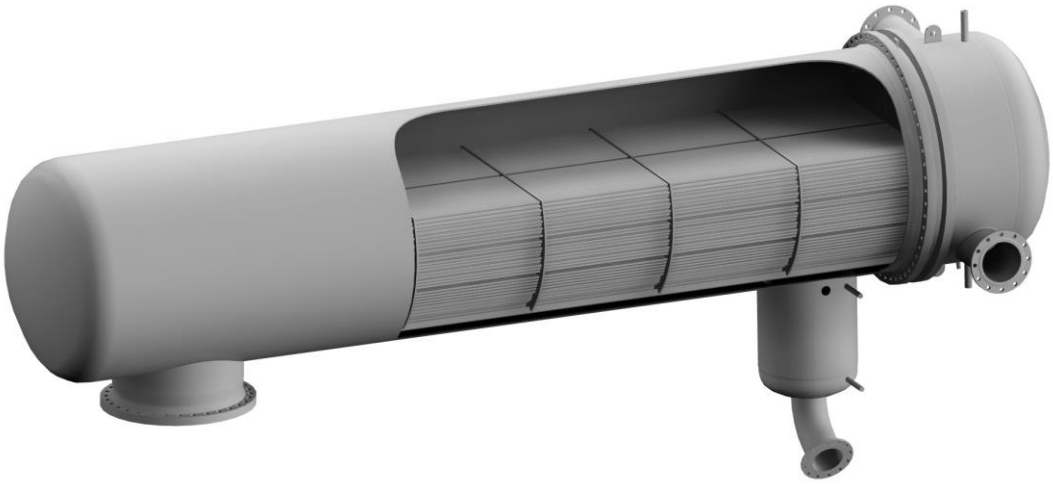

Figure 5.39: 3D-view (section) of the condenser

In this chapter the characteristics of the sink side heat exchanger, the condenser are elaborated. The following Table 5.17 gives a brief overview about all relevant parameters of the apparatus:

Table 5.17: specifications of condenser

symbol	value	unit	description
Φ_{nom}	5300	kW	nom. heat rate
Δp_1	0.05	bar	nominal pressure loss hot side
Δp_2	0.2	bar	nominal pressure loss cold side
U_{nom}	578	W/m²K	heat transfer coefficient
connector 1	800/200	DN	flange hot side
connector 2	250	DN	flange cold side
V_{tot}	5.93	m3	total shell volume
V_{dis}	1.79	m3	tube array displacement
V_1	3.448	m3	hot volume
V_2	1.145	m3	cold volume
V_3	0.17	m3	hotwell volume
V_{metal}	0.644	m3	tube metal volume
$A_{trans,log}$	321	m2	heat transfer area (log mean)
A_{trans1}	315	m2	heat transfer area (hot side)
A_{trans2}	252	m2	heat transfer area (cold side)
k_f	0.0002	m²K/W	fouling factor
D_{shl}	1.376	m	outer diameter of shell
D_{tub}	20	mm	outer diameter of tubes
d_{tub}	16	mm	inner diameter of tubes
L_{out}	5.484	m	length of shell
L_{tub}	3.6	m	net leg length of tubes
L_{u-tub}	8.172	m	average length of one u-tubes
$\dot{m}_1$	63	kg/s	nominal mass flow hot side
$\dot{m}_2$	20	kg/s	nominal mass flow cold side
γ	60		tube array pitch

5.8.6.1 Condensation and sub-cooling

Condensation of a vapour takes place under the condition that the local temperature of the vapour falls below the saturation temperature. A condensation is most likely to happen at a surface. In an ideal heat exchanger, where the vessel

contains (or rather not contains) a perfect vacuum, the condensation process would start immediately when the above conditions occur. As this perfect heat exchanger does not exist, we have to take a look into the theory of non-ideal condensation. In non-ideal condensation the pressure in the vessel is higher than the expected condensing pressure. Therefore, in a real system condenser pressure and condensing pressure are not the same and must not be mixed up.
In reality the condensers content is composed of:

- Not a surprise: the main working fluid.
- Inert gases: such as Nitrogen, Oxygen, CO, CO_2 et cetera. Incondensables that are not liquefiable within the temperature range of the cycle.
- High-boiler drops enclosed in the vapour. In ORC-units mainly higher chain compounds or lubrication oil. Their contribution to the increase of condensing pressure is negligible.
- Low-boilers, fluids that are always gaseous within the temperature range of the cycle. In ORC-modules especially chemical cracking residues and lower order relatives of the main fluid.

The absolute static pressure in a condenser is determined by the sum of all fluids and their state, as shown in the following equation:

$$p_{tot,cond} = \sum_{i=1}^{n} p_i = p_{MDM} + p_{incon} + p_{hb} + p_{lb} + p_{lub} \tag{5.81}$$

The occupied volume of liquids in the condenser plays an inferior role. Hence, the last two terms of the above Equation 5.81 can be neglected. The saturation pressure on the fluid, here simplified just MDM, is known. As a last unknown the term of incondensables remains. The composition of the organic fluids in an ORC can be measured (see Chapter 7), while the gases in an industrial condenser can only be estimated. This is the point where the physical model needs an empirical adaptation.
The role of impurities or contaminants has to be observed in detail. As mentioned earlier in the introduction, there is no such thing as a pure fluid in industrial applications. Besides the role of inert gases, that are pretty common in all condenser types and all fluid types, organic compounds have to bear fluid decomposition. After several years of operation a cycle shows a natural degradation of the fluid. Especially in the boiling and condensation the reaction

residues show undesired side-effects. Low-boilers form a non-condensible vapour cushion in the condenser. In a mixture with the original fluids vapour the heat conduction through the vapour decreases. In addition, a certain proportion of low-boilers is enclosed in the liquid condensate film, inhibiting the heat transport though the liquid to the tube. The condenser unit is a shell-and-tube heat exchanger. The silicone oil is condensed on the outside of the tube bundle. Water is pumped trough the three tiers of tubes, consisting of 697 bent u-tubes in total. The tiers consist of 219, 237 and 241 tubes. Therefore, the flow inside the tubes is slightly accelerated between the three stages. All tubes are arranged staggered in a triangle array with an axis to axis distance of 26 mm.The gaseous silicone oil enters the condenser from the bottom flowing to the upper wall. It is expected that the first tubes on the top of the array condense in droplet mode. More condensate forms on the lower tube rows, resulting in a constant curtain of liquid. This stream is collected on the bottom and flowing into the hotwell. The vapour stream is divided by four baffles. Thus, it can be assumed that four of the five chambers are vertically almost unmixed. To determine the overall U-value for the tube bundle under these flow conditions, we divide it into three heat transfer coefficients for inner and outer convection and heat conduction through the tube material:

$$\frac{1}{U_{cond}} = \frac{1}{\alpha_{cold}} + \frac{2 \times \lambda_{tube}}{d_{in} \times ln(d_{out}/d_{in})} + \frac{1}{\alpha_{cold}} + \sum_{i=1}^{n} R_{foul,i} \tag{5.82}$$

Where α_{cold} characterizes the cooling water flow inside the tubes with the Nusseltnumber of the water flow:

$$\alpha_{cold} = \frac{Nu_{cold} \times \lambda_{tube}}{d_{in}} \tag{5.83}$$

According to Gnielinsky [127] for flow regimes with $3000 < Re < 5 \times 10^6$ and $0.5 \leq Pr \leq 2000$:

$$Nu_{cold} = \frac{(f_{DW}/8) \times (Re - 1000) \times Pr}{1 + 12.7 \times (f_{DW}/8)^{1/2} \times (Pr^{2/3} - 1)} \tag{5.84}$$

Including the Darcy-Weisbach friction factor f_{DW} defined for this case by Petukhov [128] and recommended by Gnielinsky [127]:

$$f_{DW} = (0.79 \times ln(Re) - 1.64)^{-2} \tag{5.85}$$

This rather simple formulation is adequate in this case because the flow regime is fully turbulent. For the lower turbulent or the transition regime a more complicated approach, such as Serghides or Romeo et al. [107], has to be chosen. To characterize the flow behaviour of the condensing vapour outside of the tubes, the vapour around the tubes is considered at rest. It is assumed that no inert gas fractions are in the shell. It is further assumed that the condensing film flows vertically and undisturbed by horizontal forces.

In order to categorize the flow regime one can make a first approach to determine the Reynolds number of the condensing film. Therefore, the vertical velocity of the film is necessary. It is a result of the shear friction in the fluid resisting to the gravitational forces. With increasing film thickness, respectively mass flow, the velocity increases. Furthermore, a lower viscosity results in a lower shear friction. The last component in the heat transfer through the liquid film is the thermal conductivity. Both viscosity and thermal conductivity are depending on the film temperature. As it is rather difficult to measure the film velocity we deduct it from an estimated mass flow (here 20kg/s) along the vertical direction y. The Reynolds number for this case is a function of Γ, the integrated mass flow per length [110].

$$Re_{film} = \frac{4 \times \Gamma(y)}{\mu_{liq}} \tag{5.86}$$

$$Re_{film} = \frac{4 \times \dot{m}}{\mu_{liq} \times x} = \frac{4 \times \rho_{liq} \times \vec{v}_y \times \delta}{\mu_{liq}} \tag{5.87}$$

Where δ is the thickness of the film and b is the length of the surface (here length of a tube). For the case at hands (x = 3.6m, $\dot{m}$ = 20kg/s, ϑ_{liq} = 85 °C) we receive a Reynolds number of 900. This is the wavy laminar regime, but far away from the turbulence limit of Re = 1800. At the transition of the two regimes the following correlations return the Nusselt numbers [111]:

$$Nu_{lam} = 1.47 \times Re_{film}^{-1/3} \tag{5.88}$$

Which is valid for $Re \leq 30$, or the second correlation for the range of $30 \leq Re \leq 1800$ by Kutateladze [111]:

$$Nu_{wavy} = \frac{Re_{film}}{1.08 \times Re_{film}^{1.22} - 5.2} \tag{5.89}$$

From the above equations the question of regime for the case study is answered: knowing that the condensation takes place within the laminar and wavy laminar regime, a deeper look into the heat transfer is necessary.

A mean heat transfer coefficient can be predicted for one tube in the first row of the array. The following equation, based on Nusselt's condensation theory [129] on vertical plates, takes several flow regimes into account. From the first droplets, to growing drops and then to a fully developed laminar (including wavy laminar) film running around the tubes [111, 114, 130]:

$$\bar{\alpha}_D = C \times \left[\frac{g \times \rho_l \times (\rho_l - \rho_v) \times \lambda_l^3 \times h'_{fg}}{\mu_l \times (T_{sat} - T_{tube}) \times d_{outer}} \right]^{1/4} \tag{5.90}$$

It should be mentioned that the above liquid transport properties are defined for the film temperature. This film temperature is different from the liquid saturation state and the tube wall temperature.

As a simplification, it is assumed in this case that T_{tube} for each tier in the bundle of tubes is equal to the mean temperature of the tier. Under design conditions, the input of cold water would be 60 °C and the output 80 °C. In this case we obtain the mean temperature 70 °C. The condensing temperature of the MDM varies between 80 °C and 95 °C under average working conditions. We assume the condensing temperature T_{sat} 88 °C for this case. The changing number of parallel tubes per tier results in three different local velocities. With $C = 0.729$ for a tubular wall, the average convection for one tier of horizontal tubes with the number of N rows can be expressed as:

$$\bar{\alpha}_{DN} = \bar{\alpha}_D \times N_{-1/4} \tag{5.91}$$

The exponent in the above equation has been modified for various combinations to account for non-ideal behaviour or increased turbulences. Some authors

(for instance Lee and Mai[131]) recommend a more elaborate adaptation as the Eissenberg expression. Calise et al. [132] are following Butterworths proposal from

1977 and recommend to use $-\frac{1}{6}$ as exponent for the above Equation 5.91. Browne and Bansal [133] refer to numerous researchers propagating different values for the exponent. A common agreement for different applications does not seem to exist. Thus, in the case at hands the original exponent is used in the first place, and is altered if the first results indicate the necessity to do so. Yilbas and Altuntop

[134] and Cheng and Tao [135] have shown that fair results within 10% respectively 15% of variation are possible when using the original form of the equation. For the case at hands we receive deviations to the measured data of the condenser of 10% if the exponent is set to −0.4.

It should be mentioned that Browne and Bansal [133] provide a comprehensive overview on tube bundle condensation. Especially finned tubes and surface enhancements are described in detail.

According to Rohsenow [114], the following correlation for the modified latent heat of the condensate can be used considering the Jakob number:

$$h'_{fg} = h_{fg} \times (1 + 0.68 \times Ja) \tag{5.92}$$

Viscosity and thermal conductivity of the fluid are taken from the DIPPRdatabase [81]. Heat capacity and density and other required properties of MDM are calculated with the REFPROP-library [84]. Under the possible operating conditions with mass flows of cooling water between 20 m^3/h and 250 m^3/h and silicone oil mass flows between 2 kg/s and 24 kg/s, the overall heat transfer coefficients for the condenser are calculated, as shown in Figure 5.40. The weighted mean value of all three tiers are connected with a logarithmic fit.

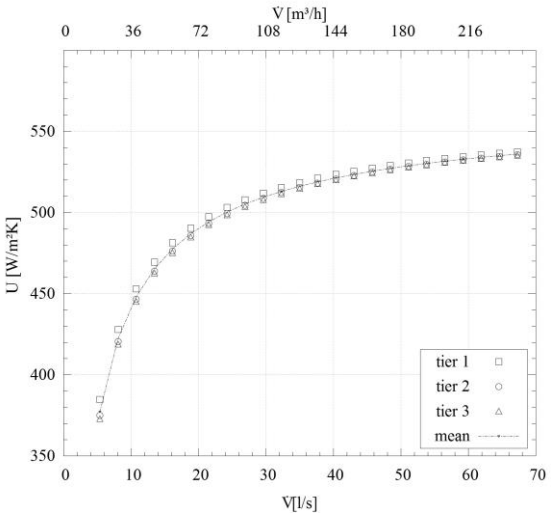

Figure 5.40: calculation of U-value for condenser with three tiers (water temperatures 60 °C/80 °C)

The fully turbulent flow inside the pipes reaches Reynold numbers up to 70000. This leads to an inner heat transfer coefficient of up to 12000 W/m^2K. The heat resistance in the pipe material is almost negligible. The heat transfer through the condensing film is dependant on the viscosity of the fluid and the density

difference between vapour and liquid. The heat transfer coefficient due to condensation at the outer surface of the tubes results much lower than that at the inner surface (about 500W/m²K), hence the overall heat exchange is limited by the condensing side.

The above mentioned behaviour should lead to the expectation that with higher mass flows on the cooling side the condensing temperature and pressure decrease. This effect is caused by the resulting increase of the overall LMTD. The LMTD for the condenser is more complex to obtain than in heat exchangers with no phase change. In cases when the super-heating and sub-cooling in the condenser occupies only a small part of the total heat transfer area the calculation is straightforward. The mean temperature of the cold side and the condensing temperature suffice to form a representative overall mean temperature. In the case at hands we have no iso-thermal condensation. The vapour enters with 110 °C to
130 °C, which leads to a significant proportion of de-super-heating (15% to 25%). In order to receive a proper LMTD the following formulation has been chosen under the assumption that the heat capacity remains constant during the single sub-processes :

$$\Delta\bar{T}_{log} = \Delta T_{log,dsh} \times \frac{\Phi_{dhs}}{\Phi_{total}} + \left(T_{sat} - \bar{T}_{cold}\right) \times \frac{\Phi_{cond}}{\Phi_{total}} + \Delta T_{log,sc} \times \frac{\Phi_{sc}}{\Phi_{total}} \qquad (5.93)$$

For the calculation of condensing film properties a modified film temperature can be used:

$$T_{film} = T_{sat} - 0.75 \times \left(T_{sat} - \bar{T}_{wall}\right) \qquad (5.94)$$

5.8.6.2 Cold side heat transfer

The before mentioned convective heat transfer delivers reasonable results over a daily average. For volatile calculations the results are not satisfying. Furthermore, for simulation purposes the complexity is too high. To derive the film transport properties several iterations (guess for film temperature and saturation pressure) are necessary. Therefore, a more robust approach is chosen. The data sets of one month have been used to find a suitable correlation. In his thesis Quoilin [48] proposes an approach for the U-value of an condenser; it correlates to the power of 0.4 with the mass flow. A similar correlation is used, except with an additional factor that takes the change in the Prandtl number into account:

$$\alpha_{cold} = \alpha_0 \times \left(\frac{\dot{m}}{m_0}\right)^a \times \left(\frac{Pr}{Pr_0}\right)^b \tag{5.95}$$

coefficient	α_0	$\dot{m}_0$	a	b
value	510.7W/m²K	20kg/s	0.73	-0.29
	PPMCC	adj.R^2	RMSE	SSE
	0.9681	0.9372	6.066	1.272e+06

The above model predicts the heat transfer of the condensing film within a accuracy range of ±10%. The Figure 5.41 depicts the calculated and measured U-value for a merged dataset of seven days (time step: 10 seconds) including the deviations as a time series. Figure 5.42 shows the same data set as a scatter plot.

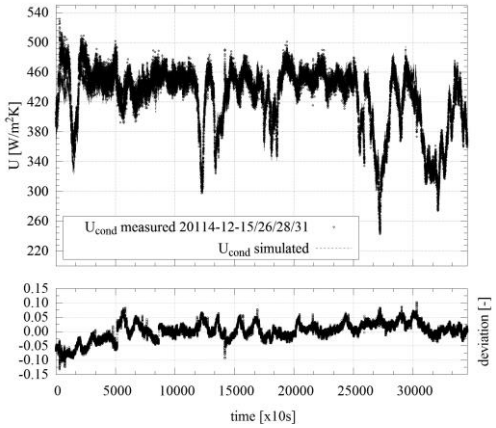

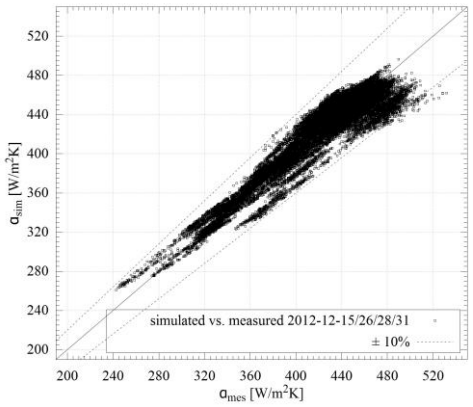

Figure 5.41: condenser convective heat transfer model and measured values vs. time

Figure 5.42: condenser convective heat transfer model vs. measured values

5.8.6.3 Dynamic condenser model

The dynamic condenser model is based on the specifications of the condenser unit in the previous section. The assumptions and simplifications for the dynamic model are the following:

- The entire vessel (Figure 5.39) is divided into two volumes: the shell itself and the hotwell.
- It is assumed, that the net vapour volume is completely filled with a vapour or vapour mixture of a homogeneous kind.

- The condensing film is instantly collecting in the hotwell. Accumulations elsewhere or travelling condensate flow on the bottom of the vessel are not respected. Therefore, the resulting time lag is ignored.
- All fluids are assumed to be compressible.
- Heat storage occurs in the tube material between the two fluids. The temperature fluctuation in the shell metal is very low, hence its thermal inertia is not relevant.

The entire model consists of the following modelica classes:

- Flow1DCONC: eExtended Flow1D class with variable heat transfer calculation according to Gnielinski's turbulent tube flow.
- ConvHT htc: heat transfer connector between variable and constant heat transfer coefficient, one each for cold and hot side.
- CounterCurrent: swap function for temperature and flux vectors.
- MetalTube: tubular conduction ,including thermal inertia, through a metal tube with one radial node and N axial nodes.
- CondenserShell: variable heat transfer based on mass flow correlation.

The vapour fraction in the shell is defined as:

$$m_{vap} = V_{vap} \times \rho_{vap} \tag{5.96}$$

where m_{vap} is the vapour mass cumulated in the shell. The liquid fluid mass is defined as:

$$m_{liq} = V_{liq} \times \rho_{liq} \tag{5.97}$$

The total volume, which consists of the shell volume without the tube bundle displacement, is a sum of the above masses:

$$m_{cond} = m_{liq} + m_{vap} \tag{5.98}$$

The change of total mass ($\frac{dm}{dt}$) during a time step is defined by the vapour entering the volume and the condensate leaving it:

$$\frac{dm}{dt} = \dot{m}_{in} - \dot{m}_{cond} \tag{5.99}$$

The according energy balance for the entire enclosed volume:

$$E = m_{liq} \times h_{liq} + m_{vap} \times h_{vap} - p \times V \tag{5.100}$$

The change of vapour and liquid mass during one time step:

$$\frac{dm_{liq}}{dt} = \frac{dV_{liq}}{dt} \times \rho_{liq} + V_{liq} \times \frac{\partial \rho_{liq}}{\partial p} \times \frac{dp}{dt} \tag{5.101}$$

$$\frac{dm_{vap}}{dt} = \frac{dV_{vap}}{dt} \times \rho_{vap} + V_{vap} \times \frac{\partial \rho_{vap}}{\partial p} \times \frac{dp}{dt} \tag{5.102}$$

where

$$\frac{dm_{cond}}{dt} = \frac{dm_{vap}}{dt} + \frac{dm_{liq}}{dt} \tag{5.103}$$

The change of energy inside the vessel:

$$\frac{dE}{dt} = \frac{dm_{liq}}{dt} \times h_{liq} + m_{liq} \times \frac{\partial h_{liq}}{\partial p} \times \frac{dp}{dt} + \frac{dm_{vap}}{dt} \times h_{vap} + m_{vap} \times \frac{\partial h_{vap}}{\partial p} \times \frac{dp}{dt} - V \times \frac{dp}{dt} \tag{5.104}$$

where $\frac{\partial h}{\partial p}$ is the partial derivative of the enthalpy.

If the metal mass of the vessel is inside the system boundary, the derivative of the stored energy ($\frac{dE_{metal}}{dt}$) can be derived from the hot side heat flow and the cold side heat flow:

$$\frac{dE_{metal}}{dt} = \phi_{cold} - \phi_{hot} = 0 \tag{5.105}$$

If the thermal inertia of the condenser is accounted for elsewhere, the above term equals zero. The change of energy during one time step is the sum of all flows crossing the system boundary and the transferred energy on the hot side:

$$\frac{dE}{dt} = \dot{m}_{vap} \times h_{vap} - \dot{m}_{liq} \times h_{liq} + \phi_{hot} \tag{5.106}$$

With α_{hot} defined as a function of the vapour's mass flow and the Prandtl number, the transferred heat on the hot side is defined as:

$$\varphi_{hot} = \alpha_{hot} \times A_{hot} \times \Delta T \tag{5.107}$$

And finally the heat flux to the cold side:

$$\varphi_{cold} = \dot{q}_{cold} \times A_{cold} \quad (5.108)$$

5.9 Piping

Within the cycle model some pipe connections are more relevant for the result quality than others. Not all pipe connections of the system are represented in the model. Some connections, such as the auxiliary evaporator turbine bypass, are neglected. As start-up and stop procedures are exceptional events, they are not relevant. The following Table 5.18 shows the modelled connections in the system:

Table 5.18: relevant pipe connections and properties

route from-to	length [m]	diameter [DN]	V [m³]	elev. [m]	bend type*?* si/do/st/3D*??*
pump-recu.	7.895	150	0.139	1.832	3x si
evap.-turbine	6.435	200	0.114	0	3D /3x si
hotwell-pump	3.2431	200	0.057	1.756	60°/60°
recu.-pre-heater	13.899	150	0.245	0.892	3D /3x si

? bends are classified according to VDI specifications: single, double, stage, 3D

?? elevation is calculated in relation to each start point - no absolute values

All above mentioned pipes have an assumed roughness of 25micron, a standard value for steel tubes of that type. In order to achieve a fast and accurate simulation the pipe connections are slightly simplified. The tube flow calculation is based on the same theory as the tube bundles in the heat exchangers. In general there are two strategies for pipe friction calculations: each time step and node is calculated separately, or the friction parameters are related to a nominal value. The second one is delivers acceptable results at low CPU load.

Table 5.19: relevant pipe friction losses

route from - to	ρ [kg/m³]	Re [m³/s]	V [-]	Pr
pump - recu	749.8	4.1E+05	0.027	9.26
evap - turb	46.2	1.1E+07	0.433	0.68
hotw - pump	747.9	3.1E+05	0.027	9.20
recu - preh	642.4	9.1E+05	0.031	5.95

route from - to	DWff [-]	Δp_{flow} [Pa]	Δp_{geo} [Pa]	Δp_{pipe} [Pa]
pump - recu	0.015	693	13476	1800
evap - turb	0.013	1785	0	5650
hotw - pump	0.016	68	-12884	100
recu - preh	0.014	1330	-5622	1200

? calculation is based on a nominal mass flow of 20kg/s. The nominal temperatures are 90 °C, 180 °C, 280 °C. The nominal pressure levels are 0.3bar and 7bar.

Time offset due to the flow path length and thermal inertia are represented in the model by the following assumptions (extending Casellas Water.Header-model):

$$E = m \times h - p \times V \tag{5.109}$$

$$m = \rho \times V \tag{5.110}$$

with mass balance

$$\frac{dm}{dt} = \dot{m}_{in} - \dot{m}_{out} = V \times \left(\frac{\partial \rho}{\partial h} \times \partial p + \frac{\partial h}{\partial p} \times \partial \rho \right) \tag{5.111}$$

and energy balance

$$\frac{dE}{dt} = h \times \frac{dm}{dt} + m \times \Delta h - V \times \Delta p$$
$$= \dot{m}_{in} \times h_{in} + \dot{m}_{out} \times h_{out} + \Phi_{loss} \quad (5.112)$$

The heat loss respectively gain is set as a constant parameter. The thermal inertia of the pipe and the temperature gradient through the pipe material are neglected.

Finally we receive the residence time or the time difference between outlet and inlet of the pipe connection:

$$\Delta t = \frac{m}{\dot{m}_{in}} \quad (5.113)$$

The following Table 5.20, lists all relevant pipe connections in the cycle and the according heat loss.

Table 5.20: heat losses of pipe connection

route -	U-value [W/m²K]	spec. loss [W/m²]	spec. loss [W/m]	surf temp. [°C]
TO feed	0.361	85	85	33.5
TO return	0.361	66	66	31.6
TO feed	0.826	46	184	29.6
TO return	0.826	59	294	30.9
turbine feed	0.361	101	648	35.1
turbine drain	0.177	140	140	39.0
hotwell-pump	0.826	45	144	29.5
pump-recuperator	0.826	36	286	28.6
recuperator-evaporator	0.431	60	840	31.0
bypass evaporator	0.431	68	307	31.8
bypass recuperator	0.431	78	155	32.8
safety valve	0.431	78	428	32.8

5.9.1 Vapour filter

In order to prevent a turbine damage by the impact of solid particles, a vapour filter is situated right before the turbine inlet flange. The type being used (ARI 35.050-DN200-PN40) is a y-pattern strainer with a stainless steel filter. The mesh width is 1.6mm, supported by a basket. Previous checks during maintenance have shown an unexpectedly high amount of loose welds

precipitating in the reservoir. Based on the fluids states and the location in the cycle, the filter is the fitting component with the highest pressure loss. According to the following formulation we receive the pressure drop as a function of the flow through the strainer:

$$\Delta p_{filter} = \zeta_{filter} \times v^2 \times \frac{\rho}{2} = \frac{\zeta_{filter} \times \dot{m}^2}{2 \times \rho \times A^2} = \Delta p_{nom} \left(\frac{\dot{m}}{\dot{m}_{nom}} \times \frac{\rho}{\rho_{nom}} \right)^2 \quad (5.114)$$

coefficient	ρ_{nom}	$\sim v$	Δp_{nom}	ζ_{filter}	$\dot{m}_{nom}$
value	64.549kg/m^3	8.74m/s	56892Pa	18.123	20kg/s

The ζ is usually given by the manufacturer or it can be calculated via the filter diameter and the void fraction of the mesh. In the dynamic model the nominal value for the pressure difference is calculated with the according nominal mass flow. The obtained value is the parameter for the calculation in the operational point mode. In this case ζ_{filter} could be obtained by several measurements. Besides the pressure characteristics the steam filter is not not respected in terms of thermal capacity, heat loss and turbulence generation.

5.10 Control components

5.10.1 Hotwell reservoir

The condenser reservoir, known as hotwell, collects condensate and provides it to the feed pump. As depicted in Figure 5.39 it is a part of the condenser vessel. Despite it is the smallest vessel in the entire cycle its role for the process is very important. By providing a stable level of liquid to the pump it avoids dry-running. At the same time the separation of gas and liquid assures smooth operation without cavitation on the feed-pump. In this case study the reservoir consists of a tube (DN600) with a height of 0.6m. The design liquid level is 0.3m. At the bottom the tube forms a spherical funnel leading into the connection flange to the feed pump (DN250). In total the hotwell consists of a volatile, measured volume of 161.8l and the spherical residual volume of 20l. The capacity of the hotwell compensates the temporal variations of the condensate mass flow. By doing so, the filling level inside this reservoir governs the behaviour of the control, the feed pump and the pressure characteristics of the cycle.
To describe the hotwell, two different modelling approaches can be used:

- The hotwell acts solely as a mass collector. The enthalpies of inlet and outlet are equal. Input and output pressure are equal. As no mixing occurs in the volume the model is simple. The volume occupied by liquid is comparably small regarding to the total container volume. Mixing effects are negligible in this case.

- The hotwell serves as mass collector, while mixing the actual content with incoming condensate during a time step. The outgoing stream enthalpy is calculated as a mixture of both. Within the vessel two pressures are present. The input opposes a pressure on the liquid surface. Consequently the outlet pressure is a result of the input pressure and the geodetic pressure from the liquid surface to the output flange. For the simulation this approach necessitates start values for initialisation.

In order to simulate the pressure characteristics of the cycle, the variation in pressure should be taken into account. Consequently, the latter strategy has been applied. The outlet pressure is as function of the inlet pressure and a geodetic pressure derived from the level of measured liquid ($l_{liq,1}$) and the height of the residual volume ($l_{liq,0}$).

$$p_{out} = p_{in} + (\rho_{liq} \times g \times (l_{liq} + l_{res})) \tag{5.115}$$

Were ρ_{liq} is the density of the mixed liquid consisting of the inlet stream and the remaining volume of the time step $n - 1$.

$$m_{liq} = V_{liq} \times \rho_{liq} \tag{5.116}$$

where the derivative of mass during one time step is defined as

$$\frac{dm_{liq}}{dt} = \dot{m}_{in} - \dot{m}_{out} \tag{5.117}$$

and the energy content of the vessel (without metal shell), related to a reference enthalpy h_0 is

$$E = m_{liq} \times (h_{in} - h_0) \tag{5.118}$$

and the derivative of the energy can be written as

$$\frac{dE}{dt} = \dot{m}_{in} \times (h_{in} - h_0) + \dot{m}_{out} \times (h_{out} - h_0) \tag{5.119}$$

This approach does not account for the heat exchange between the liquid surface in the gas opposed from the condenser. Furthermore, the heat loss to the ambient is neglected as well as the thermal inertia of the metal. The latter has no relevance as the temperature fluctuations in the hotwell are small. An adiabatic assumption seems fair in this case. Despite the hotwell is connected to the condenser, the influence on the content of the condenser shell caused by varying liquid levels are negligible. Therefore, the pressure derivatives are not accounted for. The container mixes fluid from a time step $n - 1$ with the condensate mass flow of the time step n. The liquid volume of the hotwell is composed of the residual volume and the actually measured volume:

$$V_{liq} = V_{liq,0} + V_{liq,1} = V_{liq,0} + A_{hw} \times l_{liq,1} \times \rho_{hw} \tag{5.120}$$

Where A_{hw} is the inner cross section of the hotwell. The maximum volume of the container can be expressed as follows (checked during simulation for overflow):

$$V_{max} = V_{liq,0} + V_{liq,1} + V_{vap} \tag{5.121}$$

We assume that the non-occupied volume is inert and incompressible and receive the mass balance:

$$m_{hw} = m_{liq} = V_{liq} \times \rho_{hw} \tag{5.122}$$

hence

$$\frac{dm_{hw}}{dt} = \rho_{hw} \times A_{hw} \times \frac{dl_{liq,1}}{dt} = \dot{m}_{in} + \dot{m}_{out} \tag{5.123}$$

$$E_{hw} = m_{hw} \times H_{hw} \tag{5.124}$$

For sake of completeness, in case a heat loss is used in the simulation:

$$\frac{dE}{dt} = \dot{m}_{in} \times h_{in} + \dot{m}_{out} \times h_{hw} + \sum \Phi_{loss} \tag{5.125}$$

The modelica code for this unit can be found in the Appendix A.

5.10.2 Level control

The following scheme in Figure 5.43 depicts the function structure of the feed pump control. As earlier mentioned (see Chapter 4), the level indicator returns a differential pressure. This differential pressure is converted to a geometric height by an external transducer. The maximum level of 600mm is given by the value on the left. The set-point entered via the control interface is a positive integer. In a first step it is converted into a real. This real is subtracted from the maximum level, returning a positive real difference which is feed into the PID-control block. The measured level (word DBD66) is subtracted from the maximum level value. This operation returns a positive value for the process variable. The resulting output of the PID-block is converted into an integer value, before it is sent to the frequency converter of the feed pump.

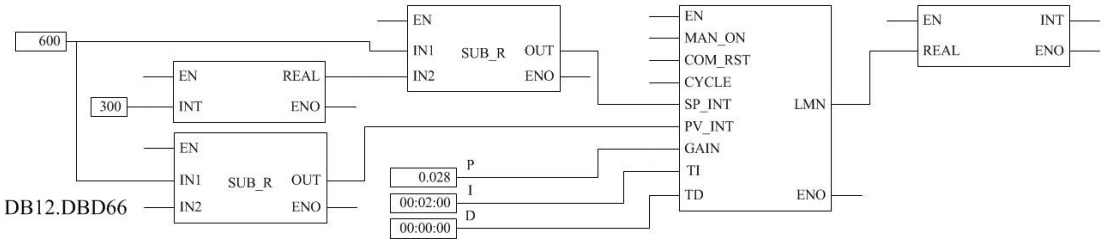

Figure 5.43: scheme of the level control functions in the Siemens S7

The following Figure 5.44 depicts a scheme of the applied modelica basic model based on Astr¨om and H¨agglund [10] which is part of the modelica library (Blocks.Continuous.LimPID).

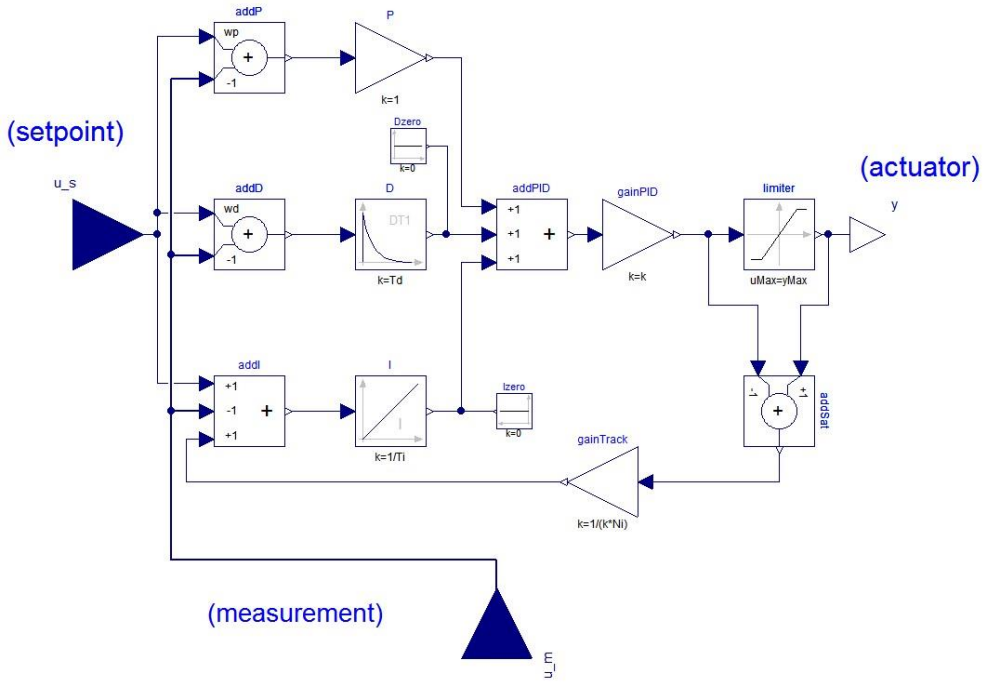

Figure 5.44: scheme of limited PID-controller model [10]

5.11 Feed pump

A six-stage circular type pump serves as feed pump in the cycle. The MSLA 125 by Sterling SIHI has a nominal speed of 1450 RPM (equivalent to 50Hz) [136].
The impeller has a variable diameter between 280mm and 305mm.

Table 5.21: feed pump specifications

value	minimum	maximum	unit
delivery rate	35.21	129.11	m^3/h
impeller diameter	280	305	mm
head		202.67	m
η_{nom}	-	76.3	%
power	29	60.7	kW
$NPSH_R$	1.22	1.75	m

The pump is driven by a frequency modulated electric drive. As described in Section 5.10 above the frequency converter is adjusted by the hotwell control loop.

According to the specifications given by the manufacturer the following behaviour can be modelled applying the law of similarity:

$$\dot{V} = \dot{V}_{nom} \times \frac{n}{n_{nom}} \tag{5.126}$$

$$H = \left(a \times \dot{V}^3 + b \times \dot{V}^2 + c \times \dot{V} + H_0\right) \times \left(\frac{n}{n_{nom}}\right)^2 \tag{5.127}$$

$$\Delta p = H \times g \times \rho_{MDM} \tag{5.128}$$

and finally the hydraulic power of the pump:

$$P_{hyd} = P_{nom} \times \left(\frac{n}{n_{nom}}\right)^3 \tag{5.129}$$

The behaviour of the feed pump for a selection of rotational speeds at nominal temperature and pressure can be seen in Figure 5.45.

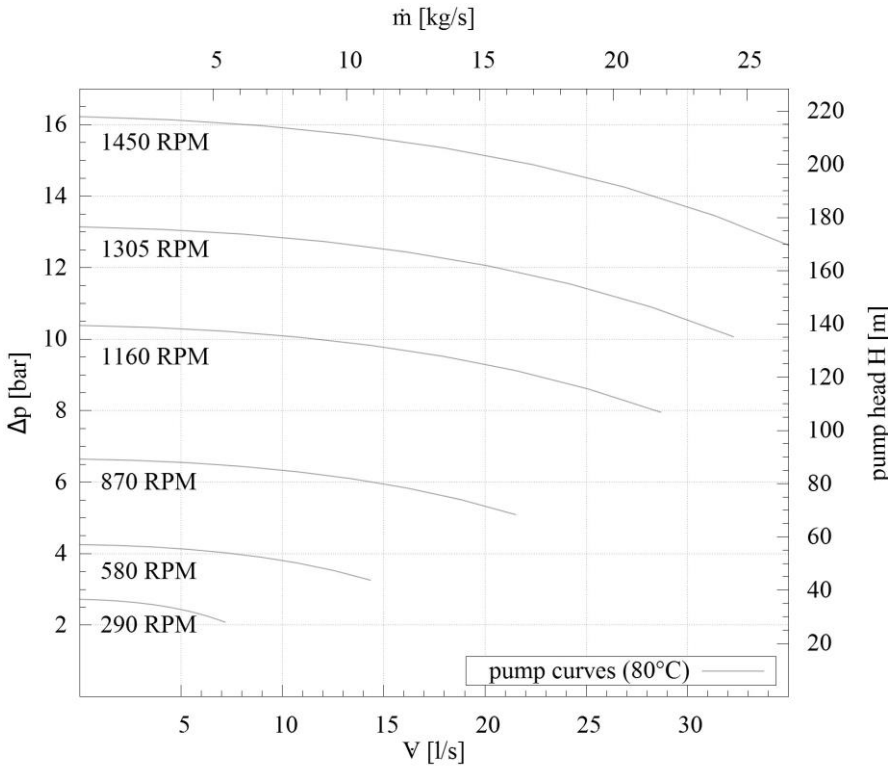

Figure 5.45: feed-pump characteristics for various rotational speeds at nominal temperature (80 °C)

5.12 Turbine

The turbine is an axial single stage turbine (modified type C10S-II) by Tuthill

Nadrowski. Originally designed for steam, the unit was modified for MDM. The radial feed tube releases the live steam into the co-axial chest. A set of 25 De Laval nozzles impinge the blades axially direction with an outflow angle of 19°. The turbine is a pure impulse type with symmetric input and output blade geometry. The design rotational speed is 3000RPM. The turbine shaft is directly connected to the alternator. The turbine is expected to work with a nominal isentropic efficiency of 78%. Previous analyses have shown that the turbine efficiency is strongly dependant on the expansion ratio. While the mean speed of the rotor is constant (158m/s), the vapour flow varies. In partial load, the resulting flow is misaligned to the blade inflow angle. Under design conditions the isentropic outflow velocity is 360 m/s. The nozzle efficiency of 92% is given by the manufacturer. This leads to a flow coefficient of 0.958 and resulting exit velocities around 300m/s. Under design conditions, Mach 1 in the critical cross section $A^?$ is approximately 130m/s. With this geometry (Figure 5.48) the maximum blade efficiency could reach 89.4%. Maximum efficiencies in high load states are around 75%. In part-load only values of 65% can be expected.

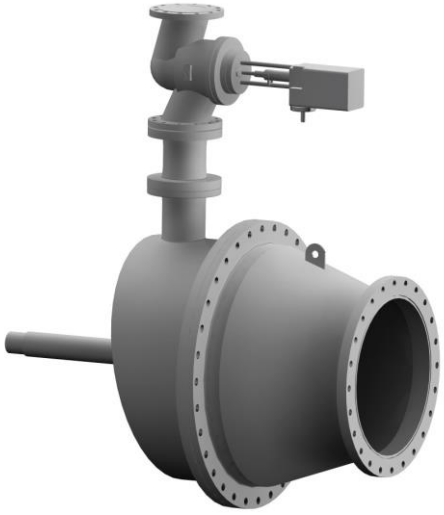

Figure 5.46: 3D-view of the turbine, without alternator unit

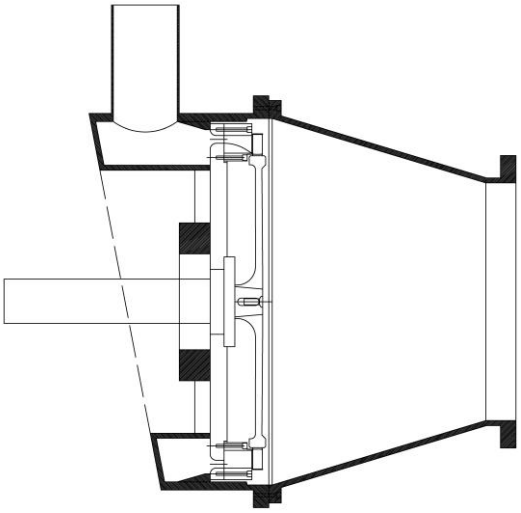

Figure 5.47: section through the turbine and diffuser

Figure 5.46 depicts a 3D-model of the turbine an its connecting flanges. The vapour enters through the turbine valve. The valves throttles the inflow to the turbine during the heat-up and synchronisation phase. In default operation the valve is fully opened. The outlet of the turbine is flanged to a diffuser, reducing the hydraulic diameter to 800mm. Figure 5.47 shows a simplified cross section though the axis of the turbine.

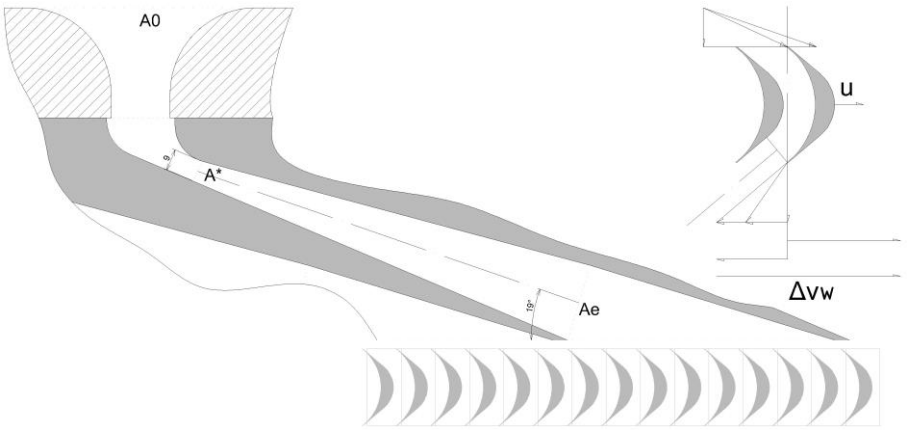

Figure 5.48: wrapped section through the nozzle and blade stage.

Figure 5.48 shows a unwrapped section of one nozzle and a bird eye view on a pair of turbine blades. The three relevant cross sections (inlet, critical, exit) are marked. Figure 5.48 is a photography the turbine rotor, taken during revision. When the rotor is removed from the turbine shaft, one can see through the exit cross section into the nozzle (Firgure 5.50).

Figure 5.49: turbine rotor during revision exit section to critical section

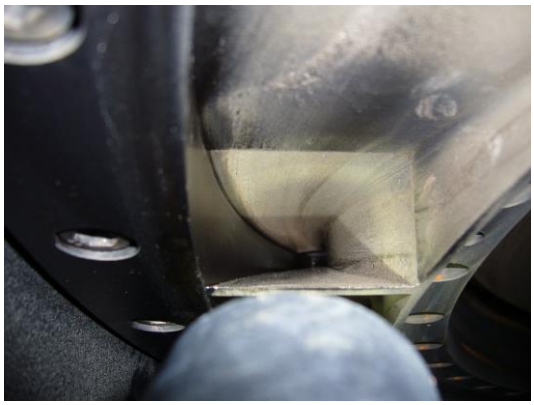

Figure 5.50: view into the nozzle from

5.12.1 Common modelling approaches for turbines

In order to find a good correlation for the behaviour of a turbine the unit is usually taken apart into sections and stages. The modelling of such an engine is basically the modelling of the sum of all its losses on the way through the unit. In turbines common losses during the different processes of conversion are:

- Throttling losses: whenever a pressure difference is converted into an increase of flow velocity that does not contribute to the fluid momentum of the blades.
- Fluid friction in the nozzle section, caused by imperfections in shape, such as edges or scratches.
- Fluid friction in the blading stage, misalignment, shock waves and resulting reflections.
- Windage losses, cause by the rotating parts in the vapour.
- Loss of fluid along around the circumference of the rotor, so called tip losses.
- Loss of fluid along the way trough the turbine. For instance though glands or the balance holes in the rotor.
- Leaving loss or Carnot's shock loss: sudden change of diameter leads to a prompt deceleration of the flow.
- Work loss, due to mechanical friction between rotating parts, such as gears, and clutches.

For the investigated system, the flow losses can be combined and reduced to two main groups: the nozzle efficiency and the blade efficiency. In addition, during the process of mechanical and electrical conversion we receive two more losses: mechanical losses of the entire power train (shaft, bearing, gear and clutch) and the electric losses of the alternator. Across the turbine various imperfections causing pressure losses in the vapour flow can be expected, the major points will be mentioned in the following. During the start-up procedure of the cycle the turbine control valve is first closed and later constantly opened. In order to reach a linear acceleration of the turbine up to the synchronous frequency of 50Hz the PLC has a PID-controller implemented. For the regular operation scenario the interaction of the valve is not relevant and can be neglected. Entering the turbine through a DN200 pipe the vapour flow enters the annular chest. It consist of a ring shaped volume. From this point the flow direction turns by 90° to enter the nozzles. Losses related with this are already respected in the above equations of the nozzle. Now, the flow converts its pressure potential into acceleration in the nozzle ring. After impinging the blades the vapour is released into the volume of the conical turbine adapter (diffuser). As a consequence of the large dilatation of

the stream a pressure drop occurs. Taking all the above mentioned points into consideration the formula for the over all power conversion efficiency can be written as:

$$\eta_{con} = \eta_{noz}(x) \times \eta_{mech}(x) \times \eta_{el}(x) \tag{5.130}$$

where x represents the state of load for each of the components. Especially the mechanical efficiency stands out. For a constant speed system, as this turbine, the mechanical friction is constant. From the inlet (1) to the outlet (2), the energy in the fluid flow that is converted across a turbine to mechanical work can be represented based on the First Law of Thermodynamics:

$$\oint_1^2 (\delta Q - \delta W) = \delta E \tag{5.131}$$

$$\Delta h_{1,2} \times \frac{dm}{dt} = \frac{dE}{dt} = \frac{dW}{dt} \tag{5.132}$$

In general the conversion can be looked at in two different ways: the conversion of a thermodynamic potential or the mechanical work of fluid on the turbine blade. The real enthalpy drop times the mass flow through the system is equal to the product of torque τ and angular velocity ω. Over the observed time period the flow applies an impulse to the blades at the average radius $\bar{r}$.

$$\dot{m} \times \Delta h_{1,2} = \tau \times \omega = \dot{m} \times \Delta \sim v_{\perp} \times \bar{r} \tag{5.133}$$

$$\eta_s = \frac{\Delta h}{\Delta h_s} = \frac{h(p_{feed}, T_{feed}) - h(p_{drain}, T_{drain})}{h(p_{feed}, T_{feed}) - h(p_{drain}, s_{feed})} \tag{5.134}$$

As a first and very simple approach one could assume a constant isentropic efficiency and calculate the turbines mechanical power by the mass flow in the system and the specific enthalpy drop. For a steady-state approach this may be sufficient. However, if the dynamic behaviour of the turbine has to be taken into account a more elaborate model has to come to use. It should be once again noted that the turbine behaviour governs the mass flow of the system. The full understanding of the dynamic cycle thermodynamic characteristics require the interaction of system pressure characteristic, turbine pressure characteristic and the feed pump. The control system finally acts as compensation for the imbalance (phase shift) between those components. As a well known approach to model the behaviour of steam turbines the Cone Law of Stodola [137, 138] is widely

accepted. With a comparably low number of parameters the main dependencies within the turbine can be derived appropriately. In order to apply this approach to the conditions of an organic fluid turbine that is operating under super-sonic conditions, we have to take a look into the theory of the nozzle flow.

5.12.2 Nozzle flow

If a pressure difference of a gaseous fluid is applied across a restriction, for instance a nozzle or orifice, a certain mass flow is transported through the cross section area of the restriction. In theory an ideal gas being expanded from a high pressure vessel to a low pressure vessel would remain at the same temperature and convert its energy of the pressure potential completely into velocity, respectively impulse. Starting with Bernoulli's continuity equation:

$$p_1 + \frac{\rho \times v_1^2}{2} = p_2 + \frac{\rho \times v_2^2}{2} \tag{5.135}$$

$$\Delta p = \frac{1}{2} \times (\rho_2 v_2^2 - \rho_1 v_1^2) \tag{5.136}$$

with the two cross sections at each side of the nozzle:

$$\Delta p = \frac{1}{2} \times \left(\rho_2 \times \left(\frac{\dot{V}}{A_2} \right)^2 - \rho_1 \times \left(\frac{\dot{V}}{A_1} \right)^2 \right) \tag{5.137}$$

solving the equation for the volume flow:

$$\dot{V}^2 = \frac{A_2^2 \times 2 \times \Delta p}{\rho \left(1 - (A_2/A_1)^2\right)} \tag{5.138}$$

substituting the cross section ratio by introducing the orifice ratio $\beta = d_2/d_1$ and separating the equation into a geometric and a thermodynamic term, we receive:

$$\dot{V} = A_2 \sqrt{\frac{1}{1-\beta^4}} \times \sqrt{2 \times \left(\frac{p_1}{\rho_1} \right) - \left(\frac{p_2}{\rho_2} \right)} \tag{5.139}$$

The discharge coefficient C_d accounts for the non-ideal effects of contraction and velocity (Toricelli's contractio venae) that occur when a flow is forced through the orifice. The product of the contraction coefficient (e.g. sharp edge 0.62) and the velocity coefficient (e.g. 0.95 to 0.99) results in overall value in a range of 0.59 to 1, for a sharp edge, respectively a perfectly rounded converging section. For the exact calculation for given situation various complex correlations

exist, such as the Reader-Harris and Gallagher equation [139]. This formulation is based on a rather large 8th degree polynomial including the Reynolds-number and the orifice ratio. The geometry of the turbine is known and has no rounded entry sections. Thus, as a first approach, the pessimistic value of 0.62 is used for the following calculations.

$$\dot{V} = C_d \times A_2 \sqrt{\frac{1}{1-\beta^4}} \times \sqrt{2 \times \left(\frac{p_1}{\rho_1}\right) - \left(\frac{p_2}{\rho_2}\right)} \tag{5.140}$$

concluding all geometrical imperfections to one coefficient C, the orifice coefficient, we can write the first root term as:

$$\dot{V} = C \times A_2 \times \sqrt{2 \times \left(\frac{p_1}{\rho_1}\right) - \left(\frac{p_2}{\rho_2}\right)} \tag{5.141}$$

finally we receive the mass flow:

$$\dot{m} = C \times A_2 \times \sqrt{2 \times (p_1\rho_1) - (p_2\rho_2)} \tag{5.142}$$

A more realistic approach accounts for the behaviour of the real gas and dissipation in the system. Therefore, an other coefficient is necessary. Ψ (as well denoted as Y) is introduced as the expansion factor:

$$\dot{m} = \Psi \times C \times A_2 \times \sqrt{2 \times (p_1\rho_1) - (p_2\rho_2)} \tag{5.143}$$

Ψ is defined for two cases, below and above the critical pressure ratio χ. In this case the critical ratio Π^* is calculated from the polytropic relation:

$$\Psi^* = \left(\frac{2}{\kappa+1}\right)^{\frac{\kappa}{\kappa-1}} \tag{5.144}$$

Assuming a state before the turbine with 270 °C and 7bar we receive a critical pressure ratio that ranges from 0.579 at 9bar to 0.6 at 4bar. In all relevant load points the turbine will exceed an inlet pressure of 3bar. Drain pressure will stay below 0.3bar during normal operation. For this case the the expansion function can be computed in the following way using the polytropic exponent κ:

$$\Psi = \sqrt{\frac{\kappa}{\kappa+1}} \tag{5.145}$$

The above expression is valid for the range $\left(\frac{2}{\kappa+1}\right)^{\frac{\kappa}{\kappa-1}} < \chi < 1$. χ is equivalent to the pressure ratio $\frac{p_2}{p_1}$. For the sake of completeness, the second case, where $\chi \leq \left(\frac{2}{\kappa+1}\right)^{\frac{\kappa}{\kappa-1}}$ should be briefly mentioned as well:

$$\Psi = \sqrt{\frac{\kappa}{\kappa - 1} \times \chi^{1/\kappa} \times (\chi^{1/\kappa} - \chi} \quad)) \tag{5.146}$$

In order to find a solution for the turbine equation one needs the exit velocity of the nozzle and the mass flow. Starting with the input state and the return pressure we can derive the isentropic enthalpy drop across the unit Δh_s. We assume the entry velocity into the turbine system to be almost zero. Using the energy balance, we receive:

$$v_2 = \mathrm{p}2 \times \Delta h_s \tag{5.147}$$

$$\dot{m}_{turb} = k_t \times \lambda \tag{5.148}$$

$$\dot{m}_{turb} = \frac{k_t}{\sqrt{T_{in}}} \times \sqrt{p_{in}^2 - p_{out}^2} \tag{5.149}$$

This theory bases on the idea that a turbine can be seen as a nozzle converting pressure difference into an impulse. As a consequence the mass flow transported through the turbine within a certain time period correlates with the pressure ratio. In order to account for the state of the inlet vapour either density or temperature can be used as a further variable. Cooke [140] found a correlation based on Stodola's theory:

$$\frac{\dot{m}_{turb}}{\sqrt{\frac{p_{in}}{v_{in}}}} \propto \sqrt{1 - \left(\frac{p_{out}}{p_{in}}\right)^{\frac{\eta_p + 1}{\eta_p}}} \tag{5.150}$$

where η_p is the polytropic efficiency which is related to the isentropic exponent κ:

$$\frac{\eta_p - 1}{\eta_p} = \eta_{stage} \times \left(\frac{\kappa - 1}{\kappa}\right) \tag{5.151}$$

introducing the Stodola coefficient k_t the correlation can be transformed to the expression:

$$\dot{m}_{turb} = k_t \times \sqrt{\frac{p_{in}}{v_{in}}} \times \sqrt{1 - \left(\frac{p_{out}}{p_{in}}\right)^{\frac{\eta_p + 1}{\eta_p}}} \tag{5.152}$$

related to the feed vapour's density:

$$\dot{m}_{turb} = k_t \times \sqrt{p_{in} \times \rho_{in}} \times \sqrt{1 - \left(\frac{p_{out}}{p_{in}}\right)^{\frac{\eta_p + 1}{\eta_p}}} \tag{5.153}$$

The pressure ratio is usually denoted as r_s. The exponent of r_s was found to be 2 [140]. He proofed this as being appropriately accurate for multi-stage steam turbines. To assure the validity of his theory three variations of the model were calculated in this work:

- Cooke's exponent, with a value of 2.
- An exponent for MDM under average load conditions (around 1.93).
- An exponent for each time step, based on the inlet vapour properties and the resulting polytropic exponent.

In order to obtain a working dynamic model for the turbine the coefficient k_t is needed. Assuming that over a longer time the mass flow trough the turbine equals the feeding pump mass flow, it can be derived from a mean value of measured data over a certain period. For this purpose a one days period has been taken and analysed to set up a first model.

5.12.3 Stage efficiency

The overall efficiency of a turbine is determined by the nozzle efficiency, the stage efficiencies and finally potential losses through shocks in a diffuser. In this case of a single stage turbine there is only one stage to calculate. It is assumed that the isentropic efficiency is a function of the pressure ratio and the rotational speed and therefore of the resulting outflow angle from the nozzle to the blade. As this unit has an almost constant speed, under normal operation, the isentropic efficiency can be described only as a function of the pressure ratio β. Quoilin [101] proposes a generic equation for volumetric expanders. Based on two reference values, the derivative of the one of the points and two parameters a unit can be described with appropriate quality.

$$\eta_s = \eta_{s,max}\gamma \times arctan(C - E \times C - arctan(C)) \tag{5.154}$$

where

$$C = b \times (\beta - \beta_0) \tag{5.155}$$

for our case a little less complicate formulation returns satisfying results in the relevant range of load:

$$\eta_s = a \times atan\left(b \times \beta^2 + \frac{c}{\beta}\right) + d \times \beta + f \tag{5.156}$$

The above correlation has been fitted using a data set of one day. The pressure ratio has been calculated from values measured before and after the turbine. The

isentropic efficiency has been calculated from the measured states. Additionally the efficiency has been validated using the electric output of the alternator calculating the enthalpy drop reversely. The results correlate within ±3% in the relevant range of β, as depicted in Figure 5.51.

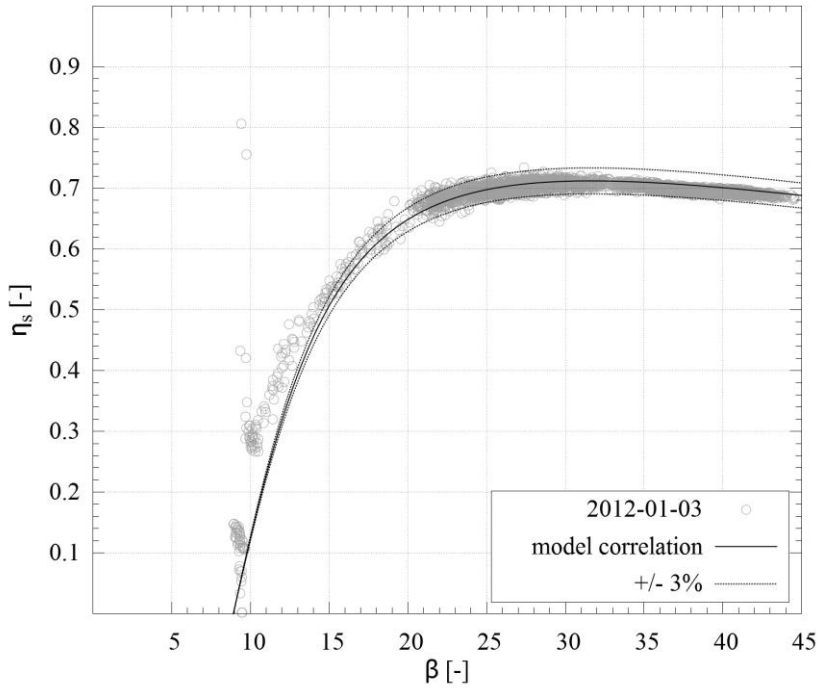

Figure 5.51: calculated η_s fitted via atan-function (2012-01-03)

Details on the above depicted correlation (parameters, statistical results) can be found in the Appendix A.3.2.

5.12.4 Pressure losses in the turbine

At the passage from the turbine blades to the exhaust diffuser the cross section dilates. This causes an irreversible pressure change according to Carnot's theory of shock loss:

$$\zeta_{dif} = \left(1 - \frac{A_1}{A_2}\right)^2 = \left(1 - \frac{0.2036}{1.1197}\right)^2 = 0.67 \tag{5.157}$$

Under design conditions (20kg/s / 0.35bar / 220 °C) we receive a pressure drop of 300Pa. Slightly more relevant than the above mentioned pressure drop is the reversible pressure change on the fluids way across the diffuser into the recuperator. The dilatation from a DN1100 to a DN800 flange causes an flow

acceleration of 89%. According to Bernoulli's conservation of energy the static pressure decreases by 400Pa.

5.12.5 Turbine correlation

In order to conclude the above theories into one final modelling approach, sets of parameters have to be obtained. If measured data are available, the predictions quality should exceed a entirely physical approach. However, the way from monitoring data to a robust turbine model proved to be not trivial in this case. In general there are three different procedures to obtain a turbine model. The choice for one of the three ways is a matter of the available data and their quality. All methods have in common that the mass flow equation is fitted in the first place. When it comes to the isentropic stage efficiency the following methods can be used:

- If reliable measured pressure data for inlet and outlet of the turbine are available, the isentropic efficiency can be directly deducted. Fitting the measured isentropic efficiency versus the expansion ratio would the final and rather trivial step in this case.

- In cases where the turbine outlet pressure values are not fully reliable (turbulences or dynamic pressure component), the isentropic efficiency can be deducted from the turbine outlet temperature. It is assumed that the temperature data are more reliable and contain less noise. For each parameter set in the fitting procedure the entire data set has to be calculated. Basically the method contains two encapsulated loops. The CPU load of this method is high.

- If the electric grid feed-in of the alternator is available, a reverse calculation back to the isentropic efficiency can be done. This is the most robust approach, as the electric power measurement is very accurate and the noise level is low. However, this method is just as good as the efficiency correlation of the alternator.

All three methods have been used in this case study.

- Obtaining the parameters and variables for the mass flow equation is vital, due to the fact that the turbine serves as a mass flow source and the cycle has to be consistent. The feed pump mass flow is used for validation, under

the assumption that the sum of all mass flows in the cycle during a long time period are equal. The first guess for the Stodola parameter k_t is calculated from the dimensions of the critical cross section in the turbine nozzle.

- In a second step, the isentropic efficiency is estimated using a reverse function of the alternators electric feed in. Under full load this method is very robust. Under part load and with rather poor information about the electric efficiency of the alternator, it may be risky.
- With the before roughly estimated efficiency characteristic the measured output temperatures of the turbine are fitted in detail.

After completing the above procedure the following correlation for the turbine mass flow has been found:

$$\dot{m}_{turb} = k_t \times \sqrt{p_{in} \times \rho_{in}} \times \sqrt{1 - \left(\frac{p_{out}}{p_{in}}\right)^{\frac{\eta_p+1}{\eta_p}}} \tag{5.158}$$

where k_t consists of the following factors:

$$k_t = x_{noz} \times y_{noz} \times N_{noz} \times C_{noz} = 0.009 \times 0.014 \times 25 \times 0.883\text{m}^2 = 0.00281317\text{m}^2 \tag{5.159}$$

5.13 Alternator

The generator (DGI 450/2L WT), produced by Weier Electric, has a rated power of 1500 kVA. The engine's load characteristic is shown in Table 5.22. It is obvious that the size of the alternator is not optimal. Even under full load conditions of the turbine the generator runs in part-load. Most of the time this alternator is working below 60% of load. This leads to additional losses that could be avoidable.

Table 5.22: load specifications of alternator [141]

load	[-]	5%	10%	25%	50%	75%	100%	125%
power input	[kW]	750	150	375	750	1125	1500	1875
gross efficiency	[%]	80.0	86.0	94.1	96.3	96.9	97.0	97.0
net efficiency *	[%]	79.2	85.1	93.1	95.3	95.9	96.0	96.0

*including cooler

Figure 5.52 depicts the gross and net efficiency of the alternator.

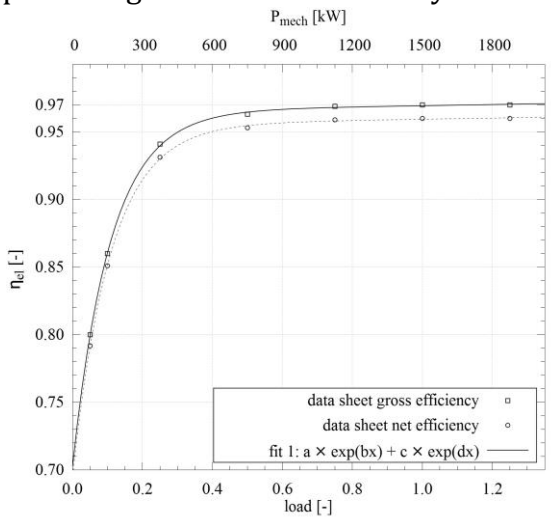

Figure 5.52: data sheet efficiencies of alternator including logarithmic fit

Table 5.23: fitting results for alternator gross efficiency

coefficient	*a*	*b*	*c*	*d*
value	0.9648	3.253e-09	-0.2617	-6.122e-06
	PPMCC	adj. R^2	RSME	SSE
	0.9998	0.9995	0.001461	6.404e-06

5.14 Mechanical dynamic properties of the power train

In the applied assembly of turbine, turbine shaft, clutch and alternator significant inertia tensors appear. In terms of dynamic modelling, those tensors have to be represented in the calculation. In this case, the variation in turbine speed is very low as it is a synchronous engine. For asynchronous generators the influence of the mechanical inertia will certainly be in a an other order of magnitude. The hereinafter listed rotating part are calculated according to the well known formula, where all points i to n of mass are integrated across the rotating axis:

$$J = \sum_{i=1}^{n} m_i \times r_i^2 \tag{5.160}$$

or:

$$J = \frac{\pi \times \rho}{2} \times \int_0^l r(z)^4 dz \tag{5.161}$$

for this case we receive:

$$J = \frac{1}{2} \times m \times r^2 \tag{5.162}$$

Figure 5.53 comprises all relevant rotational part to determine the dynamic behaviour of this drive train constellation.

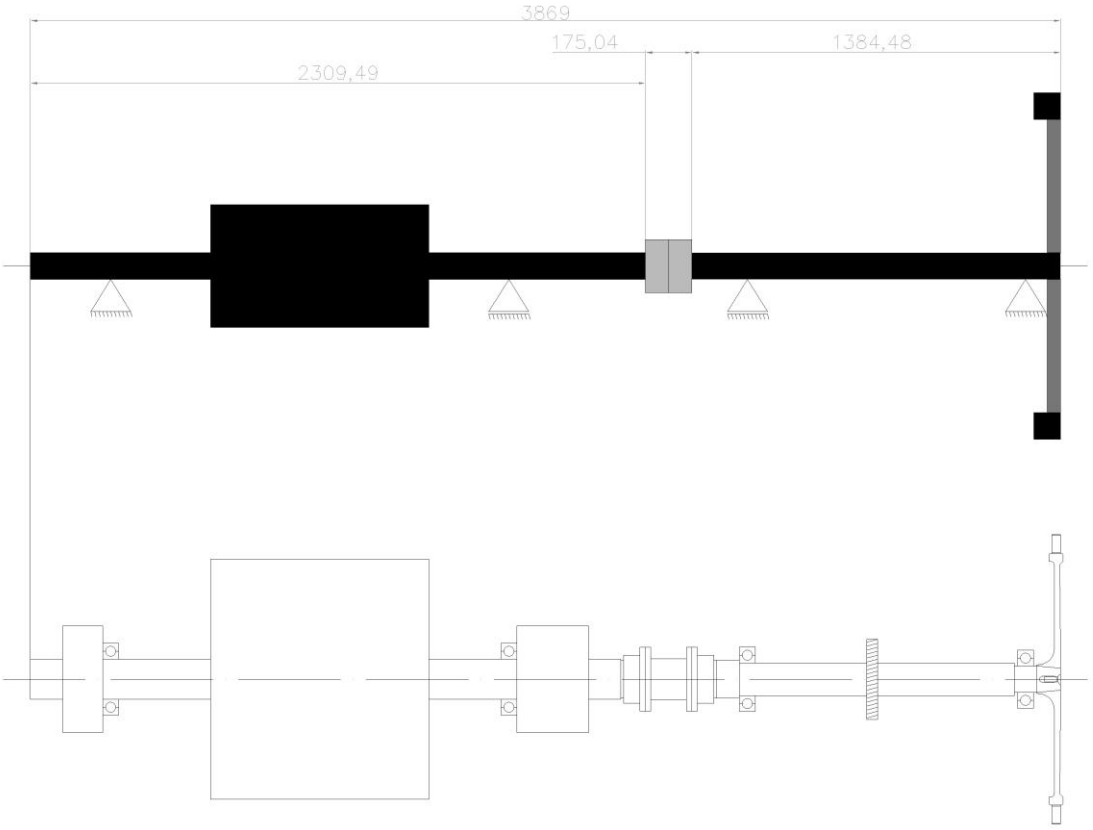

Figure 5.53: arrangement of the drive train containing turbine, shafts, clutch and alternator

The following part list (Table 5.24) represents the revolving parts in the system with significant mass and therefore influence.

Table 5.24: rotating parts in alternator-turbine unit

item	mass	tensor	amount
-	[kg]	[kgm^2]	-
turbine blade	0.1065	5.31	210
blade ring	1.79	0.525	1
turbine rotor	141.5	21.19	1

rotor sealing	37.5	n.n.	1
turbine gear	n.n.	n.n.	1
turbine shaft	127.5	0.242	1
clutch	n.n.	0.308	1
alternator	4678	70.325	1
sum	5008.7	97.9	-

As a simplification the rotating masses are assumed to have homogeneous densities. For shafts and clutches this approach has a good fit. In the case of the rotating alternator masses the distribution in the rotor (e.g. copper coils, iron rotor) is surely not constant, but the best possible guess. As shown in Table 5.24 the inertia moment of this combination is governed by the turbine and alternator rotor. In order to validate those values, a shut down procedure of the turbine can be used. Measured data of a emergency stop provide the turbine speed from 3000RPM to a full stop. The torque of friction in this system is defines as:

$$\tau_{fric} = \frac{P_{fric}}{\omega} \tag{5.163}$$

and

$$\tau_{fric} = \alpha \times J \tag{5.164}$$

where

$$\alpha = \frac{d\omega}{dt} \tag{5.165}$$

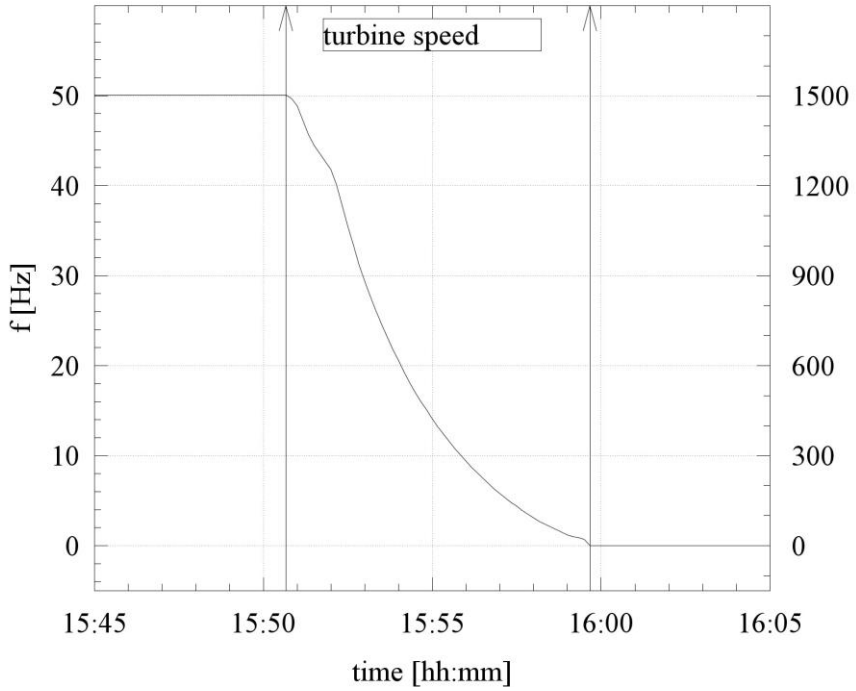

Figure 5.54: rotation measured during a turbine shut down

Having a look an average shut-down procedure (Figure 5.54) as it has been measured plenty times during the observation period, be can derive a period of 480 seconds until total stand still. The resulting mean angular acceleration is $-0.654 rad/s^2$. Neglecting fluid friction at the surface of the rotating parts and other effects (e.g. magnetic) the resulting tensor turns out to be $97.9 kgm^2$ (Table 5.24). Then we receive a friction torque of 63.7Nm. At nominal speed this torque of friction is a little more than 20kW, which is roughly 2% of the nominal mechanical power. These values seem absolutely reasonable. Concluding all above partial models, the dynamic equation for the whole drive train can be expressed as follows:

$$\left(\tau_{shaft} + \tau_{fric}(\omega) + \sum J_{i1}^{i} \times \dot{\omega}\right) \times \omega = \dot{m}_{tur} \times \Delta h_s \times \eta_s (\beta_) \tag{5.166}$$

Figure 5.55 shows the dynamic power train model, including turbine, alternator and shaft. As inputs serve the grid frequency, feed vapour temperature and pressure and the return pressure.

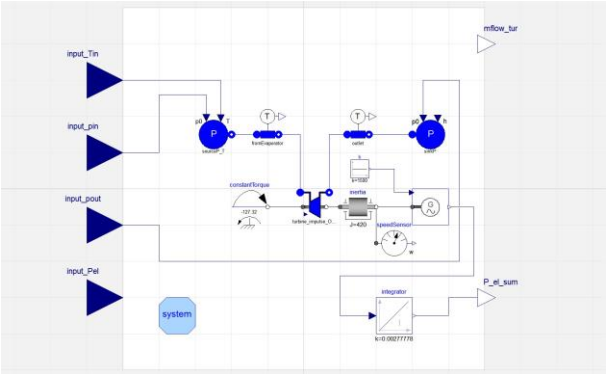

Figure 5.55: power train model with validation data-set

5.15 Dynamic cycle models

Partial cycle model 1 The next Figure 5.56 shows the the partial model number 1. It consists of the source side of the ORC-unit including the thermal oil valve. Furthermore, the pre-heater, the evaporator and the turbine including alternator are represented. The low pressure part of the cycle is substituted by a fluid sink and source. With this partial model the behaviour of the single components can be determined. Furthermore, the number of potential error sources is reduced and model calibration and validation is easier. Inputs for this model are: feed temperature, pressure and mass flow on the source side. Furthermore, the return temperature of the turbine and the fluid state after the recuperator (liquid, cold side) are defined by monitoring data.

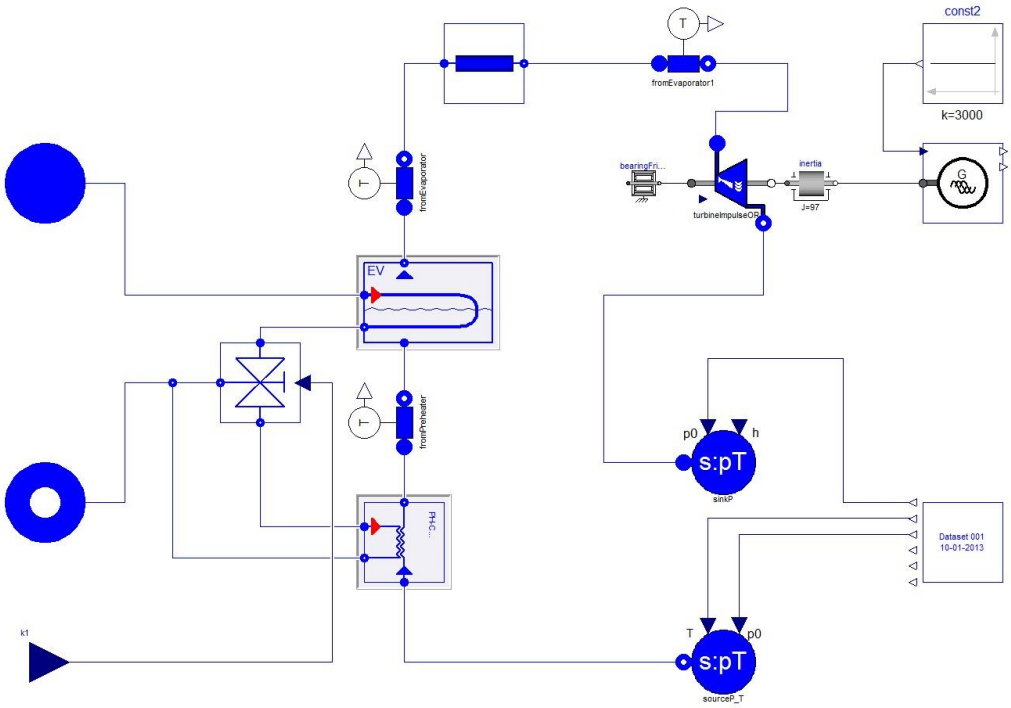

Figure 5.56: graphical layout of the hot side of the plant model

The next scheme in Figure 5.57 depicts the “cold side” of the power cycle. Again, the turbine is part of the configuration. Connected to it are: the recuperator, the condenser, the hotwell, the feed-pump and pipe friction losses. The source is defined by feed vapour temperature and pressure. On the sink side the model is connected to the district heating data. The feed pump is controlled by the PID-controller.

Partial cycle model 2

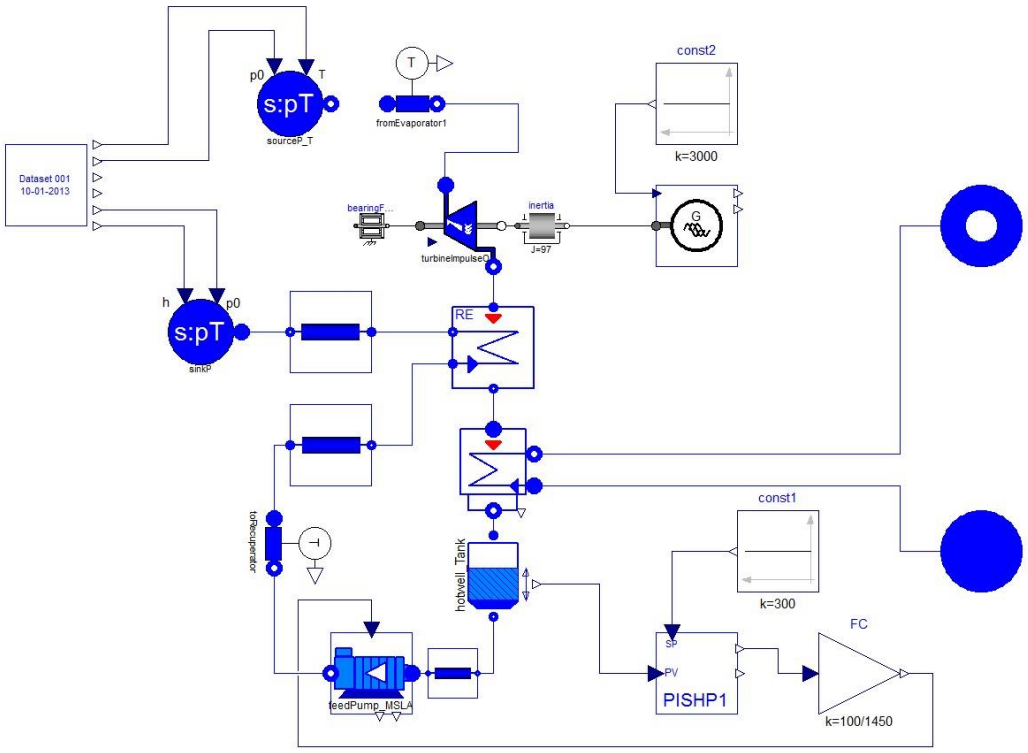

Figure 5.57: graphical layout of the cold side of the plant model

Entire cycle

The final evolutionary stage of the model is a combination of the two before described configurations. All relevant aggregates of the power cycle are represented in this model (Figure5.58).

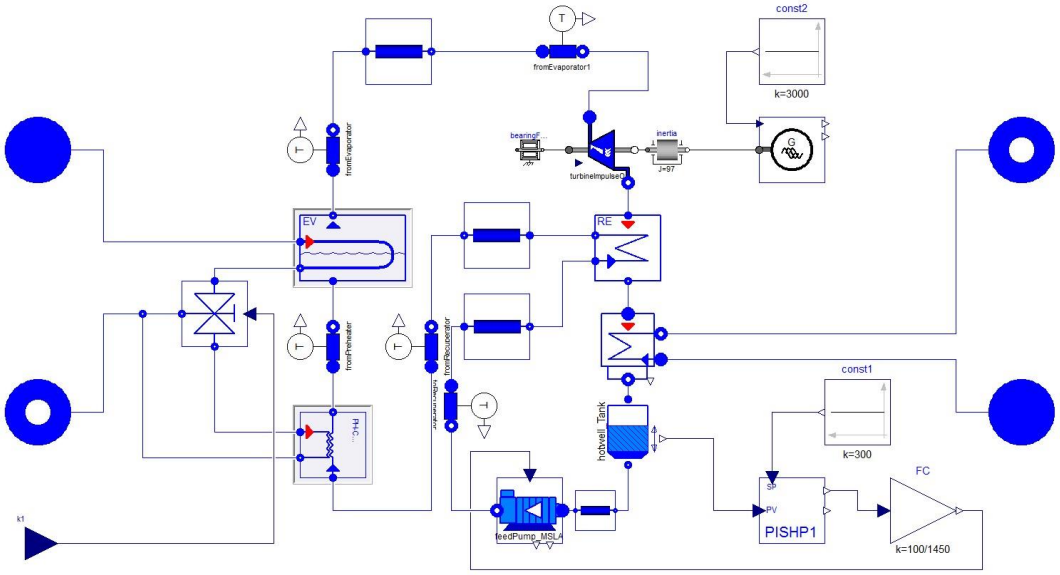

Figure 5.58: graphical layout of entire plant model

Chapter 6

Validation results

This chapter is contributed to the validation of data and models. Among the large number of sensors in the power plant a certain proportion delivers false data or imprecise values. For sensors that are not relevant for safety a revision is not likely or economically not feasible. Therefore, the data acquisition has to deal with malfunctions, short-circuits, leakage currents and defective contacts. There are three main factors influencing the data quality:

- Thermal, fluid or material stress applied on the sensors. For instance the furnace fire box temperature sensor. Ash particles and heat scrub the lances. As a consequence, double thermocouples are used to increase redundancy.
- The electric signal can be disturbed by electromagnetic influences. Leads can be be physically interrupted, connectors can be unconnected by vibration.
- Within the PLC or its bus system error due to overload, wrong protocols or software errors happen. For instance a M-Bus application and its OPCgateway do not push synchronous data, single values may freeze to a certain value.

These are just a few points that influence the data quality. Taking a look at the other side of validation - the model. The method of validation differs according to model type model purpose.

- Model type: dynamic or static, open model or closed loop.
- Time scale: fast or slow, available time step, short or long duration.
- Data quality: data errors, outliers, high frequency noise.

6.1 Steady-state validation

In order to check the validity of calculations for single components and metasystems data sets have to be prepared. If possible, the whole load range should be covered. For heat exchangers that contain a considerable thermal mass, such as large volume of liquid or large masses of metal, the dynamic effect has to be eliminated first. Three strategies can be applied to do so: using data from a very limited load range, synchronize the hot and the cold side according to the time stamp, or use mean values. All methods are used hereinafter, depending on the data quality and applicability of the method for each case.

6.1.1 Pre-heater

The data analyses of measured values from the pre-heater show that effect of the thermal inertia in the heat exchanger causes a time lag of less than 10s. As this time lag is shorter than the time step of the monitoring it can be neglected. The following plots in the Figures 6.1 to 6.4 depict four days with different load situations. It needs to be mentioned that two sensors are situated on two different end of the apparatus. The cold fluid sensor is situated in the connecting flange between pre-heater and evaporator; the hot flow is measured at the exit flange of the thermal oil return.

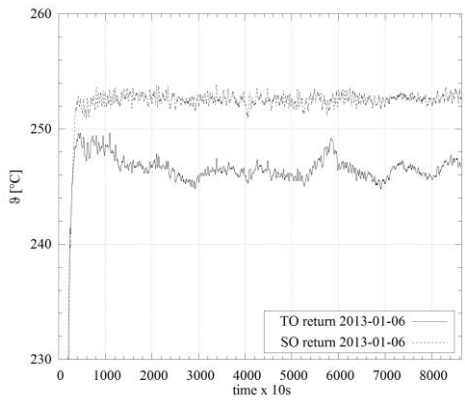

Figure 6.1: thermal oil and MDM return temperature of pre-heater (one day)

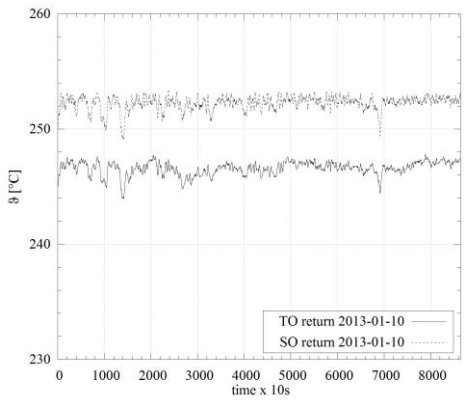

Figure 6.2: thermal oil and MDM return temperature of pre-heater (one day)

Figure 6.3 shows the MDM and Therminol66 ® return temperatures of the pre-heater during a start-up. While the profile of both temperatures is similar, the

temporal offsets differs. This is caused by the modulation of the mass flow in the cycle. Figure 6.4 depicts “normal” operating conditions with small dynamics within a range of 5K. In this case the mass flow of both sides is pretty stable which causes the linear behaviour between both sides.

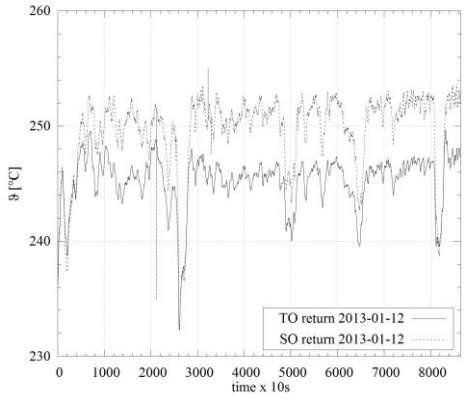

Figure 6.3: thermal oil and MDM re- temperature of pre-heater (one day)

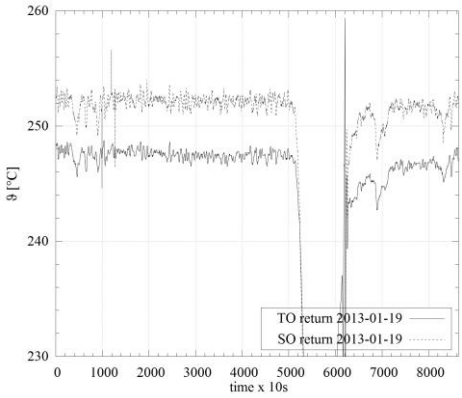

Figure 6.4: thermal oil and MDM return temperature of pre-heater (one day)

In Figure 6.3 a day with large volatility in temperature is plotted. Figure 6.4 shows a full stop of the cycle including a warm restart. The following Figures 6.5 and 6.6 show the simulation of the heat transfer of the pre-heater during one day. The model predicts within a range of deviation better than ±5%. The outliers in the lower load range are caused by a cycle shut-down. Across the relevant range of operation (230W/m²K to 350W/m²K) the prediction quality is satisfying.

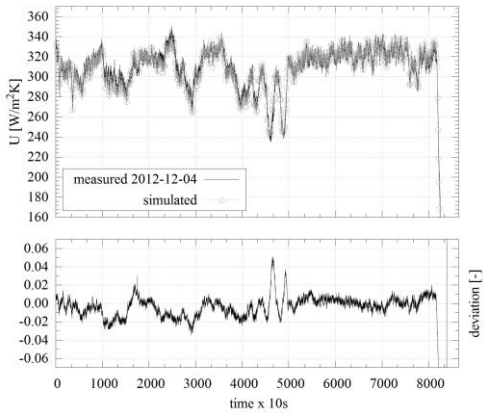

Figure 6.5: pre-heater heat transfer simulated vs. measured (1 day, 2012-

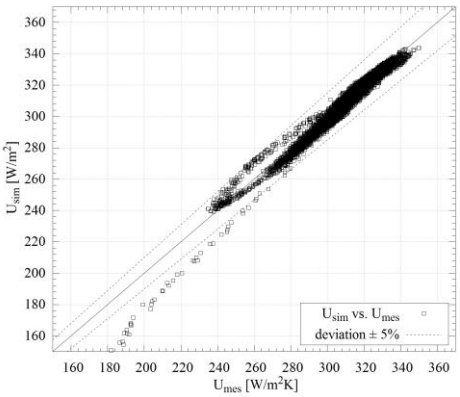

Figure 6.6: pre-heater heat transfer simulated and deviation vs. time (1

12-04) day, 2012-12-04)

6.1.2 Evaporation

The following Figures 6.7 to 6.13 depict the validation of the four different boiling correlations that have been found. In general the different variants all predict rather good. A maximum deviation of ±5% to ±8% can be expected.

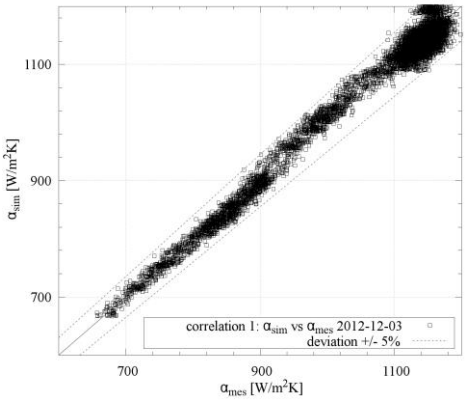

Figure 6.7: boiling correlation 1 vs. measured values (1 day, 2012-12-03)

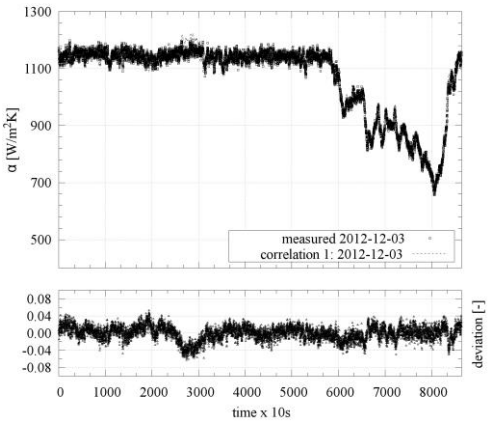

Figure 6.8: boiling correlation 1 and measured values vs. time (1 day, 2012-12-03)

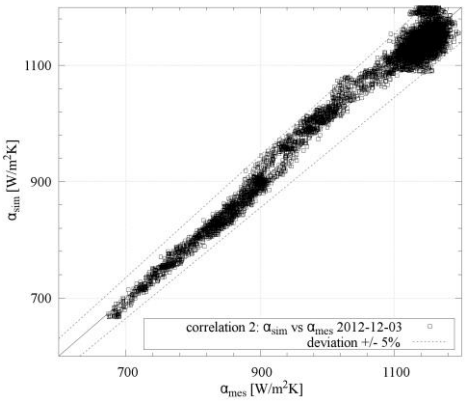

Figure 6.9: boiling correlation 2 vs. measured values (1 day, 2012-12-03)

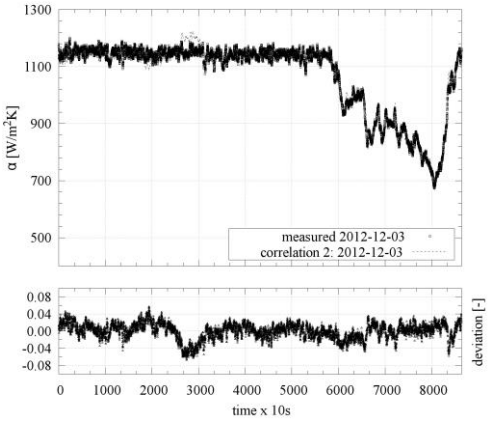

Figure 6.10: boiling correlation 2 and measured values vs. time (1 day, 2012-12-03)

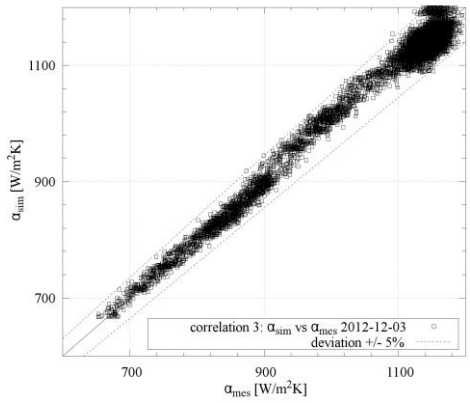

Figure 6.11: boiling correlation 3 vs. measured values (1 day, 2012-12-03)

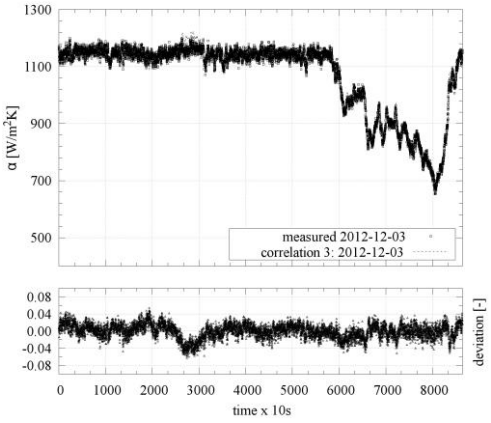

Figure 6.12: boiling correlation 3 and measured values vs. time (1 day, 2012-

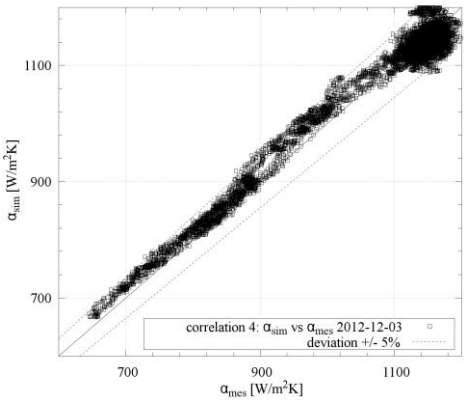

Figure 6.13: boiling correlation 4 vs. measured values (1 day, 2012-12-03)

12-03)

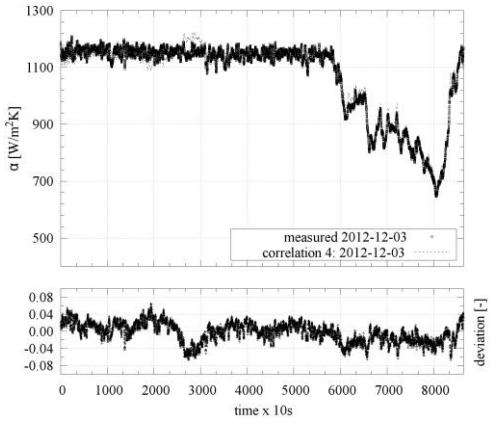

Figure 6.14: boiling correlation 4 and measured values vs. time (1 day, 2012-
12-03)

6.1.3 Heat transfer - source side

In order to give an impression on the predictive quality of the pre-heater and evaporator, the overall heat transfer of the dynamic model has been tested versus measured data.

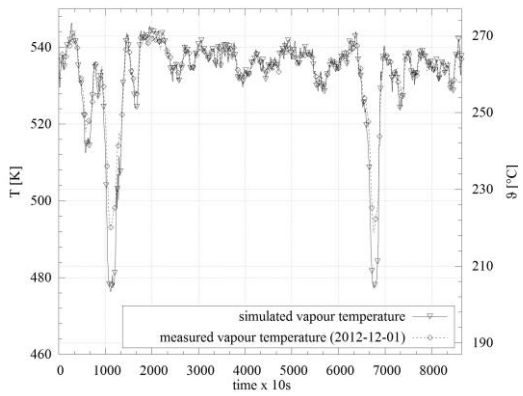

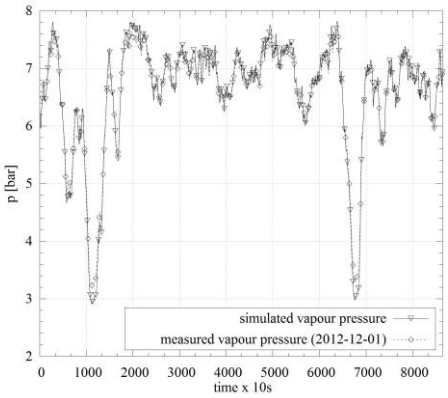

Figure 6.15: vapour outlet temperat- of evaporator, simulated vs. meas- ured (1 day, 2012-12-01)

Figure 6.16: vapour outlet pressure of evaporator, simulated vs. measured (1 day, 2012-12-01)

In the Figure 6.15 measured vapour outlet temperatures are compared with the dynamic model. On can see that the predictions quality in the relevant temperature range above 230 °C is excellent. Below that temperature the output temperature differs by almost 10K. Figure 6.16, on the right side, shows the same scenario for the measured and simulated pressure. Again, the predictions quality is very good.

6.1.4 Recuperator

The following plots depict the results of the entire heat transfer calculation for the recuperator. Figure 6.17 shows the cold side heat transfer combined with the hot side model variant number 3. In Figure 6.18 the same cold side correlation is combined with the model variant 4.

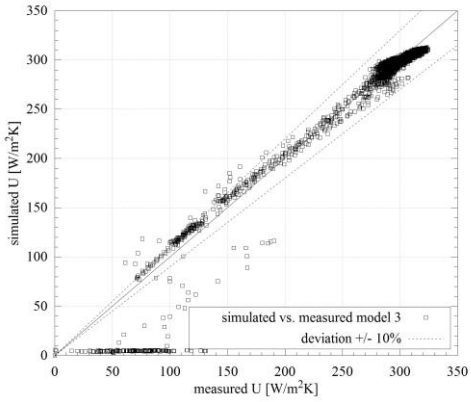

Figure 6.17: simulated vs. measured U-value of recuperator (model 3, 2012-01-10)

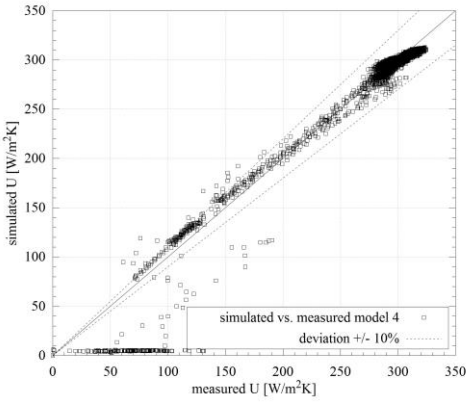

Figure 6.18: simulated vs. measured U-value of recuperator (model 4, 2012-01-10)

6.1.5 Condenser

6.1.5.1 Hot side

The following two Figures 6.19 and 6.20 depict the validation of the condensing film heat transfer. Except during a stop and start between time stamp 1200 and 1300 the model correlates well within a range of ±5% with a slight tendency to over-predict for higher values.

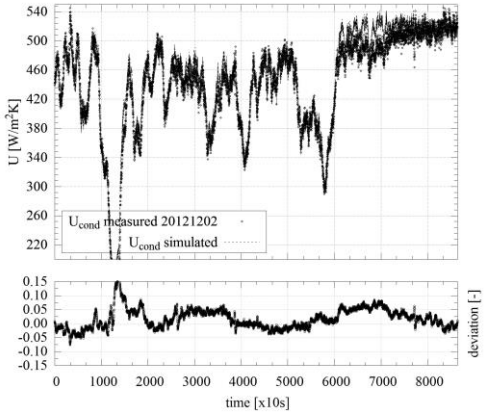

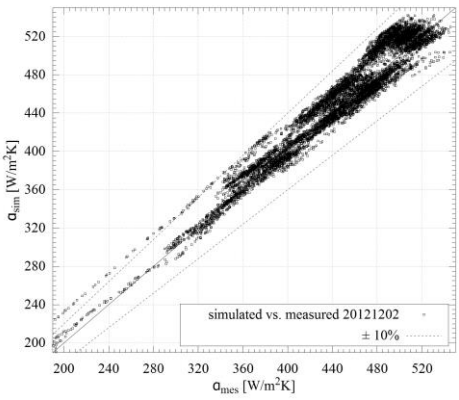

Figure 6.19: condenser convective heat transfer model and measured values vs. time (1 day, 2012-12-02)

Figure 6.20: condenser convective heat transfer model vs. measured values (1 day, 2012-12-02)

PPCP	ϵ_{min}	ϵ_{mean}
0.9797	8.11%	-8.39% - 1.45%

6.1.5.2 Entire heat transfer

Supplementing the results from the section above the next two Figures 6.21 and 6.22 show the entire heat transfer of the final condenser model.

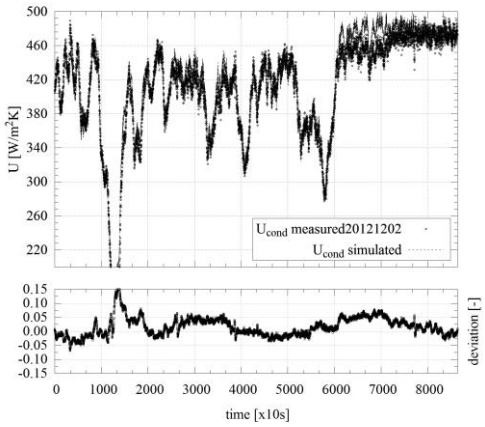

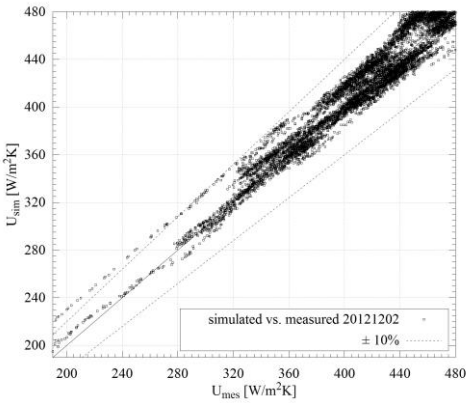

Figure 6.21: condenser convective heat transfer model and measured values vs. time (1 day, 2012-12-02)

Figure 6.22: condenser convective heat transfer model vs. measured values (1 day, 2012-12-02)

6.2 Validation of empirical models

The proposed empirical model for the investigated system has been validated with data sets from the December 2012. The following Figures 6.23 and 6.24 depict a scatter plot and a time series plot of one validation data set (1 day, 2012-12-08, 10 seconds).

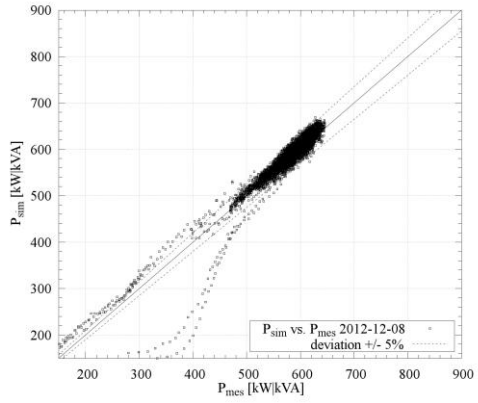

Figure 6.23: empirical model versus measmeasured values (1 day, 2012-12-08)

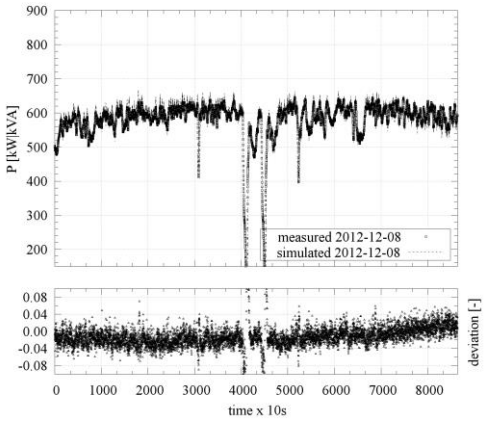

Figure 6.24: empirical model and measured values vs. time (1 day, 2012-12-08)

The model predicts the electric output of the ORC-unit with an accuracy of ±5%.

6.3 Dynamic validation

In this section the results of the validation for the single components in the cycle are shown. Due to the complexity of the meta model this approach was chosen. for each component the reliability, accuracy and contribution to the overall results are discussed. To understand the data the validation is based upon, data sets for validation are described in detail.

6.3.1 Validation of fluid calculation

As a very basis for complex models the properties calculation including all fluid libraries have to be validated first. In order to find problematic zones in the range of states for a fluids used in the models such a validation has been done.The deviations can be explained by rounding, errors in implementation or conversion of data types. The following table show the result of the comparison between calculated EOS results in REFPROP and the equivalent in modelica.

Table 6.1: deviation of REFPROP and modelica enthalpy calculation

	p [bar]					
T [°C]	0.2	1	3	5	7	mean
60	0.004%	0.082%	0.005%	0.005%	0.004%	0.020%
80	0.006%	0.006%	0.006%	0.006%	0.006%	0.006%
100	0.008%	0.008%	0.008%	0.008%	0.008%	0.008%
120	-0.008%	0.013%	0.012%	0.012%	0.013%	0.008%
140	-0.006%	0.032%	0.032%	0.032%	0.032%	0.024%
160	-0.005%	-0.005%	-0.052%	-0.051%	-0.051%	-0.033%
180	-0.004%	-0.004%	-0.014%	-0.014%	-0.014%	-0.010%
200	-0.003%	-0.003%	-0.003%	-0.008%	-0.007%	-0.005%
220	-0.003%	-0.003%	-0.003%	-0.005%	-0.005%	-0.004%
240	-0.002%	-0.002%	-0.002%	-0.002%	-0.004%	-0.003%
260	-0.002%	-0.002%	-0.002%	-0.002%	-0.002%	-0.002%
280	-0.002%	-0.002%	-0.002%	-0.002%	-0.002%	-0.002%
295	-0.002%	-0.002%	-0.002%	-0.002%	-0.002%	-0.002%
mean	-0.001%	0.009%	-0.001%	-0.002%	-0.002%	

The results in Table 6.1 show clearly that the deviation between both calculations are minor. The worst results can be expected around the phase change, due to the usage of many calculation loops.

6.3.2 Start-up data sets

The aim of a start-up data set is the stabilisation of the solving process in a simulation. In this case modelica offers a broad range to set system wide conditions and initialisation conditions. In brief the initialisation provides a set of properties where the system is in equilibrium and the set of equations is solvable.

Table 6.2: mean data and nominal data

sensor	mean	nominal	unit
$P_{el,gr}$	593.892	702.944	kVA
$T_{T66,feed}$	298.98	290.12	◦C
$T_{T66,middle}$	-	260.027	◦C
$T_{T66,return}$	246.55	235.949	◦C
$\dot{m}_{T66}$	36.75	40	kg/s
Φ_{T66}	4751.9	5346.65	kW
$p_{evap,ret}$	7.39331	7.315	bar
$T_{turb,feed}$	267.91	252.84	◦C
$p_{turb,feed}$	7.06949	6.746	bar
$T_{turb,ret}$	231.52	220	◦C
$p_{turb,ret}$	0.34744	0.40123	bar
$T_{recu,hot,ret}$	126.44	130	◦C
$p_{cond,ret}$	0.15648	0.15	bar
$T_{cond,hot,ret}$	79.60	85	◦C
$p_{pump,ret}$	-	8	bar
$\dot{V}_{MDM}$	21.775	26.342	l/s
$\dot{m}_{MDM}$	16.549	20.020	kg/s
$T_{dh,ret}$	55.05	60	◦C
$T_{dh,ret}$	72.59	80	◦C
$\dot{m}_{dh}$	54.45	53.55	kg/s

6.3.3 Component model - vapour filter

In the Figures 6.25 and 6.26 the pressure loss model of the vapour filter is validated versus a data set of ten hours. The model has a prediction quality of ±0.5% in the displayed range of 6.4bar to 7.6bar.

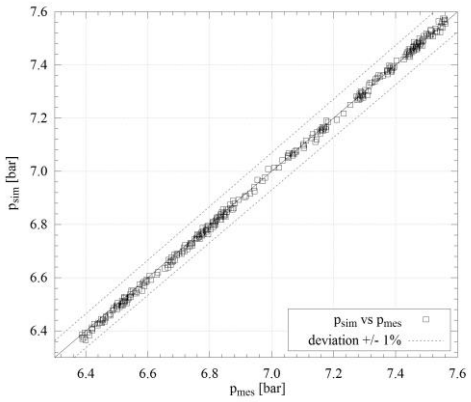

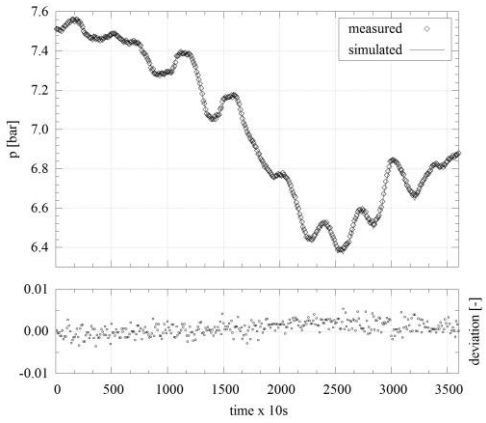

Figure 6.25: vapour filter model vs. measured results (1 day, 2012-01-01)

Figure 6.26: vapour filter model and measured results vs. time (1 day, 201201-01)

6.3.4 Component model - pre-heater

After concluding the single heat transfer correlations to component models in modelica, they have been tested versus monitoring data. The next two Figures 6.27 and 6.28 show the validations results with a one day data set (time step 10 seconds).

The model is accurate, for this data set, within a range of +0.5% and -2.5%.

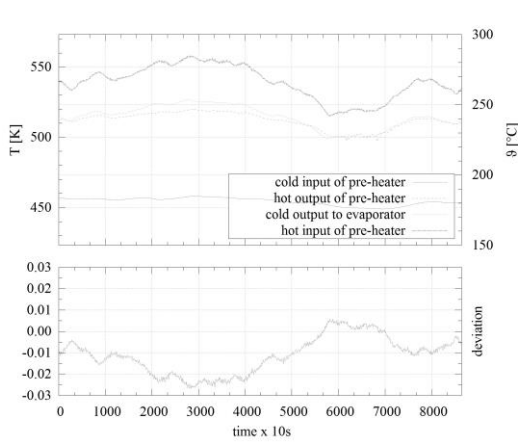

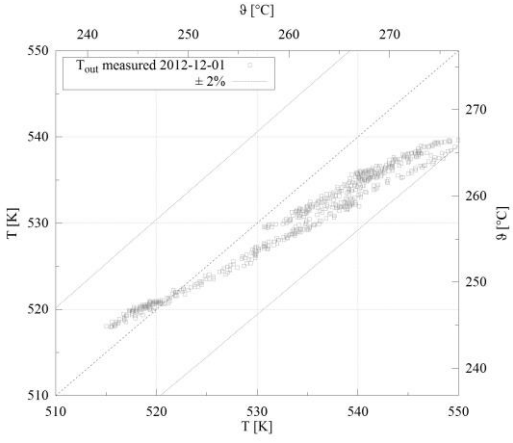

Figure 6.27: pre-heater cold side temperature simulated vs. measured (1 day, 2012-12-01)

Figure 6.28: pre-heater cold side tem- perature simulated and deviation vs. time (1 day, 2012-12-01)

6.3.5 Component model - evaporator

The same data set as in the previous Section 6.3.4 has been used to validate the dynamic evaporator model. The results in the Figures 6.29 and 6.30 show an excellent prediction of the vapour temperature. In the light of the sensitivity of the is value for the overall prediction quality, it is good news. With the investigated data set the model shows an accuracy of ±0.5%.

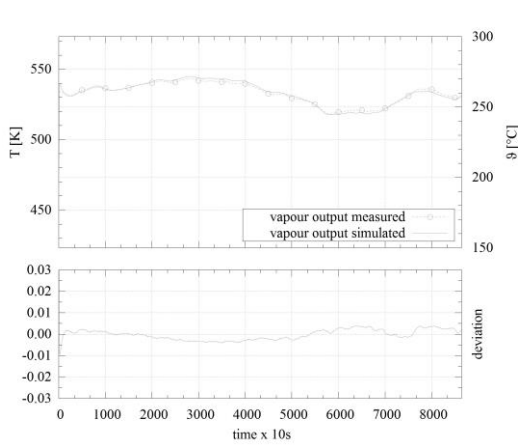

Figure 6.29: simulated versus measured vapour temperatures after evaporator (1 day, 2012-12-01)

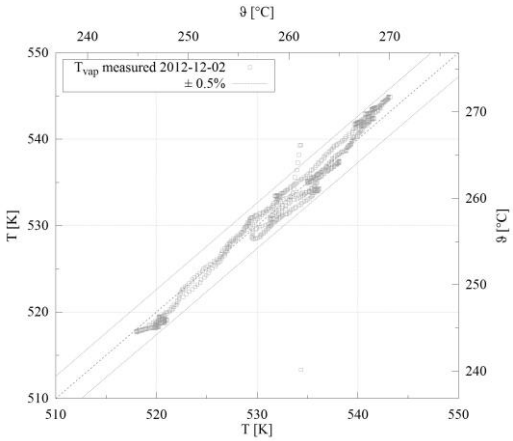

Figure 6.30: thermal oil and MDM reured turn temperature of pre-heater (1 day, 2012-12-01)

6.3.6 Component model - turbine

Three versions of the turbine model have been tested with the data sets of December 2012. The Stodola correlation remains the same, except the poly-tropic exponent. Variant one uses a poly-tropic exponent that is calculated from the inlet state of the turbine. Variant two uses Cooke's proposed simplified exponent (2). The last version uses an average value that has been calculated from the data set (1.93). All three correlations predict the electric output and the mass flow trough the turbine well. While variant three has the lowest dispersion, variant one delivers the best result for the summation of one day. As the yield prediction is in the focus variant one should be preferred. The results for one day are listed below in Table 6.3.

Table 6.3: comparison of model and measured values data sets (1 day / 10 second steps / 2012-12-01)

-	PPCP	R^2	ϵ_{min}	ϵ_{max}	$\bar{P}_{mes}$	$\bar{P}_{sim}$
$\kappa(p,T)$	0.99790	0.99580	-2.95	2.75	760284	760300
$\kappa = 2$	0.99780	0.99560	-1.15	4.18	760284	769120
$\kappa = \bar{\kappa}$	0.99782	0.99564	-1.14	1.39	760284	769020

The following Figures 6.31 and 6.32 show the behaviour of the dynamic turbine model including the drive train, shaft friction and alternator (version 1: $\kappa(p,T)$).

The shaft, respectively grid frequency are inputs in this case. Above electric outputs of 100kVA the prediction quality of this model is very high.

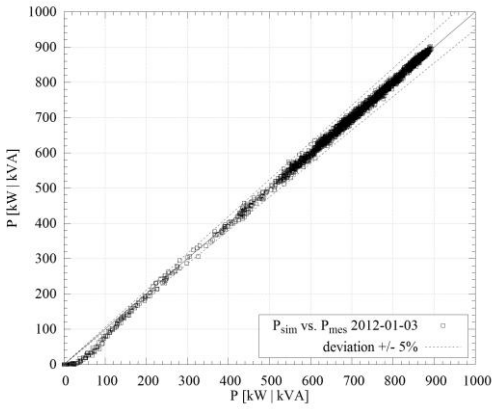

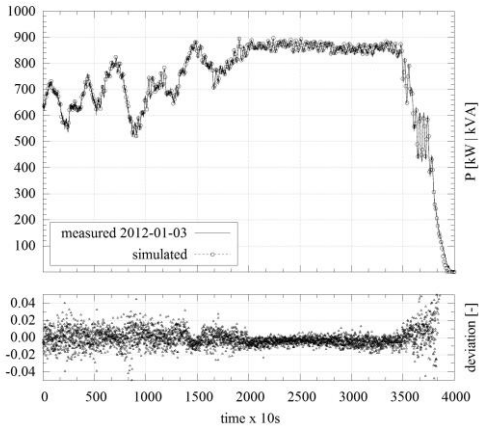

Figure 6.31: turbine electrical power, simulated vs. measured (1 day, 2012-01-03)

Figure 6.32: turbine electrical power, simulated and measured vs. time (1 day, 2012-01-03)

The according measured and simulated mass flows for the above depicted plots are shown below in the Figures 6.33 and 6.34.

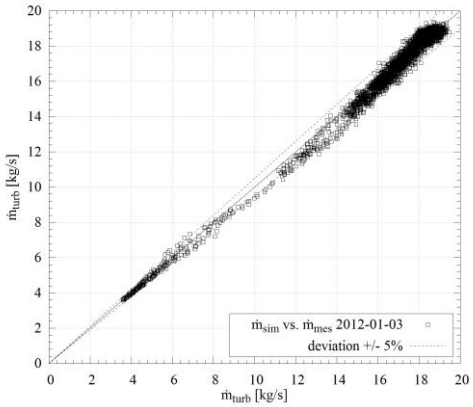

Figure 6.33: turbine mass flow, simulated vs. measured (1 day, 2012-01-03)

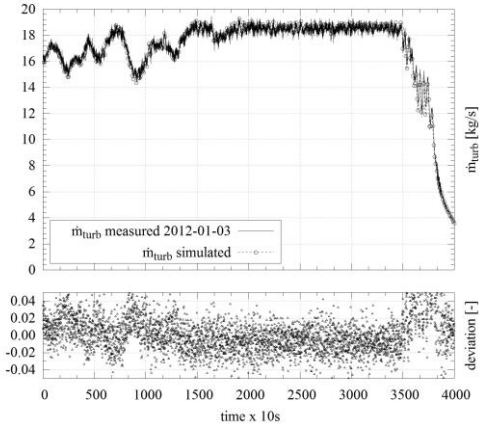

Figure 6.34: turbine mass flow, simulated and measured vs. time (1 day, 2012-01-03)

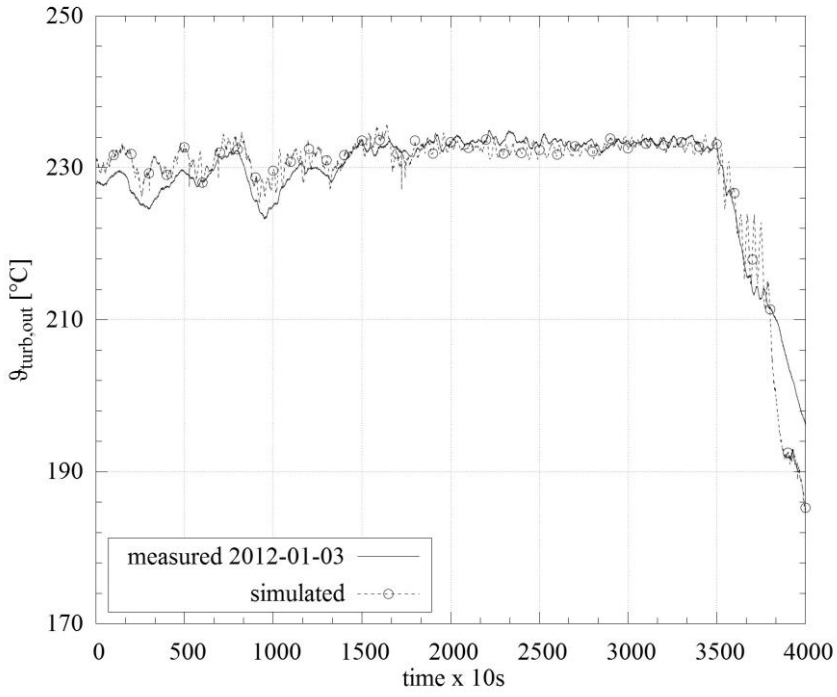

Figure 6.35: temperature after turbine, measured and simulated (1 day, 2012-01-03)

The above Figure 6.35 plots the outlet temperature of the turbine in comparison to the simulated outlet temperature. As the temperature sensor between turbine and recuperator (vapour side) shows a latent offset, the

temperature has been reverse-calculated from the heat transferred on the liquid side of the heat exchanger.

6.3.7 Component model - recuperator

The following two plots in the Figures 6.36 and 6.37 show the validation results of the dynamic recuperator model.

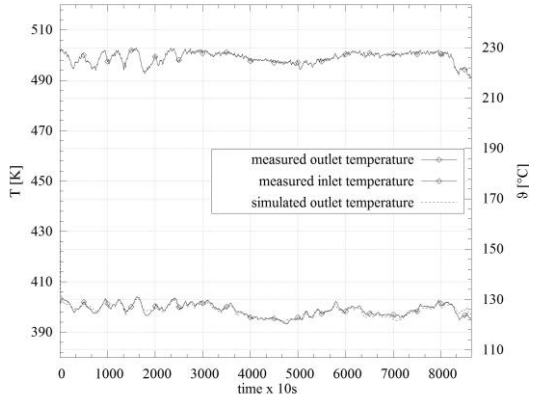

Figure 6.36: simulated and measured temperatures on hot side of recuperator (1 day, 2012-12-01)

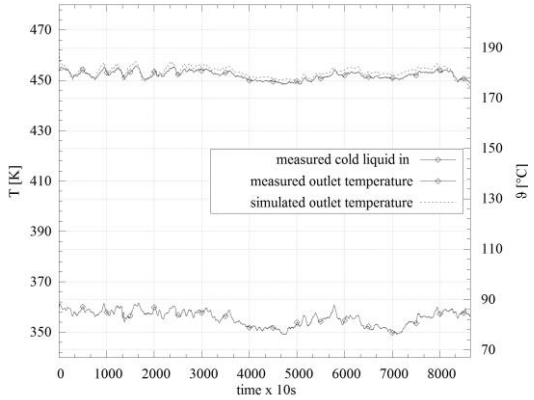

Figure 6.37: simulated and measured temperatures on cold side of recuperator (1 day, 2012-12-01)

In the above plots the relative deviation is not included, as it is solely a matter of definition for an internal heat exchanger. The absolute deviation of this model is in a range of 3K. Related to the temperature difference on the cold side, this would translate to an over-prediction of +3%.

6.3.8 Component model - control system

As previously described in Chapter 5.10.2, the control system of the cycle is based on a rather simple and robust level control. In order to set up a basic cycle model (as is) the PLCs function is programmed in modelica. For validation the output of the control function in the S7 (FC10) have been monitored. The resulting output Y is a function of the parameters *GAIN*, *TI*, *TD* and the subtraction of the control variable (hotwell level, *DB*12.*DBD*66) from the maximum filling level (here 600mm). A detailed scheme can be found in Figure 5.43. The following two Figures 6.38 and 6.39 depict the measured PLC values and the simulated results

versus time and as scatter plot. It needs to be mentioned, that the time step of 10 seconds leads to a loss of information in terms of the derivative and integrator part of the PID-controller. Therefore, a full coincidence of measured and simulated is not possible.

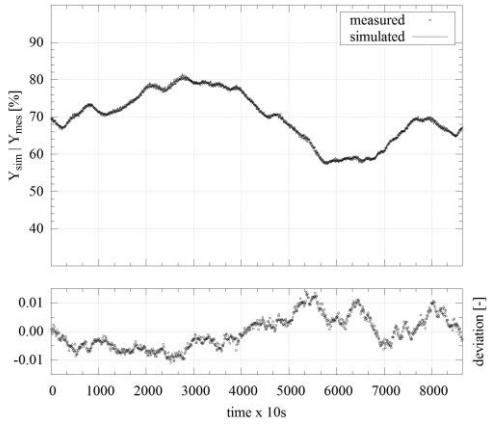

Figure 6.38: measured and simulated output of hotwell controller versus time (1 day, 2012-12-01)

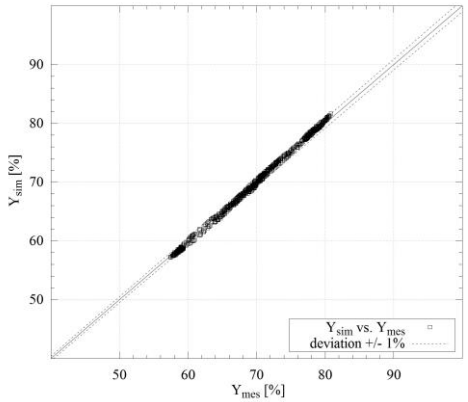

Figure 6.39: simulated versus measured output of hotwell controller (1 day, 2012-12-01)

The results show a good correlation quality. The deviation of the model is within a range of ±1%. In order to make simulation and measurement comparable, the measured output is used as initialisation value for the controller.

6.3.9 Component model - feed pump

6.3.10 Cycle model

After the validation of the before mentioned component models the entire cycle model is validated versus the a data set of mean values of one day. By doing so the validity and stability of the equation system is tested. The following figures depict the convergence of the most important variables in the system. Figure 6.40 shows electric output of the alternator, compared to the value of the mean data set. The calculation converges after 50 seconds. The simulated mass flow of MDM converges after 35 seconds (Figure 6.41).

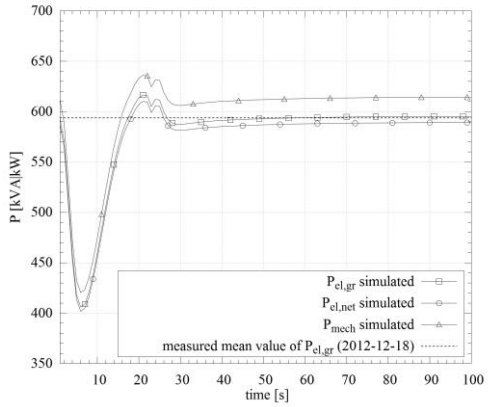

Figure 6.40: simulated and measured electric gross power of cycle (2012-12-18)

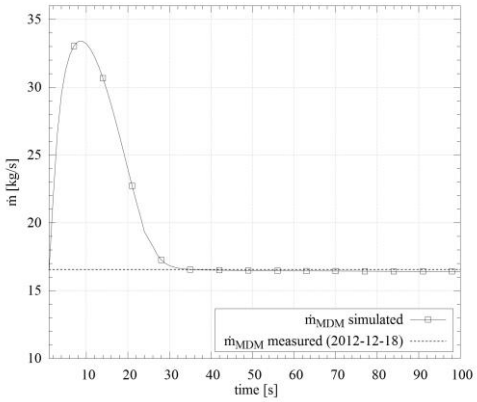

Figure 6.41: simulated and measured mass flow of cycle (2012-12-18)

According to the above mass flow calculation, the pressure values in the simulation converge after 35 seconds (Figure 6.42). Due to the thermal inertia of the system, the calculation of the cycle temperatures takes 100 seconds (Figure 6.43).

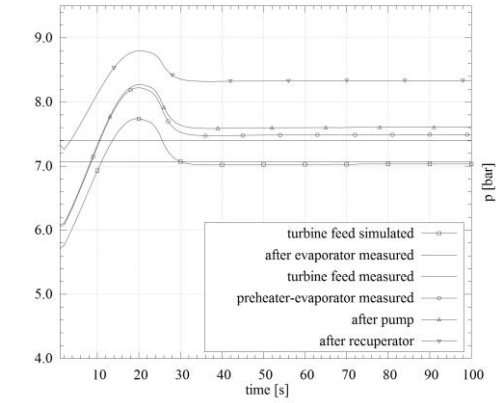

Figure 6.42: simulated and measured pressures of cycle (2012-12-18)

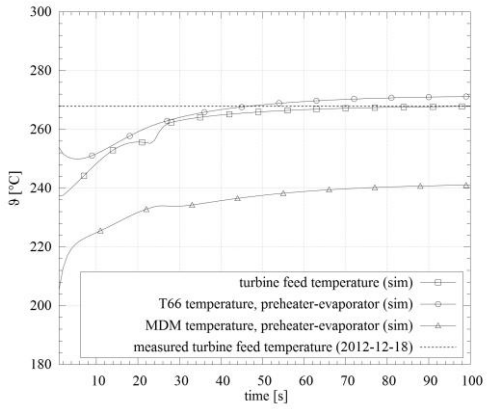

Figure 6.43: simulated and measured temperatures of cycle (2012-12-18)

The following Table 6.4 shows an overview of the most relevant cycle states in comparison.

Table 6.4: measured mean values (2012-12-18) and steady-state calculation results of dynamic cycle model

sensor	measured	simulated	unit	deviation
$P_{el,gr}$	593.892	589.963	kVA	-0.662%
$T_{T66,feed}$	298.98	298.98	◦C	-
$T_{T66,middle}$	-	271.90	◦C	-
$T_{T66,return}$	246.55	246.76	◦C	-
$\dot{m}_{T66}$	36.75	36.75	kg/s	0.000%
Φ_{T66}	4751.9	4731.9	kW	-0.421%
$p_{evap,ret}$	7.39331	7.4773	bar	1.136%
$T_{turb,feed}$	267.91	267.75	◦C	-
$p_{turb,feed}$	7.06949	7.01900	bar	-0.714%
$T_{turb,ret}$	231.52	239.21	◦C	-
$p_{turb,ret}$	0.34744	0.3305	bar	-4.876%
$T_{recu,hot,ret}$	126.44	121.635	◦C	-
$p_{cond,ret}$	0.15648	0.15648	bar	0.000%
$T_{cond,hot,ret}$	79.60	80.071	◦C	-
$p_{pump,ret}$	8	7.733	bar	-3.338%
$\dot{V}_{MDM}$	21.775	21.516	l/s	-1.190%
$\dot{m}_{MDM}$	16.549	16.3524	kg/s	-1.190%
$T_{dh,ret}$	55.05	55.05	◦C	-
$T_{dh,ret}$	72.59	72.59	◦C	-
$\dot{m}_{dh}$	54.45	54.45	kg/s	-

Chapter 7

Monitoring results - operational experience

7.1 Sink heat demand

As the case study is a heat-led plant, the sink with its heat demand is the governing adjacent system. In order to understand the necessities and the constraints during operation of the entire power plant, a brief look into the daily, weekly and seasonal behaviour is required. For the design of heat supply systems many standards can be applied. Based on the EnEV[1], DIN18599, VDI2067, VDI3985 and VDI4655

[50–52, 142] design criteria and heat demands for CHP systems can be estimated. However, these preliminary calculations are not detailed enough to obtain rules for daily operation of the plant. The fine tuning of controls has to respect partially predictable ambient conditions (weather and climate) as well as less predictable factors, such as the human behaviour. As guideline for optimisations on the system, one needs information on the volatility of the demand and the reaction times of the sub-systems and the entire system. As shown in Chapter 1, the sink side's heat demand, measured or estimated, is used as a basis for the design of a thermal power plant. The load duration curve provides a rough oversight on the expected load states. It is a summation of all load point during one season. As such it cannot give any information about the sequence of the load. In brief: it provides no information about the system dynamics. In this section the most relevant load conditions and the transient behaviour of the heat demand is analysed. Reoccurring daily and weekly patterns and seasonal deviation are observed for winter period, summer period and the transition period. These

[1] Verordnung ber energiesparenden W¨armeschutz und energiesparende Anlagentechnik bei Geb¨auden - Energy Saving Ordinance

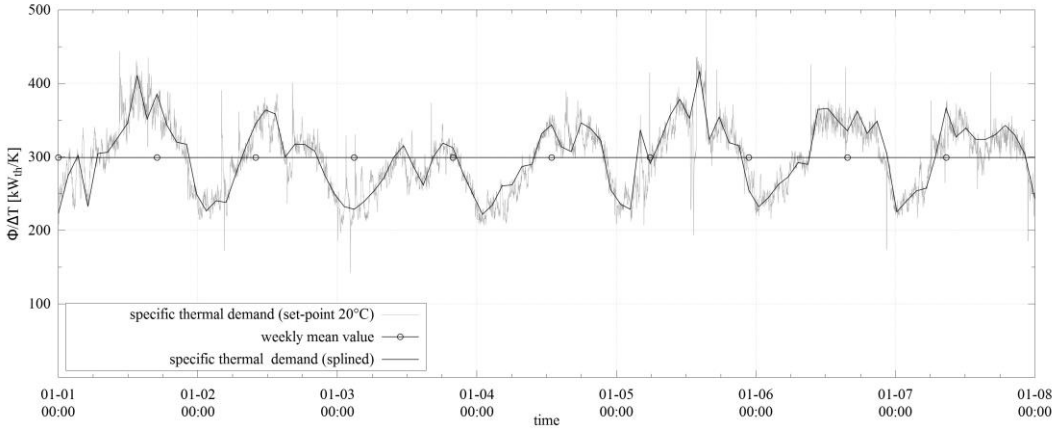

Figure 7.1: one week specific thermal demand (minute values, 2009-01-01 to 2009-01-07)

patterns may deliver useful information for predictive control systems and fuel management.

The Figure 7.1 depicts the specific thermal demand of the district heating based on the ambient temperature. The thermal power of the entire district heating network is divided by the temperature difference from a heating heating set-point of 20 °C to the ambient temperature. One can draw an average value of 299.3kW/K[1]. This means that based on the daily mean temperature one can extrapolate the average demand during winter days. Furthermore, it can be said that amplitudes (during one day) of roughly 100kW$_{th}$/K have to be expected. The volatility of demand in this case is around ±30%. Related to the useful heated space area or the number of inhabitants (at that time the above data were taken around 6000) this is a reasonable characteristic figure.

[1] Based on the specifications of the metering device, the accuracy of the values is in a range of ±0.25%

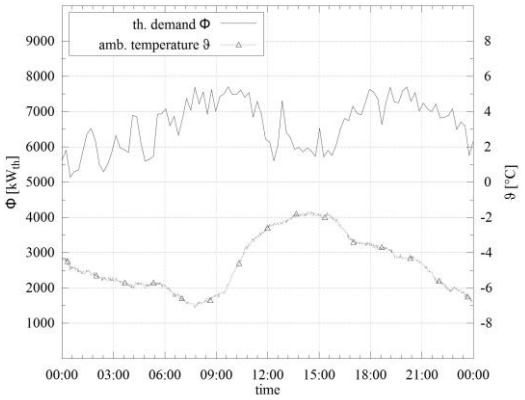

Figure 7.2: thermal demand of district heating over one day (2009-01-03)

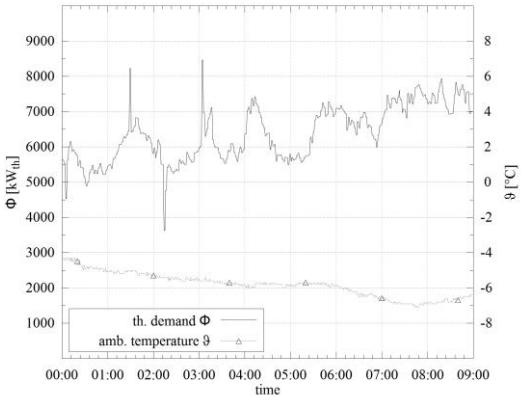

Figure 7.3: thermal demand of district heating over nine hours (2009-01-03)

Figure 7.2 shows the measured thermal power in the district heating and the ambient temperature versus a whole day (minute values). The diagram shows that ambient temperature and demand correlate to a certain extend. Taking a look at the temperature maximum between 12:00 and 15:00, the demand evolves inversely proportional. Besides the main trend, the demand has a significant dispersion. Figure 7.3 depicts the morning of the same day. The ambient temperature falls steadily from −4 °C to −7 °C. The thermal demand rises accordingly, but with several local extrema of 1MW$_{th}$ to 1.5MW$_{th}$. The peak at 4:00 can be explained by the transfer stations of multi-family homes that are programmed to pre-heat and store heat before a large domestic hot water demand at 6:00 occurs. However, the other extrema cannot be explained by the aforementioned operational strategy. It can be speculated that these extrema are the result of an inadequate and unstable control (for instance network valve control).

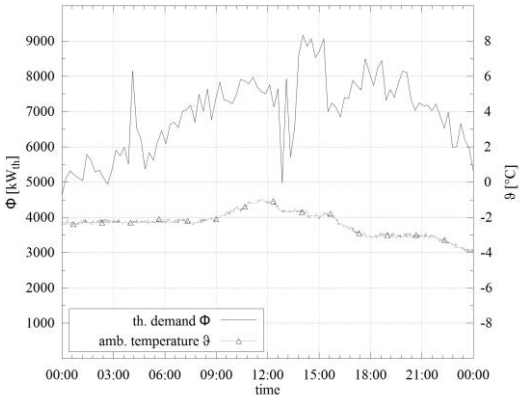

Figure 7.4: thermal demand of district heating over one day (2009-01-05)

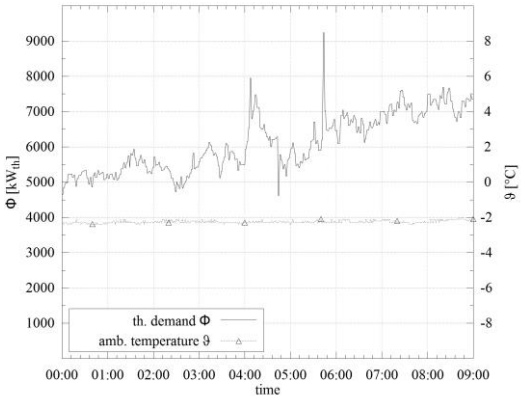

Figure 7.5: thermal demand of district heating over three hours (2009-01-05)

7.2 Load profile and utilization degree

In order to see the statistical distribution of the heat demand the district heating data of ten years (01/2004-12/2013) have been analysed. Based on these data a load profile has been generated. The demand is categorized in ten categories. With this profile optimizations on the system can be extrapolated to derive the performance gain in annual scale. Furthermore, the analysis of the load categories shows us which loads are worth the attention in terms of optimisation.

Table 7.1: degree of utilization of the CHP-unit (2007-2009)

category	load[??]	2007		2008		2009	
	from-to	[h/Y]	[%]	[h/Y]	[%]	[h/Y]	[%]
1	0-0.1	16	0.18%	18	0.21%	18	0.21%
2	0.1-0.2	1495	17.54%	854	9.83%	822	9.69%
3	0.2-0.3	1852	21.72%	1943	22.37%	2365	27.89%
4	0.3-0.4	859	10.08%	783	9.02%	920	10.84%
5	0.4-0.5	554	6.50%	576	6.63%	403	4.75%
6	0.5-0.6	540	6.34%	627	7.22%	314	3.71%
7	0.6-0.7	675	7.92%	678	7.81%	433	5.11%
8	0.7-0.8	672	7.89%	711	8.19%	498	5.87%

9	0.8-0.9	507	5.95%	674	7.77%	518	6.11%
10	0.9-1[?]	1308	15.35%	1615	18.59%	2189	25.82%

[?] values larger than 1 are included in this category

[??] related to a condenser heat rate of 5.3MW_{th}

For all years depicted above the load category three (0.2 to 0.3) is by far the most relevant one. Despite the fact that the maximum thermal power of the system is five times larger than the ORCs output, full load states are rare. This shows the necessity for part load adaptation and optimisation.

7.3 Excess cooling

Thermal power plants cannot work at all times without excess cooling. In a CHP unit cooling has to be reduced to a minimum. Nevertheless, in some situations it is indispensable. As soon as the heat demand in the district network falls below the thermal sink design output the cooler unit can be used to increase the load of the
ORC. A more relevant scenario is low demands in summer or intermediate times. When the request for heat during the day falls below 1.5MW, but during night times the demand rises the unit has to run in stand-by mode. To maintain the ORC operation during the day the excess cooling unit wastes heat. As previously described in Section 3.3 the implementation of the heat rejection system as excess cooler and emergency cooler at the same time necessitates the routing as shown in Figure 7.6.

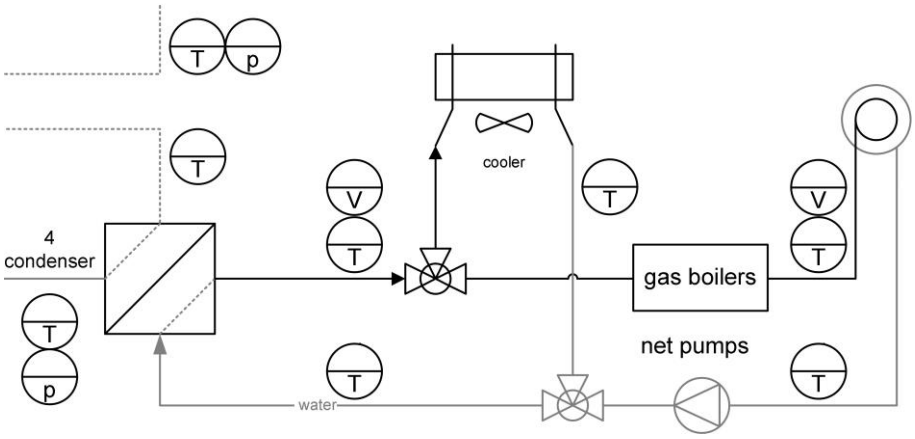

Figure 7.6: original implementation of heat rejection system

This configuration is very problematic in terms of controlling. The following two plot give an representative impression on the sink situation and the cycle behaviour during low loads in summer. Despite the district heating return temperature is low and stable, the feeding temperature has massive, reoccurring fluctuations. Even patterns can be identified. When the cooler is enable a cold temperature plug is pumped in the loop causing these disturbances.

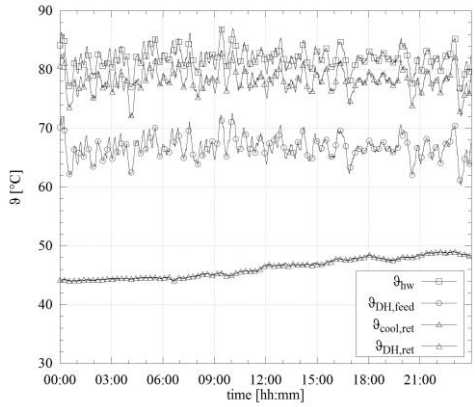

Figure 7.7: sink side temperatures: hot- well, district heating, cooler (1 day, 2011-06-02)

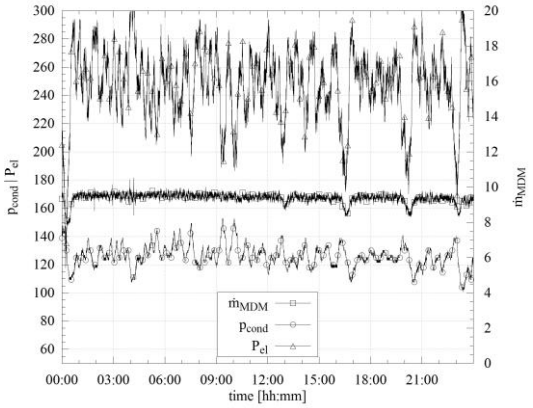

Figure 7.8: condenser pressure , mass flow and electric output (1 day, 2011-06-02)

7.4 Performance of the furnace

The demand of fuel is the main cost factor during the operation of a biomass CHP plant. Volatile or high market prices for wood chips lead to uncertain or non-profitable economics. Technically, the combustion efficiency is determined by the quality and state of the fuel and the properties of the exhaust gases. In this case the plant is non-condensing, the latent heat of the water is transported through the process but not converted to useful end energy. The basic following points are relevant for a good conversion efficiency:

- Water content: a high water content leads to long fuel drying in the precombustion zone. The latent heat of the water remains unused.
- Ash content: low ash contents assure that more convertible mass is processed through the furnace. In this case we have up to 15% of ash content.

- Load: higher loads lead to a better coverage rate of the furnace. Heat transfer, both via radiation and convection, increase.

Regarding the first of the above points, it has to be mentioned that higher water contents can have a favourable outcome in part-load. If the fuel ignites too early in the firebox the reaction temperatures may exceed the ash melting point. While the design combustion temperature was originally 1050 °C the system had to be adjusted over the years to stay below 950 °C. This was done to account for the requirements of the bad fuel quality and the furnace characteristics.

7.4.1 Exhaust gas quality

The following Table 7.2 shows average values of the fuel and exhaust gas in the investigated case study power plant.

Table 7.2: average measured exhaust gas values of 2009 and furnace design values

parameter	annotation	value	unit
ash content	maximum	15	[%]
calorific value	@25 °C	776	[kWh/m³]
ash softening point		1050	[°C]
water content	maximum	60	[%]
CO	average	0.002	[g/kWh]
λ_{com}		1.7	[-]
NO_X	average	0.589	[g/kWh]
PM(10)	average	0.016	[g/kWh]

When it comes to the improvement of efficiencies the environmental impact can be set into scale with these mean values. Although the above depicted values are far below the allowed concentration, a further reduction is always favourable.

7.5 Performance of the district heating

Together with the previous section, this chapter gives an overview on the performance of the district heating. Based on 120 monthly consumptions of the district heat network, the relation to ambient conditions (temperature, solar radiation), population and the degree days for the site have been calculated.

Results are depicted in the Figures 7.9 and 7.10. They show the correlations of heat demand and ambient conditions over the recent years.

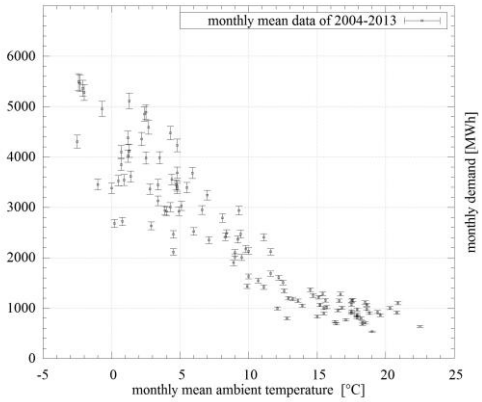

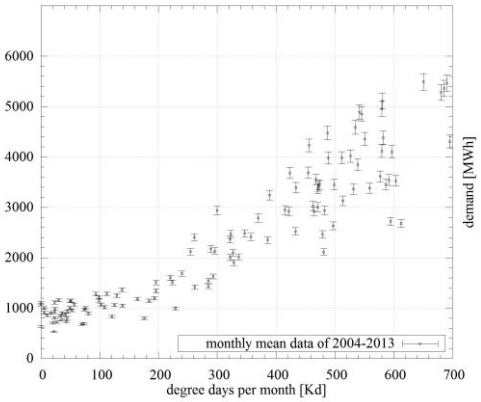

Figure 7.9: monthly heat demand vs. mean ambient temperature (2004-2013)

Figure 7.10: monthly heat demand vs. mean degree days (2004-2013)

The depicted correlations in the Figures 7.9 and 7.10 are very unique for this case study. To set the information into scale, and make it transferable to other cases, the next figures provide specific values (per capita).

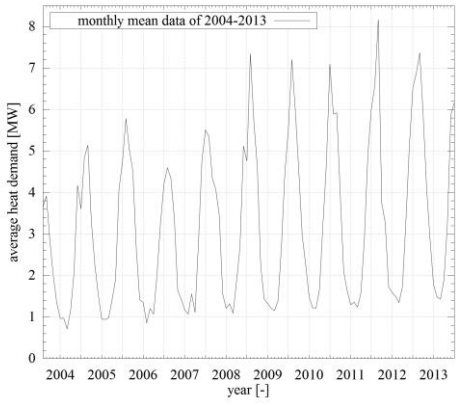

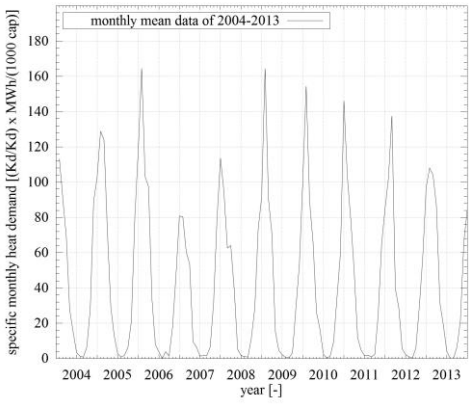

Figure 7.11: monthly mean heat demand in the district heating (2004-2013)

Figure 7.12: monthly mean heat demand in the district heating (2004-2013), degree day adjustment, related to 1000 inhabitants

Figure 7.12 depicts the monthly mean values of the years 2004 to 2013. As before shown, the population has increased almost linear during the years. This increase in population translates to a higher minimum and maximum load. However, the summer heat demand (mainly domestic water) is still very low. For

this ORC system heat rates on the sink side of 1.5MW$_{th}$ are too low. Therefore, extensive excess cooling has to be done (0.5MW$_{th}$to 1MW$_{th}$) during that period.

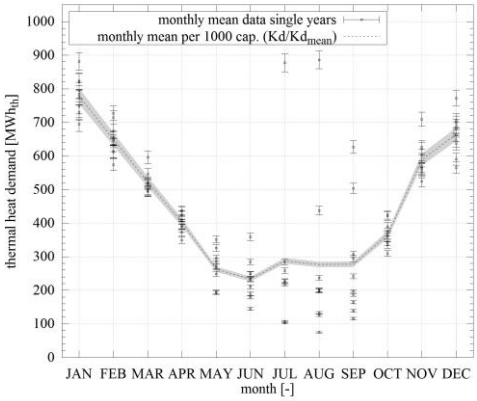

Figure 7.13: monthly heat demand per 1000 capita (scaled via degree days)

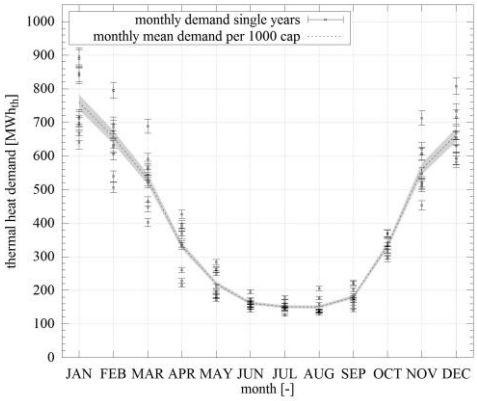

Figure 7.14: monthly heat demand per 1000 capita (absolute)

For the sake of comparability with other locations and power plants, the values in Figure 7.12 return the monthly heat demand on a basis of 1000 inhabitants, multiplied with the monthly degree days and divided by annual degree days (Kd_{month}/Kd_{year}). The degree day values have been provided by the Institut Wohnen und Umwelt (IWU) [143–146]. By doing so, one receives a straightforward indicator to compare different systems. However, the results in Figure 7.13 reveal a large deviation of the values during the summer period. A look at the degree days shows, that in very warm summer month (here July, August and September) the Kd value may deviate far from the mean of about 30Kd. For two years the values are even below 1Kd. This leads to a huge ratio of degree days to the long term mean. As a consequence, the scaled values increase. Due to the fact that the domestic water heat demand cannot be separated from the heating demand, the results depicted in Figure 7.14 are more representative for this case than in Figure 7.13. It is assumed that all depicted monthly values are accurate within a range of ±1.5%.[1]

[1] This deviation is based on the circumstance that the day of reading is known, but not the exact time of the day. Therefore, a maximum deviation of 24 hours must be assumed.

7.6 ORC engine performance

The following diagram in Figure 7.15 depicts the electric gross efficiency of the unit for the year 2008. Mean values for each hour of the year have been generated from minute values. One can see a strong correlation between the load state of the cycle and its electric output. While the full load values reach almost 15% the part-load performance is rather poor. It has to be mentioned, that the data have not been filtered according to source and sink temperature levels. That explains the large variation from the fitted curve. In the range of 3MW to 4.5MW the dots form two parallel clouds. It is an indication for different temperature levels in the evaporator. They can be caused by varying thermal oil temperature set-points or evaporator filling levels.

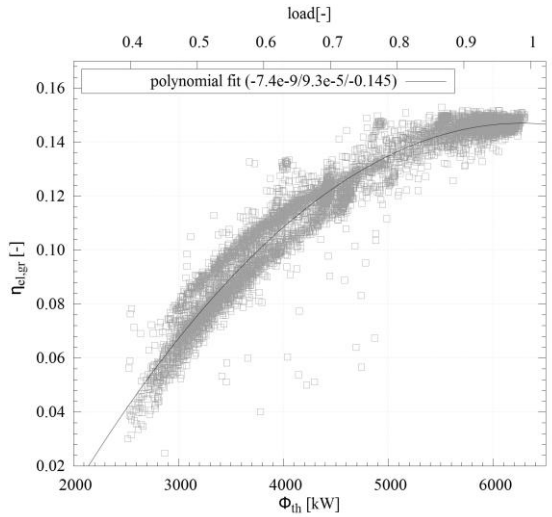

Figure 7.15: hourly mean values of electric gross efficiency versus source heat rate (year 2008)

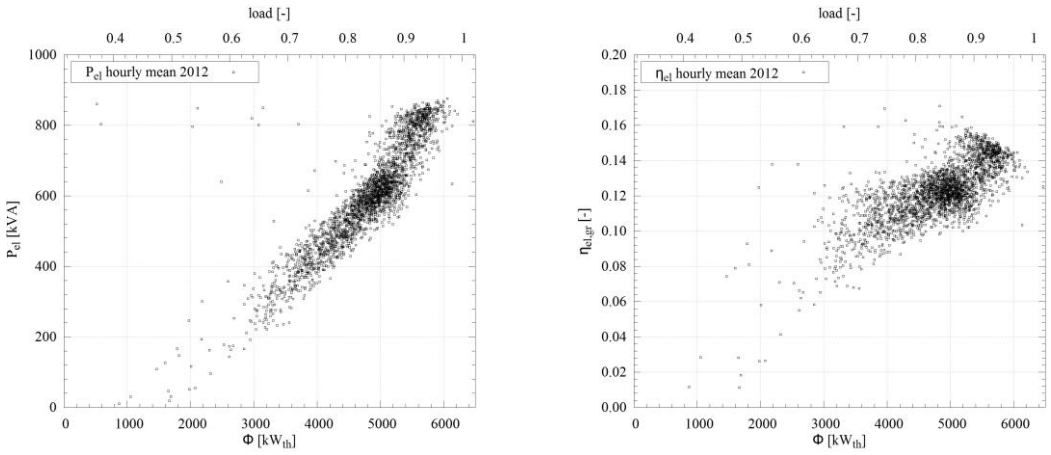

Figure 7.16: electrical grid feed-in vs. thermal input of cycle (hourly means of 2012)

Figure 7.17: electrical gross efficiency vs. thermal input of cycle (hourly means of 2012)

7.6.1 Start-up procedures

The response time in small and medium heat recovery cycles is an important criterion. If the system is not heat-led the frequent start-up and stop procedures are a relevant portion of the operation. In larger systems, such as the one at hands, shut-downs are a consequence of malfunctions or necessary maintenance has to be done. However, the behaviour of the cycle during starts and stops can give valuable information about the dynamics of the system. The following Figures 7.18 and 7.18 shall give an impression about transient procedures:

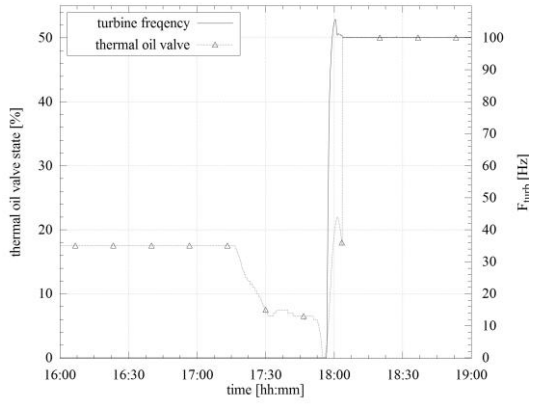

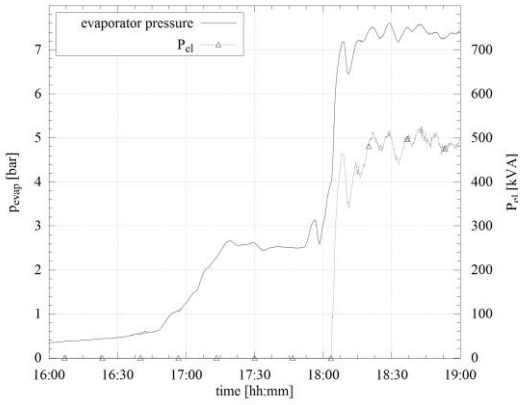

Figure 7.18: thermal oil valve state and turbine frequency during start-up

Figure 7.19: evaporator pressure and electric output during start-up

Compared to the theoretical start-up procedure mentioned in Section 3.4.1.1 some fluctuations can be seen. The length of the starting period seem to be adequate for this cycle size.

7.6.2 Cycle fluid composition

As mentioned in the introduction part, not just the cycle fluid type and its quality play a significant role for the operation of the unit. Processing sensor data at times revealed interesting and sometimes unexpected results. This led to the decision to include chemical working fluid analyses into the monitoring of the system. As a

reference for the fluid quality a barrel of fresh MDM has been analysed, the results a shown in Table 7.3. With the purity of 99.9% a high correlation of the EOS for a pure fluid can be expected.

Table 7.3: HS-GC-MS analysis of original cycle fluid

compound	abbr.	CAS	fraction
-	-	-	[%]
Octamethyltrisiloxane	L3 / MDM	107-51-7	99.9
Hexamethyldisiloxane	L2 / MM	107-46-0	0.012
Hexamethylcyclotrisiloxane	D3	107-52-8	0.003
Octamethylcyclotetrasiloxane	D4	556-67-2	0.016
Decamethyltetrasiloxane	L4 / MD2M	141-62-8	0.003
Decamethylcyclopentasiloxane	D5	541-02-6	≤0.001
Dodecanethylpentasiloxane	L5 / MD3M	141-63-9	0.004
Trimethylsilanol	MOH	1066-40-6	-

One sample of used working fluid (7.4) has been taken from the drain tap of the pre-heater after the cycle cooled down. With 79.2% the the fluid shows significant degradation. The remaining 20% of fluid represent the full range of low-boilers and high-boilers in the family of Siloxanes.

Table 7.4: HS-GC-MS analysis of cycle fluid (pre-heater, cold cycle)

compound	abbr.	CAS	fraction
-	-	-	[%]
Octamethyltrisiloxane	L3 / MDM	107-51-7	79.2
Hexamethyldisiloxane	L2 / MM	107-46-0	7.55
Hexamethylcyclotrisiloxane	D3	107-52-8	0.592
Octamethylcyclotetrasiloxane	D4	556-67-2	4.93
Decamethyltetrasiloxane	L4 / MD2M	141-62-8	5.12
Decamethylcyclopentasiloxane	D5	541-02-6	0.535
Dodecanethylpentasiloxane	L5 / MD3M	141-63-9	1.7
Trimethylsilanol	MOH	1066-40-6	-

The second used fluid sample (7.5) has been taken from the outlet of the vacuum pump. In the original design the outlet was released to the ambient. In this case the vapour is collected and fully condensed outside the cycle. The composition shows an enormous amount of MM, MDM and MM cannot be separated under the conditions of the condenser. In order to do so, temperature should to be lowered by 20K and the pressure should to be reduced to less than 60mbar.

Table 7.5: HS-GC-MS analysis of cycle fluid (vacuum pump)

compound	abbr.	CAS	fraction
-	-	-	[%]
Octamethyltrisiloxane	L3 / MDM	107-51-7	50.9
Hexamethyldisiloxane	L2 / MM	107-46-0	45.5
Hexamethylcyclotrisiloxane	D3	107-52-8	0.898
Octamethylcyclotetrasiloxane	D4	556-67-2	1.4
Decamethyltetrasiloxane	L4 / MD2M	141-62-8	0.816
Decamethylcyclopentasiloxane	D5	541-02-6	0.099
Dodecanethylpentasiloxane	L5 / MD3M	141-63-9	0.238
Trimethylsilanol	MOH	1066-40-6	-
other poly-siloxanes	-	-	0.116

The third used fluid sample (7.6) has been taken from the drain tap of the recuperator, after a full stop. The large amount of MD2M and MD3M lead to the conclusion that high-boilers condensate (if ever evaporated) and precipitate in the recuperator vessel. In this case, the effect can remain undiscovered for a long time, as the reservoir in the bottom of the recuperator has a volume of more than 600l.

Table 7.6: HS-GC-MS analysis of cycle fluid (recuperator reservoir)

compound	abbr.	CAS	fraction
-	-	-	[%]
Octamethyltrisiloxane	L3 / MDM	107-51-7	65.50
Hexamethyldisiloxane	L2 / MM	107-46-0	5.09
Hexamethylcyclotrisiloxane	D3	107-52-8	0.50

Octamethylcyclotetrasiloxane	D4	556-67-2	4.97
Decamethyltetrasiloxane	L4 / MD2M	141-62-8	11.00
Decamethylcyclopentasiloxane	D5	541-02-6	1.30
Dodecanethylpentasiloxane	L5 / MD3M	141-63-9	7.05
Trimethylsilanol	MOH	1066-40-6	-
other poly-siloxanes	-	-	4.56

The last sample (Table 7.7) has been taken during operation of the cycle after the feed-pump. The composition is similar to the one taken in the pre-heater. As the latter one has been taken in cold state, it has to be assumed that the volatile low-boilers have partially evaporated from the fluid before the sample was taken. Under normal operating conditions, the composition of the sample from the feed-pump is the most relevant. For the following aggregates such as evaporator and turbine this composition is still valid, but it changes in the recuperator.

Table 7.7: HS-GC-MS analysis of cycle fluid (feed pump)

compound	abbr.	CAS	fraction
-	-	-	[%]
Octamethyltrisiloxane	L3 / MDM	107-51-7	78.3
Hexamethyldisiloxane	L2 / MM	107-46-0	3.6
Hexamethylcyclotrisiloxane	D3	107-52-8	0.543
Octamethylcyclotetrasiloxane	D4	556-67-2	4.04
Decamethyltetrasiloxane	L4 / MD2M	141-62-8	6.55
Decamethylcyclopentasiloxane	D5	541-02-6	0.92
Dodecanethylpentasiloxane	L5 / MD3M	141-63-9	3.96
Trimethylsilanol	MOH	1066-40-6	0.001
other poly-siloxanes	-	-	1.852

From the above tables one can draw several conclusions for the operation of the cycle as well as for the comparability of simulation and reality:

- The original fluid has degraded significantly. Reasons for that can be acidity, metal contaminations, high temperatures and oxygen contamination.

- The fluid composition varies significantly within the cycle. Furthermore, it seems to make a difference whether the sample is taken from a hot or a cold cycle.
- The sample of the vacuum pump shows the lowest proportion of MDM and the highest proportion of other Siloxanes. As a consequence of the thermal conditions in the condenser and the location of the suction nozzle of the vacuum pump, mainly MDM and MM are removed in gaseous state from the condenser shell. This means, that the influence of low-boilers, especially MM has to be considered in a simulation. It does not mean that this sample is representative for the mixture in the shell volume. The good news is: the majority of contaminants can be removed with reasonable effort.
- The recuperator sample has a large proportion of high boiler contaminants (L4/L5). They form droplets after the turbine and precipitate in the shell of the recuperator. A rather large proportion of L2 in this liquid sample, which can be explained by the fact that once fluid reaches the bottom of the recuperator, it is no longer heated enough to remain vaporous. The high proportion of MDM in the liquid makes it interesting for recycling. The recuperator has a drain valve. With a vacuum pump it is possible to extract the liquid even during operation of the cycle.

7.7 Pressure losses and cycle pressure characteristics

In the following section the variations in pressure across the single components of the cycle are shown in detail.

7.7.1 Pressure characteristics of the cycle

In order to understand the cycles behaviour the volume flow (respectively mass flow) characteristics have to be observed. The following Figure 7.20 shows a data set of mean values (5 minutes, 1 week) of the differential pressure across the pump.

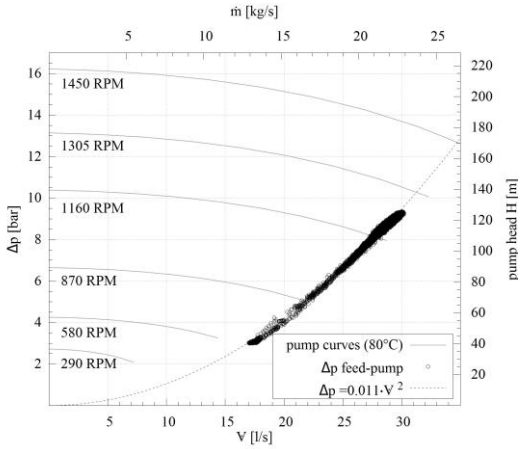

Figure 7.20: mean pressure difference across the feed-pump versus volume (1 week, 5 minutes)

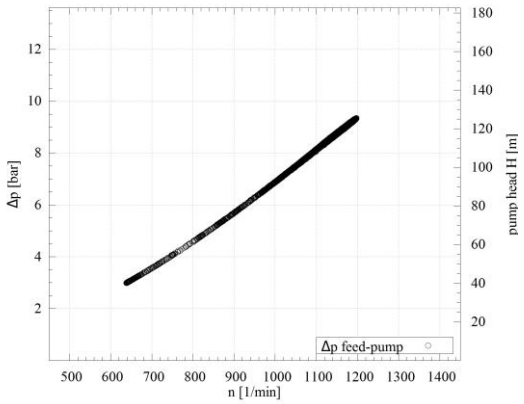

Figure 7.21: mean differential pressure across the feed-pump versus rotational flow speed (1 week, 5 minutes)

The next Figure 7.22 plots the pressure values at the turbine inlet. One month of mean values (2012-12, 5 minutes) gives an impression about the states at that point of the cycle.

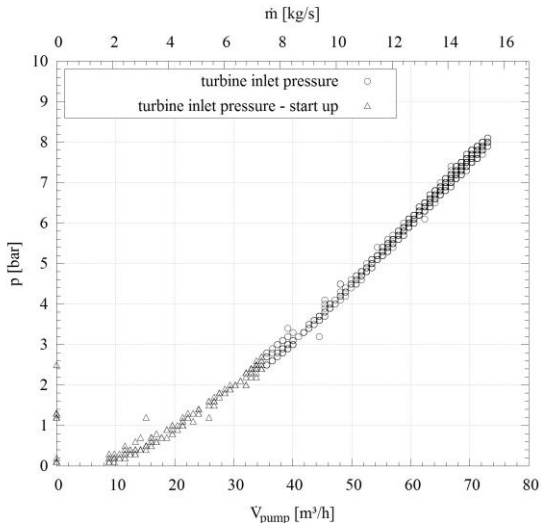

Figure 7.22: pressure before turbine, during start-up and standard operation

The data points are grouped in this case. Crosses show the behaviour during normal operation. The triangles mark the data that have been taken while the cycle was in start-up procedure.

7.7.2 Recuperator hot side pressure drop

During the observation of the cycle the data showed a massive pressure drop across the recuperator. Despite the pressure sensors have been checked and the measurement during the revisions indicated roughly the same pressure value on all cycle sensors, a suspicion remained. A difference of 5mbar to 7mbar had been discovered, but this can be explained by dispersion of the sensors or a draft in the cycle due to temperature differences. In order to prove a latent deviation of the turbine outlet pressure start ups have been analysed. The following Figure 7.23 depicts the volume flow, pressure and turbine frequency during a start-up procedure. The vapour side's pressure drop across the recuperator should be in a range of 50mbar to 150mbar. According to its rather complicated flow geometry and the tube finning in the unit, a relatively high pressure difference was expected. However, the monitored data revealed a significantly higher pressure difference (up to 300mbar).

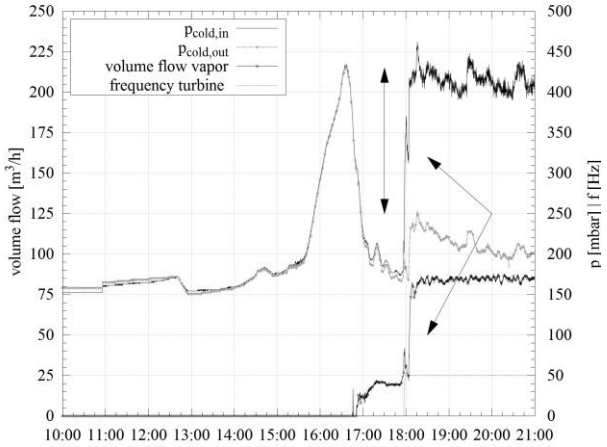

Figure 7.23: recuperator and condenser pressure during a cold start procedure (2013-02-02)

Two points can be read from this plot:

- As soon as the turbine is set under vapour the pressure difference increases enormously in a range of 200mbar (marked by the double headed arrow).
- The two other arrows point to a very interesting spots with parallel profile in the lines of the inlet pressure and the feed pump mass flow.

The above points lead one to the conclusion that the pressure measured at the inlet of the recuperator must correlate with the volume flow through the turbine. Based on the knowledge that the turbine model is very accurate and its pressure output correlate well with the measured data, the measured data seem to be correct. As a consequence, this shows that the pressure drop across the recuperator is way above the original design value. For the performance of the cycle this is a clear point for an optimisation.

Chapter 8

Simulation results and improved operation strategies

In this chapter the results of the final models are discussed. The impact of modifications are in the focus here. The assessment of the results is based on the criteria defined earlier in the Section 2.6.

8.1 Calculation results

8.1.1 Cycle case studies (steady-state)

In this section the results of case studies of the observed cycle are presented. Several cycle variants derived from the original configuration are calculated. Under necessary simplifications the different version have been calculated as a steady-state approach.

8.1.1.1 Steady-state analysis - standard configuration

The standard configuration of the cycle has a fixed live vapour temperature and a constant condensation pressure. Except the recuperator all heat exchangers are ideal, thermal losses are neglected. For the largest transfer process in the cycle, the heat transfer capability of the recuperation is correlated with an exponent of 0.6 to the mass flow. Pressure losses are modelled according to the design data and the measured data. The feed pump is based on a polynomial similarity model (3rd degree). The turbine is based on the Stodola law, the nozzles' isentropic efficiency is a correlation of the expansion ratio as described in the modelling chapter. The following nominal design values are assumed:

Table 8.1: nominal pressure differences for the case study 0.0

aggregate	Δp_{nom}	unit
recuperator liquid	-64000	[Pa]

recuperator vapour	-20742	[Pa]
pre-heater	-17600	[Pa]
evaporator	-6000	[Pa]
hotwell	1700	[Pa]
vapor filter	-32000	[Pa]

The nominal pressures in Table 8.1 are based on a nominal mass flow of 20kg/s. As a simplification the pressure drop of recuperator contains the friction loss of the pipe connection from the pump to the pre-heater.

8.1.1.2 Parametric study 1

Excessive super-heating is a widely spread phenomenon. It occurs as a consequence of over-sizing of the evaporator and pre-heater, as well as insufficient filling of the cycle. The latter can be cased by wrong design, or after a long shut-down followed by a cold restart of the cycle. Furthermore a loss of cycle fluid can cause insufficient filling in the evaporator. The following Figure depict a comparison of the standard cycle with three variants.

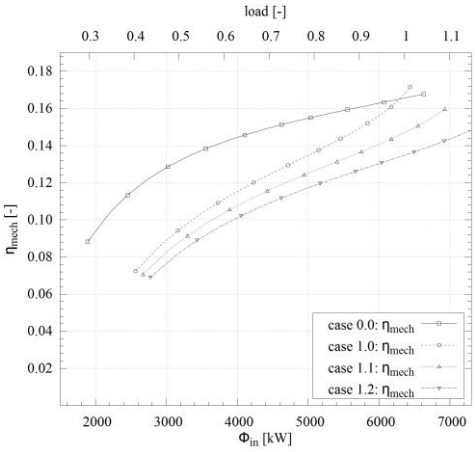

Figure 8.1: parametric studies 1.x versus 0.0 - mechanical efficiency vs. source heat

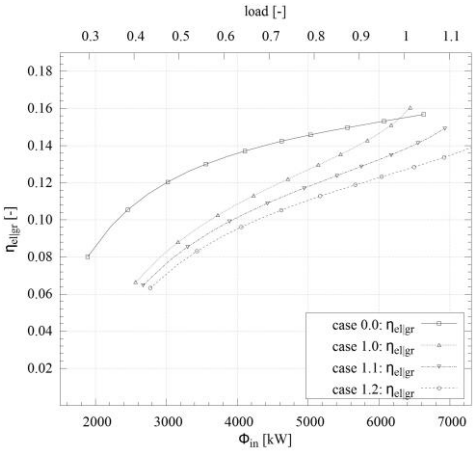

Figure 8.2: parametric studies 1.x versus 0.0 - electrical gross efficiency source heat

The Figures 8.1 and 8.2 depict the mechanical and gross electrical efficiency of the three parametric cases 1.0, 1.1 and 1.2 in comparison to the ideal standard case 0.0. For the 1.X cases a fixed evaporation temperature of 260 °C respectively 270 °C and 280 °C are assumed. The ideal case 0.0 works with an adaptive super-heating of 3K. Due to the fact that the control allows lower evaporation

temperatures than 260 °C, the ideal cycle 0.0 can start its operation at a lower source heat level. The second, very obvious difference, is the constantly higher part load efficiency.

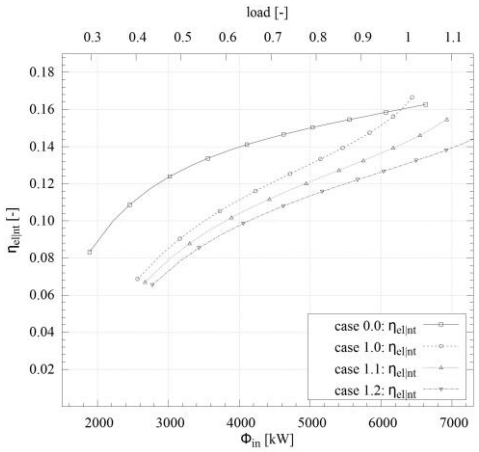

Figure 8.3: parametric study 1.X versus 0.0 - electrical net efficiency vs. source heat

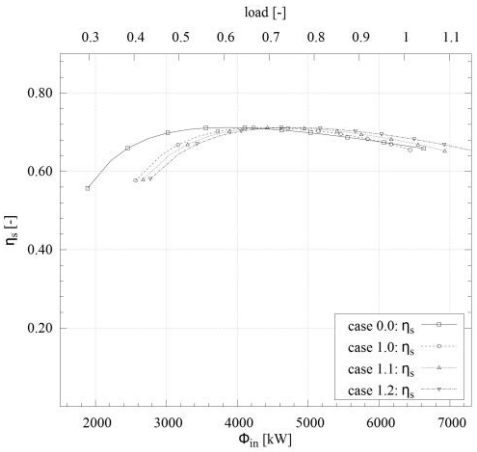

Figure 8.4: parametric study 1.X versus 0.0 - isentropic efficiency of turbine vs. source heat

Figure 8.4 gives details on the turbine's isentropic efficiency. While case 0.0 reaches its maximum efficiency around 50% to 55% of load the other cases reach the maximum at a load of 70% to 80%.

8.1.1.3 Parametric study 2.1

The calculations of the recuperators liquid side have shown comparably high pressure losses. Due to the necessary size of the heat exchanger a tube array with ten tiers in a row is used. Therefore, the flow path is very long, while the flow cross section causes a high flow friction. Based on this fact, an alternative configuration with a lower tube length and more parallel tubes per tier is tested. The results in Figures 8.5 and 8.6 show that the electric output remains almost the same in both scenarios.

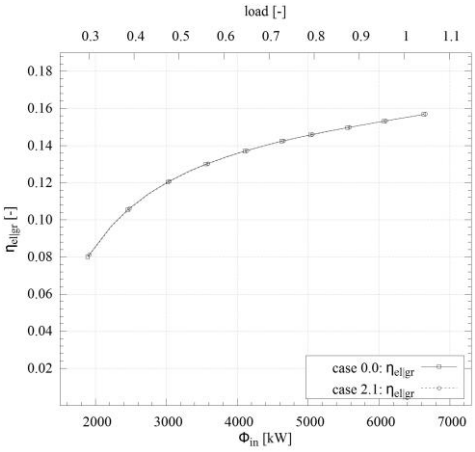

Figure 8.5: parametric study 2.0 versus 0.0 - electric gross efficiency vs. source heat

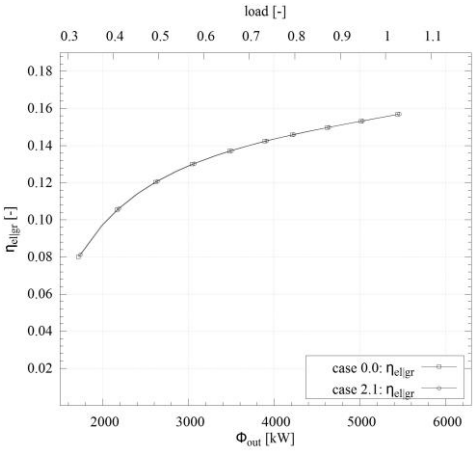

Figure 8.6: parametric study 2.0 versus 0.0 - electric gross efficiency vs. sink heat

8.1.1.4 Parametric studies 2.2 and 2.3

Besides the optimisation of the evaporation temperature, in this calculation the condenser pressure is reduced by 10mbar. Under full load the difference compared to the base case disappears. Such a little pressure difference has no big influence if the the overall pressure drop increases. Under low load conditions (0.25 to 0.6) this configuration shows an improvement 0.5% points to 0.75% points.

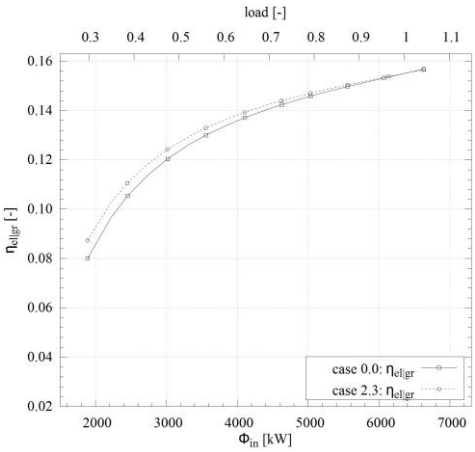

Figure 8.7: parametric study 2.3 versus 0.0 - electric gross efficiency vs. source heat

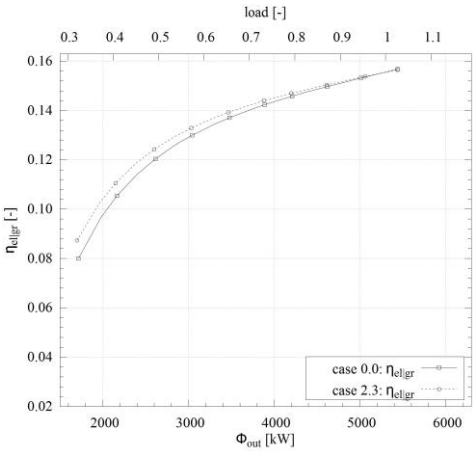

Figure 8.8: parametric study 2.3 versus 0.0 - electric gross efficiency vs. sink heat

8.1.1.5 Parametric study 3

In case study 3 several optimisations are combined. The cycle is condensing under a pressure of 135mbar. Pressure frictions are reduced to a minimum. The recuperators hot side has now a nominal loss of 70mbar, the recuperators cold side 100mbar and the vapour filter 200mbar0.

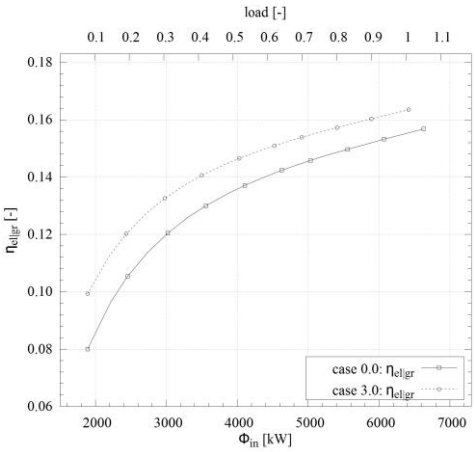

Figure 8.9: parametric study 3.0 versus - electric gross efficiency vs. source heat

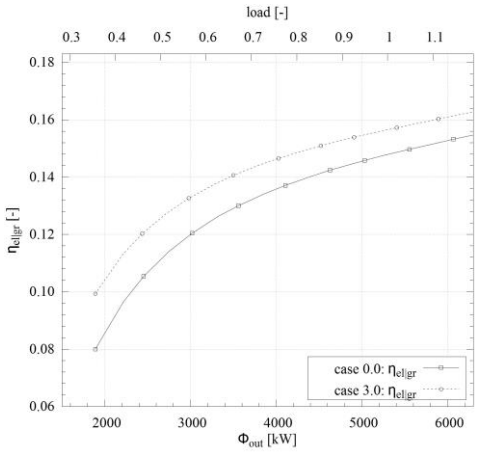

Figure 8.10: parametric study 3.0 0.0 versus 0.0 - electric gross efficiency vs. sink heat

As a sub-variant of this case study the combination of two modifications is tested: besides the lower condenser pressure the liquid side flow friction of the recuperator has been reduced to 32000Pa. In the two following Figures 8.11 and 8.12 it can be seen that a slight improvement compared to case 2.3 was achieved.

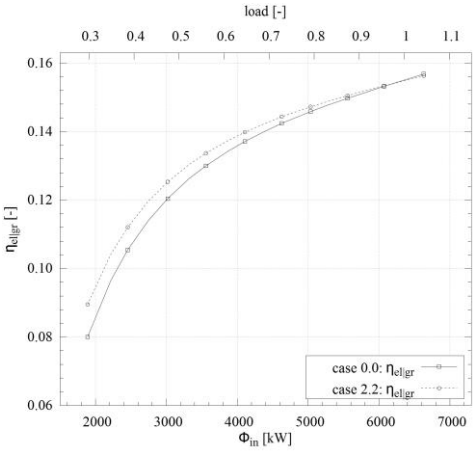

Figure 8.11: parametric study 2.2 versus 0.0 - electric gross efficiency vs. source heat

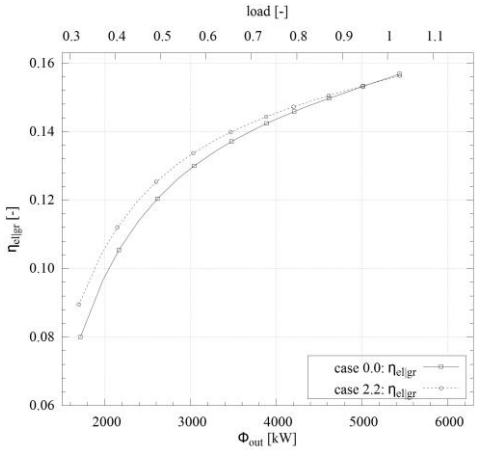

Figure 8.12: parametric study 2.2 versus 0.0 - electric gross efficiency vs. sink heat

8.1.2 Cycle response test

A response test has been run to determine the dynamics of the entire cycle model. A sudden increase of the water temperature in the district heating of 4K was fed into the system. The response in terms of temperature and electric power output is in depicted in Figure 8.13. The reaction of the cycles mass flow and the return temperature of the thermal oil are shown in Figure 8.14. For the biomass furnace control the thermal oil reaction is an input parameter for the fuel feeding frequency.

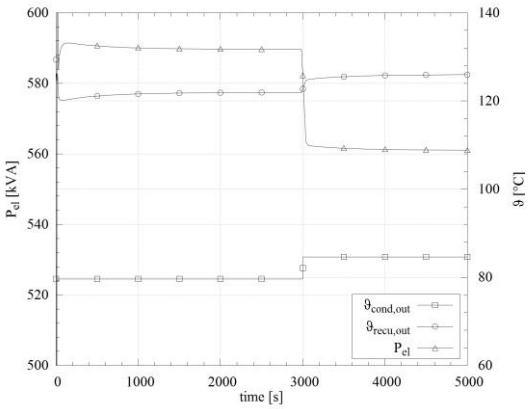

Figure 8.13: electric output and recu- perator temperature response on district heating temperature step

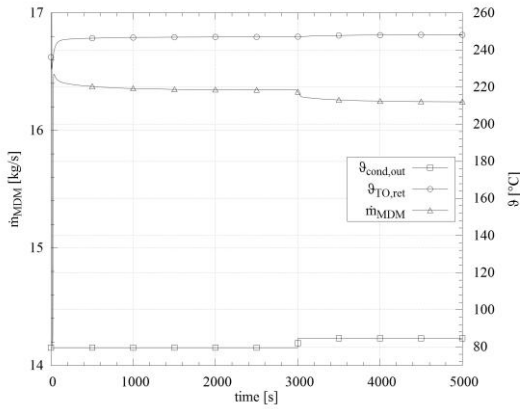

Figure 8.14: mass flow and thermal oil return temperature response on district heating temperature step

8.1.3 Reduced super-heating

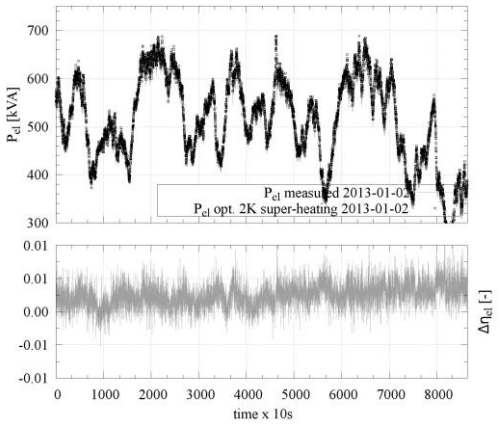

Figure 8.15: measured electric output vs. optimized super-heating of 2K

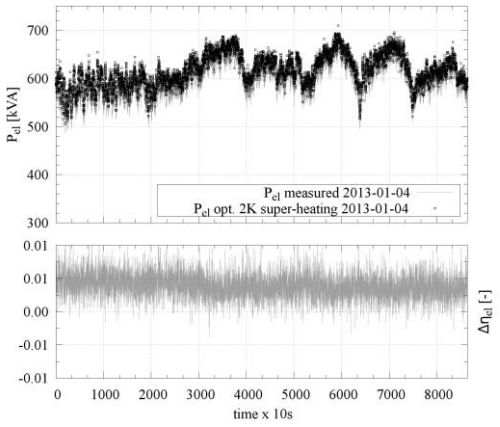

Figure 8.16: measured electric output vs. optimized super-heating of 2K

(2013-01-02) (2013-01-04)

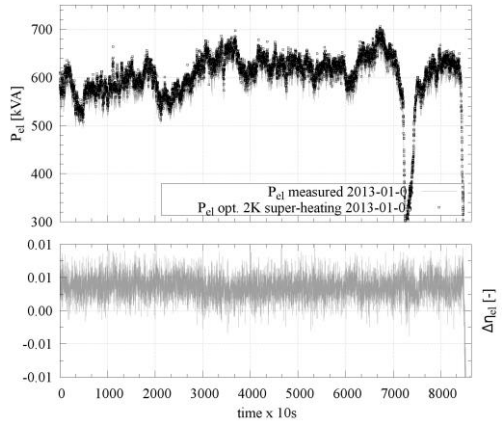

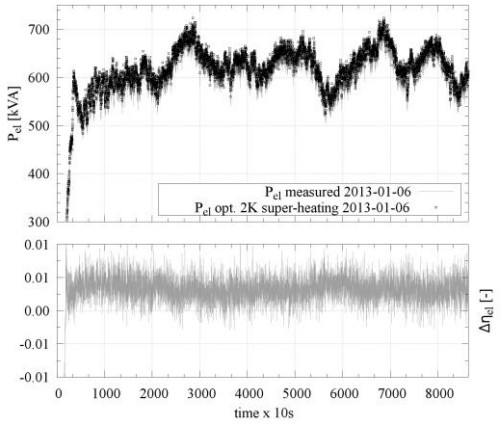

Figure 8.17: measured electric output vs. optimized super-heating of 2K (2013-01-05)

Figure 8.18: measured electric output vs. optimized super-heating of 2K (2013-01-06)

Based on the steady-state simulations the reduced super-heating has been implemented in the dynamic model. The following Figures 8.19 and 8.20 show the performance of the cycle as is (case 0) based on a load scenario of the 2012-01-03 compared to two optimized cases. The data of that day represent a wide load range (0 to 900kVA). Case 1 and case 2 shows the electric gross power output and the gross electric efficiency versus the input of heat under. The vapour temperature is reduced by 5K respectively 10K. The electric output across the whole load range increases significantly by 1% point which translates to an improvement of feed-in of roughly 6%. The cycle is limited by the amount of heat taken by the district heating. This leads to the phenomenon that the maximum power respectively efficiency is reached under a lower load state.

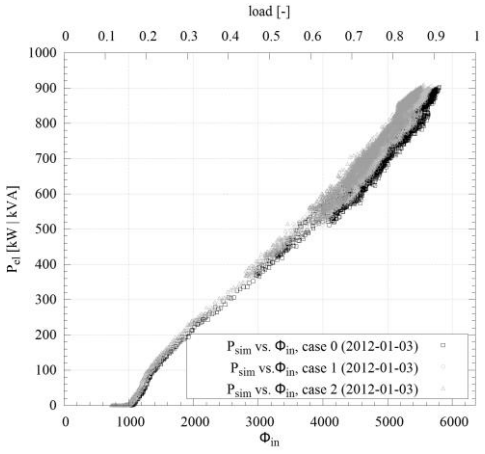

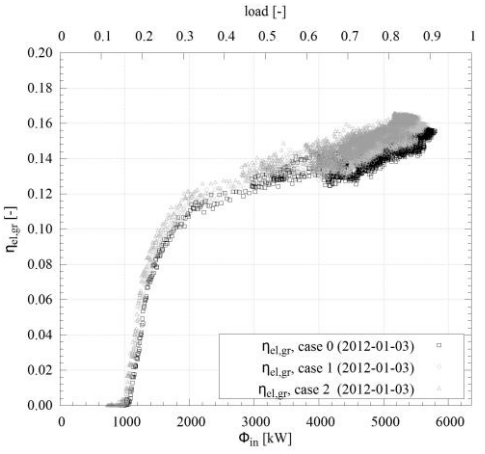

Figure 8.19: electric gross output vs. thermal input for 3 cases

Figure 8.20: electric gross efficiency vs. thermal input for 3 cases

Based on the simulation results and the temporal distribution of the load states, the economical side of the two scenarios has been calculated. The results are listed in the following Table 8.2.

Table 8.2: results for improvement of super-heating on annual basis

load	category	$\eta_{el,gr}$ case 0	$\eta_{el,gr}$ case 1	$\eta_{el,gr}$ case 2	$\Delta\eta_{el,gr}$ case 1	$\Delta\eta_{el,gr}$ case 2
0	1	-	-	-	-	-
0.1	2	-	-	-	-	-
0.2	3	5.44%	6.39%	7.32%	17.42%	34.48%
0.3	4	11.00%	11.42%	11.86%	3.79%	7.80%
0.4	5	12.21%	12.68%	13.14%	3.84%	7.62%
0.5	6	13.01%	13.45%	13.71%	3.39%	5.41%
0.6	7	13.52%	13.83%	14.19%	2.27%	4.91%
0.7	8	13.89%	14.40%	14.95%	3.64%	7.62%
0.8	9	15.13%	15.65%	16.13%	3.43%	6.62%
0.9	10	15.45%	15.93%	-	3.15%	-
distr. [h/a]	yield [kWh/h]	yield [kWh/h]	yield [kWh/h]	yield [kWh/h]	surplus [e/a]	surplus [e/a]
18	1	-	-	-	-	-
822	2	-	-	-	-	-
2365	3	57.7	67.7	77.6	5346	10582
920	4	174.9	181.5	188.6	1372	2824
403	5	258.8	268.7	278.5	901	1786
314	6	344.7	356.3	363.3	825	1319
433	7	430.1	439.8	451.2	951	2057
498	8	515.4	534.2	554.7	2103	4397
518	9	641.5	663.5	684.0	2564	4955
2189	10	736.8	760.0	-	11440	0
				P	25504	27920

The two improvement scenarios of the ORC-unit translate to an increase of turnover between 25504e and 27920e per year.

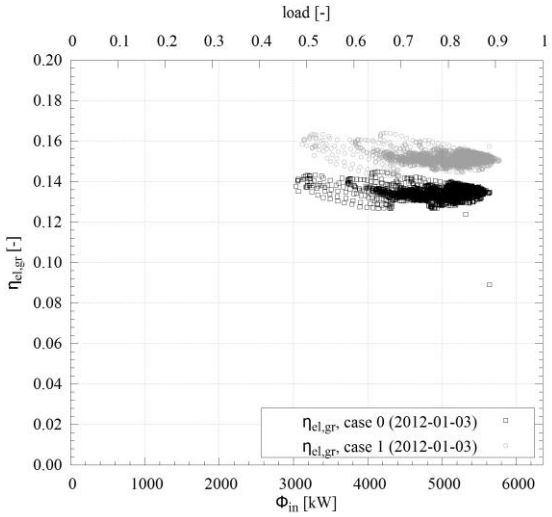

Figure 8.21: electric gross efficiency, optimized recuperator vs. base case

8.1.4 Optimized pressure drop in recuperator

Based on the results of the steady-state analysis the dynamic model of the cycle was tested with a reduced flow friction loss on the vapour side of the recuperator. This calculation was done in order to prove the necessity of redesigning the tube array. Instead of 28000Pa the nominal pressure drop parameter was to 10000Pa. The new value was estimated based on the planned layout for the hot side of the recuperator. This reduction seems immense, but it is realistic. The following Figure 8.21 gives an impression on the potential of this modification. As the results of the new cycle configuration in section 7.7.2 show, the simulation results are realistic.

8.1.5 Characteristic map of turbine

The turbine map in Figure 8.22 depicts the results of nine simulation runs. For three fixed vapour temperatures three different drain pressure levels each have been applied on the model. The influence of the temperature is very low. Under high temperatures the density of the vapour is lower whereas the specific volume rises and causes higher vapour velocities. However, the main influence is the pressure ratio. A difference of 50mbar of drain pressure translates to roughly 50kW of mechanical power output.

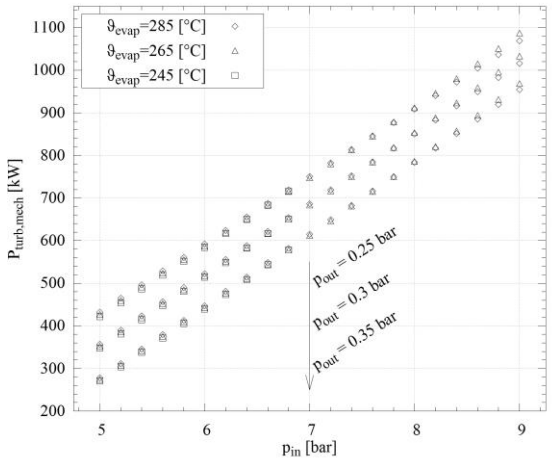

Figure 8.22: influence of various pressure conditions on the turbine model

8.1.6 Empirical cycle model

For most questions during the every day operation of an ORC the sub-systems of the cycle may not be relevant. In order to receive straightforward results for economic questions the use of an empirical model may be sufficient. For instance, in this case study the damage on the recuperator heat exchange array caused a stand still for almost two month. The power plant has an insurance contract covering losses in grid feed-in if the malfunction is an act of nature beyond control. The insurance company demands a prognosis about the quantity of the financial loss. This task can be solved with acceptable effort by using an empirical model as the one introduced in Chapter 5. By knowing the set-point temperature and set-point mass flow of the thermal oil system and the thermal demand in the district heating network the electrical generation can be predicted. The following Figure depict different load situation and compare the measured values with the simulated results.

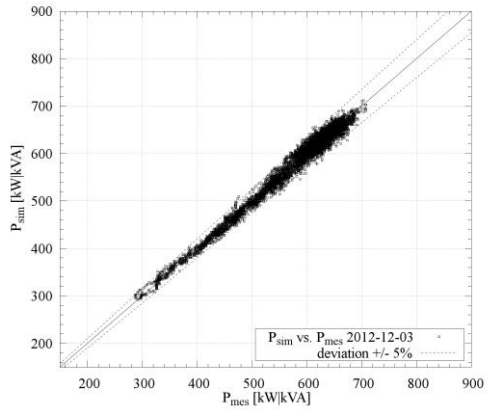

Figure 8.23: electric output of empirical cycle model vs. measured grid feed-in (2012-12-03)

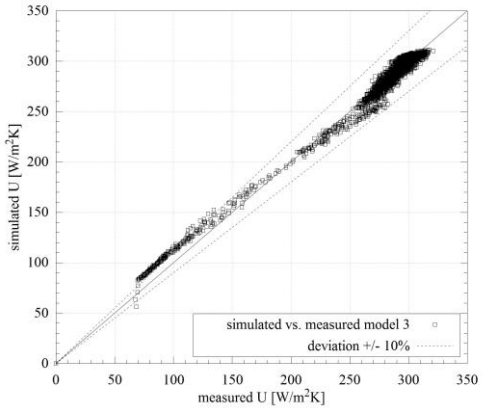

Figure 8.24: electric output of empirical cycle model and measured grid feed-in vs. time (2012-12-03)

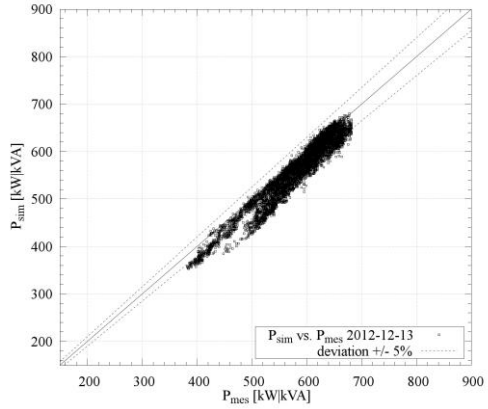

Figure 8.25: electric output of empirical cycle model vs. measured grid feed-in (2013-12-13)

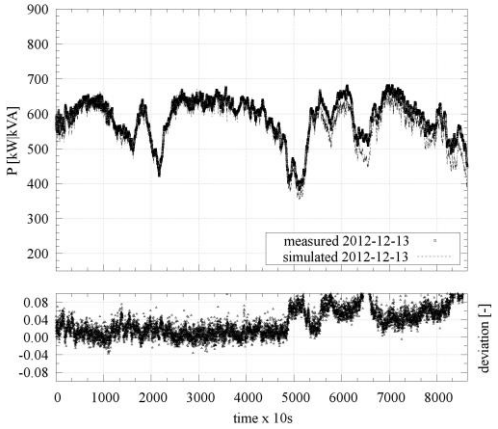

Figure 8.26: electric output of empirical cycle model and measured grid feed-in vs. time (2013-12-13)

8.2 Design improvements

This section concludes the modifications and improvements on the system that have been during this work.

8.2.1 Replacement of recuperator tube bundle

After several unsuccessful attempts to repair the recuperator tube bundle the heat exchanger was redesigned. The most relevant issues and the according changes on the system were:

- The inlet temperature of the vapour going to the condenser was too high. As the condenser, in a heat-led system, limits the condensible mass flow of MDM the optimal way to operate the apparatus is setting the focus on the transfer of latent heat. In practice this is not entirely possible, therefore there is always a de-super-heating and a sub-cooling process included. However, heat recovered from the recuperator has not to be cooled in the condenser. As a consequence the heat transfer has to increase, more heat transfer surface is necessary. The new version of the heat bundle has a gross heat transfer surface of 5800m^2.

- The flow friction losses across the hot side of the recuperator were enormous. This reduces the pressure potential across the turbine. Usually the friction correlates linearly with the heat transfer surface. In this case, despite the surface has been increased, the nominal friction loss could be reduced to 100mbar. This was achieved by changing the flow configuration. In the old configuration the vapour was deflected seven times on the hot side. With the new flow configuration the vapours direction is not changed until it enters the duct to the condenser.

- In the old recuperator the vapour entered with high velocity from the turbine and was deflected by a transverse sheet in order to avoid damage on the finning of the tubes. In the new version this sheet was spared. Unfortunately, the first rows of tubes have been damaged by the impact of the vapour. As a consequence the fins on the first four rows of tubes have been removed. Since then the recuperator is working reliably.

- Increasing the heat transfer capability of the recuperator to a point were the saturation point is reached lead to a loss of active mass flow in the system. The condensate precipitates and collects in the bottom of the vessel. Three counter-measures are available. Implementation of a three-way valve on the cold side in order to adjust the mass flow and the temperature difference. A pump to remove the condensate from the recuperator. Place the recuperator higher than the condenser, so the condensate can drain off to on its own. The last option seems appealing, but in case of fluid degradation the high-boilers cannot be separated from the system. In the case at hands the measure one and two have been combined. By doing so

the heat transfer coefficient of the recuperator is variable and in case of fouling or fin erosion it can be adjusted later on.

- As already mentioned in the above point, a drain with a pump has been connected to the bottom of the vessel. This solves two problems: Precipitating fluid can be separated from the cycle in order to purify. If cycle fluid collects after a shut-down it can be fed back into cycle. This method is more reliable, less process disturbing and time saving than the re-evaporation with the heating loop.

8.2.2 Optimisation of vacuum system

The following Figure 8.27 depicts the cycle including the design and routing changes. A larger version of this drawing can be found in the Appendix A(A). In comparison to the original layout the following items have been changed or added:

- The vacuum system does no longer release the working fluid exhaust to the atmosphere. The fluid including low-boilers are collected in an external vessel.
- Besides the primary vacuum pump a secondary pump has been added. It can be used for deep-vacuuming or evaporation of the low-boilers from the external reservoir.
- The recuperator bottom is connected to a pump. Working fluid with highboiler contaminants can be fed to a distiller unit.

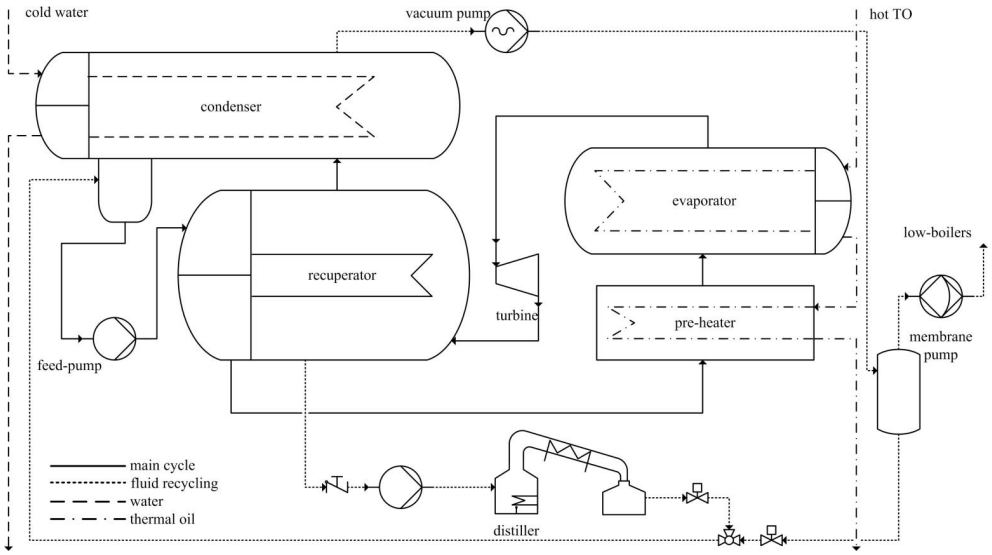

Figure 8.27: cycle layout including design changes/improvements

8.2.3 Sink side optimisation

The following sketch (Figure 8.28) shows the modifications on the excess cooler system. Besides the enlargement of the cooler heat exchanger a control has been implemented that delivers hot water to the cooler in low-flow. In this stand-by mode the fans are off. If the cooler is requested by the main control the pump mass flow is increased over a soft ramp until it reaches the set-point.

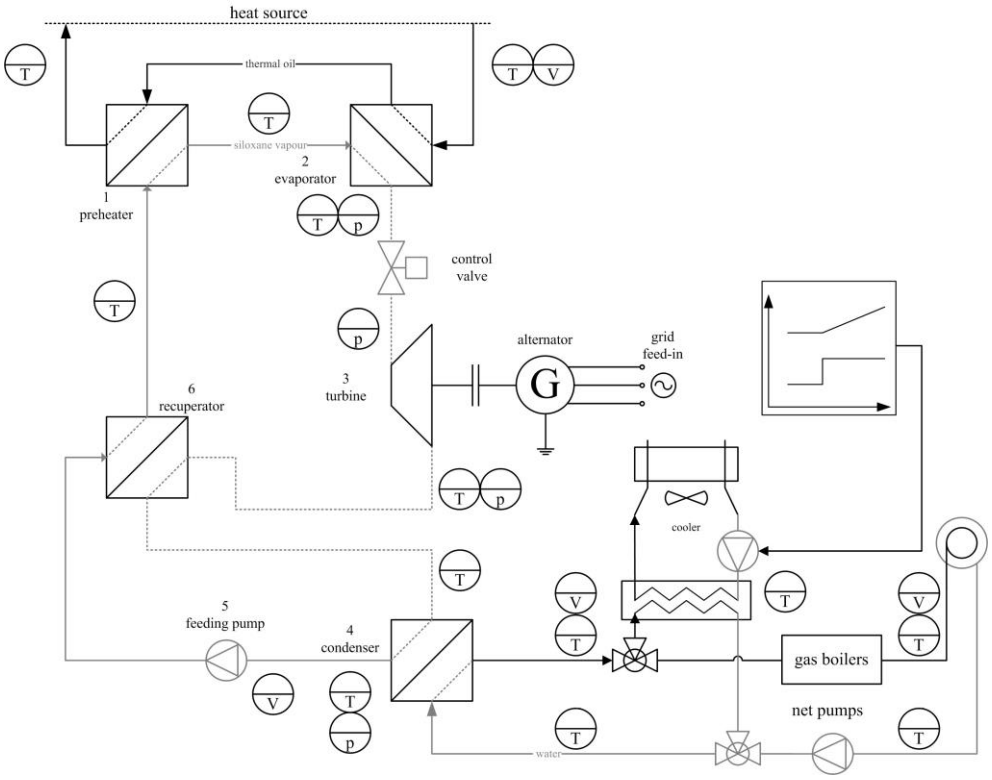

Figure 8.28: design changes in sink side and excess cooler

8.2.4 Fluid recycling

From the operational experiences and the simulation results one conclusion has to be drawn: the fluid quality is a key parameter for the optimisation of the cycle efficiency. All thermodynamic and mechanical improvements have only a little potential if the assumptions they are based on, a pure fluid, is not given. The replacement of an entire cycle filling is enormously costly, time consuming and the system is off the grid for several days. As a fluid renewal was not an option, tests with fluid recycling have been undertaken. Fluid is taken from three different sources in the cycle: from the vacuum system, the bottom of the recuperator and the pre-heater. The later one can only be drained if the system is on halt. Two samples of fluid have been distilled under laboratory conditions with a distilling apparatus. The following Figures 8.29 and 8.30 show the distilling processes of the two samples.

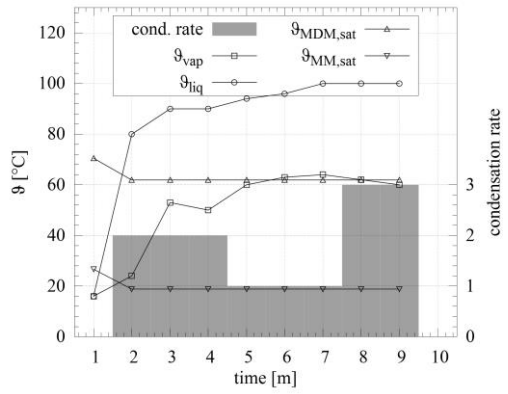

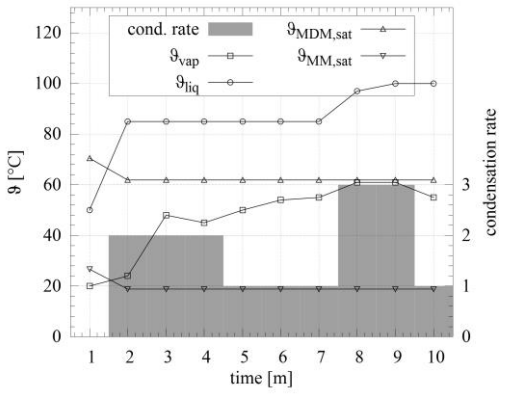

Figure 8.29: distilling of fluid sample Figure 8.30: distilling of fluid sample from vacuum pump reservoir from recuperator

Sample number one, with a start volume of 0.250l and a weight of 0.1981kg was evaporated under a pressure of 40mbar while the liquid reservoir was heated up to 100 °C. During the process two condensation mass flow peaks have been observed. Between the two peaks the collecting flask has been switched. In the second reservoir MDM with a purity of 95.2% collects (Table 8.3). The first flask MM and low-boilers accumulate. In total 0.134l of MDM could be recycled from this sample, which is a ratio if 53.8%.

Table 8.3: HS-GC-MS analysis of experiment 1, product 2

compound	abbr.	CAS	mass fraction
-	-	-	[%]
Octamethyltrisiloxane	L3 / MDM	107-51-7	95.2
Hexamethyldisiloxane	L2 / MM	107-46-0	0.883
Hexamethylcyclotrisiloxane	D3	107-52-8	0.546
Octamethylcyclotetrasiloxane	D4	556-67-2	2.4
Decamethyltetrasiloxane	L4 / MD2M	141-62-8	0.995
Decamethylcyclopentasiloxane	D5	541-02-6	0.006
Dodecanethylpentasiloxane	L5 / MD3M	141-63-9	0.018
Trimethylsilanol	MOH	1066-40-6	-
other Siloxanes	-	-	-
Petroleum	-	-	19.91

The second sample with 0.223l and a weight of 0.1745kg was processed with the same procedure. MDM with a volume of 0.14l could be recovered from this sample (64.3%). Detailed composition of the distilling product is listed in Table 8.4.

Table 8.4: HS-GC-MS analysis of experiment 2, product 2

compound	abbr.	CAS	mass fraction
-	-	-	[%]
Octamethyltrisiloxane	L3 / MDM	107-51-7	96.7
Hexamethyldisiloxane	L2 / MM	107-46-0	0.156
Hexamethylcyclotrisiloxane	D3	107-52-8	0.397
Octamethylcyclotetrasiloxane	D4	556-67-2	2.14
Decamethyltetrasiloxane	L4 / MD2M	141-62-8	0.553
Decamethylcyclopentasiloxane	D5	541-02-6	0.019
Dodecanethylpentasiloxane	L5 / MD3M	141-63-9	0.009
Trimethylsilanol	MOH	1066-40-6	-
other Siloxanes	-	-	-

After testing the distilling process under laboratory conditions a larger apparatus was designed to conduct the distilling procedure on site. The educt for the experiment was a working fluid mixture containing about 10% of lubricant, and another 10% of others siloxanes. A photography of the set up is depicted in Figure 8.31. As heat source the exhaust duct of the multi-cyclone was chosen (2). On top of the duct a container with 200l of old working fluid was placed (1). The container has been attached to a distiller (3), cooled with tap water (15 °C).

Figure 8.31: large-scale distilling apparatus prototype

The results of the experiments were MDM purities between 95% and 99%. This led to the decision to construct a stand alone distilling apparatus that can be connected to the ORC in order to recycle the fluid via a batch process.

8.2.5 Quantification of design improvements

After implementing all design optimisation measures the new version of the cycle has been tested. Figure 8.32 shows the electric power output of the cycle versus the thermal oil heat input. The maximum power output reached 940kVA, a new record compared to the monitoring results of the observed years before.

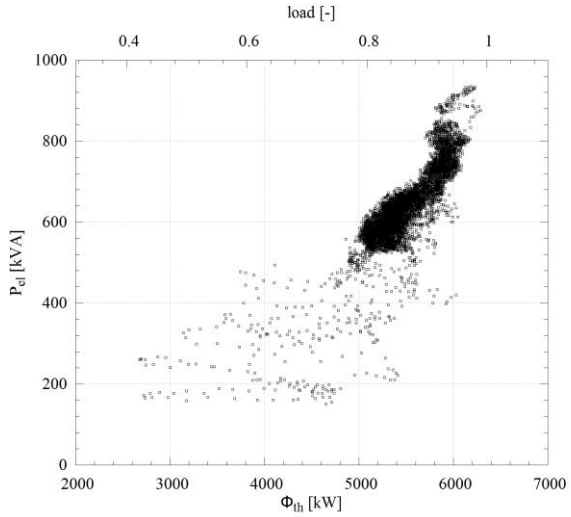

Figure 8.32: electric output vs. source heat input (10 seconds / 2014-12-27)

The results of this test run demonstrate that the redesign measures and improvements are effective. Furthermore, the validity of the model predictions both for the steady-state model as well as for the dynamic model is proved.

Chapter 9

Discussion of results - final conclusions

In the course of this thesis a large-scale biomass fuelled, heat-led ORC-power plant has been theoretically and practically examined. Based on a long-term monitoring, component models and correlations for heat and mass transfer processes have been developed. Furthermore, steady-state and dynamic cycle models have been developed. Parametric model studies serve as basis for the improvement of the system, technically and economically. Besides the theoretical modelling, the operational experience is reported as well. The collected experience on Siloxane working fluids and ORC cycle components result in recommendations for working fluid management and design improvements.

9.1 Model results

9.1.1 Alternator and drive train

The alternator model proposed in this work is simple and robust. As the frequency control of the unit is comparably fast, and the deviation of the rotation is less than ±0.5% its influence on the cycle can be neglected. Under medium and full load the electric efficiency remains stable within a range of 96% and 97% (see Table 5.22). In load states under 25% there is no efficiency information available for this unit. Due to the fact that many power plant types are not run in such low load states this is usually not relevant. For the investigated system the situation is different. The fact that the alternators nominal power was chosen too high worsens the situation. For instance, the cycle is run at 40% of its nominal power. This correlates to roughly 395kW of mechanical power in the drive train. Taking this value as mechanical input for the alternator, its load is below 25% and thus in a range where we have no information from the manufacturer about the electric efficiency. However, the lower load range was fitted from data retrieved from the electric grid feed-in, which can be assumed as very accurate and a reverse

calculation from the measured turbine states. One has to consider this limited accuracy of the alternator model when using it in low load ranges. For wide load ranges a detailed look into the current depending copper losses may be necessary. For applications with variable speed expanders, the alternator model becomes more complex. In such a case the type of frequency control of the generator has to be taken into consideration as well. Furthermore, the speed depending losses have to be observed. The mechanical friction with its constant, linear and quadratic compounds necessitates a correlation for the typical rotation frequency spectrum of the unit. The core losses in an synchronous unit remain constant, alternating frequencies in an asynchronous unit cause varying core losses. The drive train model at hand is suitable and prepared for fluctuating rotational frequencies, as shown in the validation of the dynamic turbine model.

9.1.2 Turbine model

Three different evolutionary stages of turbine models have been used in this work: The original approach of Cooke with the recommended expansion exponent (κ = 2), an average exponent for this fluid type (κ^- = 1.93) and a variable exponent calculated within each time step. All three variants predict fairly good within a range of less than ±5%. The κ^--model has the lowest scatter range (-1.14% and +1.4%) for single time steps. Nevertheless, the variable κ-approach with its larger but more symmetric dispersion (-2.95% and +2.75%) predicts better in terms of the electric yield. The prediction quality of the turbine model is the cornerstone to the validity of the cycle model and all efficiency calculations. A very critical point of the turbine model is the outlet pressure and temperature measurement. The data acquisition results have revealed the problems that come with low pressures and high flow velocities. The wake turbulence in a turbine outlet has to be taken into account as well. Taking a look at the whole picture, the turbine's outlet temperature sensor is surely not reliable. There are three reasons for that problem: The flow configuration in the original recuperator (V1) was somewhat complicated
(for instance use of the deflector sheet). Furthermore, the usage of the condensate evaporation loop at the bottom of the recuperator vessel means an uncertainty in heat input to the aggregate of 200kW. The rupture of the u-tubes in 2013 caused a deviation in vapour temperature and fluctuations in the pressure measurement.

9.1.3 Pre-heater model

The steady-state validation of the pre-heater model show a fair correlation within boundaries of ±5%. Taking a look a the correlation quality of the dynamic component model of the pre-heater, even better results can be expected. With a nodal model of only two nodes the entire calculation correlates within a range of ±0.5%. This proves that the modelling strategy was appropriate for this case.

9.1.4 Piping models

The straightforward approach of the piping models delivers good results. In comparison to the tubes in the heat exchangers the boundary layer influence is negligible. Therefore the simple quadratic approach with a mass flow correlation is sufficient. However, the influence of the thermal inertia stored in the volumes of the pipes is not respected. As the long connections, such as the route from evaporator to turbine contain 2% to 3% of the total fluid mass and the temperature drop in the connections is negligible, this assumption is valid. Furthermore, the time residence time at nominal states are all shorter than the minimum time step of 10 seconds the implementation of the runtime offset is not necessary.

9.1.5 Evaporator model

The comparison of the various pool boiling correlation in literature has shown that evaporation of siloxanes in a kettle-type tube evaporator cannot be solved without significant adaptations. While the most correlations delivered a good trend the offsets are enormous. Therefore, a new correlation for this specific case has been developed. Finally a correlation based on was chosen with the basic structure of Gorenflo's approach using the pressure correlation function of Mostinski. The prediction quality, with a range of ±8%, is fairly good for a boiling correlation.

9.1.6 Recuperator model

In terms of simulation the liquid side of the recuperator the calculation of the turbulent pipe flow is rather straightforward. As the liquid sides convective heat transfer is several magnitudes larger than the vapour side's heat transfer, errors do not have drastic consequences. During the simulation the model crashed when

the Reynolds numbers entered the regime of transition. This happens if the pipe flow calculation contains a case selection, for instance. A smoothed pipe flow calculation as Romeos approach for all turbulent regimes, the use of the explicit Churchill Usagi equation or the implicit Colebrook equation for all regimes can help here. The proposed model for the unit correlates within a range of ±5% in the relevant U-value range of 200W/m²K to 325W/m²K. The deviation for lower U-values can exceed 10%, but it is only relevant during start-ups.

9.1.7 Long term yield prediction

In many cases the forecast on electricity production is very valuable for operators of co-generation power plants. For a custom design the final efficiency characteristic under real operating conditions can be only estimated. After the commissioning period such a prediction model can be set-up and validated with first monitored data. The empirical approach developed in Chapter 5 may be a brief and robust pattern for this case. The usage of the model requires only a very limited amount of parameters and variables and delivers fair result. As long as the cycle configuration or the fluid quality and filling does not change the model predicts well within a range of ±5%.

9.1.8 Steady-state analyses

The calculation results of the case studies in Section 8.1.1.1 have result in the following conclusions:

- The reduction of super-heating enables the operator to run the cycle at lower load states with higher electric gross efficiencies.
- The highest efficiencies and electric outputs can be achieved if the flow frictions in the low pressure section of the cycle are reduced to a minimum.
- The reduction of friction losses on the high-pressure side of the cycle mainly leads to savings in feed pump power.
- Lower pressures in the condenser can improve the cycle characteristic slightly under low loads. Compared to the optimisation potential of the recuperators hot side, the condenser plays a minor role.

Based on the above points the dynamic model case studies have been conducted.

9.2 Design and operation recommendations

9.2.1 Pre-heater

The plate heat exchanger being used as pre-heating unit in this cycle, can be characterize as a very compact unit. Regarding the point of void masses in the cycle this concept is surely very effective. However, the monitoring results show that the heat transfer performance of the system stays clearly below the design values. Certainly this is mainly a consequence of fouling effects. During the fire incident in 2009 the thermal oil system was heavily contaminated with slag and char coal. These residues were a result of the contact with oxygen of the ambient and the combustion process of the thermal oil. Taking a look at the design concept of the pre-heater, the fully welded stacks of plates turn in this situation into a disadvantage. Not being able to disassemble the heat exchanger plates (or at least not without great effort the unit) makes it difficult to flush or clean the system. Instead of a revision of the heat transfer bundle a complete exchange has to be done. The surrounding vessel could remain and be reused in order to minimize the refurbishment costs. Taking a look at the flow pattern, the deflection between the two plate stacks leads to a precipitation of slag at the bottom of the vessel. If the general concept with two stacks is a necessity the deflection zone should be kept clean. This could be achieved by rotating the entire pre-heater in the longitudinal axis by 45 to 90 degrees. By doing so the coking residues are decelerated and collect still in the bottom of the vessel. As a consequence, the main flow path would free of residues. A disadvantage of the arrangement is the more complex piping geometry, less compactness and a potential accumulation of vapour in the top of the vessel. Another potential solution could be the a non-coaxial design where the deflection zone is enlarged. A general issue concerning plate heat exchangers and organic fluids has to be mentioned at this point. As the results of the fluid quality tests in Chapter 7 show, a certain proportion of impurities appears over time. If the contaminants are high-boilers they slightly decrease the heat transfer. This is unpleasant but not serious as heat exchangers are designed with allowance. In case of low-boilers in the main fluid, a sudden evaporation may occur in the pre-heater. The effective heat transfer area is significantly decreased to an extend where the design allowance can not compensate. In some cases vapour can cumulate in the vessel. In the worst case scenario the constant occurrence of low-boiler vapour bubbles may damage the plate stack. Vapour induced vibrations can lead to failure of the stack welds. This

has been observed in this case study at the very beginning of the monitoring period (see in Chapter 1).

9.2.2 Recuperator

As the largest heat exchanger in the entire system, that recovers almost two thirds of the heat being led though the cycle, a special focus has to be set upon. With the largest heat transfer surface the system as well is the heaviest and most expensive part in the cycle. The first version of the recuperator, the original design, had some design point that have to be regarded as disadvantageous:

- In order to pack as many tube tiers as possible into the vessel a the tubes have been arranged in a square. Consequently, a square shaped gasket, was necessary. It was not possible to machine the flange surfaces in a way that the smoothness was suitable for a gasket. After every reassembly of the unit multiple pressure tests had to be done. Often the gasket had to be repaired.

- The flow arrangement of the tube tiers was complicated and the multiple shock losses in the recuperator head were disadvantageous.

- In order to reduce the tube mass surface enhancements, in this case baffles were used. In theory this lead to an enlargement of the outer heat transfer surface. By doing so, the disadvantages of gaseous to liquid heat transfer can be partially compensated. However, putting this into practice, a few mistakes were made: the crimping of the baffles turned out to be too weak for the tensile and thermal stresses in the unit. As a consequence, the fins were loose enough to be disarranged by the gas flow along the tube.

- A further weak point in the design is the floating bearing of the tube bundle. Dynamic loads as well as thermal expansion cause severe expansions in the length of the u-tubes. Therefore, the bending part has to be settled on a sliding bearing. In this case the tubes were seated in bore holes. Over the last years of operation this led to abrasion at the tubes and finally ended with massive leaking.

- In cases of a shut down, the recuperator shell collects a large amount of liquid MDM (up to 600l). In the original design two u-tubes have been mounted in the bottom of the recuperator. During the heat-up phase of the cycle this heating coil is used to evaporate liquid residues. As a consequence

of the leakage in the bundle tubes, a spray of liquid MDM in a temperature range of 80 °C to 180 °C has released to the vapour volume. As far as this is not evaporated by the constant with the hot gas stream it drops down and fills up the bottom of the vessel. Since the discovery of the leak, the heating coil has been used constantly. To avoid such a constellation the void volume of the recuperator has to be kept as small as possible. By arranging the tiers in such a way that the hot side of the liquid is passing through the bottom the extra heating loop is not necessary. Another possibility is a drain connection to the vacuum system. The liquid residues can be sucked from the bottom where it accumulates and further be cooled by the vacuum condenser.

- If the bottom of the recuperator is used as a reservoir to collect high-boilers, the influence of the liquid mass should be considered. The operational experience of this case study has shown, that a rising level of liquid tends to resonate during operation. The turbines outlet stream implies a force on the liquid. This causes an oscillation of the entire liquid mass (waves) and a recurring noise and fluctuating pressures in the turbine outlet and the condenser. In order to avoid this effect a permeable deflector sheet can be mounted in the bottom (horizontal chord) of the vessel.

9.2.3 Evaporator

In order to optimize the evaporators work in the cycle two main objectives have to be put into practice. The filling level has to be adjusted accordingly to the original layout of the tube array and the thermal input to the device has to be controllable. The thermal oil valve's range in the system at hand is solely used in start-up procedures. Therefore, the opportunity to regulate the thermal input to the system is not used.

The results (Chapter 8) show that an operational mode with a low super-heating rate lead to higher thermal efficiencies. On the one hand, side this means a reduction of fuel in the furnace including all consequences. The fuel mass flow is reduced which leads to a decrease of wear on the transport systems and heat exchangers. On the other hand this strategy lowers the risk of hot spots in the ORC-system. This leads to a longer lifespan of the cycle fluid. Economically speaking this is a win-win(-win) situation. The electric efficiency improves by 1%-point almost across the whole load range. The surplus during an average year

amounts up to 28000e. Furthermore, the reduced working fluid decomposition reduces cost for replacement of the fluid. In order to use that potential, a reliable evaporator level measuring system has to be applied. A challenge has to be taken up here by installing a reliable level gauge. Based on the operational experiences of this case study, turning flap displays are not entirely sufficient. In cases when low-boilers are contained in the main working fluid the buoyancy forces of the liquid are no longer strong enough to function in a reliable way. In the design of such a cycle this fact has to be respected.

9.2.4 Condenser

The existing condenser of the system is working reliably. If the working fluid is not contaminated and the vacuuming process has been completed successfully, the pressure level is near to the ideal saturation pressure. In order to receive a maximum of pressure difference across the turbine the heat transfer and the pressure loss of the recuperator have to be optimised.

9.2.5 Vacuum system

During the observation period of this thesis, the vacuum system of the cycle has been optimised. Originally, the system was equipped with one claw pump that was operated in clocked mode (10/60 seconds). The pump turned out be not able to provide the vacuum without running it constantly. The achieved pressure level was too high. Therefore, a second pump (membrane pump) has been installed. The original unit provides the vacuum during standard operation, whereas the second pump is used after shut-downs.

Figure 9.1: primary vacuum pump (claw-type) and droplet trap

Figure 9.2: condensate reservoir of vacuum system, membrane pump

The above Figures 9.1 and 9.2 depict the latest development stage of the vacuum system. With an increasing demand for vacuuming the amount of fluid taken from the cycle rises. In the original design the exhaust was released to the ambient. Besides the environmental aspects, this leads to a constant loss of working fluid. On the one hand the costly fluid has to be replaced, on the other hand the filling level of the cycle suffers. By using the condensation trap this loss can be reduced to a minimum. During one batch process cycle the container (1) is filled up working fluid to a volume 200l. In the next step, low-boilers and inert gas residues are removed by deep-vacuuming with the membrane pump (2). The cleaned fluid, MDM of high purity, is fed back to the cycle.

9.2.6 Monitoring

Based on the monitoring system of the case study at hands the following measures are proposed to improve the analysing capabilities.

- A ring line connecting radial pressure taps at the exit section of the turbine can eliminate dynamic pressure components.

- The evaporator filling level should be monitored with an electronic indicator that is implemented in the OPC-server or main control. This would ease the fluid management significantly.
- In order to detect a leakage in the recuperator a pressure sensor after the feed pump and prior to the pre-heater could be installed.

9.2.7 Lubrication system

Using a closed turbine and gear lubrication system leads inevitably to the challenge of keeping the working fluid and the lubricant separated. As the operational experiences of this case study show, this task is not trivial. It is state of the art that lubrication systems are monitored by displacement sensors and temperature sensors. However, this covers only the observation of long-term wear. Especially changing load situations or emergency shut-downs are not covered in such a monitoring. In order to keep the system design lean, the original lubrication pump was a directly driven unit. A reliably lubrication could only be maintained during the synchronised grid operation. The need for long start-up procedures, evacuation procedures was not respected in that design. To assure a steady flow and thus a stable temperature an additional electrically driven lubrication pump has been installed. It is connected to the emergency grid and thus protects the turbine from bottoming out during a shut-down in the event of a grid failure. The above measures made the turbine operation saver and more reliable. However, a steady loss of lubricant into the working fluid cannot be avoided. Therefore, further strategies have to be applied in terms of fluid management and recycling (see Section 9.2.9 and 7.6.2).

9.2.8 Control systems

The influence of the level control is very limited. This is due to the fact that the reservoirs total capacity of 160l and its volatile capacity of 150l is almost negligible in comparison to the overall design capacity of 6000l (2.5%). In terms of energy the volatile volume equals 27MJ, which is the cumulated condenser transfer energy of a little less than 6seconds. This time period symbolizes the dilemma which has to be solved for such a cycle. Taking a look at the monitored data for the heat rejection cycle and the district heating in Chapter 7.3, one can see two external disturbance variables the cycle control has to react to. The

district heating loop with its enormous water mass, the according travel time and a broad statistical distribution for the heat demand is a very good-natured sub-system. However, the heat rejection cycle has a comparably low capacity and a quick response time. While the original purpose of the heat rejection system would be the stabilisation of the system under partial load, it leads pretty much to the opposite. The implementation of the ORC into a short cut loop leads to a quick excitation when a temperature slope is opposed on the system. In the original configuration with 2.6MW_{th} of cooling power and a quick start control the excitation could be observed in transitional seasons. The unsteady operation of the cycle was one of the prior problems at that time. In 2012 the excess cooling system has been enlarged to a nominal cooling power of 3.9MW_{th}. Furthermore the pumps have been retrofitted with frequency converters. The following changes have been made on the control system:

- The frequency converters where triggered by a separated PID-controller located in the control unit of the district heating.
- During phases where the heat rejection system is not being used a sleep mode was implemented. The fan arrays of the coolers are switched of, while the circulation pumps are running at minimum load. Two effects ensue from that measure: The cycle water is no longer divided into two different temperature “plugs”, one with ambient temperature, one with the room temperature; The smooth start-up procedure of the PID-controller is supported.
- A third point: temperature signal of the district heating and the heat rejection system are set so the same sensor. This avoids hysteresis at the threshold of two different operational modes.

On the hot source side the current control system solely delivers a maximum feed temperature to the ORC and regulates the mass flow according to the return set point (set to 240 °C). During periods when the demands from the district heating network is less than 5MW the feeding temperature as well as the return temperature of the thermal oil can be reduced. By doing so, the cycle starts at a lower load range and has a better electric efficiency in that range. Economically speaking, the biomass driven period can be enlarged, the chance for excess cooling at low loads reduced. This adaptation could be done automatically by using the vapour temperature and pressure to calculated the super-heating rate,

which is then used as input for the thermal oil valve control. The calculation of the super-heating has been implemented during this work. The plant operator can carefully adjust the temperature set points and obtains a visual feed-back from the control panel.

9.2.9 Cycle fluid replacement and recycling

In the year 2013 the bad performance of the cycle required action. After the working fluid analyses there were two options: replace the entire filling, or attempt to recycle the remaining fluid and replace the remaining difference. The second option was tested successfully. It saved more than 70000e of re-investment. Laboratory distilling tests have shown MDM recovery rates of more than 50% for fluid samples from different locations in the cycle (vacuum pump, recuperator, pre-heater). Based on these experiences an external fluid recycling unit will be built in the future. The expected recycling costs with the new system are less than 10e per litre. Besides the cost reduction, the recycling process will be possible during operation, which increases the electric efficiency and reduces the necessary down-times.

9.3 Further research

This work contributes some results and information of theoretical and practical nature to the complex field of biomass ORCs. However, some major questions have been revealed in this work, that cannot be answered. The entire process of working fluid composition is rarely discussed in literature. There a some authors, mainly in the field of chemistry and material science, that have proved decomposition of Poly-siloxanes. Nevertheless, the interaction with the conditions inside a cycle have not been observed in detail. The following points would be of interest:

- It is known that a certain degree of decomposition appears over time with rising temperatures. However, the interaction of multiple factors has, to the knowledge of the author, never been observed.
- As far as it concerns the investigated case study, a coincidence of lubrication leakages and working fluid decomposition can be drawn. A detailed

observation of this reaction complex could quantify this influence in order to give designers the possibility to avoid such events.

- From the available information it is not possible to estimate the effect of heat exchanger and piping material on the decomposition. Comparisons of cycles with different steel and aluminium alloys could deepen that knowledge.

- Long-term experiences with a fluid recycling system can very valuable for the economy of power plants. The operator of the plant can increase his own gain of value by including the recycling process into the facility. A dependency on fluctuating market prices for working fluid and external contractors can be avoided in that way. Nevertheless, this necessitates skilled personnel and a detailed quality management.

- The boiling model used in this work is empirically based. In order to enhance the possibilities of a evaporation model a physical modelling theory is necessary. Up to now such a physically based theory does not exist. Especially for frequently used apparatus types, such as the kettle type, this could be of great interest.

The End

Bibliography

[1] T. Schafgans. Picture taken by Theo Schafgans, 1888. xxv, 3

[2] Clausius Rudolf. Rudolf Clausius. *Zeitschrift f. Phys. Chemie*, 21, 1896. xxv, 3

[3] Turboden Srl. Company webpage. Technical report, Turboden Srl, Italy, Brescia Italy, 2012. xxv, 14

[4] maxxtec AG. Interview. Technical report, maxxtec AG, 2010.

[5] Koehler & Ziegler. Interview. Technical report, Koehler & Ziegler, 2012. xxv, 14

[6] Pratt & Whitney. Interview. Technical report, Pratt & Whitney, 2012. xxv, 14

[7] U. Eicker, editor. *POLYCITY - Energy Networks in Sustainable Cities*. Karl Kr¨amer Verlag, 2012. xxvi, 47, 48

[8] G. Gappmaier. UA OPC software stack. http://commons.wikimedia.org/wiki/ File:Uastack.png, 2006. xxvi, 73

[9] Ya Song Wei and Richard J. Sadus. Equations of State for the calculation of fluid-phase equilibria. *AIChE Journal*, 46(1), 2000. xxvii, 99, 100, 104

[10] K.J. ˚Astro¨m and T. Ha¨gglund. *PID controllers: Theory, design, and tuning*. Instrument Society of America, 2nd edition, 1995. xxviii, 168, 169

[11] Tobias G. Erhart. Analyse von biogen befeuerten ORC-Anlagen mit Hilfe von Computersimulationsmodellen. Master's thesis, Ulm, Stuttgart, Rottenburg a.N. University of Applied Sciences, 2006. 1

[12] VDI. DIN EN 15603 energy performance of buildings: Overarching standard
EPBD; German version 2013, 2013. 1

[13] ORC Power Systems Committee of the ASME IGTI. Knowledge Center Organic Rankine Cycle, 2013. 5

[14] I. Obernberger. Biomasse-Kraft-W¨arem-Kopplungen auf Basis des ORCProzesses - EU-Thermie-Projekt admont (a). Technical report, VDI Bericht, Nr.1588, 2001. 5

[15] I. Obernberger, Thonhofer, and Reisenhofer. Description and evaluation of the new 1000 kW_{el} Organic Rankine Cycle process integrated in the biomass CHP plant in Lienz, Austria. *Euroheat & Power*, 10:1–17, 2002. 16

[16] I. Obernberger, A. Hammerschmid, and R. Bini. Thermische Nutzung von fester Biomasse. VDI-Berichte Nr. 1588 1588, VDI, 2001. 5

[17] Bundesministerium der Justiz und fu¨r Verbraucherschutz. Gesetz fu¨r den Vorrang Erneuerbarer Energien (Erneuerbare-Energien-Gesetz - EEG), July 21 2004. 6

[18] Bundesministerium der Justiz. Gesetz fu¨r den Vorrang Erneuerbarer Energien (Erneuerbare-Energien-Gesetz - EEG), 2012. 7

[19] Bundesministerium der Justiz und fu¨r Verbraucherschutz. Gesetz fu¨r den Vorrang Erneuerbarer Energien (Erneuerbare-Energien-Gesetz - EEG), August 2014. 6

[20] Bundesverband der Energie-und Wasserwirtschaft e.V. BruttoStromerzeugung nach Energietr¨agern 2012, 2012. http://www.bdew.de. 6

[21] Ingrid Saavedra, Bruno Joan Carles, and Coronas Alberto. Thermodynamic optimisation of Organic Rankine Cycles at serveral condensing temperatures:
Case study of waste heat recovery in a natural gas compressor station. *Journal of Power and Energy 2010*, 224:917–930, 2010. 9

[22] B. Vanslambrouck, S. Guseva, T. Erhart, M. De Paepe, and M. van den Broek. Waste heat recovery via Organic Rankine Cycle: Results of a
ERA-SME technology transfer project. In *International ASME-ORC Power Systems Seminar 2013*, 10 2013.

[23] H. Legmann. Recovery of industrial heat in the cement industry by means of the ORC-process. In *Proc. IEEE-IAS/PCA 44th Cement Industry Technical*

Conference, pages 29–35, 2002. 9

[24] Fachagentur Nachwachsende Rohstoffe e.V. Basisdaten Bioenergie Deutschland August 2012, 2012. 9, 31

[25] Florian Heberle and Dieter Bru¨ggemann. Exergy based fluid selection for a geothermal Organic Rankine Cycle for combined heat and power generation. *Applied Thermal Engineering*, 30:1326–1332, 2010. 11, 21

[26] Bahaa Saleh, Gerald Koglbauer, Martin Wendland, and Johann Fischer. Working fluids for low-temperature Organic Rankine Cycles. *Energy*, 32(7):1210–1221, 2007. 11, 21

[27] Ngoc Anh Lai, Martin Wendland, and Johann Fischer. Working fluids for high-temperature Organic Rankine Cycles. *Energy*, 36(1):199–211, 2011. 11, 21, 104

[28] P. Colonna and P. Silva. Dense gas thermodynamic properties of single and multicomponent fluids for fluid dynamics simulations. *J. Fluid Eng.-T. ASME*, 125(3):414–427, 2003. 11

[29] Michael Chys, Martijn van den Broek, Bruno Vanslambrouck, and Michel De Paepe. Potential of zeotropic mixtures as working fluids in Organic Rankine Cycles. *ENERGY*, 44(1):623–632, 2012. 11, 22

[30] Oyeniyi A. Oyewunmi, Aly I. Taleb, Andrew J. Haslam, and Christos N. Markides. An assessment of working-fluid mixtures using SAFT-VR MIE for use in Organic-Rancine-Cycle systems for waste-heat recovery. *Computational Thermal Sciences: An International Journal*, 6(4):301–316, 2014. 11, 23, 104

[31] Huijuan Chen, D. Yogi Goswami, Muhammad M. Rahman, and Elias K. Stefanakos. A supercritical Rankine Cycle using zeotropic mixture working fluids for the conversion of low-grade heat into power. *Energy*, 36(1):549–555, 2011. 11, 22

[32] Gioanfranco Angelino and C. Invernizzi. Cyclic Methylsiloxanes as working fluids for space power cycles. *Journal of Solar Energy Engineering*, 115(3):130–137, 1993. 11

[33] Stoll, Vrabec, and Hasse. Vorhersage thermophysikalischer Eigenschaften realer Fluide mit molekularen Modellen. In *DECHEMA-Konferenz*, 2003. 11

[34] M. Lampe, M. Stavrou, J. Gross, and A. Bardow. Integrated process and working fluid optimization for Organic Rankine cycle (orc) using PC-SAFT. In *ASME ORC 2013 - 2nd International Seminar on ORC Power Systems*, number 2 in 2, Delft, NL, October 2013. ASME. 11

[35] Wiesbaden Statistisches Bundesamt. Daten zur Energiepreisentwicklung Lange Reihen von Januar 2000 bis April 2013, 2013. 15

[36] I. Obernberger and F. Biedermann. Combustion and gasification of solid biomass for heat ans power production in europe - state of the art and relevant future developments. Technical report, BIOS Energiesysteme GmbH, Eindhoven University of Technology, 2005. 16

[37] N. Grassie and I.G. Macfarlane. The thermal degradation of Polysiloxanes, I. Poly(dimethylsiloxane). *European Polymer Journal*, 14(11):875–884, 1978. 16, 24

[38] Bru¨ggemann, Drescher, and Lang. Energetische Bewertung verschiedener Anlagenkonzepte fu¨r Biomassekraftwerke mit Organic-Rankine-Cycle (ORC). Technical report, Universita¨t Bayreuth, 2006. 16, 34

[39] J. Kaikko, J. Backman, L. Koskelainen, and J. Larjola. Technical and economic performance comparison between recuperated and non-recuperated variable-speed microturbines in combined heat and power generation. *Applied Thermal Engineering*, 27:2173–2180, 2007. 20

[40] Wenjun Zhou, Hui Yang, Xingzhong Guo, and Jingjuan Lu. Thermal degradation behaviors of some branched and linear Polysiloxanes. *Polymer Degradation and Stability*, 91(7):1471–1475, 2006. 22

[41] Dow Corning S.A. Safety datasheet: Dow Corning OS-20, 2013. 24, 25

[42] Solutia Inc. Therminol heat transfer fluids by Solutia: A selection guide (pub. no. 7239135f), 2010. 26, 107, 110

[43] Solutia Inc. Therminol information bulletin no.6 (pub. no. 7239686), 2001.

[44] Solutia Inc. Material safety data sheet: Therminol66 heat transfer fluid, 2006. 26, 107, 110

[45] J. Larjola. Electricity from waste heat using high-speed Organic Rankine Cycle (ORC). *International Journal of Production Economics*, 41:227–235, 1995. 28

[46] Vincent Lemort, Sylvain Quoilin, Cristian Cuevas, and Jean Lebrun. Testing and modeling a scroll expander integrated into an Organic Rankine Cycle. *Applied Thermal Engineering*, 29(14-15):3094–3102, 2009. 29, 34

[47] Bayerische Landesanstalt fu¨r Wald-und Forstwirtschaft. Merkblatt 12, 2011. 31

[48] Sylvain Quoilin. *Sustainable Energy Conversion Through the Use of Organic Rankine Cycles for Waste Heat Recovery and Solar Applications*. PhD thesis, University of Li`ege, 2011. 34, 146, 158

[49] Cornell University. Eureqa website, 2012. 39

[50] VDI. Din v 18599: Energy efficiency of buildings ? calculation of the net, final and primary energy demand for heating, cooling, ventilation, domestic hot water and lighting, 2007. 50, 209

[51] VDI. VDI 2067: Economic efficiency of building installations - fundamentals and economic calculation, 2000.

[52] VDI. VDI 3985: Principles for the design, construction and acceptance of combined heat and power plants with internal combustion engines, 2004. 50, 209

[53] R. Strzalka, T.G. Erhart, and U. Eicker. Analysis and optimization of a cogeneration system based on biomass combustion. *Applied Thermal Engineering*, 50:1418–1426, 2013. 58

[54] R. Strzalka, R. Ulbrich, and U. Eicker. Proposal for a model of biomass combustion in a grate furnace. *Chemical and Process Engineering*, 4:74–75, 2010. 59

[55] R. Strzalka, R. Ulbrich, and U. Eicker. Optimisation of combustion process in a biomass-fuelled cogeneration plant. *Chemical Engineering Transactions*, 21:469–474, 2010. 59

[56] Softing. Softing OPC Toolkit, 2010. 76

[57] EN60751. Industrial platinum resistance thermometers and platinum temperature sensors (iec 60751:2008), 2008. Industrielle PlatinWiderstandsthermometer und Platin-Temperatursensoren (IEC 60751:2008),
Deutsche Fassung EN 60751:2008. 77, 78

[58] PMA Prozess und Maschinen-Automation GmbH. *Transmitter P40/P41, Pressure transmitter*, 2007. 78

[59] Kamstrup. Maxical III heat meter specifications, 2010. 82

[60] Kamstrup. Maxical 401 heat meter specifications, 2010. 82

[61] VDI. DIN EN 1434 heat meters - part 1: General requirements; German version 2007, 2007. 82

[62] Gu¨nter Leitgen. Euroheat & Power. *Euroheat & Power*, 2006. 82

[63] Gesellschaft fu¨r Verfahrenstechnik und Chemieingenieurwesen V.D.I.G.V.U. *VDI-Wa¨rmeatlas*. Springer, 2006. 93, 139, 140, 141, 142, 143, 145, 149, 150

[64] L. Abbiati and A. Barone. Object-oriented modelling and control of an Organic Rankine Cycle plant for combined heat & power generation. Master's thesis, Politecnico di Milano, 2012. 95

[65] H. Kamerlingh Onnes. Expression of the Equation of State of gases and liquids by means of series. In Kostas Gavroglu and Yorgos Goudaroulis, editors, *Through measurement to knowledge*, volume 124 of *Boston Studies in the Philosophy of Science*, pages 146–163. Springer Netherlands, 1901. 100

[66] Manson Benedict, George B. Webb, and Louis C. Rubin. An empirical equation for thermodynamic properties of light hydrocarbons and their mixtures: I. Methane, Ethane, Propane and n-Butane. *The Journal of*

Chemical Physics, 8(4):334–345, 1940. 101

[67] Giorgio Soave. Equilibrium constants from a modified Redlich-Kwong Equation of State. *Chemical Engineering Science*, 27(6):1197–1203, 1972. 101

[68] D.Y. Peng and D.B. Robinson. A new two-constant Equation of State,. *Industrial and Engineering Chemistry: Fundamentals*, 15:59–64, 1976. 101

[69] R. Stryjek and J.H. Vera. PRSV: An improved Peng-Robinson equation of state for pure compounds and mixtures. *The Canadian Journal of Chemical Engineering*, 64(2):323–333, 1986. 102

[70] P. Colonna, N.R. Nannan, and A. Guardone. Multiparameter Equations of State for Siloxanes. *Fluid Phase Equilibria*, 263:115–130, 2008. 102, 105, 106

[71] R. Span and W. Wagner. Equations of State for technical applications: I. Simultaneously optimized functional forms for non-polar and polar fluids. *International Journal of Thermophysics*, 24(1):1–39, 2003. 103

[72] R. Span and W. Wagner. Equations of State for technical applications, II. results for non-polar fluids. *International Journal of Thermophysics*, 24(1):41–109, 2003. 103

[73] Ulrike Weingerl, Martin Wendland, and Johann Fischer. Backone family of Equations of State: 2. Nonpolar and polar fluid mixtures. *AIChE Journal*, 47:705–717, 2001. 103

[74] Andreas Mu¨ller, Jochen Winkelmann, and Johann Fischer. Backone family of equations of state: 1. Non-polar and polar pure fluids. *AIChE Journal*, 42(4):1116–1126, 1996. 103

[75] W.G. Chapman, K.E. Gubbins, G. Jackson, and M. Radosz. SAFT: Equation-of-State solution model for associating fluids. *Fluid Phase Equilibria*, 52:31–38, 1989. 104

[76] Walter G. Chapman, Keith E. Gubbins, George Jackson, and Maciej Radosz. New reference equation of state for associating liquids. *Industrial & Engineering Chemistry Research*, 29(8):1709–1721, 1990.

[77] Walter G. Chapman, Sauer Sharon G., David Ting, and Auleen Ghosh. Phase behavior applications of SAFT based equations of state - from associating fluids to polydisperse, polar copolymers. *Fluid Phase Equilibria*, 217(2):137– 143, 2004. 104

[78] Ngoc Anh Lai, Martin Wendland, and Johann Fischer. Description of linear Siloxanes with PC-SAFT equation. *Fluid Phase Equilibria*, 283:22–30, 2009. 104

[79] Nawin Ryan Nannan. *Advancements in non-classical gas dynamics*. PhD thesis, TU Delft, 2009. 104

[80] Acros Organics BVBA. Safety datasheet, rev. 2, 2012. 105

[81] R.L. Rowley, W.V. Wilding, J. L. Oscarson, Y. Yang, and N. F. Giles. *DIPPR(TM), Data Compilation of Pure Chemical Properties*. Design Institute for Physical Properties, AIChE, New York, NY, 2010. 105, 157, 279

[82] E. Dickinson and I.A. McLure. Thermodynamics of n-Alkane + Dimethylsiloxane mixtures part 1: Gas-liquid critical temperatures and pressures. *J. Chem. Soc. Faraday Trans.*, 70:2313, 1974. 105

[83] P. Colonna, N.R. Nannan, A. Guardone, and E. W. Lemmon. Multiparameter equations of state for selected Siloxanes. *Fluid Phase Equilibria*, 244:193–211, 2006. 105, 279

[84] E.W. Lemmon, M.L. Huber, and M.O. McLinden. NIST Standard Reference Database 23: Reference Fluid Thermodynamic and Transport Properties REFPROP. *NIST - Standard Reference Data Program*, Version 9.0, 2010. 105, 157

[85] IUPAC. Atomic weights of the elements. *Journal of Physical Chemisty Reference Data*, 30, 3:701–712, 1999. 105, 145

[86] J. Bowers and I. A. McLure. Thermodynamics of linear Dimethylsiloxane-Perfluoroalkane mixtures, part 3: Orthobaric surface tensions of Hexamethyldisiloxane-, Octamethyltrisiloxane- or Decamethyltetrasiloxane-

Tetradecafluorohexane near the upper critical endpoint. *J. Chem. Soc., Faraday Trans. English*, 93:265–271, 1997. 106

[87] M. J. Hunter, E. L. Warrick, J. F. Hyde, and C. C. Currie. Organosilicon polymers, II. the open chain Dimethylsiloxanes with Trimethylsiloxy end groups. *J. Am. Chem. Soc. English*, 68:2284–2290, 1946.

[88] H. W. Fox and W. A. Zisman. The spreading of liquids on low energy surfaces, I. Polytetrafluoroethylene. *J. Colloid Interface Sci. English*, 5:514–531, 1950.

[89] H. I. Waterman, W. E. R. Herwijnen van, and H. W. Hartog den. Statisticalgraphical survey of series of linear and cyclic Dimethylsiloxanes. *J. Appl.*
Chem. English, 8:625–631, 1958.

[90] A. Z. Golik and P. F. Tscholpan. Surface tension of some Siloxanes. *Ukr. Khim. Zh. (Russ. Ed.)*, 28:42–46, 1962.

[91] D. Hopfe. Thermophysical data of pure substances. *Data Compilation of FIZ CHEMIE*, 1990:18, 1990.

[92] B. Edmonds and I.A. McLure. Thermodynamics of n-Alkane + Dimethylsiloxane mixtures. *J. Chem. Soc., Faraday Trans.*, 1:3319–3329, 1982.

[93] C.B. Hurd. Studies on Siloxanes, I. the specific volume and viscosity in relation to temperature and constitution. *Journal of the American Chemical Society*, 68:364, 1946. 106

[94] Solutia Inc. Therminol, unique high-temperature, low-pressure heat transfer fluid (technical bulletin 7239146d), 2010. 110

[95] W. Wagner and A. Pruss. The IAPWS formulation 1995 for the thermodynamic properties of ordinary water substance for general and scientific use. *Journal of Physical and Chemical Reference Data*, 31(2):387–535, 2002. 111

[96] M.L. Huber, R.A. Perkins, D.G. Friend, J.V. Sengers, M.J. Assael, I.N. Metaxa, K. Miyagawa, R. Hellmann, and E. Vogel. New international formulation for

the thermal conductivity of H_2O. *Journal of Physical and Chemical Reference Data*, 41(3):–, 2012. 111

[97] M. L. Huber, R. A. Perkins, La¨secke A., and D.G. Friend. New international formulation for the viscosity of H_2O. *J. Phys. Chem. Ref. Data*, 38(2):110–125, 2009. 111

[98] F. Casella and Ch. Richter. ExternalMedia: A library for easy re-use of external fluid property code in modelica. In *modelica Conference*, 2008. 112

[99] P. Colonna and T.P. van der Stelt. FluidProp: A program for the estimation of thermophysical properties of fluids. *Energy Technology Section, Delft University of Technology*, 2004. 112

[100] Eric W. Lemmon, Marcia L. Huber, and Mark O. McLinden. *NIST Reference Fluid Thermodynamic and Transport Properties-REFPROP User's guide*. National Institute of Standards and Technology, National Institute of Standards and Technology Boulder, Colorado 80305, 9.1 edition, April 2013. 112

[101] S. Quoilin, A. Desideri, I. Bell, J. Wronski, and V. Lemort. Robust and computationally efficient dynamic simulation of ORC systems: The ThermoCycle modelica library. In *2nd International Seminar on ORC Power Systems, Rotterdam*, 2013. 113, 178

[102] Francesco Casella and Alberto Leva. Object-oriented modelling and simulation of power plants with modelica. In *44th IEEE Conference on Decision and Control and European Control Conference, Seville, Spain*, pages 7597–7602, 2006. 117

[103] F. Casella, M. Otter, K. Pr¨olss, Ch. Richter, and H. Tummescheit. The modelica fluid and media library for modeling of incompressible and compressible thermo-fluid pipe networks. In Christiona Kral, editor, *Proceedings 5th International Modelica Conference*, pages 631–640. Modelica Association, 2006. 117

[104] A.G. Kanaris, A.A. Mouza, and Paras S.V. Optimal design of a plate heat exchanger with undulated surfaces. *International Journal of Thermal Sciences*, 48(6):1184–1195, 2009. 119

[105] Eastman Chemical Company. Therminol heat transfer fluid reference disk, 2014. 120

[106] M.L. Moody. An approximate formula for pipe friction factors. *Trans. ASME*, 69:1005, 1947. 129

[107] Eva Romeo, Carlos Royo, and Antonio Monzon. Improved explicit equations for estimation of the friction factor in rough and smooth pipes. *Chemical Engineering Journal*, 86:369–374, 2002. 129, 154

[108] S.W. Churchill and R. Usagi. A general expression for the correlation rates of transfer and other phenomena. *AIChE Journal 18*, 6:1121, 1972. 129

[109] S.W. Churchill. Friction factor spans all flow regimes. *Chemical Engineering*, 84:91–92, 1977. 129

[110] Frank P. Incropera, David P. DeWitt, Theodore L. Bergman, and Adrienne S.
Lavine. *Fundamentals of heat and mass transfer*. John Wiley, West Sussex, 6th edition, 2007. 130, 155

[111] Frank P. Incropera, David P. DeWitt, and Theodore L. Bergman. *Fundamentals of Heat and Mass Transfer*. John Wiley & Sons, Indianapolis, Indiana, 7th edition, 2011. 131, 155, 156

[112] A.A. Zukauskas. Heat transfer from tubes in cross-flow. *Advances in Heat Transfer*, 18:87–159, 1987. 132

[113] Luz Amaya-Bower and Lee Taehun. Single bubble rising dynamics for moderate Reynolds number using Lattice Boltzmann Method. *Computers and Fluids*, 2010. 142

[114] Frank P. Incropera, David P. DeWitt, and Theodore L. Bergman. *Fundamentals of Heat and Mass Transfer*. John Wiley & Sons, 6th edition, 2006. 142, 156

[115] I.L. Mostinski. Application of the rule of corresponding states for calculation of heat transfer and critical heat flux. *Teploenergetika*, 4:66, 1963. 143, 144

[116] I.L. Mostinski. Calculation of heat transfer and critical heat flux in boiling liquids based on the law of corresponding states. *Teploenergetika*, 10:66–71, 1963. 143, 144

[117] Warren M. Rohsenow. A method of correlating heat transfer data for surface boiling of liquids. *Technical report (Massachusetts Institute of Technology, Heat Transfer Laboratory*, 5, 1951. 143

[118] W.M. Rohsenow. A method of correlating heat transfer data for surface boiling liquids. *Trans. ASME*, 74:969, 1952. 143

[119] A. E. Bergles and W. M. Rohsenow. Determination of forced-convection surface-boiling heat transfer. *Journal of Heat Transfer*, 86(3):365–372, 1964. 144

[120] John R. Thome. *Wolverine Engineering Databook III*. Wieland-Werke AG, Germany, 2006. 144

[121] K. Stephan and M. Abdelsalam. Heat-transfer correlations for natural convection boiling. *International Journal of Heat and Mass Transfer*, 23(1):73–87, 1980. 144

[122] J.G. Collier and J.R. Thome. *Convective Boiling and Condensation*. Oxford Engineering Science Series. Clarendon Press, 1996. 145

[123] G. Vinayak Rao and A.R. Balakrishnan. Nucleate pool boiling heat transfer of multicomponent mixtures. *Trans. IChemE Chem. Eng. Res. Des.*, 82:43–52, 2004. 145

[124] S.A. Alavi Fazel and S. Roumana. Pool boiling heat transfer to pure liquids. *Continuum Mechanics, Fluids, Heat*, 2010. 145, 146

[125] Y.Y. Hsieh and T.F. Lin. Saturated flow boiling heat transfer and pressure drop of refrigerant R-410a in a vertical plate heat exchanger. *International Journal of Heat and Mass Transfer*, 45(5):1033–1044, 2002. 146

[126] J.R. Garcia-Cascales, F. Vera-Garcia, J.M. Corberan-Salvador, and J. Gonzalvez-Macia. Assessment of boiling and condensation heat transfer correlations in the modelling of plate heat exchangers. *International Journal of Refrigeration*, 30(6):1029–1041, 2007. 146

[127] V. Gnielinsky. New equations for heat and mass transfer in turbulent pipe channel flow. *International Chemical Engineering*, 16:359–368, 1976. 154

[128] B.S. Petukhov. Advances in heat transfer. *Academic Press, New York*, 6, 1970. 154

[129] W. Nusselt. Die Oberfla¨chenkondensation des Wasserdampfes. *Z. Vereines Deutsch. Ing.*, 60:541–546, 1916. 155

[130] Frank P. Incropera, David P. DeWitt, and Theodore L. Bergman. *Fundamentals of Heat and Mass Transfer*. John Wiley & Sons, 5th edition, 2001. 156

[131] W.C. Lee and J.W. Rose. Forced convection film condensation on a horizontal tube with and without non-condensing gases. *International Journal of Heat and Mass Transfer*, 27(4):519–528, 1984. 156

[132] Francesco Calise, Claudio Capuozzo, and Laura Vanoli. Design and parametric optimization of an Organic Rankine Cycle powered by solar energy. *American Journal of Engineering and Applied Sciences*, 6(2):178–204, 2013. 156

[133] M.W. Browne and P.K. Bansal. An overview of condensation heat transfer on horizontal tube bundles. *Applied Thermal Engineering*, 19:565–594, 1999. 156

[134] B.S. Yilbas and N. Altuntop. Condensing heat transfer of Freon-21 on plain horizontal tubes. *Indian Journal of Technology*, 28:100–106, 1990. 156

[135] B. Cheng and W.Q. Tao. Experimental study of R-152a film condensation on single horizontal smooth tube andenhanced tubes. *Journal of Heat Transfer*, 116:266–270, 1994. 156

[136] Busch SIHI. *Datasheet Busch: Rotary claw vacuum pumps, Mink MM 1104 A V03*, 2010. 169

[137] A. Stodola. *Dampf- und Gasturbinen*, volume 5. Julius Springer, Berlin, 1922. 174

[138] A. Stodola. *Dampf- und Gasturbinen*, volume 6. Julius Springer, Berlin, 1924. 174

[139] M.J. Reader-Harris. The equation for the expansibility factor for orifice plates. In *FLOMEKO*, pages 209–214, 1998. In Proc. of FLOMEKO Conference 98, Lund, Sweden. 175

[140] D.H. Cooke. Modeling of off-design multistage turbine pressures by Stodola's ellipse. *Proceeding PEPSE User Group Meeting*, pages 205–234, 1983. 177, 178

[141] Weier ELECTRIC GmbH. Data sheet - GET˙DGI 450/2L WT (synchronous generator), 2006. 182

[142] VDI. VDI 4655: Reference load profiles of single-family and multi-family houses for the use of chp systems, 2008. 209

[143] Institut fu¨r Wohnen und Umwelt IWU. Degree days germany, 2 2011. 218

[144] Institut fu¨r Wohnen und Umwelt IWU. Degree days germany, 2 2012.

[145] Institut fu¨r Wohnen und Umwelt IWU. Degree days germany, 2 2013.

[146] Institut fu¨r Wohnen und Umwelt IWU. Degree days germany, 2 2014. 218

Appendix A

Technical reference and source code

A.1 Auxiliary power demand

In the following sections the electric power demand for all relevant sub-systems in the power plant are listed. Furthermore the tables provide information if the component is used only in standard operation or if it is connected to the emergency power supply (Diesel generator).

A.1.1 Fuel and ash transportation system

Table A.1: nominal electric power for fuel and ash transportation

component	P_{max}	emergency power	reference
-	[kW]	[-/x/opt]	-
hyd. drive storage	15.00	-	[manufacturer]
hyd. drive cross conveyor	30.00	-	[manufacturer]
hyd. drive stoker	30.00	x	[manufacturer]
hyd. drive grate	1.50	-	[manufacturer]
hyd. drive ash disposal	3.00	-	[manufacturer]
hyd. drive feeding lock	3.00	-	[manufacturer]
through chain con.	3.00	-	[manufacturer]
alt. flaps cyclone	0.25	-	[manufacturer]
P	85.75		

A.1.2 District heating

Table A.2: nominal electric power demand for district heating network

component	P_{max}	emergency power	reference
-	[kW]	[-/x/opt]	-
dh pump 1	15.00	opt	[manufacturer]
dh pump 2	15.00	opt	[manufacturer]
P	30.00		

A.1.3 Thermal conversion - furnace

Table A.3: nominal electric power demand of biomass conversion systems

component	P_{max}	emergency power	reference
-	[kW]	[-/x/opt]	-
exhaust gas fan	75.00	x	[manufacturer]
sec. recirculation fan	7.50	-	[manufacturer]
sec. fan 1	7.50	x	[manufacturer]
sec. fan 2	7.50	x	[manufacturer]
dry-out fan	3.00	-	[manufacturer]
pri. fan	5.50	-	[manufacturer]
burn-out fan	2.20	-	[manufacturer]
flushing fans	0.35	x	[manufacturer]
P	108.55		

A.1.4 Heat transfer cycle (thermal oil)

Table A.4: nominal electric power demand of thermal oil cycle

component	P_{max}	emergency power	reference
-	[kW]	[-/x/opt]	-
pri. pump 1	55.00	-	[manufacturer]
pri. pump 2	55.00	-	[manufacturer]
emergency pump	55.00	x	[manufacturer]
drainage pump	0.75	-	[manufacturer]
P	110.75		

A.1.5 Thermal conversion

Table A.5: nominal electric power demand of furnace ventilation

component	P_{max}	emergency power	reference
-	[kW]	[-/x/opt]	-
exhaust gas fan	75.00	x	[manufacturer]
sec. recirculation fan	7.50	-	[manufacturer]
sec. fan 1	7.50	x	[manufacturer]
sec. fan 2	7.50	x	[manufacturer]
dry-out fan	3.00	-	[manufacturer]
pri. fan	5.50	-	[manufacturer]
burn-out fan	2.20	-	[manufacturer]
flushing fans	0.35	x	[manufacturer]
P	108.55		

Table A.6: nominal electric power demand of furnace cooling system

component	P_{max}	emergency power	reference
-	[kW]	[-/x/opt]	-
grate cooling 1	1.10	opt	[manufacurer]
grate cooling 2	1.10	opt	[manufacurer]
P	2.20		

A.1.6 ORC

Table A.7: nominal electric power demand of ORC unit

component	P_{max}	emergency power	reference
-	[kW]	[-/x/opt]	-
alternator	15.00	opt	[manufacturer]
alternator cooling	10.00	opt	[manufacturer]
control	1.00	opt	[manufacturer]
feed pump	60.00	opt	[manufacturer]

vacuum pump	1.10	opt	[manufacturer]
	P 87.10		

A.2 Cycle layout changes

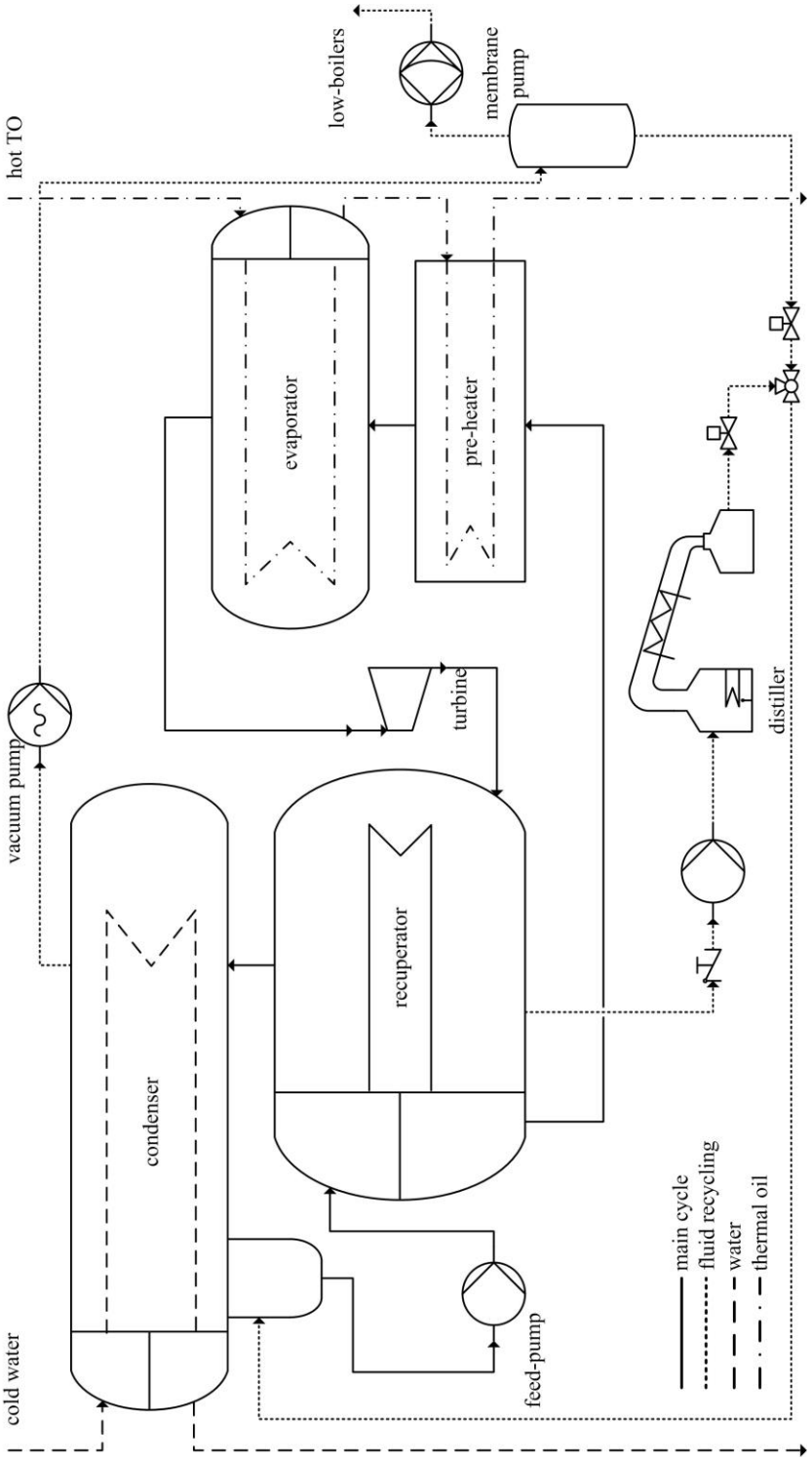

Figure A.1: cycle layout including design changes/improvements

A.3 Detailed correlation data

A.3.1 Alternator efficiency correlation

The gross efficiency of the alternator:

$$\eta_{alt,gr} = a \times exp(b \times P_{mech}) + c \times exp(d \times P_{mech}) \quad \text{(A.1)}$$

where the the load X is $X = \frac{P_{mech}}{P_{nom}}$, P_{nom} is set to 1500kW.

Table A.8: fitting results for alternator gross efficiency

coefficient	a	b	c	d
	-0.2624	-0.2624	-0.2624	0.004365
	R^2	adj. R^2	RSME	SSE
	0.9998	0.9995	0.001447	6.28e-06

The net efficiency of the alternator:

$$\eta_{alt,net} = (a \times exp(b \times X) + c \times exp(d \times X)) \quad \text{(A.2)}$$

where the the load X is $X = \frac{P_{mech}}{P_{nom}}$, P_{nom} is set to 1500kW.

Table A.9: fitting results for alternator gross efficiency (load based)

coefficient	a	b	c	d
value	-0.2596	-9.182	0.9552	0.004395
	R^2	adj. R^2	RSME	SSE
	0.9998	0.9995	0.001432	6.151e-06

Mechanical power versus electric power:

$$P_{mech,gr}(P_{el,gr}) = P_{el,gr} \times (a \times exp(b \times P_{el,gr}) + c \times exp(d \times P_{el,gr}))^{-1} \quad \text{(A.3)}$$

Table A.10: fitting results for alternator gross efficiency inverse function

coefficient	a	b	c	d
value	0.9667	0.002796	-0.001251	-4.439
	R^2	adj. R^2	RMSE	SSE
	0.9998	0.9997	0.001203	4.338e-06

A.3.2 Turbine efficiency

Turbine correlation 1:

$$\eta_{is} = a \times atan\left(\frac{b}{\beta}^2 + \frac{c}{\beta}\right) + d \times \beta + e \tag{A.4}$$

where $\beta = \frac{p_{in}}{p_{out}}$ and

Table A.11: fitting results for turbine correlation 1

coefficient	a	b	c	d	e
value	0.9649	-112.9	4.811	-0.002609	0.7741
	R^2	adj. R^2	RMSE	SSE	
	0.9928	0.9928	0.007912	0.2511	

Turbine correlation 2:

$$\eta_{is} = a \times atan\left(\frac{b}{\beta}^2 + \frac{c}{\beta}\right) + d \times \beta + e \tag{A.5}$$

where $\beta = \frac{p_{in}}{p_{out}}$ and

Table A.12: fitting results for turbine correlation 1

coefficient	a	b	c	d	e
value	0.9659	-128.2	2.28	-0.005512	0.9727
	R^2	adj. R^2	RMSE	SSE	
	0.9865	0.9865	0.009902	3.404	

This correlation is based on a long-term data set (2010-11-01/2010-11-05)

A.3.3 Pre-heater

$$\alpha_{ph,hot} = \alpha_0 \times \left(\frac{\dot{m}}{\dot{m}_0}\right)^b \tag{A.6}$$

Table A.13: fitting results for pre-heater hot side correlation

coefficient	a	b	$\dot{m}_0$
value	678	0.95	20

$$Nu_{ph,cold} = C_1 \times Re^m \times Pr^n \times p_r^l \quad \text{(A.7)}$$

Table A.14: fitting results for pre-heater hot side Nusselt correlation

coefficient	C_1	m	n	l
value	0.1025	0.8	0.42	1.25

A.3.4 Evaporator

$$alpha_{evap,boil} = C_1 \times \alpha_0 \times F_p \times \left(\frac{\dot{m}}{\dot{m}_0}\right)^n \quad \text{(A.8)}$$

$$F_p = 1.8 \times p_r^0.17 + 4 \times p_r^1.2 + 10 \times p_r^10; \quad \text{(A.9)}$$

Table A.15: fitting results for evaporator pool boiling correlation

coefficient	α_0	C_1	n	$\dot{m}_0$
value	1325	0.23522	0.372	20

A.3.5 Recuperator - type 1

$$\alpha_{hot} = C_1 \times Re_m \times Pr_n \quad \text{(A.10)}$$

Table A.16: fitting results for recuperator hot side Nusselt correlation

coefficient	$\dot{C}1$	m	n
value	0.003874	0.8956	0.33

A.3.6 Condenser

$$\alpha_{hot} = \alpha_0 \times \left(\frac{\dot{m}}{\dot{m}_0}\right)^b \quad \text{(A.11)}$$

Table A.17: fitting results for condenser vapour side correlation

coefficient	a	b	$\dot{m}_0$
value	510.7	0.73	20

$$Nu_{hot} = a \times \left(\frac{\dot{m}}{\dot{m}_0}\right)^b \times Pr_{film}^c \quad \text{(A.12)}$$

Table A.18: fitting results for condenser vapour side correlation

coefficient	a	b	c	
value	0.4091	0.7542	-1.261	
	R_2	$adj.R^2$	RMSE	SSE
	0.9627	0.9627	0.004842	0.2025

A.4 Solids properties

```
Function Steel_ThCon ( t As Double , Unit As String ) As Double
Dim AST As Double Dim
BST As Double
Dim CST As Double
 "thermal conductivity of Steel 235 GH [W/mK ]according to
    Waerme Atlas"
AST = 0.0000130794
1
2
3
4
5
6
```

```
BST =       0.024334
CST = 55.6364
 Select Case Unit

          Case Is = "C"          " for      temperature      in      C "

              Steel _ThCon = AST * t ^ 2 + BST * t + CST

       Case Is = "K" " for temperature in K" t = t + 273.15
              Steel _ThCon = AST * t ^ 2 + BST * t + CST

End Select
```

```
Function Alu_ThCon( x_in As Double ,                    Unit As Integer ) As Double
"thermal conductivity for pure Aluminium types EW 1XXX" temp = 0#
      " coefficients "
      A   = 252.212021673555
      B   = 2.79348507151663E 0 4C = 208.261326742849
      D =
         308.761052445552 f =
         140.44635307017
      g =
         54.2665507155588 h =
         213.556540034445 i =
         207.500329353761
Select Case Unit
      Case Is = 0 " for temperature in C " temp = A * Exp ( B * x_in ) + C * Exp( 1# * ( x in D)
       * ( x_in
                    D) / ( f * f ) ) + g * Exp( 1# * ( x_in                h) * ( x in            h) / ( i
           * i ) )
       Case Is = 1 " for temperature in K" x_in = x_in 273.15 temp = A * Exp ( B * x_in ) +
       C * Exp( 1# * ( x in D) *
                    ( xin                D) / ( f * f ) ) + g * Exp( 1# * ( x inh) *
                    ( xinh) / ( i * i ) )
End Select
```

19

A.5 Fluid data

Table A.19: overview of linear Siloxanes appearing in ORC-applications

		hexa-methyldi-siloxane	octa-methyltri-siloxane	deca-methyltetra-siloxane	dodeca-methylpenta-siloxane	tetra-methyhexa-siloxane
property	unit	C6H18OSi2	C8H24O2Si3	C10H30O3Si4	C12H36O4Si5	C14H42O5Si6
CAS		107-46-0	107-51-7	141-62-8	141-63-9	107-52-8
Abbreviation		MM, L2	MDM, L3	MD2M, L4	MD3M, L5	MD4M, L6
Mol. Weight	[g/mol]	162.378	236.531	310.685	384.839	458.993
Crit. Temp.	[K]	518.700	564.090	599.400	628.360	653.200
Crit. Pressure	[bar]	19.39	14.15	12.27	9.45	8.77
Crit. Volume	[m^3/kg]	0.003285	0.003895	0.003519	0.003789	0.003501
Crit. Comp.	[-]	0.24	0.28	0.27	0.26	0.26
Melting Point	[K]	374.04	426.40	468.27	503.84	533.57
Acentric Factor	[-]	0.42	0.53	0.67	0.73	0.79
Flashpoint	[K]	271.15	302.15	335	352.15	375.15
Reference		[83]	[83]	[83]	[83]	[83]

Table A.20: overview of Cyclo-siloxanes appearing in ORC-applications

		hexa-methylcyclotri-siloxane	octa-cylcomethytetra-siloxane	deca-methylcyclopenta siloxane	dodeca-methylcyclohexa-siloxane
property	unit				
formula		C6H18O3Si3	C8H24O4Si4	C10H30O5 Si5	C12H36O6Si6
CAS		541-05-9	556-67-2	541-02-6	540-97-6
Abbreviation		D3	D4	D5	D6
Mol. Weight	[g/mol]	222.462	296.616	370.770	444.924
Crit. Temp.	[K]	554.200	586.491	619.235	645.780
Crit. Pressure	[bar]	16.80	13.32	11.61	9.61
Crit. Volume	[m^3/kg]	0.245916	0.003257	0.003418	0.003583
Crit. Comp.	[-]	0.23	0.26	0.29	0.29
Melting Point	[K]	408.26	449.24	484.85	244.96
Acentric Factor	[-]	0.47	0.59	0.67	0.74
Flashpoint	[K]	308.15	330.15	350.15	397.55
Reference		[81]	[83]	[83]	[83]

A.6 Fluid property code (EES)

A.6.1 Header files

A.6.1.1 REFPROP header file

```
#ifndef H
#define H

typedef void (stdcall *fp INFOdllTYPE) ( long &,double &,double &,double &,double &,double
        &,double &,double &,double &,double &,double &); typedef void (stdcall *fp SETUPdllTYPE) ( long &,char*,char*,char*, long &,char*, long
                , long
        , long , long ) ; typedef void (stdcall *fp THERMdllTYPE) ( double &,double &,double *,double &,double
        &,double &,double &,double &,double &,double &,double &); typedef void (stdcall *fp TPRHOdllTYPE) ( double &,double &,double *, long &,long
&,double
        &,long &,char*, long ) ; typedef void (stdcall *fp TRNPRPdllTYPE) ( double &,double &,double *,double &,double &,long &,char*, long ) ;
```

```
typedef void (stdcall *fp SATTdllTYPE) ( double &,double *, long &,double &,double &,double &,double
        &,double *,double *, long &,char*, long &); typedef void (stdcall *fp TPFLSHdllTYPE) ( double &,double &,double *,double &,double
        &,double &,double *,double *,double &,double &,double &,double &,double &,double
        &,double &,long &,char*, long ) ; typedef void (stdcall *fp PSFLSHdllTYPE) ( double &,double &,double *,double &,double
        &,double &,double &,double *,double *,double &,double &,double &,double &,double
        &,double &,long &,char*, long &); typedef void (stdcall *fp SATDdllTYPE) ( double &,double *, long &,long &,double &,double
        &,double &,double &,double *,double *, long &,char*, long ) ; typedef void (stdcall *fp SATEdllTYPE) ( double &,double *, long &,long &,long
&,double
        &,double &,double &,long &,double &,double &,double &,long &,char*, long &); typedef void (stdcall *fp SATHdllTYPE) ( double &,double *,
long &,long &,long &,double
        &,double &,double &,long &,double &,double &,double &,long &,char*, long &); typedef void (stdcall *fp SATSdllTYPE) ( double &,double *,
long &,long &,long &,double
        &,double &,double &,long &,double &,double &,double &,long &,double &,double &,double
        &,long &,char*, long &); typedef void (stdcall *fp ABFL1dllTYPE) ( double &,double &,double *, long &,double &,double
        &,double &,double &,double &,double &,long &,char*, long &); typedef void (stdcall *fp ABFL2dllTYPE) ( double &,double &,double *, long &,long
&,double
        &,double &,double &,double &,double &,double &,double *,double *,double
        &,double &,double &,double &,double *,double *,double &,long &,char*, long ) ; typedef void (stdcall *fp ACTVYdllTYPE) ( double &,double
&,double *,double &); typedef void (stdcall *fp AGdllTYPE) ( double &,double &,double *,double &,double &); typedef void (stdcall *fp
CCRITdllTYPE) ( double &,double &,double &,double *,double
        &,double &,double &,double &,long &,char*, long ) ; typedef void (stdcall *fp CP0dllTYPE) ( double &,double *,double &);
typedef void (stdcall *fp CRITPdllTYPE) ( double *,double &,double &,double &,long
        &,char*, long ) ; typedef void (stdcall *fp CSATKdllTYPE) ( long &,double &,long &,double &,double &,double
        &,long &,char*, long ) ; typedef void (stdcall *fp CV2PKdllTYPE) ( long &,double &,double &,double &,double &,long
        &,char*, long ) ; typedef void (stdcall *fp CVCPKdllTYPE) ( long &,double &,double &,double &,double &); typedef void (stdcall *fp
CVCPdllTYPE) ( double &,double &,double *,double &,double &); typedef void (stdcall *fp DBDTdllTYPE) ( double &,double *,double &); typedef void
(stdcall *fp DBFL1dllTYPE) ( double &,double &,double *,double &,double
        &,double &,long &,char*, long ) ; typedef void (stdcall *fp DBFL2dllTYPE) ( double &,double &,double *, long &,double &,double
        &,double &,double &,double &,double *,double *,double &,long &,char*, long ) ; typedef void (stdcall *fp DDDPdllTYPE) ( double &,double
&,double *,double &); typedef void (stdcall *fp DDDTdllTYPE) ( double &,double &,double *,double &); typedef void (stdcall *fp DEFLSHdllTYPE)
( double &,double &,double *,double &,double
        &,double &,double &,double *,double &,double &,double &,double &,double
        &,double &,long &,char*, long ) ; typedef void (stdcall *fp DHD1dllTYPE) ( double &,double &,double *,double &,double &,double
        &,double &,double &,double &); typedef void (stdcall *fp DHFLSHdllTYPE) ( double &,double &,double *,double &,double
        &,double &,double &,double *,double *,double &,double &,double &,double &,double
        &,double &,long &,char*, long ) ; typedef void (stdcall *fp DIELECdllTYPE) ( double &,double &,double *,double &); typedef void
(stdcall *fp DOTFILLdllTYPE) ( long &,double *,double &,double &,long
        &,char*, long ) ; typedef void (stdcall *fp DPDD2dllTYPE) ( double &,double &,double *,double &); typedef void (stdcall *fp
DPDDKdllTYPE) ( long &,double &,double &,double &); typedef void (stdcall *fp DPDDdllTYPE) ( double &,double &,double *,double &);
typedef void (stdcall *fp DPDTKdllTYPE) ( long &,double &,double &,double &); typedef void (stdcall *fp DPDTdllTYPE) ( double
&,double &,double *,double &);
typedef void (stdcall *fp DPTSATKdllTYPE) ( long &,double &,long &,double &,double &,double
        &,double &,long &,char*, long ) ; typedef void (stdcall *fp DSFLSHdllTYPE) ( double &,double &,double *,double &,double
        &,double &,double &,double *,double &,double &,double &,double &,double
        &,double &,long &,char*, long ) ; typedef void (stdcall *fp ENTHALdllTYPE) ( double &,double &,double *,double &); typedef void (stdcall
*fp ENTROdllTYPE) ( double &,double &,double *,double &); typedef void (stdcall *fp ESFLSHdllTYPE) ( double &,double &,double *,double
&,double
        &,double &,double &,double &,double *,double *,double &,double &,double &,double
        &,double &,long &,char*, long ) ; typedef void (stdcall *fp FGCTYdllTYPE) ( double &,double &,double *,double *) ; typedef void (stdcall *fp
FPVdllTYPE) ( double &,double &,double &,double *,double &); typedef void (stdcall *fp GERG04dllTYPE) ( long &,long &,long &,char*, long ) ; typedef
void (stdcall *fp GETFIJdllTYPE) ( char*,double *,char*,char*, long , long , long ) ; typedef void (stdcall *fp GETKTVdllTYPE) ( long &,long &,char*,double
        *,char*,char*,char*,char*, long , long , long , long , long ) ; typedef void (stdcall *fp GIBBSdllTYPE) ( double &,double &,double *,double &,double
&); typedef void (stdcall *fp HSFLSHdllTYPE) ( double &,double &,double *,double &,double
        &,double &,double &,double &,double *,double *,double &,double &,double &,double
```

9

```
        &,double &,long &,char*, long ) ; typedef void (stdcall *fp INFOdllTYPE) ( long &,double &,double &,double &,double &,double
        &,double &,double &,double &,double &,double &); typedef void (stdcall *fp LIMITKdllTYPE) ( char*, long &,double &,double &,double &,double
        &,double &,double &,double &,long &,char*, long, long ) ; typedef void (stdcall *fp LIMITSdllTYPE) ( char*,double *,double &,double &,double
&,double
        &,long ) ; typedef void (stdcall *fp LIMITXdllTYPE) ( char*,double &,double &,double &,double *,double
        &,double &,double &,double &,long &,char*, long, long ) ; typedef void (stdcall *fp MELTPdllTYPE) ( double &,double *,double &,long &,char*,
long ) ; typedef void (stdcall *fp MELTTdllTYPE) ( double &,double *,double &,long &,char*, long ) ; typedef void (stdcall *fp MLTH2OdllTYPE) ( double
&,double &,double &); typedef void (stdcall *fp NAMEdllTYPE) ( long &,char*,char*,char*, long , long , long ) ; typedef void (stdcall *fp
PDFL1dllTYPE) ( double &,double &,double *,double &,long
        &,char*, long ) ; typedef void (stdcall *fp PDFLSHdllTYPE) ( double &,double &,double *,double &,double
        &,double &,double *,double *,double &,double &,double &,double &,double &,double
        &,double &,long &,char*, long ) ; typedef void (stdcall *fp PEFLSHdllTYPE) ( double &,double &,double *,double &,double
        &,double &,double &,double *,double *,double &,double &,double &,double &,double
        &,double &,long &,char*, long ) ; typedef void (stdcall *fp PHFL1dllTYPE) ( double &,double &,double *, long &,double &,double
        &,long &,char*, long ) ; typedef void (stdcall *fp PHFLSHdllTYPE) ( double &,double &,double *,double &,double
        &,double &,double &,double *,double *,double &,double &,double &,double &,double
        &,double &,long &,char*, long ) ; typedef void (stdcall *fp PQFLSHdllTYPE) ( double &,double &,double *, long &,double &,double
        &,double &,double &,double *,double *,double &,double &,double &,double &,double
        &,double &,long &,char*, long ) ; typedef void (stdcall *fp PREOSdllTYPE) (
long &);
typedef void (stdcall *fp PRESSdllTYPE) ( double &,double &,double *,double &); typedef void (stdcall *fp PSFL1dllTYPE) ( double &,double &,double *,
long &,double &,double
        &,long &,char*, long ) ; typedef void (stdcall *fp PSFLSHdllTYPE) ( double &,double &,double *,double &,double
        &,double &,double &,double *,double *,double &,double &,double &,double &,double
        &,double &,long &,char*, long ) ; typedef void (stdcall *fp PUREFLDdllTYPE) ( long &); typedef void (stdcall *fp QMASSdllTYPE) ( double
&,double *,double *,double &,double
        *,double *,double &,double &,long &,char*, long &); typedef void (stdcall *fp QMOLEdllTYPE) ( double &,double *,double *,double
&,double
        *,double *,double &,double &,long &,char*, long &); typedef void (stdcall *fp SATDdllTYPE) ( double &,double *, long &,long &,double &,double
        &,double &,double &,double *,double *, long &,char*, long &); typedef void (stdcall *fp SATEdllTYPE) ( double &,double *, long &,long
&,long &,double
        &,double &,double &,long &,double &,double &,double &,long &,char*, long ) ; typedef void (stdcall *fp SATHdllTYPE) ( double &,double *,
long &,long &,long &,double
        &,double &,double &,long &,double &,double &,double &,long &,char*, long ) ; typedef void (stdcall *fp SATPdllTYPE) ( double &,double *, long
&,double &,double &,double
        &,double *,double *, long &,char*, long ) ; typedef void (stdcall *fp SATSdllTYPE) ( double &,double *, long &,long &,long &,double
        &,double &,double &,long &,double &,double &,double &,long &,double &,double &,double
        &,long &,char*, long ) ; typedef void (stdcall *fp SATTdllTYPE) ( double &,double *, long &,double &,double &,double
        &,double *,double *, long &,char*, long ) ; typedef void (stdcall *fp SETAGAdllTYPE) ( long &,char*, long ) ; typedef void (stdcall *fp
SETKTVdllTYPE) ( long &,long &,char*,double *,char*, long
        &,char*, long , long , long ) ; typedef void (stdcall *fp SETMIXdllTYPE) ( char*,char*,char*, long &,char*,double *, long
        &,char*, long , long , long , long , long ) ; typedef void (stdcall *fp SETMODdllTYPE) ( long &,char*,char*,char*, long &,char*, long , long
        , long , long ) ; typedef void (stdcall *fp SETREFdllTYPE) ( char*, long &,double *,double &,double &,double
        &,double &,long &,char*, long , long ) ; typedef void (stdcall *fp SETUPdllTYPE) ( long &,char*,char*,char*, long &,char*, long , long
        , long , long ) ; typedef void (stdcall *fp SPECGRdllTYPE) ( double &,double &,double &,double &); typedef void (stdcall *fp SUBLPdllTYPE) (
double &,double *,double &,long &,char*, long ) ; typedef void (stdcall *fp SUBLTdllTYPE) ( double &,double *,double &,long &,char*, long ) ; typedef void
(stdcall *fp SURFTdllTYPE) ( double &,double &,double *,double &,long
        &,char*, long ) ; typedef void (stdcall *fp SURTENdllTYPE) ( double &,double &,double &,double *,double
        *,double &,long &,char*, long ) ; typedef void (stdcall *fp TDFLSHdllTYPE) ( double &,double &,double *,double &,double
        &,double &,double *,double *,double &,double &,double &,double &,double &,double
        &,double &,long &,char*, long ) ; typedef void (stdcall *fp TEFLSHdllTYPE) ( double &,double &,double *, long &,double &,double
        &,double &,double &,double *,double *,double &,double &,double &,double &,double
```

53 54

```
                                &,double &,long &,char*, long ) ;
typedef void (stdcall *fpTHERM0dllTYPE) ( double &,double &,double *,double &,double
        &,double &,double &,double &,double &,double &,double &,double &); typedef void (stdcall *fpTHERM2dllTYPE) ( double &,double
&,double *,double &,double
        &,double &,double &,double &,double &,double &,double *,double &,double &,double &,double &,double &,double &,double &,double
        &,double &,double &,double
        &,double &,double &); typedef void (stdcall *fp THERM3dllTYPE) ( double &,double &,double *,double &,double
        &,double &,double &,double &,double &,double &,double &,double &); typedef void (stdcall *fp THERMdllTYPE) ( double
&,double &,double *,double &,double
        &,double &,double &,double &,double &,double &,double &); typedef void (stdcall *fp THFLSHdllTYPE) ( double &,double &,double *, long &,double
&,double
        &,double &,double &,double *,double *,double &,double &,double &,double &,double
        &,double &,long &,char*, long ) ; typedef void (stdcall *fp TPRHOdllTYPE) ( double &,double &,double *, long &,long &,double
        &,long &,char*, long ) ; typedef void (stdcall *fp TQFLSHdllTYPE) ( double &,double &,double *, long &,double &,double
        &,double &,double &,double *,double *,double &,double &,double &,double &,double
        &,double &,long &,char*, long ) ; typedef void (stdcall *fp TRNPRPdllTYPE) ( double &,double &,double *,double &,double &,long
        &,char*, long ) ; typedef void (stdcall *fpTSFLSHdllTYPE) ( double &,double &,double *, long &,double &,double
        &,double &,double &,double *,double *,double &,double &,double &,double &,double
        &,double &,long &,char*, long ) ; typedef void (stdcall *fp VIRBdllTYPE) ( double &,double *,double &); typedef
void (stdcall *fp VIRCdllTYPE) ( double &,double *,double &); typedef void (stdcall *fp WMOLdllTYPE) ( double *,double
&); typedef void (stdcall *fp XMASSdllTYPE) ( double *,double *,double &); typedef void (stdcall *fp XMOLEdllTYPE) (
double *,double *,double &);

        const long refpropcharlength =255; const long
                filepathlength =255; const long
                lengthofreference =3; const long
        errormessagelength =255; const long ncmax=20; const
        long numparams=72; const long maxcoefs=50;

#endif
```

A.6.1.2 Header file 1

```
* secondary authors : T. Erhart , A.                    Trinkle
* University of Applied Sciences                        Stuttgart
  * March 2012

  * mdm_ees.h header      f i l e          for usage of Reprop through DLP interface          in EES * based on :
  * primary author :
  * June 2001
* Bruno ROSE                b. rose@sherpa       eng .com
  * Sherpa Engineering
  * 269 287 , rue de la Garenne
* 92000 Nanterre                    France
  *
  */
#pragma once
//#include "mdm ees record .h"                                  // Type and class          declaration          for handling ees
        records

// Tell C++ to use the "C" style calling conventions rather than the C++ // mangled names


#ifdef _ _cplusplus extern "C" {
#endif

/* tell EES which functions and procedures are exported in the library
* declare                functions and procedures
* in DLF calling                style */


    declspec ( dllexport ) void DLFNames( char* Names) ; declspec ( dllexport ) double h ptx mdm( char s [256] , int mode, EES PARAM REC *rec_
    in ) ; declspec ( dllexport ) double s ptx mdm( char s [256] , int mode, EES PARAM REC *rec in ) ;
```

```
    declspec ( dllexport ) double v ptx mdm( char s [256] ,          int mode, EES PARAM REC *rec in ) ;
```

```
--                                                  -       -                                                    -
--declspec ( dllexport ) double rho ptx mdm( char s [256] , -     int mode, EES PARAM REC *rec in ) ;                  -
--declspec ( dllexport ) double cv ptx mdm( char s [256] , -      int mode, EES PARAM REC *rec in ) ;                 -
--declspec ( dllexport ) double cp ptx mdm( char s [256] , -      int mode, EES PARAM REC *rec in ) ;                 -
--declspec ( dllexport ) double kinvis ptx mdm( char s [256] ,    int mode, EES PARAM REC *rec in ) ;                      -
--declspec ( dllexport ) double thcon ptx mdm( char s [256] ,   -int mode, EES PARAM REC *rec in ) ;                     -
--declspec ( dllexport ) double ts p mdm( char s [256] ,-         int mode, EES PARAM REC *rec in ) ;                -
--declspec ( dllexport ) double ps t mdm( char s [256] ,          int mode, EES PARAM REC *rec in ) ;                -
--declspec ( dllexport ) double t ph mdm( char s [256] ,-        int mode, EES PARAM REC *rec in ) ;                 -
--declspec ( dllexport ) double s ph mdm( char s [256] ,-        int mode, EES PARAM REC *rec in ) ;                 -
--declspec ( dllexport ) double t psx mdm( char s [256] ,-       int mode, EES PARAM REC *rec in ) ;                  -
--declspec ( dllexport ) double h psx mdm( char s [256] ,-       int mode, EES PARAM REC *rec in ) ;                  -
--declspec ( dllexport ) double hevap t mdm( char s [256] ,      int mode, EES PARAM REC *rec in ) ;                    -

#ifdef    cplusplus
};
#endif
```

```
/* secondary authors : T. Erhart , A. Trinkle * University of Applied Sciences
  Stuttgart
  *

  * mdm _ees. cpp f i l e for usage of Reprop through DLP interface in EES * based on :
  * primary author :
  * June 2001
* Bruno ROSE                    b. rose@sherpa          eng .com
  * Sherpa Engineering
  * 269 287 , rue de la Garenne
* 92000 Nanterre                        France
  */
#pragma warning( disable : 4996)
#include "mdm ees record .h"
#include "mdm ees.h"
#include <windows .h>
#include <math.h>
#include <stdio .h>
// Defines the entry point                              for the        dll
BOOL APIENTRY DllMain( HANDLE hModule ,
                                          DWORD                ul reason for call ,
                                          LPVOID lpReserved
                                        )
{ return TRUE; }

// Tells EES which functions and procedures are exported in the library                                    :
// List of DLF format functions declspec ( dllexport ) void DLFNames( char*
    Names)                                                                                                          --
                                                                                                                    {
        strcpy (Names, "h psx mdm , t psx mdm ,s ph mdm ,t ph mdm , ps t mdm , ts p mdm ,h ptx mdm ,
        s ptx mdm , rho ptx mdm ,v ptx mdm , cp ptx mdm , cv ptx mdm , kinvis ptx mdm , thcon ptx mdm , hevap t mdm") ;
}
```

A.6.1.3 Header file 2

```
/* secondary authors : T. Erhart , A. Trinkle
 * University of Applied Sciences Stuttgart
 * March 2012
 * mdm -ees -record .h header file for usage of Reprop through DLP interface in EES
 * based on :
 * primary author :
 * June 2001
 * Bruno ROSE b.rose@sherpa eng .com
 * Sherpa Engineering
 * 269 287 , rue de la Garenne
 * 92000 Nanterre France
 */


#pragma once
```

```
#ifdef _ _cplusplus extern "C" {
#endif


// Structure for parameter records in DLF and DLP formats typedef struct EES PARAM REC {
double value ; struct EES PARAM REC *next ; } EES PARAM REC;



#ifdef              _ _cplusplus
};
#endif


// Declare C++ interface      for handling records chained                  l i s t s class     ees _record {

                EES PARAM REC * begin ;                                  // Pointer on the              f i rs t              record as private member

public          :


        ees _record (EES PARAM REC * begin _init ) ; // Constructor

         int          length () ;                                                  // Return         l i s t                                  length ( useful to get number of I/O)
        double& operator [ ] ( const int ) ; // Overloaded subscript operator to access I/O for r/w operations
};
```

```
/* secondary authors : T. Erhart , A. Trinkle * University of Applied Sciences
  Stuttgart
  * March 2012
  * mdm ees recors . cpp f i l e for usage of Reprop through DLP interface in EES * based on :
  * primary author :
  * June 2001
* Bruno ROSE                    b. rose@sherpa          eng .com
  * Sherpa Engineering
  * 269 287 , rue de la Garenne
* 92000 Nanterre                        France
  */

#include "mdm ees record .h"


// Constructor i ni t ia l iz e the begin pointer to the fi r st record ees _record : : ees record (EES PARAM REC * begin _init

) : begin ( begin _init )
{
}



// Return the l i s t length int ees _record : :
length ()
{
        EES PARAM REC * i _rec = begin ; int len = 0;

        while ( i rec != 0)
                {
                i rec = i rec >next ; len++;
                }

        return len ;
}


// Subscript operator to access the l i s t elements double& ees _record : : operator [ ] ( const int
i )
{
        EES PARAM REC * i _rec = begin ; int j = 0;

        while (j<i )
```

```
                {

                i _rec = i _rec >next ; j++;
                }


}       return          i _rec > value ;
```

```
#pragma warning( disable : 4996)
#include "mdm ees record .h"
#include "mdm ees.h"
#include <windows .h>
#include <math.h>
#include <stdio .h>
// Defines the entry point                          for the       dll
BOOL APIENTRY DllMain( HANDLE hModule ,
                       DWORD                ul reason for call ,
                       LPVOID lpReserved
                     )
{ return TRUE; }

// Tells EES which functions and procedures are exported in the library                                                    :
// List of DLF format functions declspec ( dllexport ) void DLFNames( char*
   Names)

      strcpy (Names, "h psx mdm , t psx mdm ,s ph mdm ,t ph mdm , ps t_mdm , ts p mdm ,
      h ptx mdm , s ptx mdm , rho ptx mdm ,v ptx mdm , cp ptx mdm , cv ptx mdm ,
      kinvis ptx mdm , thcon ptx mdm , hevap t_mdm") ;
}
```

```
--
 {
```

A.6.2 Property wrapper functions

A.6.2.1 Enthalpy $h(p,t,x)$ function code for MDM

```
#include "mdm ees record .h"
#include "mdm ees.h"
#include <windows .h>
#include <math.h>
#include "refprop .h"
#include <stdio .h>


declspec ( dllexport ) double h ptx mdm( char s [256] ,                                    int mode, EES PARAM REC *rec _in )


    ees _record        inputs ( rec in ) ;              // Use ees _record      class    for    convenience

  int NInputs = inputs . length () ;

  // refprop pointer inplementation fp INFOdllTYPE
     - INFOdll ; fp SETUPdllTYPE SETUPdll; fp
     - THERMdllTYPE THERMdll; fp TPRHOdllTYPE
     - TPRHOdll; fp TRNPRPdllTYPE TRNPRPdll; fp
     - TPFLSHdllTYPE TPFLSHdll; fp SATTdllTYPE
     - SATTdll;
     - HINSTANCE RefpropdllInstance ;

  // necessary variables for RefProp functions double x[ncmax] , xliq [ncmax] , xvap [ncmax]
  ,wm, ttp , tnbp , tc , pc , dc , zc , acf , dip , rgas ,d, ss , cv , cp ,w, t ,p, hjt , dl ,dv ,q , e ,h;


  long ierr , info _index=1,j=1,tmp _int=0, i =1; char *FLD PATH; char hf [ refpropcharlength*ncmax] ,
  hrf [ lengthofreference +1], herr [ errormessagelength +1],hfmix [ refpropcharlength +1];
1
2
3
4
5
6
7
8 --
9 {
10
11
12
13
14
15
16
17
18
19
20
21
22
23
24
25
26
27
28
29
30
31
32
33
```

```
//    load RefProp DLL
        RefpropdllInstance = LoadLibrary("C:\\Program Files \\REFPROP\\refprop . dll ") ;

//    efine          explicit          function          pointers
        INFOdll = (fp INFOdllTYPE) GetProcAddress( RefpropdllInstance , "INFOdll") ;
        SETUPdll = (fp SETUPdllTYPE) GetProcAddress( RefpropdllInstance , "SETUPdll") ;
        THERMdll = (fp THERMdllTYPE) GetProcAddress( RefpropdllInstance , "THERMdll") ;
        TPRHOdll = (fp TPRHOdllTYPE) GetProcAddress( RefpropdllInstance , "TPRHOdll") ;
        TRNPRPdll = (fp TRNPRPdllTYPE) GetProcAddress( RefpropdllInstance , "TRNPRPdll") ;
        TPFLSHdll = (fp TPFLSHdllTYPE) GetProcAddress( RefpropdllInstance , "TPFLSHdll") ;
        SATTdll = (fp SATTdllTYPE) GetProcAddress( RefpropdllInstance , "SATTdll") ;
//    set the           fluid         f i l e PATH
        FLD PATH = "C:\\Program Files \\REFPROP\\ fluids \\" ;


        strcpy _s (hf ,FLD PATH) ;
                  s (hfmix ,FLD PATH) ;
        strcpy _

                  s (hf , "mdm. fld ") ;
        strcpy _

                  s (hfmix , "hmx. bnc") ;
        strcpy _

                  s ( hrf , "DEF") ;
        strcpy _

                  s ( herr , "Ok") ;
        strcpy _

//
      all SETUPdll to i ni t ia l iz e the program SETUPdll( i , hf , hfmix , hrf , ierr
       , herr , refpropcharlength*ncmax, refpropcharlength , lengthofreference
       , errormessagelength ) ;

//    return          calling          syntax when mode ==          1


if    (mode== 1)

       { strcpy _s (s ,256 ,"h return
                                    (p;T;x)") ;
       0;
       }

//    check the number of                inputs


if    (NInputs!=3)

       { strcpy _s (s ,256 ,"h return
                                    (p;T;x) expects three                inputs       [ bar ;K; ] ") ;
       0;
       }

      i n it i al i ze              the fluid
//
       INFOdll( info _index ,wm, ttp , tnbp , tc , pc , dc , zc , acf , dip , rgas ) ;
//

p=inputs [0]*100;                  // pressure input                [kPa]
t=inputs [ 1 ] ;                   //temperature [K]


x[0   ]=1;

if    ( inputs [0] <0)
       {
       double h l , s l , cv l , cp l , h v , s v , cv v , cp v ;
       SATTdll (t ,x , i ,p, dl ,dv , xliq , xvap , ierr , herr , errormessagelength ) ;
       THERMdll(t , dl ,x ,p, e , h l , s l , cv l , cp l ,w, hjt ) ;
       THERMdll(t ,dv ,x ,p, e , h v , s v , cv v , cp v ,w, hjt ) ; h=h l+(h v h l )*inputs [ 2 ] ;
       }
```

```
        if     ( inputs [2]== 1)
                {
                TPFLSHdll(t ,p,x ,d, dl ,dv , xliq , xvap ,q , e ,h, ss , cv , cp ,w, ierr , herr , errormessagelength ) ;
                }

             if    ( inputs[2]==0 || inputs [2]==1)
                {
                j=long ( inputs [2]) +1;      //steam quality                 if                 necessary      in case of      f (p,T)          it                 is set to " 1"

                TPRHOdll(t ,p,x , j , tmp _int ,d, ierr , herr , errormessagelength ) ;
                THERMdll(t ,d,x ,p, e ,h, ss , cv , cp ,w, hjt ) ;
                }

                // unload the library
                FreeLibrary ( RefpropdllInstance ) ;
                //


        return (h/wm) ;                        //devide by molar mass ,                          return enthalpy           [ kJ/kg ]
}
```

A.6.2.2 Entropy $s(p,h,x)$ function code for MDM

```
    //          in i ti a li z e          the fluid

            INFOdll( info -index ,wm, ttp , tnbp , tc , pc , dc , zc , acf , dip , rgas ) ;
    //

    x[0]=1; //steam quality if necessary in case of f (p,T) it is set to " 1" h=inputs [1]*wm; //enthalpy kJ/kg p=inputs [0]*100; // pressure
    input [kPa]

        PHFLSHdll (p,h,x , tt ,dd , dl ,dv , xliq , xvap ,q , e , ss , cv , cp ,w, ierr , herr , errormessagelength ) ;

            // unload the library
            FreeLibrary ( RefpropdllInstance ) ;
            //

    return ( ss/wm) ;                       // entropy in          [ kJ/(Kg.K) ]
}
...
```

The header and code of all property functions are basically the same until the fluid initialisation. Therefore the following code snippets contain only relevant code after that point.

A.6.2.3 Entropy $s(p,t,x)$ function code for MDM

```
                                        uid
// i n it i al i ze the INFOdll( info_  ,wm, ttp , tnbp , tc , pc , dc , zc , acf , dip , rgas ) ;
//


p=inputs [0]*100;                       // pressure input                [kPa]
t=inputs [ 1 ] ;                        //temperature [K]


if     1;

      ( inputs [0] <0)
        {
        double h l , s l , cv l , cp l , h v , s v , cv v , cp v ;
        SATTdll (t ,x , i ,p, dl ,dv , xliq , xvap , ierr , herr , errormessagelength ) ;
        THERMdll(t , dl ,x ,p, e , h l , s l , cv l , cp l ,w, hjt ) ;
        THERMdll(t ,dv ,x ,p, e , h v , s v , cv v , cp v ,w, hjt ) ; ss=s l +(s v s l )*inputs [ 2 ] ;
        }


if
      ( inputs [2]== 1)
        {
        TPFLSHdll(t ,p,x ,d, dl ,dv , xliq , xvap ,q , e ,h, ss , cv , cp ,w, ierr , herr , errormessagelength ) ;
        }
  if    ( inputs[2]==0 || inputs [2]==1)
        {
        j=long ( inputs [2]) +1;     //steam quality              if              necessary     in case of     f (p,T)        it              is set to " 1"

        TPRHOdll(t ,p,x , j , tmp _int ,d, ierr , herr , errormessagelength ) ;
        THERMdll(t ,d,x ,p, e ,h, ss , cv , cp ,w, hjt ) ;
        }

        // unload the library
        FreeLibrary ( RefpropdllInstance ) ;
        //
return ( ss/wm) ;                       // entropy [ kJ/(kg .K) ]
```

A.6.2.4 Density $\rho(p,T,x)$ function code for MDM

```
    // i n it i al i ze the INFOdll( info
                                    uid
          -                         ,wm, ttp , tnbp , tc , pc , dc , zc , acf , dip , rgas ) ;
    //

    p=inputs [0]*100;               // pressure input              [kPa]
    t=inputs [ 1 ] ;                //temperature [K]


    if    1;
          ( inputs [0] <0)
            {
            double h l , s l , cv l , cp l , h v , s v , cv v , cp v ,v , vl , vv ;
            SATTdll (t ,x , i ,p, dl ,dv , xliq , xvap , ierr , herr , errormessagelength ) ;
            THERMdll(t , dl ,x ,p, e , h l , s l , cv l , cp l ,w, hjt ) ;
            THERMdll(t ,dv ,x ,p, e , h v , s v , cv v , cp v ,w, hjt ) ; vv=1/dv; vl=1/dl ;
            v=inputs [2]* vl +(1 inputs [2]) *vv ; d=1/v;
            }



    if
          ( inputs [2]== 1)
            {
            TPFLSHdll(t ,p,x ,d, dl ,dv , xliq , xvap ,q , e ,h, ss , cv , cp ,w, ierr , herr , errormessagelength ) ;
            }

    if                                                                                  in  case  of  f (p,T)  it  is
          ( inputs[2]==0 || inputs [2]==1)
            {
            j=long ( inputs [2]) +1; //steam quality if necessary set to " 1"

            TPRHOdll(t ,p,x , j , tmp _int ,d, ierr , herr , errormessagelength ) ;
            THERMdll(t ,d,x ,p, e ,h, ss , cv , cp ,w, hjt ) ;
            }

            // unload the library
            FreeLibrary ( RefpropdllInstance ) ;
            //

    return (d*wm) ;                 // density kg/m^3


}
```

1 . . .

A.6.2.5 Kinematic viscosity *kinvis*(*p,t,x*) function of MDM

```
#include "mdm ees record .h"

#include "mdm _ees.h"

#include <windows .h>

#include <math.h>

#include "refprop .h"

#include <stdio .h>

declspec ( dllexport ) double kinvis ptx mdm( char s [256] , int mode, EES PARAM REC *rec _in )
                                                                    class for convenience
    ees _record inputs ( rec _in ) ;                    // Use ees _record

    int NInputs = inputs . length () ;

    // refprop pointer inplementation fp INFOdllTYPE
        INFOdll ; fp SETUPdllTYPE SETUPdll; fp
        THERMdllTYPE THERMdll; fp TPRHOdllTYPE
        TPRHOdll; fp TRNPRPdllTYPE TRNPRPdll; fp
        TPFLSHdllTYPE TPFLSHdll; fp SATTdllTYPE
        SATTdll;
        HINSTANCE RefpropdllInstance ;

    // necessary variables for RefProp functions double x[ncmax] , xliq [ncmax] , xv
    [ncmax] ,wm, ttp , tnbp ,
            tc , pc , dc , zc , acf , dip , rgas ,d, ss , cv , cp ,w, t ,p, dl ,dv ,q , e ,h, eta , tcx ;

    long ierr , info _index=1,j=1,tmp _int=0, i =1; char *FLD PATH;

--
{
```

```
char hf [ refpropcharlength*ncmax] , hrf [ lengthofreference +1], herr [ errormessagelength +1],hfmix [
        refpropcharlength +1];


// load RefProp DLL
        RefpropdllInstance = LoadLibrary("C:\\Program Files \\REFPROP\\refprop . dll ") ;

//Define          explicit        function        pointers
        INFOdll = (fp INFOdllTYPE) GetProcAddress( RefpropdllInstance , "INFOdll") ;
        SETUPdll = (fp SETUPdllTYPE) GetProcAddress( RefpropdllInstance , "SETUPdll") ;
        THERMdll = (fp THERMdllTYPE) GetProcAddress( RefpropdllInstance , "THERMdll") ;
        TPRHOdll = (fp TPRHOdllTYPE) GetProcAddress( RefpropdllInstance , "TPRHOdll") ;
        TRNPRPdll = (fp TRNPRPdllTYPE) GetProcAddress( RefpropdllInstance , "TRNPRPdll") ;
        TPFLSHdll = (fp TPFLSHdllTYPE) GetProcAddress( RefpropdllInstance , "TPFLSHdll") ;
        SATTdll = (fp SATTdllTYPE) GetProcAddress( RefpropdllInstance , "SATTdll") ;

// set the              fluid       f i l e PATH
        FLD PATH = "C:\\Program Files \\REFPROP\\ fluids \\" ;

        strcpys (hf     _   ,FLD PATH) ; strcpys
        (hfmix ,FLD     _   PATH) ; strcpys (hf ,
        "mdm. fld ") ;  _   strcpys (hfmix , "hmx.
        bnc") ;         _   strcpys ( hrf , "DEF") ;
        strcpys ( herr  _   , "Ok") ;


// . . . Call SETUPdll to i ni t ia l iz e the program SETUPdll( i , hf , hfmix , hrf ,
        ierr    ,   herr    ,   refpropcharlength*ncmax,    refpropcharlength   ,
        lengthofreference , errormessagelength ) ;

// Return calling syntax when mode == 1 if (mode== 1)
        {
        strcpy _s (s ,256 ," kinetic viscosity (p;T;x)") ; return 0;
        }

// Check the number of inputs if (NInputs!=3)
        {
        strcpy _s (s ,256 ," (p;T;x) needs three inputs [ bar ;K; ] ") ; return 0;
        }


//          i n it i al i ze        the fluid

        INFOdll( info _index ,wm, ttp , tnbp , tc , pc , dc , zc , acf , dip , rgas ) ;
//


p=inputs [0]*100;                       // pressure input          [kPa]
t=inputs [ 1 ] ;                        //temperature [K]
x[0]=1;

if      ( inputs [0] <0)
        {
        double h l , s l , cv l , cp l , h v , s v , cv v , cp v , hjt ;
        SATTdll (t ,x , i ,p, dl ,dv , xliq , xvap , ierr , herr , errormessagelength ) ;
        THERMdll(t , dl ,x ,p, e , h l , s l , cv l , cp l ,w, hjt ) ;
        THERMdll(t ,dv ,x ,p, e , h v , s v , cv v , cp v ,w, hjt ) ;
        }

if      ( inputs [2]== 1)
        {
        TPFLSHdll(t ,p,x ,d, dl ,dv , xliq , xvap ,q , e ,h, ss , cv , cp ,w, ierr , herr , errormessagelength ) ;
        } if    ( inputs[2]==0 || inputs [2]==1)
        {
        j=long ( inputs [2]) +1;            //steam quality           if          necessary   in case of  f (p,T)     it          is set
                to " 1"

        TPRHOdll(t ,p,x , j , tmp _int ,d, ierr , herr , errormessagelength ) ; }

        TRNPRPdll (t ,d,x , eta , tcx , ierr , herr , errormessagelength ) ;
```

```
        // unload the library
        FreeLibrary ( RefpropdllInstance ) ;
        //

    return ( eta*10E 6 ) ;                          // return kinematic
}                                                                   viscosity       [ Pa . s      >Pa. s ]
106 107
108
109
110
111
112
113
```

A.6.2.6 Enthalpy of evaporation $h_{evap}(T)$ function code of MDM

```
    //      i n it i al i ze        the fluid

        INFOdll( info _index ,wm, ttp , tnbp , tc , pc , dc , zc , acf , dip , rgas ) ;
    //


    //x[0]= inputs [ 2 ] ;                        //steam quality       if      necessary           in case   of    f (p,T)     it    is    set    to
          " 1"
    //p=inputs   [0]*100;  //pressure   input   [kPa]   t=inputs   [   0   ]   ;
    //temperature [K] x[0]=1;
    i =2;
    SATTdll(t ,x , i ,p, dl ,dv , xliq , xvap , ierr , herr , errormessagelength ) ; THERMdll(t ,dv ,x ,p, e v , h v , s v , cv
    v , cp v ,w, hjt ) ; i =1;
    SATTdll(t ,x , i ,p, dl ,dv , xliq , xvap , ierr , herr , errormessagelength ) ;
    THERMdll(t , dl ,x ,p, e l , h l , s l , cv l , cp l ,w, hjt ) ;



        // unload the library
        FreeLibrary ( RefpropdllInstance ) ;
        //

    return (( h v           h l )/wm) ;             // return enthalpy in          [ kJ/kg ]

}
1 . . .
2
3
4
5
6
7

8
9
10
11
12
13
14
15
16
17
18
19
20
21
22
23
24
25
```

A.6.2.7 Saturation temperature $T_{sat}(p)$ function code of MDM

```
#include "mdm ees record .h"
#include "mdm ees.h"
#include <windows .h>
#include <math.h>
#include "refprop .h"
#include <stdio .h>


declspec ( dllexport ) double ts p mdm( char s [256] ,                                    int mode, EES PARAM REC *rec _in )

    ees _record    inputs ( rec in ) ;                  // Use ees _record    class    for    convenience

  int NInputs = inputs . length () ;

  // refprop pointer inplementation fpINFOdllTYPE INFOdll
    -   ; fp  SETUPdllTYPE  SETUPdll;  fpSATPdllTYPE
    -   SATPdll ;
    -
   HINSTANCE RefpropdllInstance ;

  // necessary variables for RefProp functions double x[ncmax] ,wm, ttp , tnbp , tc , pc , dc , zc , acf , dip , rgas , dl ,dv , xliq [ncmax] , xvap [ncmax] , ts ,p;


  long ierr , info _index=1,j=1,tmp _int=0, i =1; char *FLD PATH; char hf [ refpropcharlength*ncmax] ,
  hrf [ lengthofreference +1], herr [ errormessagelength +1],hfmix [ refpropcharlength +1];


  // load RefProp DLL
```

```
        RefpropdllInstance = LoadLibrary("C:\\Program Files \\REFPROP\\refprop . dll ") ;

    //Define          explicit        function        pointers
        INFOdll             = (fp INFOdllTYPE)                  GetProcAddress( RefpropdllInstance , "INFOdll") ;
        SETUPdll            = (fp SETUPdllTYPE)                 GetProcAddress( RefpropdllInstance , "SETUPdll") ;
      SATPdll = (fp SATPdllTYPE) GetProcAddress( RefpropdllInstance , "SATPdll") ;

    // set the             fluid       f i l e PATH
      FLD PATH = "C:\\Program Files \\REFPROP\\ fluids \\" ;


        strcpy_s (hf ,FLD PATH) ;
                 s (hfmix ,FLD PATH) ;
        strcpy_
                 s (hf , "mdm. fld ") ;
        strcpy_
                 s (hfmix , "hmx. bnc") ;
        strcpy_
                 s ( hrf , "DEF") ;
        strcpy_
                 s ( herr , "Ok") ;
        strcpy_



    // . . . Call SETUPdll to i ni t ia l iz e the program SETUPdll( i , hf , hfmix , hrf ,
        ierr    ,   herr    ,   refpropcharlength*ncmax,    refpropcharlength   ,
        lengthofreference , errormessagelength ) ;

    // Return calling              syntax when mode ==         1
    if      (mode== 1)
        { strcpy_s (s ,256 ,"Ts                 (p)") ;
        return 0;
        }

    // Check the number of             inputs
    if      (NInputs!=1)
        { strcpy_s (s ,256 ,"Ts                 (p) expects one             input       [ bar ] ") ;
        return 0;
        }


    //      i n it i al i ze        the fluid

        INFOdll ( info_index ,wm, ttp , tnbp , tc , pc , dc , zc , acf , dip , rgas ) ;
    //

    p=inputs [0]*100;                       //pressure          [ bar >kPa]

    SATPdll (p,x , i , ts , dl ,dv , xliq , xvap , ierr , herr , errormessagelength ) ;

        // unload the library
        FreeLibrary ( RefpropdllInstance ) ;
        //

    return ( ts ) ;                             // saturation temperature [K]
}
```

A.6.2.8 Saturation pressure p(T) function code for MDM

```
#include "mdm ees record .h"

#include "mdm _ees.h"
#include <windows .h>
#include <math.h>
#include "refprop .h"
#include <stdio .h>

declspec ( dllexport ) double t psx mdm( char s [256] , int mode, EES PARAM REC *rec _in )
ees _record inputs ( rec _in ) ; // Use ees _record class for convenience
int NInputs = inputs . length () ;
// refprop pointer inplementation fpINFOdllTYPE INFOdll
_ ; fp SETUPdllTYPE SETUPdll; fp PSFLSHdllTYPE
_ PSFLSHdll ;
```

```
1
2
3
4
5
6
7
8 --
9 {
10
11
12
13
14
15
16
17
```

```
18
19      HINSTANCE RefpropdllInstance;
20
21      // necessary variables for RefProp functions
22      double x[ncmax],wm,ttp,tnbp,tc,pc,dc,zc,acf,dip,rgas,ss,e,h_,
23             cv,cp,w,p,tt,dd,dl,dv,xliq[ncmax],xvap[ncmax],q;
24
25      long ierr,info_index=1,j=1,tmp_int=0,i=1;
26      char *FLD PATH;
27      char hf[refpropcharlength*ncmax], hrf[lengthofreference+1],
28           herr[errormessagelength+1],hfmix[refpropcharlength+1];
29
30
31      // load RefProp DLL
32           RefpropdllInstance = LoadLibrary("C:\\Program Files\\REFPROP\\refprop.dll");
33
34      //Define explicit function pointers
35           INFOdll = (fp_INFOdllTYPE) GetProcAddress(RefpropdllInstance,"INFOdll");
36           SETUPdll = (fp_SETUPdllTYPE) GetProcAddress(RefpropdllInstance,"SETUPdll");
37           PSFLSHdll = (fp_PHFLSHdllTYPE) GetProcAddress(RefpropdllInstance,"PHFLSHdll");
38
39      // set the fluid file PATH
40           FLD PATH = "C:\\Program Files\\REFPROP\\fluids\\";
41
42           strcpy_s(hf,FLD PATH);
43           strcpy_s(hfmix,FLD PATH);
44           strcpy_s(hf,"mdm.fld");
45           strcpy_s(hfmix,"hmx.bnc");
46           strcpy_s(hrf,"DEF");
47           strcpy_s(herr,"Ok");
48
49
50      //...Call SETUPdll to initialize the program
51           SETUPdll(i, hf, hfmix, hrf, ierr, herr,
52           refpropcharlength*ncmax,refpropcharlength,
53           lengthofreference,errormessagelength);
54
55      // Return calling syntax when mode == 1
56      if (mode==1)
57           {
58           strcpy_s(s,256,"T (p;s;x)");
59           return 0;
60           }
61
62      // Check the number of inputs
63      if (NInputs!=3)
64           {
65           strcpy_s(s,256,"T (p;s;x) expects three inputs [bar;kJ/(kg.K); ]");
66           return 0;
67           }
68
69
70      //  initialize the fluid
71           INFOdll(info_index,wm,ttp,tnbp,tc,pc,dc,zc,acf,dip,rgas);
72      //
73
74      x[0]=inputs[2];      //steam quality if necessary   in case of f(p,T) it is set to "1"
75      ss=inputs[1]*wm;          //entropy [kJ/(kg.K)]
76      p=inputs[0]*100;     //pressure input [kPa]
77
78        //PHFLSHdll (p,h,x,tt,dd,dl,dv,xliq,xvap,q,e,s_,cv,cp,w,ierr,herr,errormessagelength);
79
80        PSFLSHdll (p,ss,x,tt,dd,dl,dv,xliq,xvap,q,e,h_,cv,cp,w,ierr,herr,errormessagelength);
81
82
83           // unload the library
84           FreeLibrary(RefpropdllInstance);
85           //
86
87      return (tt);     // temperature [K]
88 }
```

A.6.2.9 Specific volume *v*(*p*,*t*,*x*) function code of MDM

```
//          i n it i al i ze              the uid
                                          :x ,wm, ttp , tnbp , tc , pc , dc , zc , acf , dip , rgas ) ;
                    INFOdll( info _ind
//
                                          // pressure input                [kPa]
p=inputs [0]*100;
t=inputs [ 1 ] ;                          //temperature [K]


if     1;

      ( inputs [0] <0)
        {
        double h l , s l , cv l , cp l , h v , s v , cv v , cp v ,v , vl , vv ;
        SATTdll (t ,x , i ,p, dl ,dv , xliq , xvap , ierr , herr , errormessagelength ) ;
        THERMdll(t , dl ,x ,p, e , h l , s l , cv l , cp l ,w, hjt ) ;
        THERMdll(t ,dv ,x ,p, e , h v , s v , cv v , cp v ,w, hjt ) ; vv=1/dv; vl=1/dl ;
        v=inputs [2]* vl +(1 inputs [2]) *vv ; d=1/v;
        }



if     ( inputs [2]== 1)
        {
        TPFLSHdll(t ,p,x ,d, dl ,dv , xliq , xvap ,q , e ,h, ss , cv , cp ,w, ierr , herr , errormessagelength ) ;
        }
   if     ( inputs[2]==0 || inputs [2]==1)
        {
        j=long ( inputs [2]) +1;     //steam quality              if              necessary     in case of     f (p,T)          it              is set to " 1"

        TPRHOdll(t ,p,x , j , tmp _int ,d, ierr , herr , errormessagelength ) ;
        THERMdll(t ,d,x ,p, e ,h, ss , cv , cp ,w, hjt ) ;
        }

        // unload the library
        FreeLibrary ( RefpropdllInstance ) ;
        //

return 1/(d*wm) ;                         // spec . volume m^3/kg


}
```

A.6.2.10 Thermal conductivity k(p,T,x) function code for MDM

```
#include "mdm ees record .h"
#include "mdm ees.h"
#include <windows .h>
#include <math.h>
#include "refprop .h"
#include <stdio .h>

                declspec ( dllexport ) double thcon ptx mdm( char s [256] ,                                    int mode, EES PARAM REC *rec _in )

    ees _record          inputs ( rec _in ) ;                    // Use ees _record          class     for     convenience

    int NInputs = inputs . length () ;

    // refprop pointer inplementation fp INFOdllTYPE
        - INFOdll ; fp SETUPdllTYPE SETUPdll; fp
        - THERMdllTYPE THERMdll; fp TPRHOdllTYPE
        - TPRHOdll; fp TRNPRPdllTYPE TRNPRPdll; fp
        - TPFLSHdllTYPE TPFLSHdll; fp SATTdllTYPE
        -
        - SATTdll;
        - HINSTANCE RefpropdllInstance ;

    // necessary variables for RefProp functions double x[ncmax] , xliq [ncmax] , xvap
    [ncmax] ,wm, ttp , tnbp ,
            tc , pc , dc , zc , acf , dip , rgas ,d, ss , cv , cp ,w, t ,p, dl ,dv ,q , e ,h, eta , tcx ,
            hjt ;


    long ierr , info _index=1,j=1,tmp _int=0, i =1; char *FLD PATH; char hf [ refpropcharlength*ncmax] ,
    hrf [ lengthofreference +1],
--
{
```

```
27
28
29
30
31
32                herr [ errormessagelength +1],hfmix [ refpropcharlength +1];
```

```
// load RefProp DLL
        RefpropdllInstance = LoadLibrary("C:\\Program Files \\REFPROP\\refprop . dll ") ;

//Define              explicit          function          pointers
        INFOdll = (fp INFOdllTYPE) GetProcAddress( RefpropdllInstance , "INFOdll") ;
        SETUPdll = (fp SETUPdllTYPE) GetProcAddress( RefpropdllInstance , "SETUPdll") ;
        THERMdll = (fp THERMdllTYPE) GetProcAddress( RefpropdllInstance , "THERMdll") ;
        TPRHOdll = (fp TPRHOdllTYPE) GetProcAddress( RefpropdllInstance , "TPRHOdll") ;
        TRNPRPdll = (fp TRNPRPdllTYPE) GetProcAddress( RefpropdllInstance , "TRNPRPdll") ;
        TPFLSHdll = (fp TPFLSHdllTYPE) GetProcAddress( RefpropdllInstance , "TPFLSHdll") ;
        SATTdll = (fp SATTdllTYPE) GetProcAddress( RefpropdllInstance , "SATTdll") ;

// set the              fluid        f i l e PATH
        FLD PATH = "C:\\Program Files \\REFPROP\\ fluids \\" ;

        strcpys (hf      _    ,FLD PATH) ; strcpys
        (hfmix ,FLD      _    PATH) ; strcpys (hf ,
        "mdm. fld ") ;   _    strcpys (hfmix , "hmx.
        bnc") ;          _    strcpys ( hrf , "DEF") ;
        strcpys ( herr   _    , "Ok") ;


// . . . Call SETUPdll to i ni t ia l iz e the program SETUPdll( i , hf , hfmix , hrf ,
        ierr   ,   herr   ,   refpropcharlength*ncmax,   refpropcharlength   ,
        lengthofreference , errormessagelength ) ;

// Return calling syntax when mode == 1 if (mode== 1)

        { strcpy_s (s ,256 ,"alpha (p;T;x)") ; return 0;
        }

// Check the number of inputs if (NInputs!=3)
        {

        strcpy_s (s ,256 ,"alpha (p;T;x) expects three inputs [ bar ;K; ] ") ; return 0;
        }


//          i n it i al i ze          the fluid

        INFOdll( info_index ,wm, ttp , tnbp , tc , pc , dc , zc , acf , dip , rgas ) ;
//

p=inputs [0]*100;                       // pressure input          [kPa]
t=inputs [ 1 ] ;                        //temperature [K]
x[0]=1;

if        ( inputs [0] <0)
        {
        double h l , s l , cv l , cp l , h v , s v , cv v , cp v ;
        SATTdll (t ,x , i ,p, dl ,dv , xliq , xvap , ierr , herr , errormessagelength ) ;
        THERMdll(t , dl ,x ,p, e , h l , s l , cv l , cp l ,w, hjt ) ;
        THERMdll(t ,dv ,x ,p, e , h v , s v , cv v , cp v ,w, hjt ) ;
        }

if          ( inputs [2]== 1)
        {
        TPFLSHdll(t ,p,x ,d, dl ,dv , xliq , xvap ,q , e ,h, ss , cv , cp ,w, ierr , herr , errormessagelength ) ;
        } if      ( inputs[2]==0 || inputs [2]==1)
        {
        j=long ( inputs [2]) +1;            //steam quality          if          necessary     in case of     f (p,T)       it          is set
                to " 1"

        TPRHOdll(t ,p,x , j , tmp_int ,d, ierr , herr , errormessagelength ) ;
        }
```

```
102
103
104                         TRNPRPdll (t ,d,x , eta , tcx , ierr , herr , errormessagelength ) ;
105
106             // unload the library
107             FreeLibrary ( RefpropdllInstance ) ;

        return      ( tcx ) ;               //  return      thermal      conductivity          in    [W/(m.K) ]


}
108             //
109
110
111
112
```

A.6.2.11 Temperature T(p,h,x) function code for MDM

```
#include "mdm ees record .h"
#include "mdm ees.h"
#include <windows .h>
#include <math.h>
#include "refprop .h"
#include <stdio .h>

declspec ( dllexport ) double t ph mdm( char s [256] , int mode, EES PARAM REC *rec _in )
{

ees _record inputs ( rec in ) ; // Use ees _record class for convenience

int NInputs = inputs . length () ;

// refprop pointer inplementation fpINFOdllTYPE INFOdll
– ; fp SETUPdllTYPE SETUPdll; fp PHFLSHdllTYPE
– PHFLSHdll;
–
HINSTANCE RefpropdllInstance ;

// necessary variables for RefProp functions double x[ncmax] ,wm, ttp , tnbp , tc , pc , dc , zc , acf , dip

, rgas , s _ , e ,h, cv , cp ,w,p, tt ,dd , dl ,dv , xliq [ncmax] , xvap [ncmax] ,q;

long ierr , info _index=1,j=1,tmp _int=0, i =1; char *FLD PATH; char hf [ refpropcharlength*ncmax] ,
hrf [ lengthofreference +1], herr [ errormessagelength +1],hfmix [ refpropcharlength +1];

// load RefProp DLL
RefpropdllInstance = LoadLibrary("C:\\Program Files \\REFPROP\\refprop . dll ") ;

//Define explicit function pointers
INFOdll = (fp INFOdllTYPE) GetProcAddress( RefpropdllInstance , "INFOdll") ;
SETUPdll = (fp SETUPdllTYPE) GetProcAddress( RefpropdllInstance , "SETUPdll") ;
PHFLSHdll = (fp PHFLSHdllTYPE) GetProcAddress( RefpropdllInstance , "PHFLSHdll") ;

// set the fluid f i l e PATH
FLD PATH = "C:\\Program Files \\REFPROP\\ fluids \\" ;

– strcpys (hf ,FLD PATH) ;
– strcpys (hfmix ,FLD PATH) ;
– strcpys (hf , "mdm. fld ") ;
– strcpys (hfmix , "hmx. bnc") ;
– strcpys ( hrf , "DEF") ;
– strcpys ( herr , "Ok") ;

// . . . Call SETUPdll to i ni t ia l iz e the program SETUPdll( i , hf , hfmix , hrf ,
ierr , herr , refpropcharlength*ncmax, refpropcharlength ,
lengthofreference , errormessagelength ) ;

// Return calling syntax when mode == 1 if (mode== 1)

{ strcpy _s (s ,256 ,"T (p;h)") ; return 0;
}
```

```
6
7


10



15
16
17

19


23



28


32


35
36
37


40

42
43
44
45
46
47


51
52
53



58


// Check the number of inputs if (NInputs!=2)
 {

 65 strcpy_s (s ,256 ,"T (p;h;x) expects two inputs [ bar ; kJ/kg ] ") ; return 0;
```

```
            }

    //          i n it i al i ze          the fluid

            INFOdll( info _index ,wm, ttp , tnbp , tc , pc , dc , zc , acf , dip , rgas ) ;
    //

    x[0]=1;                                     //steam quality      if      necessary          in case of      f (p,T)     it     is          set to " 1"
    h=inputs [1]*wm;                    //enthalpy kJ/kg


    p=inputs [0]*100;                   // pressure input          [kPa]



        PHFLSHdll (p,h,x , tt ,dd , dl ,dv , xliq , xvap ,q , e , s _ , cv , cp ,w, ierr , herr , errormessagelength ) ;

            // unload the library
            FreeLibrary ( RefpropdllInstance ) ;
            //

}   return ( tt ) ;                     // temperature [K]
```

A.6.2.12 Temperature T(p,s,x) function code for MDM

```
#include "mdm ees record .h"
#include "mdm ees.h"
#include <windows .h>
#include <math.h>
#include "refprop .h"
#include <stdio .h>

declspec ( dllexport ) double t psx mdm( char s [256] ,          int mode, EES PARAM REC *rec _in )
{

  ees _record      inputs ( rec in ) ;        // Use ees _record   class   for   convenience

  int NInputs = inputs . length () ;

  // refprop pointer inplementation fpINFOdllTYPE INFOdll
   _   ; fp SETUPdllTYPE SETUPdll; fpPSFLSHdllTYPE
   _   PSFLSHdll ;
   _
  HINSTANCE RefpropdllInstance ;

  // necessary variables for RefProp functions double x[ncmax] ,wm, ttp , tnbp , tc , pc , dc , zc , acf , dip ,

  rgas , ss , e , h _ , cv , cp ,w,p, tt ,dd , dl ,dv , xliq [ncmax] , xvap [ncmax] ,q;


  long ierr , info _index=1,j=1,tmp _int=0, i =1; char *FLD PATH;
  char hf [ refpropcharlength*ncmax] , hrf [ lengthofreference +1], herr [ errormessagelength +1],hfmix [
        refpropcharlength +1];


  // load RefProp DLL
        RefpropdllInstance = LoadLibrary("C:\\Program Files \\REFPROP\\refprop . dll ") ;

    //Define     explicit     function     pointers
        INFOdll = (fp INFOdllTYPE) GetProcAddress( RefpropdllInstance , "INFOdll") ;
        SETUPdll = (fp SETUPdllTYPE) GetProcAddress( RefpropdllInstance , "SETUPdll") ;
        PSFLSHdll = (fp PHFLSHdllTYPE) GetProcAddress( RefpropdllInstance , "PHFLSHdll") ;

     // set the     fluid     f i l e PATH
        FLD PATH = "C:\\Program Files \\REFPROP\\ fluids \\" ;

                 _   strcpys (hf ,FLD PATH) ;
                 _   strcpys (hfmix ,FLD PATH) ;
                 _   strcpys (hf , "mdm. fld ") ;
                 _   strcpys (hfmix , "hmx. bnc") ;
        strcpy s ( hrf , "DEF") ;
```

```
19
23
28
32
35
36
37
40
42
43
44
45
46
47                  strcpy_s ( herr , "Ok") ;

                // . . . Call SETUPdll to  i ni t ia l iz e  the program
51              SETUPdll( i , hf , hfmix ,  hrf ,  ierr , herr ,
52              refpropcharlength*ncmax, refpropcharlength ,
```

```
53                lengthofreference , errormessagelength ) ;
54
55            // Return calling                syntax when mode ==          1
56        if    ( mode  ==1)
57              {
58              strcpy     -s (s ,256 ,     "T   ( p ; s ; x)  " ) ;
59              return      0 ;
60              }
61
62        //   Check     the    number     of    inputs
63        if    ( NInputs     !=3)
64              {
65              strcpy     -s (s ,256 ,     "T   ( p ; s ; x)    expects      three      inputs      [ bar   ; kJ   /( kg  .K)   ; ]   " ) ;
66              return      0 ;
67              }
68
69
70        //     i n it i al i ze        the     flu   id
71              INFOdll( info         -ind   ex ,wm, ttp , tnbp , tc , pc , dc , zc , acf , dip , rgas ) ;
72        //
73
74        x[0]= inputs [ 2 ] ;                  //steam       quality        if     necessary             in     case     of    f ( p ,T)     it     is     set     to     " 1"
75        ss=inputs [1]         * wm;                  // entropy       [ kJ   /( kg  .K)   ]
76        p=inputs [0]        * 100   ;         // pressure        input       [ kPa   ]
77
78           //PHFLSHdll         ( p , h , x , tt   , dd  , dl  , dv  , xliq    , xvap    , q , e , s - , cv  , cp  ,w,   ierr    , herr    , errormessagelength            ) ;
79
80           PSFLSHdll (p, ss ,x , tt ,dd , dl ,dv , xliq , xvap ,q , e , h                                  - , cv , cp ,w, ierr , herr , errormessagelength ) ;
81
82
83              //   unload      the     library
84              FreeLibrary ( RefpropdllInstance ) ;
85              //
86
87        return      ( tt ) ;          //    temperature         [K ]
88  }
```

A.7 Code of cycle components (VBA)

A.7.1 Feed pump

```
Function pump001 _p(V As Double , n As Double) As Double Dim n ref As Double


 n ref = 1450

A =              0.0000411995
B =              0.000989611
C =          0.01732591
l = 16.22951399

             -    pump001p = A * V ^ 3 + B * V ^ 2 + C * V + d
             -
                  pump001 p = pump001 _p * (n ^ 2) * ( n _ref ^                2)

End Function
```

```
9

11
12
13
14
15
```

```
Function pump001 _eta(V As Double , n As Double) As Double Dim n ref As Double


 n ref = 1450

A = 0.000850366
B =            0.124628028
C  =  5.489142766  10  d  =
08277477
```

```
1
2
3
4
5
6

8
11
12  pump001eta = A ∗ V ^ 3 + B ∗ V ^ 2 + C ∗ V + d
                _
13  pump001_eta = pump001 _eta ∗ (n ^ 1) ∗ ( n _ref ^   1)
14
15 End Function
```

```
Public Function eta s ( p in As Double , p _out As Double) As Double

Dim A As Double Dim B As
Double Dim C As Double Dim
D As Double Dim E As Double
Dim beta As Double

beta = p in / p out

            A = 0.9649
            B = 112.9 C = 4.811
            D  =              0.002609
            E  = 0.7741


        eta _s = A ∗ Atn(B / beta ^ 2 + C / beta ) + D ∗ beta + E

End Function
```

```
1
2
3
4
5
6
7
8
9
10
11
12
13
```

```
14
15
16
17
18
19
20
```

```
Function turbine(p_in As Double, T_in As Double, p_out As Double) As Variant

Dim temp(7) As Variant
Dim eta_is As Double
Dim u As Double
Dim m_turb As Double
Dim r_s As Double
Dim rho As Double
Dim A_exit As Double
Dim V As Double
Dim h_in As Double
Dim s_in As Double
Dim h_out As Double
Dim dh As Double
Dim dh_s As Double
Dim h_out_s As Double
Dim P_mech As Double
Dim v_exit As Double

r_s = p_out / p_in

u = 80

h_in = h_ptx(p_in, T_in, 1)

s_in = s_ptx(p_in, T_in, 1)

T_s = t_ps(p_out, s_in)

h_out_s = h_ptx(p_out, T_s, 1)

dh_s = h_in   h_out_s

rho = rho_ptx(p_in, T_in, 1)

V = v_ptx(p_out, T_in   20, 1)

A_exit = 0.057 * 0.0375 * 25

m_turb = k_t * (rho * p_in * 100000) ^ 0.5 * (1   r_s ^ 1.9137) ^ 0.5

C = m_turb * V / A_exit

eta_is = eta_s(p_in, p_out)

2
```

```
23
25
27
29
31
33
35
37
39
46 h -out=h        -in        eta   -is   *   dh -s
47
48 dh=h       -in        h -out
50 P -mech=dh         *   m -turb
52 v -exit = m        -turb / A       -exit / rho        -ptx (p    -out ,      1 ,   1)
54 temp(0) = h         -out
55 temp(1) = t         -ph (p   -out , h      -out )
56 temp(2) = dh          -s
57 temp(3) = dh
58 temp(4) = m         -turb
59 temp(5) = P         -mech
60 temp(6) = eta           -is
61
62 turbine = temp
63
64 End    Function
41
43
49
51
53
```

A.8 Code of cycle components (modelica)

Can be downloaded under: https://sourceforge.net/projects/ thesis-shp-orc/files/

A.9 Definitions of characteristic numbers

Darcy-Weisbach friction factor:

$$f_{DW} = \frac{2 \times \Delta p \times D}{L \times \rho \times v^2} \tag{A.13}$$

Fanning friction factor:

$$C_F = \frac{2 \times \tau}{\rho \times v^2} \tag{A.14}$$

Boiling number:

$$Bo = \frac{g \times (\rho_l - \rho_v) \times L^2}{\sigma} \tag{A.15}$$

Grashof number:

$$Gr = \frac{g \times \beta\,(T_s - T_\infty) \times L^3}{\nu^2} \tag{A.16}$$

modified Nusselt number for condensation on tubes:

$$Nu_{mod} = \frac{\bar{\alpha}_{film} \times \left(\nu_{film}^2 / g\right)^{(1/3)}}{\lambda_{film}} \tag{A.17}$$

Reynolds number for condensing film:

$$Re_{film} = \frac{4 \times \Gamma\,(y)}{\mu_{liq}} \tag{A.18}$$

Appendix B

Publications of the author

B.1 Books

- Eicker U. (Ed.)
  POLYCITY - Energy Networks in Sustainable Cities, Karl Kr¨amer Verlag Stuttgart, 2012 (co-author)

B.2 Conference publications

- Eicker U. and Strzalka A. and Erhart T.G.
  Energy efficient buildings and renewable supply within the German POLY-CITY project,
  Proceedings of Polycity Final Conference, Stuttgart, Germany, 2010

- Eicker U. and Strzalka A. and Erhart T.G.
  Energy efficient buildings and renewable supply within the German POLY-CITY project,
  Proceedings of POLYCITY Final Conference, Stuttgart, 2010

- Erhart T. and Strzalka R. and Eicker U. and Infield D.
  Performance Analysis of a Biomass ORC Poly-generation System,
  2nd European Conference on Poly-generation, 2011

- Erhart T. and Eicker U. and Infield D.
  Part-load characteristics of Organic-Rankine-Cycles, 2nd European Conference on Poly-generation, 2011

- Vanslambrouck B. and Guseva S. and Erhart T. and De Paepe M. and van den Broek M.

  Waste heat recovery via Organic Rankine Cycle: Results of a ERA-SME

Technology Transfer Project, International ASME-ORC Power Systems Seminar 2013, 2013

- Erhart T. and van den Broek M. and Eicker U.
  Dynamic models of a heat-led Organic Rankine Cycle, International ASMEORC Power Systems Seminar 2013, 2013

- Tobias Erhart and Ju¨rgen G¨olz and Ursula Eicker and Martijn van den Broek
  Fluid stability in large scale ORCs using Siloxanes Long-term experiences and fluid recycling
  The 3rd International Seminar on ORC Power Systems (ASME ORC 2015), Brussels, Belgium, 2015

B.3 Conference presentations

- Erhart T.G. and Eicker U. and Infield D.
  Part-load characteristics of Organic-Rankine-Cycles,
  2nd European Conference on Poly-generation, Taragona, Spain, 2011

- Erhart T.G. and Eicker U. and Infield D.
  Influence of Condenser Conditions on Organic-Rankine-Cycle Load Characteristics,
  First International Seminar on ORC Power Systems, Kortijk, Belgium, 2011

- Erhart T.G.
  Dynamic simulation of OR-cycles
  Waste Heat Valorisation Symposium 2012, Kortrijk, Belgium, 2012

- Erhart T.G. and van den Broek M. and Eicker U.
  Dynamic models of a heat-led Organic Rankine Cycle,
  International ASME-ORC Power Systems Seminar, Rotterdam, Netherlands, 2013

- Vanslambrouck B. and Guseva S. and Erhart T. and De Paepe M. and van den Broek M.
  Waste heat recovery via Organic Rankine Cycle: Results of a ERA-SME Technology Transfer Project,

International ASME-ORC Power Systems Seminar, Rotterdam, Netherlands, 2013

- Tobias Erhart
  Fluid stability in large scale ORCs using Siloxanes Long-term experiences and fluid recycling
  The 3rd International Seminar on ORC Power Systems (ASME ORC 2015), Brussels, Belgium, 2015

B.4 Poster presentations

- Erhart T.G. and Benhassine I. and Strzalka R.
  Polycity Final Conference 2010, Stuttgart, Germany, 2010

- Erhart T.G. and Strzalka R. and Eicker U. and Infield D.
  Performance Analysis of a Biomass ORC Poly-generation System, 2nd European Conference on Polygeneration, Taragona, Spain, 2011

- Erhart T.G. and Infield D. and Eicker U.
  Performance analysis of an Organic-Rankine-Cycle co-generation unit, Glasgow Research Partnership in Engineering (GRPe), Ross Priory Research Workshop, Glasgow, Scotland, 2012

- Erhart T.G. and Infield D. and Eicker U.
  Optimisation of heat-led CHPs based upon ORC-technology, Glasgow Research Partnership in Engineering (GRPe) Conference, Glasgow, Scotland, 2013

B.5 Journal publications

- Eicker U. and Erhart T.G. and Hettler F. and Pietzsch U. and Strzalka A. Gebaeude-Energieeffizienz und erneuerbare Energieversorgung in urbanem
  Massstab - Auf dem Weg zum nachhaltigen Modellstadtviertel, Oekologisches Wirtschaften, 2011

- Eicker U. and Erhart T.G. and Hettler F.and Pietzsch U. and Strzalka A. Die nachhaltige Modellstadt - Energieeffizienz und erneuerbare Energieversorgung im urbanen Massstab, Ingenieurblatt, 2, 2011
- Erhart T.G. and Herrmann M. and Hettler F. and Jansen K.-J. Nachhaltige Stadtquartiere mit Niedrigenergiegeb¨auden und erneuerbarer Versorgung - Ein Pilotprojekt in Deutschland, St¨adtebauwelt, 2011

B.6 Peer-reviewed journal publications

- Eicker U. and Strzalka A. and Erhart T.G. and Balestieri J. Low energy city quarters with high renewable fractions: Monitoring results and potential for replication, International Journal of Sustainable Building Technology and Urban Development - SUSB, 3, 69-79, 2011

- Strzalka R. and Erhart T.G. and Eicker U. Analysis and optimization of a co-generation system based on biomass combustion, Applied Thermal Engineering, 50, 1418-1426, 2011

- Erhart T.G. and Eicker U. and Infield D. Influence of Condenser Conditions on Organic-Rankine-Cycle Load Characteristics, ASME Journal of Engineering for Gas Turbines and Power, 135(4), doi: 10.1115/1.4023113, 2013